PHOTOPHYSICS OF INFRARED MULTIPHOTON ABSORPTION BY THIOPHOSGENE

by

MARK NELSON SPENCER

B.A., University of Pennsylvania
(1978)

SUBMITTED TO THE DEPARTMENT OF
CHEMISTRY IN PARTIAL
FULFILLMENT OF THE
REQUIREMENTS FOR THE
DEGREE OF

DOCTOR OF PHILOSOPHY

at the

MASSACHUSETTS INSTITUTE OF TECHNOLOGY

DECEMBER 1982

[i.e. Feb, 1982]

c Massachusetts Institute of Technology

Signature redacted

Signature of the Author _____
Mark N. Spencer
Department of Chemistry

Signature redacted

Certified by _____
Jeffrey I. Steinfeld
Thesis Supervisor

Signature redacted

Accepted by _____
Glenn A. Berchtold
Chairman, Departmental Committee

Archives

MASSACHUSETTS INSTITUTE
OF TECHNOLOGY

MAR 31 1983

LIBRARIES

This doctoral thesis has been examined by a Committee of the Department of Chemistry as follows:

Professor Robert J. Silbey Signature redacted Chairman

Professor Jeffrey I. Steinfeld Signature redacted Thesis Supervisor

Professor Robert W. Field Signature redacted

PHOTOPHYSICS OF INFRARED MULTIPHOTON ABSORPTION BY THIOPHOSGENE

by

MARK NELSON SPENCER

Submitted to the Department of Chemistry
on December , 1982 in partial fulfillment of the
requirements for the Degree of Doctor of Philosophy in Chemistry

ABSTRACT

Infrared-visible double resonance experiments were done on thiophosgene under collisionless conditions and in a bulb to determine the dynamics of infrared multiphoton absorption in its sparse density of states region. In the absence of collisions thiophosgene absorbs at all excitation frequencies. Measurements of the ground state depletion as a function of CO_2 laser frequency do not correlate at all with the conventional infrared absorption spectrum. At excitation frequencies coincident with the ν_4 overtone, no population build-up is observed in excited states of the $2\nu_4$ manifold.

The depletion of the ground state induced by the CO_2 laser decreases rapidly as the pressure of thiophosgene increases beyond 2 mTorr. Mixed gas experiments show that this collisional effect is proportional to long range intermolecular forces.

Computer solution of the density matrix equations for the infrared excitation of prototypical five level vibrational ladders were carried out in conjunction with the experiments. They demonstrate that the observed phenomena are consistent with a model in which a system of extremely weak combination bands lying between 940 and 1100 cm^{-1} provide an absorption continuum for CO_2 laser radiation in this frequency region. The computer simulations also allow us to hypothesize that the observed collisional effect is due to pressure broadening of rovibrational transitions in these very weak combination bands. However, the unusually high efficiency with which pressure broadening must occur in order to make this explanation work leaves open the possibility that other mechanisms are responsible for this behavior.

Thesis Supervisor: Dr. Jeffrey I. Steinfeld

Title: Professor of Chemistry

TABLE OF CONTENTS

ABSTRACT 3

ACKNOWLEDGEMENTS 7

I. INTRODUCTION 4

II. INFRARED -VISIBLE DOUBLE RESONANCE EXPERIMENTS 25

Ammonia 29

Osmium Tetroxide 32

Biacetyl. 32

Formaldehyde 34

Propynal. 37

III. THIOPHOSGENE 41

A. Ground State ($\tilde{X}\ ^1A_1$). 42

B. Electronically Excited States 49

First Excited Singlet States ($\tilde{A}(^1A_2)$) 49

Second Excited Singlet ($\tilde{B}(^1A_1)$) 53

Triplet State ($\tilde{a}(^3A_2)$) 54

IV. THEORY. 56

A. Schrödinger Formulation 56

Two-Photon Absorption 60

B. Density Matrix Formulation 67

C. Density Matrix Solution: Computer Model 82

V. EXPERIMENTAL 95

A. Materials 95

1. Thiophosgene 95

2. Added Gases 96

B. Delivery System 96

1. Effusive Beam 96

2. Supersonic Beam. 97

3. Bulb Experiments 98

C. Molecular Beam Machine. 98

D. CO_2 Laser 106

E. Dye Laser 109

F. Detection System 111

G. Triggering System 115

VI. Results 118

A. Collisonless Experiments 118

1. Ground (Vibrationless State). 118

2. Excited States 143

B. Static Gas Experiments 146

1. Vibrationless Ground State 146

2. Excited Vibrational States 165

VII. DISCUSSION. 188

A. Collisionless Experiments 188

B. Bulb Experiments 195

REFERENCES 228

Appendix A. Measurement of Branching Ratios for the $2_0^1 3_0^1 4_{2n}^1$ Progression 230

Appendix B. Listing of Program Density Matrix Computer Solution Program 245

Appendix C. Reprint of "Influence of collisions on coherent IR multiphoton absorption in thiophosgene" 253

Appendix D. Reprint of "Photophysics of infrared multiphoton excitation in thiophosgene." 256

Acknowledgements

My first thanks go to my advisor, Jeff Steinfeld, who decided that I would be less of a menace to MIT by doing my experimental work at Brookhaven. Doug Brenner deserves special acknowledgement: He drilled in me the importance of not making mistakes---three diffusion pumps later, I believe I have finally achieved perfection. If the southern California sun doesn't mellow Doug out I suggest phenobarbitol. To the other members of my committee: Robert W. Field once told me that, contrary to popular belief, he would be impressed with a solid piece of spectroscopic work done on a molecule having more than two atoms--Sorry, Bob. I recommend that Professor Field attempt to break the Soviet endurance record for orbiting the earth in a space station. Bob Silbey deserves much credit for my development as a scientist. Perhaps after reading this thesis, he will relieve himself of his duties on the admissions committee.

I must express my gratitude to certain senior members of the Steinfeld group: My eternal thanks to Chris Reiser for his electronics expertise, for his computer know-how and for his careless leaving behind of 5.76 problem sets. To Craig Jensen for leaving me a drug store when he left me his desk. And to Melissa Charron for showing us all how to be child-like without being childish. Maybe this Christmas Santa will bring her a puppy.

Of my peers: Since I've known Joseph Salvadore Francisco I can honestly say that some of my best friends are black. Techniques that Joe taught me at MIT will prove to be indispensable at Columbia and throughout my entire life. He even knows a little science. I wish Dave

Harradine much financial success in his future; sex change operations are very expensive. Eric Schweitzer is one person I believe who would benefit immensely from hallucinogenic drugs. Bobbi Roop will always be remembered for her fascinating group seminars. Perhaps a quaalude in her beer would help her delivery. Since I've met Leo Laux, I've learned that you can't judge a person by his name. (Could his middle name be Bagelan?) Unabashed thanks goes to Neil Shinn, Dave Reisner, Precila Ip, Daisy Chawla, Amit Sinha, Dan Imre, Don Kormos, Pierre Tutundjian, James Mack, and any other nationality I have left out.

Most of the ideas expressed in the discussion are the result of long and fruitful discussions with Hal Galbraith and Jay Ackerhalt of Los Alamos National Laboratory and I owe them an eternal debt. When not doing theory, Hal is tinkering in his woodworking shop. I suspect that when this thesis is published, he will be tinkering full time. Thanks also go to the theoretical team of Goodman, Stone and Thiele for their unique insights. Where else, but in southern California, can one find a biologist, a chemist trained by John Ross and an anarchist doing theory together?

I am especially in debt - spiritually and financially - to Vera Spanos for typing this manuscript and for putting up with my many missed deadlines. Any mistakes you find in this thesis are Vera's fault - not mine.

None of the experiments described in this thesis could have been done without the work of the support staffs of Brookhaven and MIT. Their contribution to my research has been immeasurable and they must, therefore, share the blame for it.

Thanks to Ken Lew and Tom Fox of Children's Hopsital Medical Center who gave me the best career opportunity of my life when they offered to write a recommendation for me to medical school.

And, lastly, special thanks to my parents who wisely persuaded me not to become a bricklayer.

I. INTRODUCTION

The invention of the laser two decades ago has changed the direction of research in the physical sciences and created a new field of science--nonlinear optics. At the heart of the theory behind this new discipline is the ability of matter to absorb or emit radiation from an electromagnetic field through higher powers in the electric field. In mathematical language:

$$\vec{P} = \sum_{n=1}^{\infty} \chi^{(n)} \vec{E}^n$$

in which $\vec{P}$ is the polarization of the medium interacting with radiation, $\vec{E}$ is the electric field and $\chi^{(n)}$ is the complex susceptibility of the material. In general, as n increases the contribution that $\chi^{(n)}$ makes to the overall absorption or emission of radiation decreases rapidly. In fact, only through the use of the laser can the scientist obtain the field intensity needed to observe nonlinear effects (n>1) of most systems. Among the various nonlinear effects that have been observed are: stimulated Raman scattering[1], coherent anti-Stokes Raman scattering[2], self-induced transparency[3,4], superradiance[2,5], and multiphoton transitions[2,5].

It is the last of these phenomena to which this thesis is addressed. To be more specific, I shall describe the experiments and calculations that were done by Steinfeld, Brenner and me to unravel the dynamics of multiphoton absorption in the infrared regime by thiophosgene molecules. Although the theory behind all multiphoton processes is derived from one source--the time-dependent Schrödinger equation--certain features of infrared multiphoton absorption (IRMPA) make it amenable to a mathematical treatment that is distinct from multiphoton absorption

in other frequency regimes. For instance, the large difference between the rovibrational density of states and the electronic density of states in polyatomic molecules makes IRMPA a characteristically different process from multiphoton ionization (MPI)--the absorption by atoms and molecules through a manifold of electronic states. In particular the regularity of spacing in a vibrational ladder introduces mathematical simplifications into the theory of IRMPA that cannot be used in the theory of MPI.

In this chapter I shall briefly describe several of the pioneering investigations of infrared multiphoton absorption that paved the way to the experiments reported in this thesis. They began as crude attempts to irradiate gaseous samples with a continuous wave infrared laser--but which resulted merely in thermal heating of the molecules--and have progressed to carefully controlled experiments in which the spectroscopic and collisional parameters of the infrared pumping process have been determined.

Credit for the first such efforts to excite molecules with a c.w. infrared laser goes to the team of Bordé, Henry and Henry[6]. In 1966 they focussed the undispersed radiation from their CO_2 laser onto a cell of ammonia, the latter being resonant with the laser at three lines in the 10.6 μm branch. The resulting yellow light was identified as fluorescence from electronically excited NH_2 fragments and thus demonstrated the ability of the infrared laser to induce decomposition in a gas (albeit through bulk heating).

Similar experiments on boron trichloride[7-9] again demonstrated the feasibility of using infrared lasers to initiate chemical reactions, but it was not until 1974 that any collisionless excitation of this molecule

was observed. In fact, Karlov, et al.[7] recorded infrared fluorescence from BCl_3 irradiated by a c.w. laser resulting from the excitation of four vibrational modes although only one was in resonance with the CO_2 laser.

If "real" infrared multiphoton absorption (characterized by some sort of vibrational selectivity in the pumping process) were ever to be observed, then a pulsed laser would have to replace the continuous wave laser in the excitation process.

In 1970 Isenor and Richardson[10] first reported a series of experiments in which a pulsed CO_2 laser was used to excite gaseous samples of SiF_4, CH_3Cl, CCl_2F_2, NH_3 and several hydrocarbons. More systematic experiments[11] followed which focussed on the temporal characteristics of the luminescence signal resulting from excitation of SiF_4. In these latter experiments a focussed CO_2 laser having an output power of approximately 1 MW dissociated samples of silicon tetrafluoride at various pressures. The fluorescence from the decomposition fragments was time resolved and, at low pressures, a fast component was observed to follow the laser pulse within 20 nsec. At pressures greater than 5 Torr they also observed a slow fluorescence component (~1 μsec) whose magnitude increased with pressure and at the expense of the fast component. The Canadian team was able to assign most of the fast fluorescence to excited SiF fragments and the slow fluorescence to SiF and SiF_2 fragments. Measurement of the fast luminescence signal as a function of foreign gas pressure and laser power, along with determination of the fluorescence lifetime as a function of gas pressure, confirmed the idea that this process resulted from direct excitation of SiF_4 all the way to dissociation.

One startling point to be made about these experiments is the fact that SiF_4 has no fundamental vibrational frequencies in the vicinity of the CO_2 laser excitation frequency of 946 cm^{-1}. The laser-induced decomposition could be explained only by the pumping of combination bands. This work was also the first to postulate the role of the vibrational quasicontinuum in allowing IRMPA to overcome anharmonic bottlenecks.

Similar observations of a fast fluorescence signal following laser-decomposition were made by Letokhov, et al. on boron trichloride[9]. BCl_3 at various pressures was excited by the P(14) line of a TEA laser having an output energy of 0.3 J and pulse duration of 400 nsec. At pressures less than 6 Torr the fast luminescence signal followed the infrared laser pulse by less than 20 nsec. At higher pressures only the slow component of the fluorescence signal appeared.

In the reports of both experiments just described the authors invoked the idea of a collisionless excitation pathway during multiphoton absorption at low pressures. This hypothesis was given further credence by a series of experiments done on C_2F_3Cl by Letokhov, Ryabov and Tumanov [12,13]. As in the previous investigations, a CO_2 laser was focussed on gaseous samples of C_2F_3Cl (and NH_3) and the luminescence resulting from the dissociation products was collected and, in some cases, dispersed by a monochromator before being imaged onto a photomultiplier. Although the fluorescence decreased with increasing pressure, the short delay (30 nsec) between the laser pulse and the fluorescence pulse ruled out thermal heating as the cause of dissociation.

The difference between Boltzmann type heating and IRMPA was under-

scored dramatically in 1974 with the discovery by Ambartzumian et al.[14] of isotope selectivity of the excitation of boron trichloride. A natural mixture of $^{10}BCl_3$ and $^{11}BCl_3$ (^{10}B:^{11}B = 1:4.32) was mixed with oxygen and subjected to CO_2 laser pulses tuned to excite the $^{11}BCl_3$ absorption maximum (P(26), 10.6 μm). The dissociation that followed laser excitation led to excited BO formation and fluorescence, the latter of which was dispersed and recorded. The 30 Å shift between band heads of the electronic emission spectra of both radical isotopes allowed the Russians to observe a preponderance of the Boron isotope, in the products, that was selectively excited.

The newly discovered selectivity of multiphoton excitation was put on a more quantitative basis by Ambartzumian, et al.[15] by mass analyzing the dissociation products of sulfur hexafluoride. When SF_6, having a natural mixture of sulfur isotopes (^{32}S-95%, ^{33}S-0.75%, ^{34}S-4.2%, ^{35}S-0.017%) was excited and dissociated by an infrared laser tuned to the absorption maximum of one of the isotopes the spectra of the remaining reactant showed almost complete removal of the excited isotope. For instance, exposure of SF_6 at 0.1 Torr to 2000 laser pulses in resonance with the $^{32}SF_6$ species (947 cm^{-1}) produced an enrichment factor

$$\frac{(^{34}S/^{32}S)_{after}}{(^{34}S/^{32}S)_{before}}$$

of 2800! As the pressure of the absorbing gas increased, the enrichment factor dropped exponentially; at 1 Torr it was essentially one, i.e. no enrichment. This constituted the first hard evidence that IRMPA resulted in a nonthermal distribution of vibrational energy.

Using hydrogen as a scavenger of dissociated SF_6 molecules

Lyman, et al.[16,17] performed similar experiments on the isotope selectivity of infrared multiphoton dissociation of SF_6. The CO_2 laser lines used in these experiments were chosen to be coincident with three maxima in the infrared absorption spectrum. Two lines, P(16) and P(20) (10.6 μm), excited hot bands and the third line excited the ground state ν_3-Q branch. Depletion of the $^{32}SF_6$ content confirmed the earlier Russian results but the $^{34}SF_6$ isotope enrichment factor did not vary much with the choice of laser line as was previously reported.

With the completion of the pioneering experiments a qualitative picture of IRMPA emerged. In contrast to thermal heating, in which maximum entropy is preserved in all degrees of freedom and at all times during heating, excitation with a CO_2 laser (under the appropriate conditions) apparently excited only certain vibrational modes and left all others cold.

Although the experiments so far demonstrated a positive role for collisions in assisting the overall absorption process, they did not show that infrared absorption could not proceed in the absence of them. In fact, as the isotope experiments just discussed demonstrated, collisions destroyed the rovibrational selectivity of absorption. These latter observations underscore the need to study IRMPA under truly collisionless conditions so that the quantum mechanical basis of the pumping process, unperturbed by collisions, can be understood.

The stream of experiments that gave the scientific community its crude understanding of IRMPA up to this point (1975) then became a flood. Motivated by the prospect of developing mode-selective chemistry, physicists searched for multiphoton excitation pathways in nearly every molecule known to absorb CO_2 laser radiation. Steinfeld, in his

compilation of infrared laser-induced chemical reaction[18], lists over one hundred distinct chemical species that have been put in the path of an infrared laser.

Characterizing the absorption process has been done by one of the following four methods: First, the molecule is dissociated and the product yield determined from luminescence of the new species[6,7,9,10,11,19,20] from the infrared spectrum of the products[21-23], gas chromatography[24,25], mass spectroscopy[26-31], or laser-induced fluorescence of the products[32-41]. Second, in what is really a special application of this technique, the isotope enrichment factor is determined from infrared spectroscopy[14,42] or, more commonly, mass spectrometry[15-17,43-49]. Third, absorption of the CO_2 laser pulse as a function of various parameters may be used to yield absorption cross sections[13,49-61]. Fourth, double resonance techniques can be used to determine population distributions resulting from IRMPA; this last method will be discussed in the next chapter.

For the remainder of this chapter, I will mention only a few key experiments and theoretical studies that have improved our understanding of IRMPA and I will follow it, in chapter II, with a discussion of those experiments that have drawn on the same technique as we have used in attempting to unravel the dynamics of multiphton absorption --infrared-visible double resonance.

Even with the awareness that infrared multiphoton absorption proceeded through only a small subset of vibrational space, workers still could not explain the ability of a molecule to absorb the many photons needed for it to dissociate. In SF_6, for example, excitation of the ν_3 mode by 944 cm^{-1} photons leads to breaking of the S-F bond--a process

that consumes 95 kcal/mole or 33 photons[62]. That SF_6 does absorb this number of photons is even more surprising in view of the anharmonicity of the (pumped) mode--2.9 cm^{-1}. This decreasing vibrational energy level spacing as excitation of the ladder proceeds means that an infrared light field in resonance with the (0→1) transition is already out of resonance for the (1→2) transition (for a field intensity of 10 MW/cm and a power broadened width of 0.3 cm^{-1})[62]. This so-called anharmonic bottleneck ought to limit absorption to, at most, two photons. The fact that it doesn't implies that it is insufficient to consider only the vibrational structure of a molecule in attempting to understand IRMPA.

One missing piece to the puzzle is the rotational structure at each vibrational level. For the ν_3 manifold of SF_6, including the rotational contribution to multiphoton absorption means associating with each vibrational level in the pumped mode ladder a "width" of approximately 20 cm^{-1}. Specific rovibrational excitation pathways can then be envisioned in which infrared photons can find a series of resonant transitions through several quanta of the pumped mode.

The first few models to incorporate rotational structure into a multiphoton absorption scheme proposed very specific pathways of excitation but could account for the absorption of, at most, three photons. Ambartzumian, et al.[19] suggested a scheme for SF_6 in which an initial (0→1) P branch transition is followed by a Q branch transition. They used this model to explain an experiment in which they measured dissociation yield as a function of CO_2 laser frequency. The dissociation curve (a sort of absorption spectrum) had a width of ~30 cm^{-1} and was red shifted from the Q branch ν_3 absorption band by 8 cm^{-1} indicating

absorption through high vibrational states. (A more satisfactory explanation of these observations will soon be obvious.) In another scheme set forth by Bloembergen, Cantrell and Larsen[62] a four-photon excitation model was proposed in which the largest detuning in the ladder was 1.4 cm^{-1}. Although still grossly oversimplified, these attempts provided the basis for more refined models.

As the excitation models became more sophisticated so did the mathematical treatment needed to carry out the calculations suggested by the models. Bloembergen, et al.[62] presented, along with their crude excitation scheme, a second order perturbation calculation of the effective Rabi frequency for the overall multiphoton transition. Lin and Morris[63] produced a comprehensive model for calculating populations in a three-level system interacting with a CO_2 laser. By using a density matrix formalism, they were able to include the effects of collisional relaxation on the resulting population distribution. The expressions they derived were intended to be used to choose the optimum frequency at which any given molecule should be excited in order to promote the greatest fraction of population to the third level.

The concept of compensating for anharmonicity by adding rotational energy was carried one step further for molecules having a degenerate pumped mode. For these species, splitting of the degenerate vibrational sublevels through first order Coriolis interactions and anharmonic coupling with other modes could provide an additional means of fine tuning the energy of excitation and, hence, of minimizing the detunings. Cantrell and Galbraith[64] calculated the energy levels of the degenerate ν_3 ladder of SF_6 perturbed by octahedral and spherical anharmonicity and Coriolis coupling. At a vibrational level of $2\nu_3$ they found that the

splitting produced by the perturbations (5.3 cm^{-1}) exceeded even the rotational width for that level. By choosing a laser frequency that was 4 cm^{-1} to red of the ν_3 Q branch, they showed that excitation beyond $5\nu_3$ was quite possible.

More recently, Patterson, et al.[65,66] have analyzed ultrahigh resolution diode laser spectra of SF_6 and have confirmed these calculations. In fact, they have shown that excitation to $8\nu_3$ is feasible.

Absorption all the way to $8\nu_3$ of SF_6 still, however, falls far short of the 33 photons needed for dissociation. The final missing piece of the explanation was first suggested in 1973 by Isenor, et al.[11]. The reader will remember that the Canadian team observed laser-induced dissociation of SiF_4 even though no fundamental frequencies coincided with the frequency of the CO_2 laser. Combination bands, they reasoned, could absorb a few photons, after which anharmonic and Coriolis coupling (second order) with background states could "siphon" off some of the oscillator strength to these nonpumped states. (This sort of quantum mechanical coupling is not to be confused with the kind of coupling calculated by Cantrell and Galbraith which included perturbations only within the ν_3 manifold, i.e. it did not include cross anharmonicities or second order Coriolis coupling needed to couple the pumped mode states to nonpumped states.) Presumably, this spreading of oscillator strength into background states would increase as the vibrational density of states increased. At a high enough density of states such that the coupling can be considered irreversible and absorption occurs predominantly in the background states, the energy region is called the quasicontinuum.

One prediction that might be made on the basis of the newly-invoked quasicontinuum would be that, once a molecule is excited into this region, an infrared field of any frequency should be able to pump the molecule further up the energy axis. Ambartzumian, et al.[67] confirmed this by performing a two-frequency experiment on SF_6. They used two pulsed CO_2 lasers: The first was tuned to excite the ν_3 mode at 942 cm^{-1} and had an output energy of 0.5 J. The second was delayed in time with respect to the first, had an output energy of 3 J, and was tuned higher in frequency than the first (to insure that it did not excite the ν_3 mode). Only when both lasers were fired was there any dissociation. By measuring the dissociation rate as a function of the frequency of the first laser the Russians obtained a sort of absorption spectrum that was considerably narrower than the corresponding high intensity, one-frequency dissociation spectrum mentioned earlier[19]. The maximum of the dissociation curve was still red shifted with respect to the infrared spectrum but was blue shifted with respect to the one color spectrum; the former confirmed the existence of hot band pumping while the latter was attributed to the smaller power broadening at the less intense field. Lowering the SF_6 temperature decreased the width of the dissociation curve even further by decreasing the thermal population in the excited states and reducing hot band pumping. The dissociation curve obtained by varying the frequency of the second laser had a very broad width that extended to 1100 cm^{-1} and peaked strongly in the vicinity of the ν_3 fundamental. The hypothesis of nonselective pumping in the quasicontinuum was therefore verified.

With these basic characteristics of IRMPA established, physicists could now spend their time filling in the details of the photophysics and

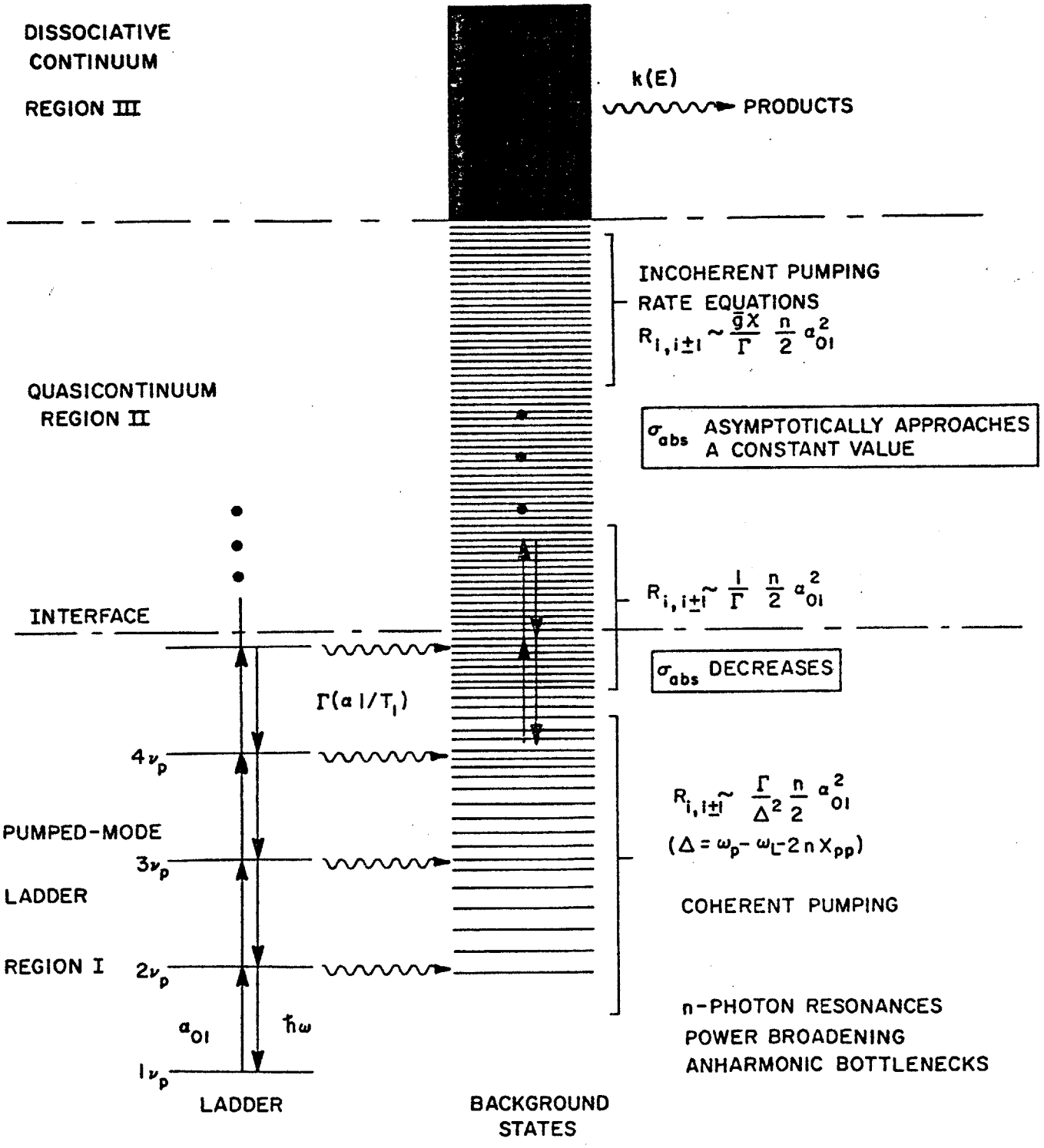
producing a more sophisticated theory. As a means of summarizing, I shall now present a qualitative picture of IRMPA as it is understood today. A more quantitative explanation of the dynamics in the region relative to our experiments will be given in the chapter on theory.

Multiphoton excitation occurs in three stages (or energy regions). (Fig. I.1) Absorption in the first region--the sparse density of states region--is quantum mechanical in nature and must be modeled using the time-dependent Schrödinger (or Heisenberg) equation. If collisional relaxation is to be accounted for, then one must modify the Schrödinger equation to phenomenologically include these interactions--the result is the density matrix formalism.

The behavior of the discrete region is determined by the molecular properties of the system, especially those of the pumped mode such as vibrational spacing, anharmonicity, rotational constants, dipole moment, and anharmonic and Coriolis coupling within the ladder--if it is degenerate--and with nonpumped states. Properties of the light field--the degree of coherence, monochromaticity, intensity and temporal shape--contribute with the molecular properties to determine the characteristics of IRMPA that distinugish one molecule from another. Detunings between the light field and the vibrational energy levels are compensated for by rotational energy increments and, in degenerate modes, by splittings of the degenerate sublevels through Coriolis and anharmonic perturbations.

As anharmonic and second-order Coriolis interactions couple and mix states of the pumped mode with isoenergetic background states, part of the oscillator strength is spread into these other states. Depending on

Fig. I.1 Postulated Mechanism of Infrared Multiphoton Absorption


DISSOCIATIVE CONTINUUM
REGION III
k(E)
PRODUCTS
INCOHERENT PUMPING
RATE EQUATIONS
$R_{i,i\pm1} \sim \frac{\bar{g}\chi}{\Gamma} \frac{n}{2} a_{01}^2$
QUASICONTINUUM
REGION II
σ_{abs} ASYMPTOTICALLY APPROACHES A CONSTANT VALUE
$R_{i,i\pm1} \sim \frac{1}{\Gamma} \frac{n}{2} a_{01}^2$
INTERFACE
σ_{abs} DECREASES
$\Gamma(a\,1/T_1)$
$4\nu_p$
$R_{i,i\pm1} \sim \frac{\Gamma}{\Delta^2} \frac{n}{2} a_{01}^2$
$(\Delta = \omega_p - \omega_L - 2n\chi_{pp})$
PUMPED-MODE
$3\nu_p$
LADDER
COHERENT PUMPING
REGION I
$2\nu_p$
n-PHOTON RESONANCES
POWER BROADENING
ANHARMONIC BOTTLENECKS
a_{01}
$\hbar\omega$
$1\nu_p$
LADDER
BACKGROUND STATES

the relative magnitude of the Rabi frequency (ω_R) and the coupling matrix element connecting a pumped mode state with a background state (Γ) excitation to these interacting states can be described either as a transition to a pure pumped mode state followed by transfer of population to the coupled state ($\omega_R >> \Gamma$) or as a transition directly to a mixed state ($\Gamma >> \omega_R$).

Since the density of vibrational states increases with increasing energy, absorption eventually takes place exclusively within these combination states; this energy region is the quasicontinuum.

Initially in the quasicontinuum, relaxation into combination states has a secondary effect of broadening the transition linewidth and decreasing the overall oscillator strength. At higher energies, however, the number of coupled background states increases and compensates for the lower transition strength of each absorbing mixed state. Eventually the decreasing absorption cross section levels off and, depending on the molecule, may even rise.

As the potential energy surface of the pumped mode flattens out, corresponding to dissociation, the quasicontinuum becomes a true continuum. Molecules in this region dissociate at a rate that can be calculated using RRKM theory.

This concludes our capsule summary of the dynamics of infrared multiphoton absorption. For a thorough and mathematical treatment of this phenomenon, including model calculations done on SF_6 and S_2F_{10}, the reader is referred to the excellent review article by Ackerhalt and Galbraith[68].

II. INFRARED VISIBLE DOUBLE RESONANCE EXPERIMENTS

The ultimate aim of all investigations of the infrared multiphoton absorption process is to be able to characterize its dynamics--especially in the low density of states region where a molecule's response to an infrared field is most unique. This requires determination of the population distribution of the absorbing molecule over all its rovibrational states as a function of time--during and after the laser pulse.

In the preceding chapter, the experiments that were cited all sought to obtain this information either by measuring the dissociation yield of a compound following irradiation by CO_2 laser pulses or by measuring the absorption of infrared energy in a laser pulse subsequent to excitation. The first method only measures the total population that is excited beyond the dissociation threshold; two distributions may differ radically in their shape prior to the energy of dissociation and still give the same decomposition rates. The second method is sensitive only to the first moment of the population distribution--the average energy absorbed--so that two different distributions that have the same first moment will give the same absorption data.

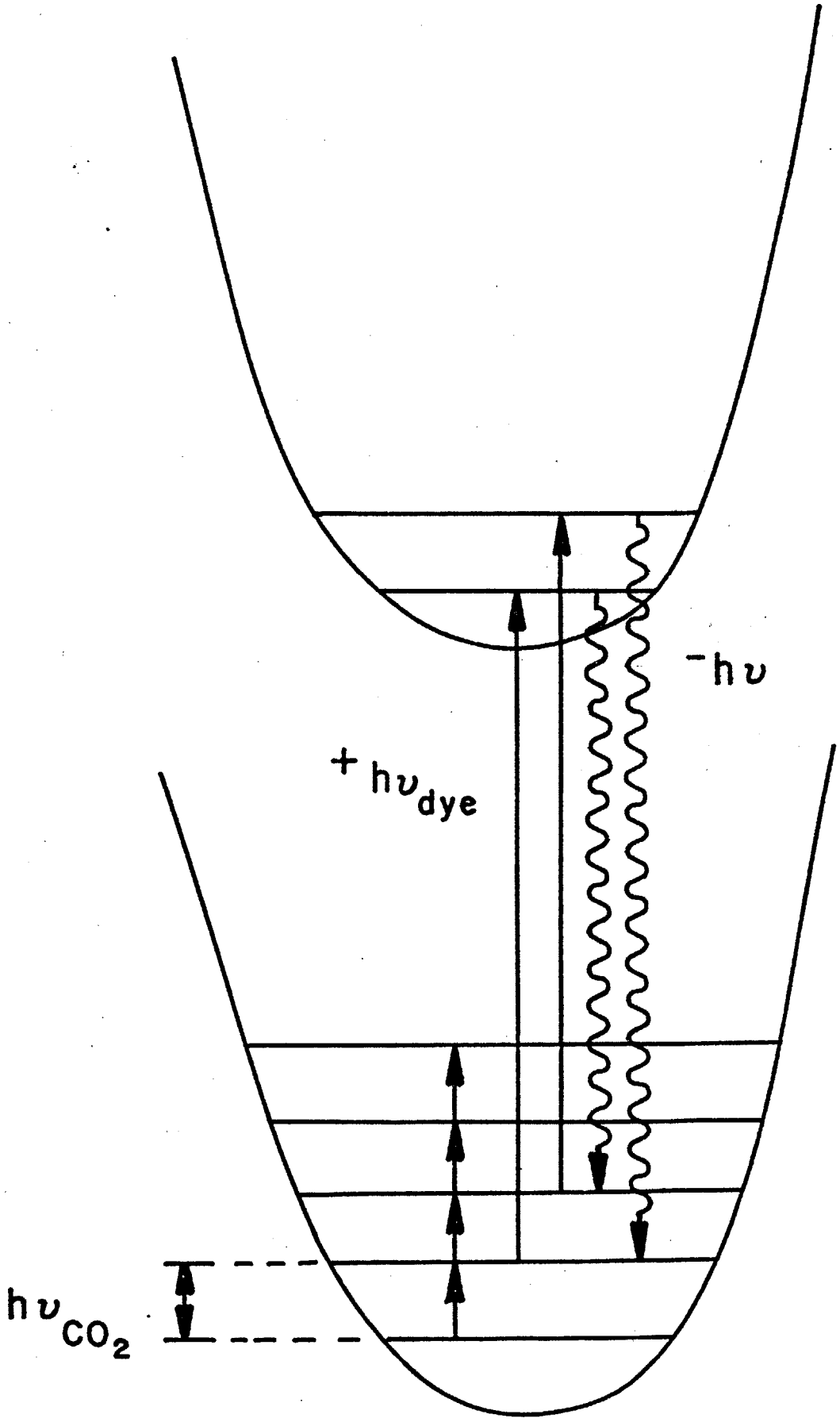
Any method that attempts to obtain specific information about the dynamics of IRMPA in the low density of states energy region must measure the changes in individual level populations that result from infrared laser excitation. The most direct way of doing this is to observe the changes in a molecule's absorption spectrum during, and subsequent to, infrared pumping. This is the basis of all double resonance experiments. While the molecule is in some vibrationally excited state an absorption spectrum is taken (Fig. II.1). Changes in the intensities of absorption bands can be traced to changes induced by the infrared laser--the "pump".

From these changes in the spectrum, changes in the populations of the absorbing states can be deduced.

The light source that is used to record the absorption spectrum may excite transitions in the microwave, infrared, visible or ultraviolet wavelength regions. For an excellent review of all of these schemes the reader is advised to consult Steinfeld's review article[69]. Of the three, recording changes in an infrared spectrum subsequent to irradiation-infrared-infrared [double-resonance (IR-IR-DR)] has been used the most. Unfortunately, interpretation of IR-IR-DR experiments is complicated by two factors: First, since the pump and probe operate in the same wavelength region, the probe can also pump the transitions that it is supposed to interrogate. This effect is minimized by keeping the power of the probe (usually another laser) as low as possible. Second, complications arise from the even spacing of the vibrational levels; this often makes the assignment of the pumped transitions difficult.

Infrared-visible (ultraviolet) double-resonance (IR-VIS[UV]-DR) techniques circumvent both these problems. The infrared transition induced by the infrared source are in a totally separate spectral region from the visible probe that takes the absorption "snapshot" and, hence, can in no way alter the population distribution created by the CO_2 laser. In general, dissimilarities in the vibrational frequencies of the ground and excited states are different so that an unambiguous assignment of the electronic spectrum is possible. IR-VIS-DR experiments have an additional advantage over their IR-IR-DR counterparts when the electronic absorption spectrum is taken via laser-induced fluorescence. In this case the detection of visible fluorescence can be done with much greater signal-to-noise ratio and with simpler technology than the recording of

Fig. II.1 Schematic representation of the concept of infrared-invisible double resonance. In this diagram the first and second excited vibrational states of the pumped mode ladder are being probed.


$-h\upsilon$
$+h\upsilon_{dye}$
$h\upsilon_{CO_2}$

an infrared absorption spectrum.

The remainder of the chapter is devoted to a summary of experimental investigations that have used the technique of infrared-visible double resonance to study IRMPA by several molecules. Their numbers are severely limited because of one constraint that this technique imposes on them--the requirement that the molecule to be studied possesses a discrete and assignable electronic absorption spectrum that does not lie too deeply in the ultraviolet.

Ammonia

The first molecule to be subjected to an infrared-ultraviolet double resonance experiment was ammonia. Ambartzumian et al.[69,70] tuned their CO_2 laser to emit 50 mJ pulses at 933.0 cm^{-1}. Coincident with this frequency (within 45 GHz) is the asQ(5,3) component of the ν_2 mode. Inversion doubling causes the overtones of this mode to be irregularly spaced. Consequently, only the fundamental (both symmetry components) and the asymmetric component of the first overtone lie at energies that are in resonance with infrared light at 933 cm^{-1}.

For a probe source they used a stabilized hydrogen spectral lamp focussed with a condenser and dispersed by a monochromator. The spectral region monitored lay between 2000 Å and 2500 Å. Absorption of the pulsed infrared radiation was monitored by recording the transient change in the electronic absorption spectrum as the sample was excited into higher vibrational levels. As in previously discussed experiments[10-13], the change in transmittance of the ultraviolet probe manifested itself as a short (collisionless) pulse approximately 0.3 μsec long followed by a pressure dependent tail of duration 0.3 to 1 μsec. The population changes that Ambartzumian and co-workers reported were those remaining after the tail and, hence, represented a thermal population. At a

pressure of 240 Torr, the ammonia was heated by the CO_2 laser to a temperature of 900 K. At this vibrational temperature 40% of the ammonia molecules were excited to the v=1 level (ν_2) and 6% were promoted to the v=2 level. (We must remember that the excited state population of 40% includes a 17% contribution that is there at room temperature in the absence of the CO_2 laser.)

In order to model their results the Russian workers also set up a set of rate equations including radiative and collisional (V→T) transfer of population for a two level system. From the solution of the equations they obtained a value of 25-30 nsec (at 240 Torr) for the vibrational relaxation time of excited ammonia molecules. Since this time is far shorter than the delay between infrared excitation and observation of spectral shifts (>1 μsec), there was no doubt about the thermal nature of the excited vibrational distribution.

In additional experiments[71] filling of the $1\nu_2$ level was studied in greater detail by measuring the effects of buffer gases (Ar, O_2 and Xe) on the vibrational relaxation rate of this level and on the intermolecular V-V transfer rate from the $^{14}NH_3$ isotope to the $^{15}NH_3$ isotope (also at v=1). The resulting V→T relaxation times varied from (1.9 ± 0.2 nsec atm) for pure ammonia to (240±20 nsec atm) for NH_3-Xe mixtures. The isotope (V→V) exchange rate was determined, using these values, to be (1.2±0.4 nsec atm).

These early IR-UV-DR experiments on ammonia highlighted the need to repeat them at lower pressures so that the nonthermal radiative transfer of population to excited vibrational states could be studied. Tablas, et al.[72] did just this within several months of the Russian experiments. In most of the experiments, the CO_2 laser was tuned to the same frequency

(933.0 cm^{-1}) used in Ambartzumian's experiments and a xenon flash tube with a pulse duration of 10 μsec served as the probe excitation source for the electronic transition $\tilde{A}(^1A_2) \leftarrow \tilde{X}(^1A_1)$(2168 Å). Other experiments, however, were done with the infrared laser tuned to CO_2 lines in the 10.6 μm branch other than the resonant P(32) line. Surprisingly, the German team found that the R(14) (971.9 cm^{-1}) and R(6) (966.3 cm^{-1}) lines deposited as much energy in the ammonia gas as the P(32) line even though ammonia is transparent at these frequencies in the normal infrared spectrum! Of the many different experiments done by Tablas, those most significant were performed on ammonia at a pressure of 2 Torr. Population changes in the $1\nu_2(+)$, $2\nu_2(+)$ and $2\nu_2(-)$ states were observed to follow temporally the laser pulse. With a knowledge of the absorption coefficients for the vibronic transitions that probed these levels, they deduced the following population changes for the three levels absorbing 5 J pulses (with a peak power of not more than 10 MW cm^{-1}). (The values in the table are expressed as a fractional change in population due to infrared excitation.)

	NH_3 pressure=1.4 torr	NH_3 pressure=2.1 torr
ground state	-0.20	-0.22
$1\nu_2(+)$	19.6	18.9
$1\nu_2(-)$	8.0	7.8
$2\nu_2(-)$	3.1	2.5

In another surprise finding Tablas, Schmid and Kompa observed population increases in levels as high as $5\nu_2$. This they attributed to collisional coupling between the $1\nu_2(+)$ state and $1\nu_4$ and/or between

$2\nu_2(-)$ and $1\nu_4+1\nu_2$.

Osmium Tetroxide

The only known IR-VIS-DR experiments on OsO_4 were done by Ambartzumian, et al.[73]. The reason for the apparent lack of interest in this molecule is obvious: The vibrational mode which absorbs CO_2 laser radiation--ν_3 (960 cm^{-1})--is absent in the electronic absorption spectrum. A Raman active transition--(971 cm^{-1})--is nearly isoenergetic with and does appear in the electronic spectrum; this mode was monitored for population changes through collisional population transfer from the driven ladder.

An IFP flash lamp whose output was dispersed by a monochromator was the source of ultraviolet radiation. Only light of frequencies lying to the red of the 1_1^0 band were allowed to pass through the monochromator. Upon excitation of 0.4 Torr of osmium tetroxide by focused 3 J pulses, the long wavelength of the absorption spectrum shifted 10,000 cm^{-1} to the red indicating the absorption of approximately ten infrared photons. That the increases in the ν_1 ladder occurred only after the firing of the CO_2 laser, constituted further evidence that absorption was initially in the ν_3 mode and was followed by fast intramolecular relaxation into ν_1 and, possibly, other modes.

Biacetyl

Attempts to unravel the photophysics of IRMPA in biacetyl all met with the following obstacle: The lack of structure in the electronic absorption (room temperature) spectrum makes it impossible to assign specific vibronic transitions and, hence, trace the infrared laser-induced excitation pathways. However, as Campargue and Soep[74] have shown, cooling thiophosgene in a supersonic jet yields a well-structured

and identifiable spectrum that should allow future investigators to study this molecule successfully.

Yogev and Haas[75] irradiated biacetyl at pressures of 1 to 30 Torr with 5 MW cm^{-2} pulses from the P(20), 10.6 μm line of the CO_2 laser (944.2 cm^{-1}). The mode targeted for absorption was the b_u CH_3 rocking mode. A 12V, 100W quartz iodine lamp fed through a monochromator excited the $n\rightarrow\pi^*(\tilde{A}(^1A_u)\leftarrow\tilde{X}(^1Ag)$ transition. Unfortunately, the huge spectral linewidth of the probe radiation (200 cm^{-1}) only allowed Yogev and Haas to observe changes in the envelope of the absorption spectrum.

At a pressure of 29 Torr, they saw a decrease in absorption between 21,800 cm^{-1} and 26,000 cm^{-1} that lasted for 30 μsec; at 1 Torr, the decrease lasted 10 μsec. Between 19,600 cm^{-1} and 21,700 cm^{-1} they observed absorption increases. In both cases the changes only amounted to a fraction of a percent and in neither case was a shift in the long wavelength limit of the spectrum observed. In view of the lack of suitable resolution, no useful information concerning the path of IRMPA can be deduced from this work.

All of the experiments discussed so far employed high intensity spectral lamps as probe sources. Unfortunately, the discharge from these lamps, whether they are flashlamps or continuous sources, is long enough so that it overlaps in time with the infrared laser pulse. This introduces the uncertainty, when analyzing an IR-UV-DR experiment, of whether the infrared laser pumps the electronic ground state--as it should--or the excited state. Furthermore, the large spectral width of these incoherent light sources means that there is low power density at the desired probe wavelength. If the electronic transition that probes the vibrational distributions is weak, then a lamp might not be intense

enough to enable observation of these transitions.

For these two reasons it is advantageous to use a laser instead of a lamp as the probe. The short pulses of light (~20 nsec) obtainable from them allows the timing of probing the vibrationally hot and short-lived population to be accurately controlled and the high intensity per frequency unit allows even "forbidden" electronic transitions to be used to monitor IRMPA.

Credit for the first use of a laser as a probe, though not a pulsed laser, goes to Orr[76] who used a 15 mW continuous wave He-Cd laser on biacetyl. At a frequency of 441.6 nm several unidentified vibronic transitions in the $\tilde{A}(^1Au) \leftarrow \tilde{X}(^1Ag)$ system were excited. Counterpropagating with the visible laser beam was a CO_2 laser operating, as in the previous experiments, on the P(20), 10.6 μm line and emitting 150 mJ pulses. (A 150 W Xenon lamp was also used in other experiments but this yielded no additional information.)

Because of the lack of knowledge of the vibronic transitions doing the probing, identification of the vibrational modes excited by the CO_2 laser was impossible. In addition, singlet to triplet crossing in the excited state gave two temporal components to the fluorescence and made it difficult to interpret the change in fluorescence following infrared excitation. Lastly, as Burak, Quelley and Steinfeld[77] showed in time-resolved experiments, the CO_2 laser pumped the excited state (prepared by the visible laser) in addition to the ground state.

Formaldehyde

In one of the most thorough investigations of IRMPA dynamics ever carried out, using the IR-UV-DR technique, Orr and co-workers[78-82] analyzed the radiative and collisional transfer of population through the

first two excited states of deuterated formaldehyde (HDCO and D_2CO). Their identification of the specific rovibrational transitions pumped by the CO_2 laser along with the measurement of rotational relaxation rates at different levels of excitation demonstrate beautifully the usefulness of the infrared-ultraviolet double resonance method.

In their first experiments[78] D_2CO at a nominal pressure of 5 mTorr was irradiated with 0.5 J pulses of infrared photons. At a frequency of 929.0 cm^{-1} the CO_2 laser excited the ν_4 $8_{1,7} \leftarrow 2_{1,7}$ transition. The specific rovibronic transitions that were used to monitor the ν_4 $8_{1,7}$ state in the electronic absorption spectrum, were those in the 4_1^0 band (365 nm), e.g. $9_{2,8} \leftarrow 8_{1,7}$. These electronic transitions were produced by a pulsed dye laser with a time delay that could be varied (with respect to the firing of the CO_2 laser) to allow them to study the relaxation of the $8_{1,7}$ state into neighboring rotational states. Alternatively, these relaxation parameters could be measured by keeping the dye laser delay fixed and varying the pressure of the gas. Using the former method, Orr and co-workers estimated that relaxation out of the $8_{1,7}$ state occurred with a time constant of not more than 10 nsec Torr.

In subsequent studies[80] the ν_4 $^rQ_2^{(e)}(12)$ $(12_{3,10} \leftarrow 2_{2,10})$ transition was also excited by the P(16), 10.6 μm line (947.7 cm^{-1}) of the CO_2 laser. In a more detailed study of rotational relaxation out of the pumped mode state and into neighboring "satellite" states Orr and Nutt[79] concluded that relaxation into this molecule's pumped mode is principally electric dipole governed and obeys the propensity rule: $\Delta J = \pm 1$. Population increases in satellite levels connected by $\Delta J = 0$ collision-induced transitions were observed but these were shown to be far less efficient that the $\Delta J = \pm 1$ transitions. As before,

a relaxation time of less than 10 nsec Torr was inferred.

Similar experiments on HDCO[79] exploited several CO_2 laser frequencies coincident with transitions in four vibrational bands but the electronic probe transitions out of the excited vibrational states were too weak to be of much value.

Orr and Nutt ascribed two other characteristics of IRMPA to deuterated formaldehyde: First, given a dipole moment of 0.01 D for the $\nu_4 \leftarrow 0$ transition and a laser intensity of 10 MW cm^{-2}, the resulting Rabi frequency is approximately 0.01 cm^{-1}. Hence, only those transitions within 0.01 cm^{-1} of the CO_2 laser frequency could be expected to be pumped and give rise to an IR-UV-DR signal; this was verified in all of their studies. Second, infrared pumping resulted in a hundred-fold enhancement of population in the specified rotational level of ν_4. Both of these results stand in sharp contrast to those obtained by us with thiophosgene.

Further time delay studies[81] monitored relaxation into states coupled to the pumped state through weak collisional transfer mechanisms: $\Delta K_a = \pm 2$ transitions, quadrupole type transitions and V-V relaxation ($\nu_6 \leftarrow \nu_4$). An estimate of the rate of these slower processes was given as 10 μsec^{-1} $torr^{-1}$.

In order to obtain more precise measurements the Australian team[82] set up matrix rate equations (See ref. 83) and used their experimental data to calculate the desired rates. They determined them to be:

$$k(\Delta J = \pm 1) = 50 \pm 10\ \mu sec^{-1} Torr^{-1}$$

$$k(\Delta J = 0) = 25 \pm 10\ \mu sec^{-1} Torr^{-1}$$

$$k(\Delta J = \pm 2)\ \text{(quadrupole-type)} = 6\ \mu sec^{-1} Torr^{-1}$$

$$k(\Delta J = \pm 1)\ \text{(quadrupole-type)} = 12\ \mu sec^{-1} Torr^{-1}.$$

Investigations of the $2\nu_4$ state showed that pumping at 949.5 cm^{-1} (P(14), 10.6 μm) increased population in that state but did not induce any changes in the $1\nu_4$ state. Apparently the low Rabi width of the transition and the anharmonicity of the fundamental was preventing absorption through more than two vibrational quanta. Rotational relaxation out of the second excited state into neighboring J and K_a states was also measured (although with less precision than for the first excited state).

In spite of the explicit and detailed information Orr et al. extracted on the dynamics of infrared absorption by D_2CO it is unfortu-nate that they were unable to observe absorption of two or more photons by either deuterated species. This stands in sharp contrast to the work on Koren et al.[26-29] in which a much higher powered CO_2 laser (20 MW vs. ~1 MW) dissociated samples of H_2CO, HDCO and D_2CO. Although decomposition by the undeuterated species was believed to be thermal, HDCO was found to absorb 14±5 photons[29]. In the light of this information, it seems worthwhile to repeat the IR-UV-DR experiments with more intense infrared excitation so that real multiphoton processes may be studied.

Propynal

Because of its well-characterized electronic absorption spectrum and the occurrence of two vibrational frequencies in the CO_2 laser range, propynal is an ideal candidate for IR-UV-DR experiments. Lesiecki et al.[84] studied the radiative transfer of population between the ground and first excited states of the mode by comparing the laser-induced fluorescence spectra of propynal before and after excitation with a CO_2 laser operating on the P(10), 10.6 μm line (953 cm^{-1}). By measuring the

fluorescence signal as a function of delay in the same manner used in Orr's experiments, they also measured the rate of relaxation into nonpopulated rotational states of $1\nu_6$ and into nonpumped vibrational states isoenergetic with this level. Unfortunately, the kinetic model which they used to extract the relaxation parameters from their fluorescence vs. time delay experiments contained parameters describing collisionless (intramolecular) rotational relaxation which, of course, is a violation of the law of conservation of angular momentum. Furthermore, the unsuitability of using a kinetic scheme, instead of quantum mechanical expressions, to model the excitation and relaxation of the low energy region of propynal renders their quantitative conclusions meaningless.

A far more satisfactory performance of these types of experiments on propynal were done by Brenner et al.[85-87]. In one of the first uses of a molecular beam in a double resonance experiment, they studied IRMPA under collisionless and--when desired--single collision conditions. (The possibility that an experiment done at pressures as low as 5 mTorr may not be collisionless, as many investigators have claimed, will become apparent later in this thesis.)

The molecular beam Brenner, Curtis and Brezinsky used was an effusive beam skimmed 2 mm from the source with a 3 mm slit. The number density resulting from this configuration at the detection region was 10^{11} cm^{-3}. CO_2 laser excitation of the ν_6 mode (943.7 cm^{-1}) and the ν_{10} mode (981.2 cm^{-1}) was accomplished by tuning the laser to the 10.6 μm, P(12) 951.2 cm^{-1}) and R(22), (977.2 cm^{-1}) lines, respectively. Monitoring the ν_{10} state was done generally via the 10_1^1 band (~25,600 cm^{-1}); for observing the $1\nu_6$ level, the probe transition 6_1^0 (~25,200 cm^{-1}) was chosen. A pulsed dye laser served as the probe.

At an intensity of 3 MW cm^{-2}, not surprisingly, only excitation at 977 cm^{-1} produced any population change in $2\nu_{10}$. However, population increases at that level were observed when pumping at all infrared wavelengths between 938.7 cm^{-1} and 952.9 cm^{-1}. The greatest increases were observed for pumping the ^{R}Q sub-band at 942 cm^{-1}. These results are in sharp contrast to those for formaldehyde[78-82] in which only the CO_2 laser line closest in frequency to the pumped mode succeeded in depopulating the ground state.

In another unexpected result, photoacoustic measurements of the absorption of propynal at 200 mTorr as a function of CO_2 laser wavelength, correlated well with a conventional infrared spectrum but not with the double resonance data[86]. In addition, more rovibrational transitions were excited by the CO_2 laser than could be accounted for by power broadening. They hypothesis that Brenner proposed to explain these peculiar findings was that combination transitions were being driven by the CO_2 laser at various frequencies, e.g. at 951.9 cm^{-1}. These bands are too weak to be observed in a normal infrared spectrum, but as we shall later see, can still be strong enough to be excited under collisionless conditions.

Mixed gas experiments were also performed in which a foreign gas (Ar, CO, NO, CCl_4, CH_3F, SiF_4, CF_4, CH_4, or C_2H_6) was introduced into the beam machine at a low enough pressure to insure that not more than one collision occurred between an added gas molecule and a propynal molecule. The following results were obtained:

Pumping ν_6 and probing $1\nu_{10}$ showed no population increase in the latter mode in the absence or in the presence of an added gas. For the opposite case-pumping ν_{10} and monitoring $1\nu_6$--population did increase but

only where SiF_4 was added.

The addition of less than 0.5 mTorr of helium or argon to the detection region did not lead to any enhanced population in $1\nu_6$ when pumping this mode. This piece of evidence was used to eliminate the possibility of vibrational relaxation occurring at this low pressure.

In order to extract rate constants for V→V energy transfer processes in the ν_6 ladder involving only single quantum changes, foreign gases having a fundamental vibrational frequency near 1000 cm^{-1} were used--SiF_4, CH_3F and CF_4. For observation of two quantum changes induced by collisions, molecules having fundamental vibrational modes near 2000 cm^{-1} were used--CO and NO. The observed increases for the added gas experiments, together with an appropriate kinetic model for V→V energy transfer led the Brookhaven group to the surprising conclusion that, at an infrared intensity of 12 MW cm^{-2}, the $3\nu_6 \rightarrow \nu 1\nu_6$ rate was similar in magnitude to the $2\nu_6 \rightarrow \nu_6$ rate although at, 5 MW cm^{-2}, the rate was near zero.

III. Thiophosgene

In spite of the tremendous usefullness of the infrared-visible technique in studying IRMPA, the number of molecules that are suitable for use in an IR-VIS-DR experiment is severely limited by the following two constraints: First, the molecular candidate must be able to absorb light from a suitable high powered infrared laser. For CO_2 laser excitation this means the molecule must possess a vibrational frequency at around 1000 cm^{-1}. Second, the molecule must also possess an electronic absorption spectrum that lies within the range of a visible or ultraviolet laser. Furthermore, the absorption spectrum must be well-resolved and assigned at least on the vibrational level and, preferably, on the rotational level.

Remaining from the field of potential candidates, after these two restrictions are made, is a handful of molecules. Among them are formaldehyde (including its deuterated derivatives), propynal, ammonia, tetrazine, glyoxal, thioformaldehyde and thiophosgene.

The last of these mentioned--thiophosgene--is the one chosen for our studies. Although it has no fundamental vibrational frequencies in the vicinity of the CO_2, one of its overtones--$2\nu_4$--absorbs with an oscillator strength that is anomalously large for such a "forbidden" transition (0.012 D). It also has a visible absorption spectrum that has already been extensively studied and identified. This chapter is devoted to a description of thiophosgene--the rotational parameters of the ground state, its vibrational frequencies and its known excited electronic states.

A. Ground State ($\tilde{X}\ ^1A_1$)

In its vibrationless ground state thiophosgene is a planar molecule having the same structure as that of formaldehyde. From the electron diffraction studies of Pauling et al.[88,89] we know the interatomic distances to be r(C=S) = 1.601 Å, r(C-Cl) = 1.729 Å, and Cl-C-Cl angle = 111.2° (Fig. III.1). Since the C-Cl distance for a substituted alkane is 1.76 Å and, for a substituted alkene, is 1.58 Å, the intermediate value for thiophosgene indicates partial double bond character (12%) for the C-Cl bond. This lessens the reactivity of the chlorine atom to electrophillic reagents (and explains why thiophosgene is not the toxic gas that phosgene is).

From another early study[90] the dipole moment was determined to be 9.3×10^{-31} Cm (0.28 D). Using these interatomic distances and the atomic masses known, I have calculated the following kinetic facts for thiophosgene, at a temperature of 298 K, which will be needed for the interpretation of the double resonance experiments:

hard sphere collision diameter = 2.6×10^{-8} cm

number density = 3.27×10^{16} cm^{-3} $Torr^{-1}$

mean free path = 0.0101 cm Torr

mean molecular velocity = 2.33×10^{4} cm s^{-1}

collision frequency = 3.77×10^{22} s^{-1} cm^{-3} $Torr^{-1}$

= 1.15×10^{6} s^{-1} $molec^{-1}$ $Torr^{-1}$

The similar masses of the chlorine and sulfur atoms make thiophosgene a near oblate top. Nevertheless, the axis of symmetry is along the C=S bond so that a type I representation must be used when analyzing its spectra (rather than a type III representation reserved for

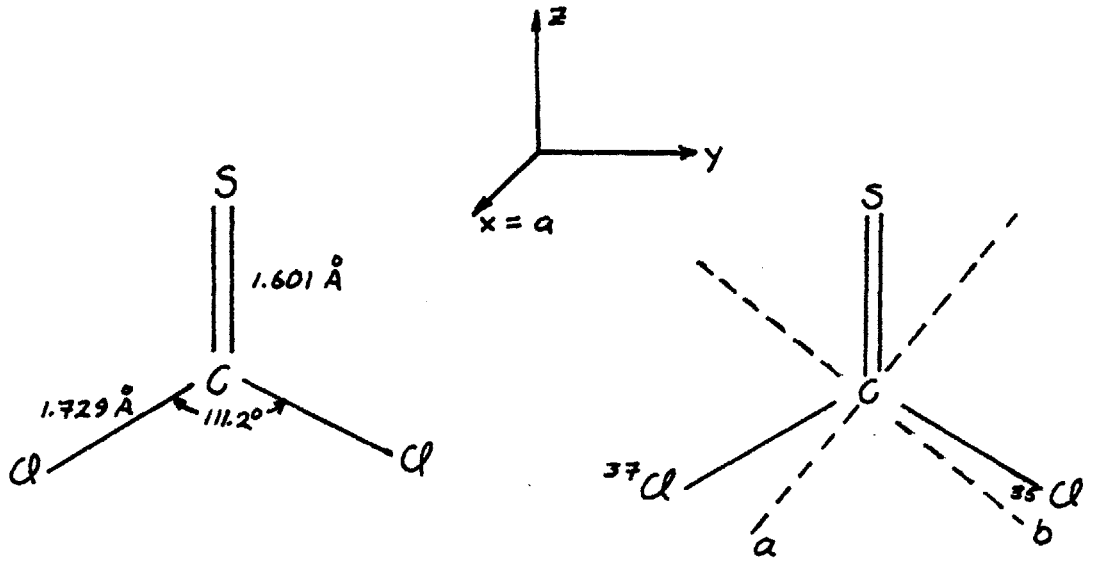


Fig. III.1

(a) Structure of Thiophosgene Orientation of molecule-fixed axes is shown in the middle.

(b) Placement of axes, a and b, for mixed isotope $^{35}Cl^{37}ClCS$. The c axis is perpendicular to the plane of the molecule.

true oblate tops).

The placement of the axes of rotation poses a few more problems (Fig. III.1). The c axis (axis of greatest moment of inertia) is unambiguously fixed to the out of plane x axis. Based on the microwave work of Carpenter et al[91], for the $^{35}Cl^{35}ClCS$ isotope, the a axis is parallel with the z axis (C=S bond). For the $^{35}Cl^{37}ClCS$ isotope, however, the a and b axes switch and the b axis lines up with the C=S bond. For the mixed isotope, $^{35}Cl^{37}ClCS$, the a and b orthogonal axes lie between these two limiting cases.

Carpenter et al.[91] calculated the inertial defect ($I_c-I_b-I_a$) to be 0.319 amu $Å^2$. This near zero value indicates a nearly planar molecule. Other rotational constants for the vibrationless ground state that are needed for spectrum analysis are taken from Carpenter's work and tabulated below.

Table III.1

Rotational Constants for the $X(^1A_1)$ State of Thiophosgene

	$^{35}Cl^{35}Cl$ CS	$^{35}Cl^{37}Cl$ CS	$^{37}Cl^{37}Cl$CS
A(MHz)	3557.3089(3)	3503.3107(4)	3402.751(6)
B	3464.1108(3)	3391.29871(3)	3365.254(5)
C	1753.1000(2)	1721.3039(2)	1690.109(3)
Δ_J(kHz)	0.6508(6)	0.6652(4)	0.863(16)
Δ_{JK}	-0.2680	-0.1910(6)	-1.429(47)
Δ_K	1.2997(7)	0.9504(4)	1.911(56)
δ_J	0.2782(2)	0.2865(1)	0.380(3)
δ_K	0.5395(6)	0.6164(2)	0.287(17)
$\Sigma_i \alpha_i^{AA}$(MHz)	-10.888	-10.175	-10.847
$\Sigma_i \alpha_i^{BB}$	-9.345	-9.476	-8.824
$\Sigma_i \alpha_i^{CC}$	-1.128	-1.096	-1.090

$(A_Z = A_0 + \Sigma_i \alpha_i\ h/2,$ etc.)

$\kappa = 0.844$

The relatively small values of the rotational constants, especially of C, has unfortunate implications for the interpretation of vibrational or electronic spectra. The separation between adjacent rotational levels is very small and, consequently, the frequency difference between consecutive J transitions is no greater than 0.01 cm^{-1}. This difference is less than the spectral width of most dye lasers and infrared spectrometers and therefore makes it difficult to obtain rotationally resolved spectra. Two other complications combine to make the extraction

of information on the rotational state selectivity of IRMPA impossible to obtain: The small value for C also means that population is found at very high J values (up to J≅100 at room temperature). As a result, overlapping among transitions of equal K but different J is common. Lastly, the existence of the two chlorine isotopes in the ration $^{35}Cl:^{37}Cl$ = 1:2 results in the spectra of the two major isotopic thiophosgene species ($^{35}Cl^{35}ClCS$ and $^{35}Cl^{37}ClCS$) overlapping each other and observing a lot of rotational structure.

Determination of the normal mode frequencies is made difficult by the fact that four out of the six vibrational modes have frequencies no greater than approximately 500 cm^{-1} and by the accidental degeneracy of two of them. Force field calculations have been carried out by Brand et al.[92], Carpenter et al.[91], and Frenzel et al.[93]. In addition to doing normal coordinate analyses, the latter have also recorded and identified the infrared (and Raman) spectra of thiophosgene in all three phases and in the dimer and trimer form. The assigned frequencies of vibration and the calculated Coriolis coefficients that are generally accepted are taken from references 91, 93 and 102 and reproduced in Table III.2.

Table III.2

Vibrational Frequencies (cm^{-1})

Mode	$^{35}Cl^{35}ClCS$	$^{35}Cl^{37}ClCS$	$^{37}Cl^{37}ClCS$	Symmetry	Description
ν_1	1139.0	1138.8	1138.6	a_1	C=S stretch
ν_2	503.5	499.4	494.9	a_1	C-Cl stretch
ν_3	288.5	285.8	282.4	a_1	C-Cl bend
ν_4	471.0	470.7	470.2	b_1	out-of-plane bend
ν_5	818	817	815	b_2	C-Cl asym.str.
ν_6	305	302	300	b_2	C-Cl rock

Coriolis Coefficients*

			Sum
$\zeta^a_{64} = -0.9590$	$\zeta^a_{65} = 0.2833$		0.9993
$\zeta^b_{61} = 0.9703$	$\zeta^b_{62} = -0.1891$	ζ^b_{63} 0.1506	0.9999
$\zeta^c_{14} = 0.8731$	$\zeta^c_{24} = -0.2657$	ζ^c_{34} 0.4088	1.0000
$\zeta^c_{15} = -0.4694$	$\zeta^c_{25} = -0.2317$	ζ^c_{35} 0.8521	1.0000

*Calculated using method of Meal and Polo[99].

Overtone and Combination Bands

Identity	Frequency (cm^{-1})	Species	Observed?
$\nu_2+\nu_3$	781.5	a_1	yes
$2\nu_4$	875	b_2	no
$2\nu_4$	942	a_1	yes
$\nu_2+\nu_4$	974	b_1	no
$2\nu_2$	1006	a_1	no
$2\nu_3+\nu_4$	1047	b_1	no
$2\nu_6+\nu_4$	1081	b_1	no
$\nu_3+\nu_6+\nu_4$	1064	a_2	no
$\nu_2+2\nu_3$	1089	a_1	yes
$\nu_3+\nu_5$	1106	b_2	no
$\nu_2+2\nu_6$	1113	a_1	no
$\nu_2+\nu_3+\nu_6$	1096	b_1	no
$\nu_5+\nu_6$	1123	a_1	yes

One would expect the chlorine isotope shift to be greatest for modes having the greatest chlorine atom displacements. Inspection of Table III.2 verifies this. The normal mode ν_2 (C-Cl stretch) shows the greatest difference in frequency between the three isotopes. Vibrational modes ν_3, ν_5 and ν_6 show intermediate shifts while ν_1 (C=S stretch) and ν_4 (out-of-plane bend) show very small differences.

Of particular importance for the analysis of the double resonance experiments discussed in this thesis is the identification of combination and overtone bands. Frenzel et al.[93] have identified two: $2\nu_4$ at 942 cm^{-1} and $\nu_2+\nu_3$ at 790 cm^{-1}. (The anomalously large intensity for the $2\nu_4$ overtone has defied explanation to this day.) Butler and English[94] have recorded the (laser) Raman spectrum of thiophosgene and identified other combination bands: $\nu_5+\nu_3$ at 1123 cm^{-1}, $\nu_2+2\nu_3$ at 1089 cm^{-1}, and the previously identified $\nu_2+\nu_3$ at 781.5 cm^{-1}. These known combination bands are listed in Table III.2 along with the bands whose existence has never been verified but which are predicted simply on the basis of adding the frequencies of fundamentals. This listing of combination modes will be referred to in the discussion section.

B. Electronically Excited States

Thiophosgene's visible absorption spectrum was first recorded by Henri and Duchesne in 1939[95] but only the $^3A_2 \leftarrow {}^1A_1$, transition was assigned. Seventeen years later Burnell[96] identified three more electronic band systems: an $n \rightarrow \pi^*$ ($^1A_2 \leftarrow {}^1A_1$) between 3900 and 5700 Å, an $n \rightarrow \sigma^*$ transition localized in the C=S bond and lying in the region 2970-2690 Å and an $n \rightarrow \sigma^*$ ($^1A_1 \leftarrow {}^1A_1$) found between 2770 and 2390 Å. For the remainder of the chapter, I shall review what has been learned about the three major excited states: the two singlet states, whose separation is nearly the same as that between the first singlet and the ground state, and the triplet, located just beneath the first excited singlet. Because this latter state is the one exploited in our double resonance experiments I will discuss only this one in detail.

First Excited Singlet States ($\tilde{A}(^1A_2)$)

This symmetry species of this state (a_1) makes optical transitions between it and the electronic ground state electric dipole-forbidden. However, coupling between the electronic and vibrational degrees of freedom (Herzberg-Teller coupling) allows those vibronic transitions in which the symmetry species of the product of the vibrational and electronic wave functions for the ground state with those of the excited state is the same as that of the dipole moment operator, i.e.:

$$\Gamma(\psi''_{el}) \times \Gamma(\psi''_{vib}) \times \Gamma(\psi'_{el}) \times \Gamma(\psi'_{vib}) = \Gamma(\mu)$$

Only by including the ν_4 mode (b_1) in a vibronic transition (in such a way that the quantum change in ν_4 is odd) and by using the y dipole

moment operator (b_2) can the $\tilde{A}(^1A_2) \leftarrow \tilde{X}(^1A_1)$ transition become allowed ($a_1 x a_2 x b_2 x a_2 x a_1 = a_1$) The oscillator strength for this weak transition is 1.2×10^{-4} [96].

The first spectroscopic study of this band to result in the assignment of its vibrational structure was done by Brand et al[92]. They found all bands to degrade toward the red. The important mode in the excited state was characterized by a double well potential with a barrier that they calculated to be approximately 600 cm^{-1} and a resulting out-of-plane bend of approximately 32°. At the bottom of the double well there is only slight splitting of the first degenerate pair of vibrational states (0.2 cm^{-1}); the odd member provides a "false" origin to the electronic absorption system (4_0^1) that is less than 1 cm^{-1} away from where the true origin would be.

(Although the $^1A_2$ state is strictly of C_S symmetry it is customary to assume C_{2v} symmetry when designating vibrational states. This is acceptable in view of the low inversion barrier of the mode and the convenience in keeping the same symmetry species for the excited singlet as for the ground state when denoting transitions between the two.

From the visible absorption spectra of Brand and laser fluorescence excitation spectra of Clouthier and Moule[97] we now know four out of the five other excited state vibrational frequencies. They are listed in Table III.3 along with the frequencies of the ground state and the triplet state.

Table III.3

Vibrational Frequencies of the Three Lowest Electronic States (cm^{-1})

$\tilde{X}(^1A_1)$		$\tilde{A}(^1A_2)$		$\tilde{a}(^3A_2)$	
35/35	35/37	35/35	35/37	35/35	35/37
1139.0	1138.8	907.4	906.8	923	
503.5	499.4	480.0	476.7	474.2	
288.5	285.8	245.0	243.5	247.3	246.7
471.0	470.7	0.4	0.4	0.2	0.2
941.9	941.3	279.6	278.4	298.1	297.0
818		-		-	
305		189		-	

In 1980 Vasudev et al.[98] changed some of Brand's vibronic assignments based on rotationally cooled laser fluorescence excitation spectra. Of particular significance was their change of the identity of the band at 19440.9 cm^{-1} from $2_0^1 3_0^1 4_0^1$ to $2_0^2 3_0^1 4_0^1$ and the subsequent reassignment of the former as a shoulder at 19433.0 cm^{-1}. Their motivation for doing so was the apparent decrease in intensity of the 19440.9 cm^{-1} feature upon rotational cooling which seemed to indicate that it was a hot band. However, computer simulation by us (Fig. V.1) and by Clouthier and Birss[104] of this band demostrate that this intensity decrease is really the result of a redistribution of oscillator strength among the rotational states of the ground electronic state.

Since the $2_0^1 3_0^1 4_0^1$ absorption band is the one we used to monitor the ground state, I will comment briefly on its spectroscopy. Lombardi[105] has analyzed the absorption spectrum of this band and

extracted from it several rotational parameters for the upper state. In spite of the overlapping of the band for the 35/35 isotope with that for the 35/37 isotope and the overlapping of both with the $1_0^1 4_1^2$ band, Lombardi was able to find a region in the spectrum in which the 35/35 isotope predominated. Using a spectrum simulation program[106] he analyzed this region and deduced the following constants fpr the $^1A_2$ state:

$$A = 0.11401 \text{ cm}^{-1}$$

$$B = 0.10990 \text{ cm}^{-1}$$

$$C = 0.05631 \text{ cm}^{-1}$$

$$\Delta(=I_c-I_b-I_a) = -1.82 \text{ amu Å}^2$$

$$\kappa = 0.858$$

From these parameters he determined the C-Cl distance to be 1.745 Å, the Cl-C-Cl angle to be 112.3°, and the out-of-plane angle to be 27.2°.

The fluorescence spectra of thiophosgene excited via argon ion laser excitation of the $2_0^1 3_0^1 4_0^1$ transition has been recorded and assigned by Brand, Hardwick and Teo[107]. As predicted by intensity rules[108] and observed in the absorption spectrum, the most intense lines in the emission spectrum were those for which $\Delta J = \Delta K$ (the ^PP and ^RR subbands). Observation of the first six members of the progression $2_0^1 3_0^1 4_0^1$ supported the earlier deductions[92,105] of a pyramidal shape for the excited singlet state. Franck-Condon factors for these transitions have been determined in this thesis and are presented in Appendix A.

Quenching rates and lifetimes of the $^1A_2$ state have been studied by McDonald and Brus[109]. At pressures less than 100 mTorr and vibrational energies (above the excited singlet origin) of less than ~3400 cm^{-1} fluorescence is exponential over three lifetimes and fits a Stern-Volmer relationship[110] nicely. From a least squares fitting of the lifetime

data to a Stern-Volmer plot, McDonald and Brus determined the zero pressure lifetime to be 35±4 μsec and the quenching cross section to be 157±30 Å. The calculated lifetime is consistent with a fluorescence maximum at 750 nm and an oscillator strength of 1.2×10^{-4} [111]. At energies above 3400 cm^{-1} the fluorescence lifetime drops sharply to less than 150 nsec. The most likely mechanism responsible for this abrupt change is internal conversion or pre-dissociation into a nearby electronic state (the triplet state perhaps).

Second Excited Singlet ($\tilde{B}(^1A_1)$)

Thiophosgene, and several other thiocarbonyl compounds, belong to a very select group of molecules that do not obey Kasha's Rule[95] which states that a molecule will emit preferentially from the lowest excited state of a given multiplicity. For most molecules, radiationless processes dominate at energies associated with the upper excited electronic states so that the quantum yield of emission from them is very small. Azulene[101-103] is the best known example of a molecule which does not obey this rule. Because of its forbidden $\tilde{A}(^1A_2)\leftarrow\tilde{X}(^1A_1)$ transition, thiophosgene and its relatives are other exceptions. It is because of this molecule's unique behavior that we know as much as we do about its second singlet state.

The $\tilde{B}(^1A_1)$ is located approximately 3600 cm^{-1} (30nm) above the ground state. Because of its a_1 symmetry the electronic transition terminating at this state is allowed and has an oscillator strength of 0.1. Like the first excited singlet state, the $\tilde{B}(^1A_1)$ state is characterized by a pyramidal shape: it has an out-of-plane angle of 20°

and an inversion barrier of 126 cm^{-1} [113]. The origin is presumed to lie at 35,112 cm^{-1} [113].

Fluorescence has been observed[112] only from the states 4^0, 4^1, and 3^1. Vibrational states at higher energies than the inversion barrier do not fluoresce due to competition with radiationliess transitions. Most active in emission and absorption are vibrational modes 1,3 and 4. As with the $\tilde{A}(^1A_2) \leftarrow \tilde{X}(^1A_1)$ transition, the selection rule that only odd changes in the ν_4 mode are allowed holds for this system as well[120].

Excitation of the $B(^1A_1)$ state with radiation of wavelength less than 283 nm leads to dissociation ($Cl_2CS \rightarrow Cl\bullet + CSCl\bullet$)[113] and results in a diffuse and unresolvable absorption spectrum. The abrupt change in fluorescence quantum yield above this energy is probably due to the sharp increase in the density of background vibrational states and the large energy gap between the first two excited singlet states.

Before ending this section it is worth noting that a novel way of accessing the second singlet state has been reported by Clouthier et al.[115]. Taking advantage of the nearly equal spacing between the ground state and the first singlet and between the first singlet and second singlet states they used a pulsed dye laser to sequentially two-photon pump the B state. The possibility was raised, however, that excitation of the upper singlet may have been due to collisional "pooling" of two molecules in the S_1 state to yield one molecule in the S_2 state and one ground state molecule.

Triplet State ($\tilde{a}(^3A_2)$)

The origin of the $\tilde{a}(^3A_2)$ state is at 17,492 cm^{-1} [116]. Oscillator

strength for the spin forbidden singlet to triplet transition is borrowed from mixing of the $\tilde{B}(^1A_1)$ state with the $\tilde{a}(^3A_2)$ state so that the polarization and selection rules for this transition are the same as those for the $\tilde{B}(^1A_1)\leftarrow\tilde{X}(^1A_1)$ transition. Because of the small energy gap between the triplet and first excited singlet this intensity borrowing is particularly strong and gives rise to an unusually large oscillator strength--2×10^{-5} [116].

As with the other two excited electronic states, thiophosgene in the triplet state is in a pyramidal configuration; the inversion barrier is 726 cm^{-1} [116] and the out-of-plane angle is calculated to be 32° [116]. Reports of laser induced phosphorescence from the triplet state[117] have been proved to be in error[118]. The luminescence observed in these studies was, in fact, fluorescence from the $\tilde{A}(^1A_2)$ state.

The absorption spectrum of this state has been most successfully recorded by Clouthier and Moule[119] using magnetic rotation spectroscopy. This spectroscopic technique, which only yields a signal from a state having a magnetic moment, gave well resolved spectra which allowed the two to determine the vibrational frequencies listed in Table III.2.

IV. Theory

A. Schrödinger Formulation

In solving the equations of motion for a system interacting with a radiation field, one starts off with the time-dependent Schrödinger equation

$$i\hbar \frac{d}{dt} |\psi(t)\rangle = H|\psi(t)\rangle \qquad \text{(IV.1)}$$

in which $H = H_0 + W(t) = H_0 + \lambda W(t)$ where λ is a dimensionless ordering parameter much less than 1 and $\tilde{W}(t)$ is of the same order of magnitude as H_0.

Before we can define what each of the terms above represents, we must choose between treating the problem semiclassically or fully quantum mechanically. In the former H_0 is the unperturbed Hamiltonian for the isolated molecule, $W(t)$ is the interaction between the molecules and radiation field and $|\psi(t)\rangle$ represents the state of the molecule only. In the latter formalism H_0 is the Hamiltonian for the isolated molecule plus the isolated quantized radiation field, $W(t)$ is again the interaction Hamiltonian, and $|\psi(t)\rangle$ represents both the state of the molecule and the state of the radiation field (the latter in terms of the occupation numbers of each of the modes of the field). For a full discussion of the quantum theory of radiation, the reader is advised to read Chapter 14 of Sargent, Scully and Lamb[4]. The general process of multiphoton absorption using a fully quantum mechanical representation is very well treated by Peticolas[5]. For problems in which spontaneous emission does not need to be treated, the semiclassical approach is quite sufficient and will be used exclusively in this chapter.

To solve the time-dependent Schrödinger equation one writes it out in the orthonormal basis of the unperturbed Hamiltonian:

$$H_0|\phi_i\rangle = E_i|\phi_i\rangle \quad i = 1,\cdots,N \tag{IV.2}$$

When the state vector $|\psi(t)\rangle$ is expanded upon this basis

$$|\psi(t)\rangle = \sum_k c_k(t)|\phi_k\rangle \tag{IV.3}$$

and substituted into Eq. (IV.1) the resulting expression is[2]:

$$i\hbar \frac{dc_j(t)}{dt} = c_j(t)\ E_j + \lambda \sum_{k=1}^{N} c(t)\tilde{W}_{jk}(t) \tag{IV.4}$$

$$(\tilde{W}_{jk} = \langle\phi_j|\tilde{W}(t)|\phi_k\rangle)$$

We are thus left with a set of N coupled differential equations from which we must solve for the time-dependent coefficients of basis sets. Unfortunately, two factors make the exact solution this set of equations impossible: the time dependence of $\tilde{W}(t)$ which renders the equations nonhomogeneous and the very large number of coefficients (or equations) that need to be solved for virtually all real systems. What follows from Eq. (IV.4), then, is a series of approximations which eventually reduce the equations to a form suitable for standard algebraic or numerical techniques.

Before proceeding with these approximations we first must set the stage for the first of them by performing the transformation:

$$c_k(t) = b_k(t)e^{-iE_k/h} \qquad \text{(IV.5)}$$

This transformation is equivalent to a change from the Schrödinger representation to the interaction picture in which the state vector is given by:

$$|\psi^I(t)\rangle = e^{iW(t)t/\hbar}|\psi(0)\rangle \qquad \text{(IV.6)}$$

and the Schrödinger equation is:

$$\frac{|d\psi^I(t)\rangle}{dt} = \frac{-i}{\hbar} W(t)|\psi^I(t)\rangle \qquad \text{(IV.7)}$$

In carrying out the change of representation we are effectively removing rapid time variations of the coefficients corresponding to the Bohr frequencies by absorbing them into the coefficients themselves. This is similar, but not the same as placing the molecule in a frame that rotates with the sinusoidal perturbation; we shall use this transformation later.

Transformation (IV.5) changes (IV.4) to:

$$i\hbar\frac{db_j(t)}{dt} = \lambda \sum_{k=1} b_k(t)\, e^{i\omega_{jk}t}\tilde{W}_{jk}(t) \qquad \text{(IV.8)}$$

$$\omega_{jk} = \frac{E_j - E_k}{t}$$

Eq. (IV.8) cannot be solved exactly but, by expanding the $b_k(t)$'s in a power series in λ, we can yet carry its solution to any degree desired.

$$b_i(t) = b^{(0)}(t) + \lambda b_n(1)(t) + \lambda^2 b_n(2) + \lambda^r b_n(r)(t) + \cdots \qquad \text{(IV.9)}$$

Substitution of Eq. (IV.9) into Eq. (IV.8) and equating coefficients of λ^r on both sides gives:

$$i\hbar \frac{d}{dt} b_j^{(0)}(t) = 0 \qquad \text{(IV.10)}$$

$$i\hbar \frac{d}{dt} b_j^{(r)}(t) = \sum_k e^{i\omega_{jk}t} \tilde{W}_{kj}(t) b_k^{(r-1)}(t)$$

The zeroth and first order solutions are:

$$b_j^{(0)} = \delta_{ji} \qquad \text{(IV.11)}$$

and

$$\frac{d}{dt} b_j^{(1)}(t) = \sum_k e^{i\omega_{jk}t} \tilde{W}_{jk}(t)\delta_{ji} = e^{i\omega_{ji}t}\tilde{W}_{ji}(t) \qquad \text{(IV.12)}$$

In conventional spectroscopy one uses an incoherent light source which, because of the broad spectral width, is weak in intensity at any one given wavelength. For describing this type of interaction then, first order perturbation theory is quite sufficient. For atomic or molecular systems in which electronic or vibrational states are excited by the intense field of a laser the perturbation W(t) is no longer small (λ is not much less than one). Second order perturbation theory can be used if, as we will soon see, the intermediate state in the perturbation expression doesn't lie near a photon frequency and cause it to diverge. For atomic electronic energy levels this is usually not a problem. From the second order correction, the phenomenon of two photon transitions arises. Higher order photon transitions require correspondingly higher order perturbation theory.

If the radiation source is an infrared laser tuned to excite a nearly evenly spaced manifold of vibrational states then resonances between the field and energy level spacings will occur and one must diagonalize the full interaction Hamiltonian. This technique of course will work for all

three cases and is correct to all orders of perturbation but the lack of physical insight it imparts to the problem solver and the time and expense required to diagonalize the large matrices usually involved (N×N) for a N level system) make this technique one of last resort. However, infrared multiphoton absorption must be treated in this way.

The use of higher-order perturbation theory to describe multiphoton transitions and the use of numerical methods to describe sequential multiple-photon transitions will now be put on a mathematical base. Since the discussion of the first phenomenon is not central to the topic of this thesis, the treatment will be limited only to a formulation of 2-photon transitions. For more lengthy coverage of the theory of multiphoton transitions the reader should consult any of references[1,5,122,124].

Two-Photon Absorption

To derive an expression for the probability of a system making a two-photon transition from a state i to a state k through an intermediate state j, let us start with Eq. (IV.12). Using the dipole approximation for $W_{ij}(t)$ we get:

$$\tilde{W}_{ji}(t) = -\mu_{ji}E_0 \cos \omega t \qquad \text{(IV.13)}$$

and integrating the differential equation gives:

$$b_j^{(1)}(t) = \frac{\mu_{ji}E_0}{2\hbar}\left[\frac{e^{i(\omega_{ji}+\omega)t}-1}{i(\omega_{ji}+\omega)} + \frac{e^{i(\omega_{ji}-\omega)t}-1}{i(\omega_{ji}-\omega)}\right] \qquad \text{(IV.14a)}$$

Let us take $E_j > E_i$ so that ω_{ji} is positive. For fields close to resonance ($\omega_{ji} \simeq \omega$) we can invoke the Rotating Wave Approximation (RWA) and discard the nonresonant term in Eq. (IV.14).

$$b_j^{(1)}(t) = \frac{\mu_{ji}E_0}{2\hbar} \frac{e^{i(\omega_{ji}-\omega)t}-1}{\omega_{ji}-\omega} \qquad \text{(IV.14b)}$$

The transition probability for absorption from state i to state j is found by multiplying Eq. (IV.14) by its complex conjugate, to yield

$$P_{j\leftarrow i}^{(1)}(t) = |b_j^{(1)}(t)|^2 = \left|\frac{\Omega_{ji}}{(\omega_{ji}-\omega)}\right|^2 \sin^2(\omega_{ji}-\omega)t \qquad \text{(IV.15)}$$

This is just the expression for the absorption by a 2-level system of coherent monochromatic radiation. The square of the probability amplitude $b_j^{(1)}(t)$ gives the probability of finding the system in the upper state j and is maximum for a resonant field ($\omega_{ji}=\omega$). Note that the expression for $|b_j^{(1)}(t)|^2$ does not diverge when ω_{ji} approaches ω as we might think from looking at the denominator of Eq. (14), because the resulting probability expression approaches that of the Dirac-Delta function. The treatment of this problem is found in nearly all quantum mechanics textbooks[122].

We must carry Eq. (IV.15) to one more level of perturbation. To do so we insert Eq. (IV.15) into the right-hand side of Eq. (IV.10) and, again, invoke the dipole approximation and RWA. The resulting differential equation, when integrated, yields:

$$b_k^{(2)}(t) = \left(\frac{\Omega_{kj}\Omega_{ji}}{4}\right) \frac{e^{i(\omega_{ki}-2\omega)t}-1}{(\omega_{ki}-2\omega)(\omega_{ji}-\omega)} - \frac{e^{i(\omega_{kj}-\omega)t}-1}{(\omega_{kj}-\omega)(\omega_{ji}-\omega)} \qquad \text{(IV.16)}$$



The Libraries
Massachusetts Institute of Technology
Cambridge, Massachusetts 02139

Institute Archives and Special Collections
Room 14N-118
(617) 253-5688

There is no text material missing here.
Pages have been incorrectly numbered.

in which $E_k > E_j > E_1$ and

$$\Omega_{kj} = \frac{\mu_{kj} E_0}{2\hbar}.$$

Multiplying Eq. (IV.16) by its complex conjugate gives the desired probability of finding the system in state k:

$$P_{k \leftarrow i}(t) = \left[\frac{\Omega_{kj}\Omega_{ji}}{2(\omega_{ji}-\omega)}\right]^2 \frac{\sin^2\left(\frac{\omega_{ki}-2\omega}{2}\right)t}{(\omega_{ki}-2\omega)^2} + \frac{\sin^2\left(\frac{\omega_{kj}-\omega}{2}\right)}{(\omega_{kj}-\omega)^2}$$

$$+ \frac{\sin^2\left(\frac{\omega_{ki}-2\omega}{2}\right)t + \sin^2\left(\frac{\omega_{kj}-\omega}{2}\right)t - \sin^2\left(\frac{\omega_{ji}-\omega}{2}\right)t}{(\omega_{ki}-2\omega)(\omega_{kj}-\omega)} \Bigg] \qquad \text{(IV.17)}$$

The most serious approximation made in arriving at Eq. (IV.16) is the RWA at each of the two levels of perturbation. For a 2-level system the RWA is an excellent approximation but, for describing multiphoton transitions among states of an unequally spaced ladder, the approximation of neglecting the nonresonant contribution to the b_k's can lead to serious error. Nonetheless, the algebra is much simpler and the essential physics of 2-photon absorption can be seen if the RWA is made.

Examination of Eq. (IV.17) shows that in addition to two one-photon resonances between state k and the intermediate states j and between the initial state i and j, there is also a <u>two</u>-photon resonance between the state k and the initial state i. Furthermore, there need not be any state in resonance with the "first" photon; what Eq. (IV.17) shows, then, is the possibility of a molecule or atom absorbing 2 photons without going through a real intermediate state. The "ghost" state at energy

$E_i+h\omega$ is appropriately called a virtual intermediate state because there may be no gain in population at this energy level as excitation from state i to state k proceeds. The intermediate state j receives little population during absorption if it is far off resonance with a photon. Nevertheless, its presence is necessary to make the i→k transition go.

It appears as if conservation of energy is violated since a molecule can be excited to an energy level $jh\omega$ for which there is no energy eigenstate. However, according to the Heisenberg uncertainty principle ($\Delta E \Delta t \geq \hbar$) the uncertainty in energy can be very large if the lifetime of the virtual state is very short. In fact, one may estimate this lifetime and the time it takes a molecule to undergo a two-photon transition using the uncertainty relation. For a CO_2 laser photon of frequency 1000 cm^{-1} interacting with a molecule whose first accessible state is located at 2000 cm^{-1} above the gound state absorption of the second photon must proceed within $\sim 10^{-14}$ seconds of the first one.

Notice, in Eq. (IV.17), that there may be a state j which does involve itself in absorption even though it may never gain in population. Although our convention in deriving Eq. (IV.17) was to assume $E_k > E_j > E_i$ this was done only for mathematical convenience (to insure that ω_{ji} and ω_{kj} were positive). It is quite possible that the "intermediate" states j could lie above state k; in fact, when the upper state is a symmetry doublet, one member of the pair can serve as the real upper state to which a dipole transition can be made and the other can serve as the intermediate.

However, for the 3-level system, as the state j moves closer and closer into resonance with the first photon, the transition probability $P_{k\leftarrow i}(t)$ increases dramatically. One can show using Eq. (IV.17) that as

this gap narrows increasing amounts of population can be found in state j and stays there for a longer and longer time. Use of the uncertainty principle bears this out as well; as the real state j approaches the virtual state at energy $E_j+h\omega$, ΔE decreases and Δt, the time the system spends in the virtual state, increases. The phenomenon of increased absorption probability of state j as it moves into resonance with the light field is called resonance-enhanced multiphoton absorption. In the limit where j is exactly on resonance 100% of the population passes through the intermediate state on its way to state k and the expression, sequential multiple photon absorption, is more appropriate.

Hence, the distinction between this process and time multiphoton transition is one of degree only; the former is merely a limiting case of the latter. Nonetheless, this distinction must be kept in mind when interpreting the experimental data for thiophosgene. For this molecule it appears that infrared excitation proceeds through sequential one photon absorption.

We could apply these perturbation expressions to a multilevel system, in order to study the photophysics of an atom or molecule interacting with a coherent monochromatic light field. For dealing with realistic systems, however, in which the field is not absolutely coherent and in which interactions between the molecule (or atom) and its surroundings disrupt the molecule field interaction, the Schrödinger equation in the form of Eq. (IV.8) is no longer applicable. To be more specific, Eq. (IV.8) is applicable for a single molecule or atom interacting with a radiation field. As soon as we start to deal with an ensemble of molecules interacting with each other we must add to the perturbing

Hamiltonian W(t) interactions, such as dipole-dipole interactions or van der Waals forces. This becomes totally intractable for a system having more than two molecules so that for describing real samples of molecules an alternative approach must be used.

The solution to this problem is to invoke the density matrix formalism and to treat molecular interactions phenomenologically as collisions affecting the density matrix elements on two levels. The Schrödinger equation (IV.8) is recast into the corresponding density matrix equation and the collisional terms are simply "tacked" on. The resulting equations are considerably more difficult to solve, even with first order perturbation theory, but fortunately we can turn to numerical techniques for their solution. These allow very large systems to be studied and an exact calculation to be performed free of the approximations introduced with perturbation theory (but inexact insofar as certain other approximations, such as the RWA, are made).

B. Density Matrix Formulation

The density matrix operator $\underset{\sim}{\rho}$ is defined as

$$\underset{\sim}{\rho} = |\psi\rangle\langle\psi| \tag{IV.18}$$

where $|\psi\rangle$ is the state vector which can be expanded on the eigenstates the unperturbed Hamiltonian (Eq. I.2).:

$$|\psi\rangle = \sum_i c_i(t)|\phi_i\rangle \tag{IV.19}$$

In this basis the matrix elements of $\underset{\sim}{\rho}$ are:

$$\rho_{ij} = \langle\phi_i|\psi\rangle\langle\psi|\phi_j\rangle = c_i c_j^* \tag{IV.20}$$

and the time derivative of ρ_{ij} is:

$$\frac{\partial \rho_{ij}}{\partial t} = c_i \frac{\partial c_j^*}{\partial t} + c_j \frac{\partial c_j^*}{\partial t} \tag{IV.21}$$

We know the time derivatives of the coefficients c_i from the Schrödinger equation (IV.4)

$$i\hbar \frac{\partial c_i}{\partial t} = \sum_j c_i H_{ij} \quad (H=H_0+\lambda W(t)) \tag{IV.22}$$

Substituting (IV.22) into (IV.21) and using the definition of ρ_{ij} (Eq. (IV.20)), yields:

$$\frac{\partial \rho_{ij}}{\partial t} = \frac{i}{\hbar} \sum_j [\rho_{ik}H_{kj}-\rho_{kj}H_{ik}] = \frac{i}{\hbar} [(\rho H)_{ij}-(H\rho)_{ij}] \tag{IV.23}$$

Finally, expressing Eq. (IV.23) in matrix notation we get:

$$\partial \underset{\sim}{\rho}/\partial t = \frac{i}{\hbar} [\underset{\sim}{\rho}, H] \tag{IV.24}$$

The diagonal density matrix element, ρ_{ii}, is the populations at level

normalized to unity. For a 2-level system the real part of the off-diagonal density matrix element, ρ_{ij}, is proportional to the ensemble averaged dipole moment, i.e.

$$\langle \mu_{ab} \rangle = Tr(\rho\mu) = 2\mu_{ab} \; Re(\rho_{ab}) \qquad \text{(IV.25)}$$

For a multilevel system the ρ_{ij}'s are not as simply related. In general, one calls them the coherences as they represent the phase relationship between the basis states. A collision can affect the molecule in one of two ways: It can induce transitions between energy levels or it can leave the molecule in the same state and just disrupt the phase between the molecule and the field. The first is incorporated into the density master equation (IV.24) by adding a loss term to the diagonal elements and the second by adding a loss term to the off-diagonal elements. Effect of unimolecular decay out of the levels on $\partial\rho/\partial t$ can also be incorporated. Using the notation of Goodman, Stone and Thiele[128]. Eq. (IV.24) becomes:

$$\frac{\partial \underset{\sim}{\rho}}{\partial t} = \frac{i}{\hbar}[\underset{\sim}{\rho}, \underset{\sim}{H}] + \frac{1}{\tau} \underset{\approx}{K}\underset{\sim}{\rho} - \frac{1}{\tau} \underset{i=0}{\underset{\sim}{\rho}} - \frac{1}{\hbar} \sum_{i=1}^{N-1} \frac{\Gamma_i}{2}(\underset{\sim}{\rho}\underset{\sim}{P_i} + \underset{\sim}{P_i}\underset{\sim}{\rho}) \qquad \text{(IV.26)}$$

where:

$\frac{1}{\tau}$ is the collision frequency

$\underset{\approx}{K}$ is a superoperator describing state changing collisions

$\underset{\sim}{P_i}$ is the projection operator onto the state $|\psi\rangle$

Γ_i is the unimolecular decay constant for the ith level

Let us now derive explicit expressions for the matrix elements of Eq. (IV.26) in the $|\phi_n\rangle$ basis. For now we shall consider the case

of a harmonic oscillator since this is the system with which we will model thiophosgene. Including anharmonicity to first order is trivial and will be done later.

In the harmonic oscillator basis, the matrix elements of Eq. (II.9) are

$$H_{nm} = [\underset{\sim}{H}_0+\underset{\sim}{W}(t)]_{nm} = \delta_{nm}\, nh\omega + \delta_{m,n\pm1}\, \mu_{nm}\, E_0 \cos \chi t \tag{IV.27}$$

where $h\omega$ is the harmonic oscillator spacing, and the dipole approximation again is invoked for the second term of (IV.27).

$$(K\rho)_{nm} = \delta_{nm} \sum_{i=0}^{N} P_{n\leftarrow i}\rho_{ii} \tag{IV.28}$$

$$(P_i)_{nm} = \delta_{nm}(P_i)_{nm} = (P_i)_{nn}\delta_{in} = \rho_{nn}\delta_{nm} \tag{IV.29}$$

In writing out Eq. (IV.28) the strong collision limit is assumed, i.e. the collision is considered to be instantaneous and to cause a correspondingly instantaneous energy transition.

Let us first write out the molecule-radiation interaction term:

$$[\underset{\sim}{\rho},\underset{\sim}{H}]_{nm} = \sum_k [\rho_{nk}H_{km}-H_{nk}\rho_{km}] \quad 0\leq n,\ m\leq N-1$$

$$= \rho_{n,m+1}H_{m+1,m} + \rho_{n,m-1}H_{m-1,m} - H_{n,n+1}\rho_{n+1,m} - H_{n,n-1}\rho_{n-1,m}$$

$$+ \rho_{nm}H_{mm} - H_{nn}\rho_{nm} \tag{IV.30}$$

$$= - [\rho_{n,m+1}\mu_{m+1,m} + \rho_{n,m-1}\mu_{m,m-1} - \rho_{n+1,m}\mu_{n+1,n} - \rho_{n-1,m}\mu_{n,n-1}] E_0 \cos xt$$

$$+ \rho_{nm}(m-n)\hbar\omega \qquad \text{(IV.31)}$$

in which use has been made of the fact that:

$$\mu_{nm} = \mu_{mn}$$

Substituting Eq. (IV.31) into (IV.24) and writing cos χt as a sum of exponentials we get:

$$\left(\frac{\partial \rho_{nm}}{\partial t}\right)_{rad} = i\omega(m-n)\rho_{nm} - \frac{iE}{2\hbar} (e^{i\chi t}+e^{-i\chi t})$$

$$\times[\rho_{n,m+1}\mu_{m+1,m} + \rho_{n,m-1}\mu_{m,m-1} - \rho_{n+1,m}\mu_{n+1,n} - \rho_{n-1,m}\mu_{n,n-1}]$$

$$= i\omega(m-n)\rho_{nm} - i(e^{ixt} + e^{-ixt})\Omega_m\rho_{n,m-1} + \Omega_{m+1}\rho_{n,m+1}$$

$$- \Omega_{n+1}\rho_{n+1,m} - \Omega_n\rho_{n-1,m}] \qquad \text{(IV.32)}$$

where Ω_n is the Rabi frequency for the n-1→n transition (with the n-1 subscript being understood).

Let us now write out the collisional relaxation terms. By definition (Goodman, Stone and Thiele[128]) the first such term represents vibrational relaxation and is written as:

$$\left(\frac{1}{\tau} k\rho\right)_{nm} = \frac{1}{\tau} \sum_{i=0}^{N=1} P_{n\leftarrow i}\rho_{ii}\delta_{nm} \qquad \text{(IV.33)}$$

$P_{n\leftarrow i}$ represents the probability that, upon collision, an oscillator in state i will make a transition to state n. In this formalism the colliding partner is a monoatomic gas that serves as a heat bath into which the oscillator vibrationally relaxes. Since this type of collision term causes a shift in population among energy levels, it can affect the density matrix only through the latter's diagonal matrix elements. This process does not conserve energy <u>within</u> the harmonic oscillator ladder, although the missing energy is taken up by the heat bath.

The other collision term in Eq. (IV.26) represents an elastic collision in which the phase between the dipole moment and the field is temporarily disrupted, and is commonly referred to as T_2-type relaxation (or T_2'-type relaxation to distinguish it from V→V relaxation). It is written out as:

$$-\frac{1}{\tau}\rho_{nm}(1-\delta_{nm}) \qquad \text{(IV.34)}$$

in which the term in parenthesis insures that only the off-diagonal density matrix elements are affected.

The last terms on the right-hand side of Eq. (IV.26) represent unimolecular decay out of the harmonic oscillator ladder; this term conserves neither population nor energy. In actual molecules it can represent dissociation of highly excited molecules or it can represent V→V relaxation from a state in the pumped mode to one in a nonpumped mode. It is written as:

$$-\frac{1}{2\hbar}\sum_{i=0}^{N-1}[\Gamma_i(\rho P_i+P_i\rho)]_{nm} = -\frac{1}{2\hbar}\sum_{i=0}^{N-1}[\Gamma_i(\rho P_i)_{nm}] - \frac{1}{2\hbar}\sum_{i=0}^{N-1}[\Gamma_i(P_i\rho)_{nm}]$$

$$= -\frac{1}{2\hbar}\sum_{i=0}^{N-1}\Gamma_i\sum_k \rho_{nk}(P_i)_{km} - \frac{1}{2\hbar}\sum_{i=0}^{N-1}\Gamma_i\sum_k (P_i)_{nk}\rho_{km}$$

(where P_i, the projection operator onto state i: $(P_i = |u_i\rangle\langle u_i|)$:

$$((P_i)_{km} = \delta_{mi}\delta_{ik})$$

$$= -\frac{1}{2\hbar}\Gamma_m\rho_{nm} - \frac{1}{2\hbar}\Gamma_n\rho_{nm} = \frac{\Gamma_n+\Gamma_m}{2\hbar}\rho_{nm} \qquad \text{(IV.35)}$$

Notice that unimolecular decay affects not only the diagonal matrix elements but also the off-diagonal elements.

Combining all the separate contributions to Eq. (IV.26) gives the final equation of motion in component form:

$$\frac{\partial\rho_{nm}}{\partial t} = i\omega(m-n)\rho_{nm} - i(e^{i\chi t}+e^{-i\chi t})(\Omega_m\rho_{n,m-1} + \Omega_{m+1}\rho_{n,m+1}$$

$$- \Omega_n\rho_{n-1,m} - \Omega_{n+1}\rho_{n+1,m} + \frac{1}{\tau}\sum_i P_{n\leftarrow i}\rho_{ii}\delta_{nm} - \frac{1}{\tau}\rho_{nm}$$

$$- \frac{\Gamma_n+\Gamma_m}{2\hbar}\rho_{nm} \qquad \text{(IV.36)}$$

Unfortunately, the time dependence of the light field makes this set of coupled differential equations impossible to solve analytically. As

we did in the preceding Schrödinger equation treatment, we shall make a transformation of variables:

$$\psi_n = a_n \, e^{-in\chi t} \tag{IV.37}$$

Notice that this is not quite the same as Eq. (IV.5). There, the result of the transformation was that the system rotated at its Bohr frequency ($\omega_k = E_k/\hbar$) and was therefore equivalent to the interaction representation. Here the transformation results in the system rotating with the light field frequency, χ, and is equivalent to the "dressed-atom" formalism or rotating frame transformation.

The density matrix elements are now rewritten as:

$$\rho_{nm}(t) = c_n(t)c_m^*(t) = a_n(t)a_m^*(t) \, e^{i(m-n)\chi t} \equiv a_{nm} \, e^{i(m-n)\chi t} \tag{IV.38}$$

Let us substitute Eq. (II.19) into Eq. (II.17) and discard all terms that go as $e^{\pm 2i\chi t}$ (RWA):

$$\frac{\partial \rho_{nm}}{\partial t} = i(m-n)\chi e^{i(m-n)\chi t} \, a_{nm} + \frac{\partial a_{nm}}{\partial t} \, e^{i(m-n)\chi t}$$

$$= i(m-n)\omega a_{nm} e^{i(m-n)\chi t}$$

$$- \frac{i}{2} \left[\Omega_m a_{n,m-1} + \Omega_{m+1} a_{n,m+1} - \Omega_n a_{n-1,m} - \Omega_{n+1} a_{n+1,m}\right] e^{i(m-n)\chi t}$$

$$+ \frac{1}{\tau} \sum_{i=0}^{N-1} P_{n+i} a_{ii} \delta_{nm} - \frac{1}{\tau} a_{nm}(i-\delta_{nm}) e^{i(m-n)\chi t} - \frac{\Gamma_m + \Gamma_m}{2\hbar} \, a_{nm}$$

(IV.39)

which rearranges to:

$$\frac{\partial a_{nm}}{\partial t} = \left[i(m-n)(\omega-\chi) - \frac{\Gamma_n+\Gamma_m}{2\hbar} - \frac{1}{\tau}(1-\delta_{nm})\right] a_{nm}$$

$$- \frac{i}{2}\left[\Omega_m a_{n,m-1} + \Omega_{m+1} a_{n,m+1} - \Omega_n a_{n-1,m} - \Omega_{n+1} a_{n+1,m}\right]$$

$$+ \frac{1}{\tau} \sum_{i=0}^{N-1} P_{n+i} a_{ii} \delta_{nm} \qquad \text{(IV.40)}$$

As a result of the rotating frame transformation and rotating wave approximation, we are left with a set of coupled differential equations with constant coefficients. The removal of the time dependence allows us to write (IV.40) in matrix form:

$$\frac{d\underset{\approx}{a}(t)}{dt} = \underset{\approx}{R}\,\underset{\approx}{a}(t) \qquad \text{(IV.41)}$$

in which $\underset{\approx}{R}$ is a time independent matrix. The following short proof shows how such an eigenvalue equation can be solved using matrix techniques:

Let the diagonal eigenvalues matrix of $\underset{\approx}{R}$ be $\underset{\approx}{\lambda}$ and the eigenvector matrix of $\underset{\approx}{R}$ be $\underset{\approx}{V}$:

$$\underset{\approx\approx}{RV} = \underset{\approx\approx}{V\lambda} \rightarrow \underset{\approx}{R} = \underset{\approx\approx\approx}{V\lambda V^{-1}} \qquad \text{(IV.42)}$$

Substitute this back into Eq. (II.22)§

$$\frac{d\underset{\approx}{a}(t)}{dt} = \underset{\approx\approx\approx}{V\lambda V^{-1}}\,\underset{\approx}{a}(t) \qquad \text{(IV.43)}$$

Let us define the matrix $\underset{\approx}{\phi}$ as:

$$\underset{\approx}{\phi} \equiv \underset{\approx}{V}^{-1} \underset{\approx}{a}(t) \tag{IV.44}$$

and insert this into Eq. (IV.43)

$$\frac{d\underset{\approx}{a}}{dt} = \underset{\approx}{V}\underset{\approx}{\lambda}\underset{\approx}{\phi} \rightarrow \underset{\approx}{\lambda}\underset{\approx}{\phi} = \underset{\approx}{V}^{-1}\frac{d\underset{\approx}{a}}{dt} = \frac{d}{dt}(\underset{\approx}{V}^{-1}\underset{\approx}{a}) = \frac{d\underset{\approx}{\phi}}{dt}$$

which has the solution

$$\underset{\approx}{\phi}(t) = \underset{\approx}{\phi}(0)e^{\underset{\approx}{\lambda}t} \tag{IV.45}$$

Substituting Eq. (IV.44) into Eq. (IV.45) finally yields:

$$\underset{\approx}{V}^{-1}\underset{\approx}{a}(t) = e^{\underset{\approx}{\lambda}t}\underset{\approx}{V}^{-1}\underset{\approx}{a}(0)$$

$$\underset{\approx}{a}(t) = \underset{\approx}{V}e^{\underset{\approx}{\lambda}t}\underset{\approx}{V}^{-1}\underset{\approx}{a}(0), \text{ Q.E.D.} \tag{IV.46}$$

where $\underset{\approx}{a}(0)$ is the density matrix at time zero.

Thus all we need to do is diagonalize the coefficient matrix, $\underset{\approx}{R}$, invert the resulting eigenvector matrix and carry out the matrix multiplication indicated in Eq. (IV.46) and all the information about the system will be known. With the use of standard matrix manipulation routines available with most large computers (e.g. the International Mathematical and Scientific Library) the solution of Eq. (IV.46) is quite easy.

As a simple illustration of the density matrix formalism, let us use it to solve the equations of motion for a 2-level system analytically and then show how the same problem would be set up for numerical solution by a computer.

The 2-level system we will model is characterized by a Rabi frequency Ω, and a decay rate from the top level Γ. Using Eq. (IV.40), we write out the equations of motion for the four density matrix elements.

$$\frac{\partial a_{00}}{\partial t} = -\frac{i}{2}\Omega[a_{01}-a_{10}] + \frac{1}{\tau}P_{0\leftarrow 1}a_{11} - \frac{1}{\tau}P_{1\leftarrow 0}a_{00} \qquad \text{(IV.47)}$$

$$\frac{\partial a_{01}}{\partial t} = \left[\, i(\omega-\chi) - \frac{\Gamma}{2\hbar} - \frac{1}{\tau}\right] a_{01} - \frac{i\Omega}{2}[a_{00}-a_{11}] \qquad \text{(IV.48)}$$

$$\frac{\partial a_{10}}{\partial t} = \frac{\partial a_{01}^{*}}{\partial t} = [-i(\omega-\chi) - \frac{\Gamma}{2\hbar} - \frac{1}{\tau}\,]\, a_{10} - \frac{i\Omega}{2}[a_{11}-a_{00}] \qquad \text{(IV.49)}$$

$$\frac{\partial a_{11}}{\partial t} = -\frac{\Gamma}{\hbar}a_{11} - \frac{i\Omega}{2}[a_{10}-a_{01}] + \frac{1}{\tau}P_{1\leftarrow 0}a_{00} - \frac{1}{\tau}P_{0\leftarrow 1}a_{11} \qquad \text{(IV.50)}$$

Exact solutions to the 2-level system can be found in Goodman, Stone and Thiele[125,126]. For now let us solve the set of equations (IV.47-IV.50) at "quasi-equilibrium" i.e. after fast transients occurring on the timescale of τ have damped out oscillations in the populations. True equilibrium, $\partial a_{ii}/\partial t = 0$, would not be attained until all population had left the system via top level decay. What we are interested in is equilibrium defined by the condition that the time derivatives of the off-diagonal matrix elements equal zero:

$$\left(\frac{\partial a_{01}}{\partial t}\right)_{ss} = 0 = [i(\omega-\chi) - \frac{\Gamma}{2\hbar} - \frac{1}{\tau}\,]\, a_{01}^{ss} - \frac{i\Omega}{2}\,(a_{00}^{ss}-a_{11}^{ss}) \qquad \text{(IV.51)}$$

where the subscript ss signifies steady state. (It is not necessary to solve for Eq. (IV.49) since it is just the complex conjugate of IV.42.)

$$a_{01}^{ss} = \frac{\frac{i\Omega}{2}\ (a_{00}^{ss}-a_{11}^{ss})}{i(\omega-\chi)-\frac{\Gamma}{2\hbar}-\frac{1}{\tau}} = \frac{\Omega}{2}\ (a_{00}^{ss}-a_{11}^{ss})\ \frac{(\omega-\chi)^2-i(1/\tau+\Gamma/2\hbar)}{(\frac{1}{\tau}+\frac{\Gamma}{2\hbar})^2\ (\omega-\chi)^2} \qquad \text{(IV.52)}$$

$$a_{01}^{ss}-a_{10}^{ss} = i\Omega(a_{11}^{ss}-a_{00}^{ss})\ \frac{(\frac{1}{\tau}+\frac{\Gamma}{2\hbar})}{(\frac{1}{\tau}+\frac{\Gamma}{2\hbar})^2+(\omega-\chi)^2} \qquad \text{(IV.54)}$$

$$\frac{\partial P_0}{\partial t}\Big|_{ss} = \frac{\Omega^2}{2}\ (P_1^{ss}-P_0^{ss})\ \frac{(\frac{1}{\tau}+\frac{\Gamma}{2\hbar})}{(\frac{1}{\tau}+\frac{\Gamma}{2\hbar})^2+(\omega-\chi)^2} + \frac{1}{\tau}P_{0\leftarrow1}a_{11}^{ss} - \frac{1}{\tau}P_{1\leftarrow0}a_{00}^{ss} \qquad \text{(IV.55)}$$

where $a_i^{ss} = P_i^{ss}$ (population of level i).

In the absence of unimolecular decay the two right-hand terms in equation (IV.55) can be rewritten as

$$\frac{1}{\tau}(P_{0\leftarrow1}+P_{1\leftarrow0})(P_0{}^0-P_0)$$

where $(P_0{}^0)$ is the ambient ground state population in the absence of radiation.

Since the rate of photon absorption for a 2-level system is equal to the <u>negative</u> of the rate of population change out of the ground state,

Eq.(IV.55) is also proportional to the (incoherent) absorption rate by a 2-level system (Notice that $p^{ss}_1 < p^{ss}_0$ so that the ground state population change is negative and the absorption rate is positive as it should be):

$$P_{net} = \hbar\omega \frac{\Omega^2}{2} (p^{ss}_0 - p^{ss}_1) \frac{(\frac{1}{\tau} + \frac{\Gamma}{2\hbar})}{(\frac{1}{\tau} + \frac{\Gamma}{2\hbar})^2 + (\omega - x)^2} + \frac{1}{\tau} P_{0\leftarrow 1} a^{ss}_{11} - \frac{1}{\tau} P_{1\leftarrow 0} a^{ss}_{00} \quad \text{(IV.56)}$$

Eq. (IV.56) is identical to the expression for the pressure broadened width of 2 level absorption, i.e. absorption in the limit in which $1/\tau >> \Omega$.

Two points are in order. First, Eq. (IV.55) is a rate equation in which the dependent variable (p^{ss}_i) appears on both sides of the equation. The problem has been solved only to first order with the assumption that the populations are constant (the same assumption that was used in the first order perturbation result in the Schrödinger equation development

of multiphoton absorption). To obtain the second order solution to photon absorption one would have to solve Eq. (IV. 55) for the $P^{SS}{}_i$'s, reinsert it back into Eq. IV.48 and solve it for the off-diagonal matrix elements, and reinsert the solutions into Eqns. (IV.47) and (IV.50). Secondly, $1/\tau$ is ambiguously defined as the collision frequency. It may be equated to the dephasing rate $1/T_2$ which is often much faster than the hard sphere collision frequency and, hence, is not necessarily equal to the latter. Whatever deviation of $1/\tau$ from the gas kinetic rate is, it does not affect the V→T relaxation rates, $1/\tau(P_{i\leftarrow j})$, since the $P_{i\leftarrow j}$'s can always be adjusted to force agreement with the known rate.

The coefficient matrix, R, defined in (IV.41) is:

$$\frac{\partial}{\partial t}\begin{bmatrix} a_{00} \\ a_{01} \\ a_{10} \\ a_{11} \end{bmatrix} = \begin{bmatrix} -\frac{1}{\tau}P_{1\leftarrow 0} & -\frac{i\Omega}{2} & \frac{i\Omega}{2} & \frac{1}{\tau}P_{0\leftarrow 1} \\ -\frac{i\Omega}{2} & i(\omega-x)-\frac{\Gamma}{2\hbar}-\frac{1}{\tau} & 0 & \frac{i\Omega}{2} \\ -\frac{i\Omega}{2} & 0 & -i(\omega-x)-\frac{\Gamma}{2\hbar}-\frac{1}{\tau} & -\frac{i\Omega}{2} \\ \frac{1}{\tau}P_{1\leftarrow 0} & +\frac{i\Omega}{2} & -\frac{i\Omega}{2} & -\frac{\Gamma}{2\hbar}-\frac{1}{\tau} \end{bmatrix} \begin{bmatrix} a_{00} \\ a_{01} \\ a_{10} \\ a_{11} \end{bmatrix}$$

The matrix $\underset{\approx}{R}$ is symmetric complex but not Hermitian. Once the eigenvectors and eigenvalues of $\underset{\approx}{R}$ have been determined and the inverse of the eigenvector matrix has been found, Eq. IV.46) can be called on to calculate the time dependent density matrix elements. Ordinarily one would only be concerned with the time development of the populations, a_{00} and a_{11}.

For a 3-level system carrying out the algebra shown above explicitly reveals the same two photon resonances resulting from the Schrödinger equation solution done earlier. We must resort to computer solution of the matrix equation (IV.41) for a system of more than 3 levels. In the next chapter I shall discuss the choice of the parameters used in Eq. (IV.40) to model thiophosgene's response to an infrared field.

B. Density Matrix Solution: Computer Model

Numerical solution of the density matrix equations for a general N-level system was accomplished with a computer program (Copath) whose prototype version was loaned to us by Harold Galbraith and Jay Ackerhalt of Los Alamos National Laboratory. This version was extensively modified to allow simulation of a rovibrational ladder interacting with a monochromatic infrared field and undergoing phase-changing and state-changing collisions. A listing of the program can be found in Appendix B.

In Table (IV.I) the reader will find a tabulation of the input parameters that are read into the computer each time Copath is run. In this discussion of the computer model, the following must be remembered: Knowledge of all the parameters listed in Table (IV.1) would permit us to reproduce quantitatively thiophosgene's observed behavior when it is irradiated with a coherent infrared field. However, our very incomplete understanding of this molecule's spectroscopy allows us to use the model only to gain qualitative understanding of the IRMPA dynamics, i.e. to enable us to reject or accept hypotheses on the basis of the range of values of the parameters needed to make the model work.

Table IV. 1. Input Parameters to Copath

Parameter	Algebraic/Computer Symbol	Value(s) used
Molecular Properties		
Number of levels	N	5
Harmonic oscillator Frequency	ω_0/WO	944 cm^{-1}
Anharmonicity	x_{pp}/XPP	0-1 cm^{-1}
Rotational energy Increment	E_{rot}/EROT(I)	0-1 cm^{-1}
Unimolecular decay Rate	r/UNI(I)	0-10^{12} sec^{-1}
Properties of the Light Field		
Laser frequency	ω_L/WL	942 cm^{-1}
Laser pulse duration	τ_L/TIMLZR	200 nsec
		10-2000 nsec*
Laser dephasing rate	$1/T_2$(LASER)/T2LZR	0-$10^9$$sec^{-1}$
Rabi frequency	ω_R/RABI	10^{-4}-$10^{-2}$$cm^{-1}$
Collision Parameters		
Pure dephasing rate	$(1/T_2)_{ij}$/T2(I,J)	0-$10^{12}$$sec^{-1}$$Torr^{-1}$
Vibrational relaxation		
Rate	$1/T_1(i\leftarrow j)$/T1(I,J)	0-10^{12} $sec^{-1}$$Torr^{-1}$
Pressure	p/PRES	1-200 mTorr
Temperature	T/TEMP	298 K

*In pulse shape convolution

For the remainder of the chapter, I will discuss the reasoning behind the choice of the input parameters and describe qualitatively how the program works.

The number of oscillator levels (N) chosen should, ideally, be very large (>10). However, the density matrix equations of motion produce an $N^2 \times N^2$ matrix that must be diagonalized (as opposed to an N×N matrix the Schrödinger equation yields). For values of N greater than 5, the computer cost of solving the equations becomes prohibitively expensive. Since the low-density-of-states region of a molecule generally persists for less than 10 vibrational quanta before the quasicontinuum sets in, no more than that many levels, with the appropriate relaxation rates included at each level, need be chosen. Furthermore we have convinced ourselves that the results achieved with a 5-level system do not differ enough from results obtained with larger systems to warrant using the latter.

The parameter to which the density matrix equations are most sensitive is the frequency mismatch (the "detuning" between the light field and each of the rovibrational transitions the molecule makes). Minute changes in Δ can produce drastic changes in the pumping efficiency. In actual molecules, pumping at a single frequency causes the simultaneous excitation of many ladders, with each such ladder having its own set of detunings. For a perfectly coherent light source and in the absence of dephasing collisions, each of these individual systems would "Rabi oscillate" up and down the ladder at a frequency determined by the energy mismatches. For a system responding to a somewhat incoherent field or suffering phase changing collisions, the interaction

between the molecule and the radiation field can no longer be described by Rabi oscillations, but is more correctly referred to by a rate of absorption which is also controlled by the set of detunings[127] for each ladder.

Since we do not know the different excitation pathways for thiophosgene at any CO_2 laser wavelength and, hence, do not know the detunings to input into the computer model, we have studied the behavior of several prototypical ladders undergoing absorption--each with a different set of detunings. Some ladders, for instance, have no rotational energy increments added to the anharmonic oscillator levels and, accordingly, have the largest detunings and slowest pumping rates. Others have the appropriate increments added to make them completely resonant with the field and, as a result, are pumped up the ladder the fastest. All others in this series of simulations are intermediate between these two cases and some of these have resonances (or near resonances) at various transitions. A sample calculation using various sets of detunings can be found in Fig. VII.5 and in the companion paper to this thesis (Appendix D).

The unimolecular decay rate represents a sum of two different physical processes. It may contain contributions from actual unimolecular reaction (dissociation) or from V→V relaxation into isoenergetic nonpumped vibrational modes. In accordance with the bi-directional nature of vibrational energy transfer the latter should strictly be incorporated into the model via a gain term, in addition to a loss term, at each level in the ladder. However, as I will describe at the end of this chapter, this would involve the considerable complication of adding a second ladder representing the nonpumped states and having "in" and "out" rates connecting both systems at every level. Moreover,

once the density of background states, is much greater than the intramolecular coupling between the pumped mode ladder and background states relaxation can be considered to occur irreversibly and can be described with unidirectional rates. Letting all the relaxation rates be unidirectional causes some unwanted loss of population but, since we are not concerned with the fine details of the pumping process, this is not detrimental to our goals. In the model calculations only Γ for the top level (Γ_5) is nonzero. Adding relaxation terms to the four other levels does not change the final results appreciably and is not warranted in view of the lack of experimentally determined parameters. The relative insensitivity to the choice of the top level Γ of the ground state depopulation is demonstrated in Fig. VII.3 in which Γ_5 is varied by three orders of magnitude and the corresponding ground state depletion vs. pressure curves are calculated.

The excitation frequency chosen for all of the simulations is 944 cm^{-1}. Whether or not thiophosgene's pumped mode, at this frequency, is $2\nu_4$ (as was initially believed) will be elaborated upon and will be the subject for a more extensive discussion in the final chapter.

Copath can be run in two different modes corresponding to the shape of the laser pulse desired. In the simplest--and most frequently used--version, the laser pulse is approximated by a rectangular pulse with a duration of 200 nsec and a Rabi frequency that varies from 10^{-4} to 0.02 cm^{-1}. (The electric field is fed into the program as a Rabi frequency rather than as an actual field since the two are proportional and since the former is of interest when comparing thiophosgene with other molecules.) The choice of ω_R and τ_L are dictated by the constraint

that the pulse amplitude (ω_R) integrated over the pulse duration gives the same value as the actual CO_2 laser pulse (shown in Fig. V4).

If a more accurate representation of the laser pulse is desired, the second mode of operation may be used. In this version the pulse is approximated by a series of rectangular pulses. The program is run through several iterations with each iteration using a rectangular pulse that represents one time "slice" of the real pulse shape. The initial density matrix ($\underset{\sim}{\rho}(0)$ is changed at each run to correspond to the population resulting from the previous run. The accuracy of this procedure is limited only by the (computer) expense of breaking the pulse up into smaller and smaller intervals. No matter how the pulse is represented, however, the integrated pulse area must always be equal to the same value.

To describe the partial incoherence that is inherent in all CO_2 laser pulses the single parameter $1/T_2$(laser) is used. Goodman, Stone and Thiele[126] have shown that, although phase randomization of the field is fundamentally different from collisional randomization, the two broadening rates can be summed together to give one overall rate. This prescription is used in the computer code. One can estimate the dephasing rate of the laser by measuring the width of the individual spikes of the pulse (Fig.V.4). This crude measurement Fourier limits the coherence time and, hence, gives a lower bound to the dephasing rate. For our laser the coherence time is estimated to be >10 nsec. For computer simulations in which the Rabi frequency is equal to 0.02 cm^{-1}, any reasonable laser dephasing rate has a negligible effect on the final population distribution. However for simulations using a Rabi frequency

of less than 0.01 cm^{-1}, the choice of $1/T_2$ (laser) significantly affects the population distribution through its broadening effect. For this reason many of the pressure dependence calculations were done with a dephasing rate of zero. Since this rate is added with the pressure broadening coefficient, determining the effect of a nonzero $1/T_2$(laser) is trivial.

The Rabi frequency for pumping of the $2\nu_4$ mode with a 100 mJ pulse (0.02 cm^{-1}) was calculated from an FTIR spectrum of the transition, recorded here at MIT and calibrated in absorptivity. The transition moment rigorously should be that for a rovibrational transition, i.e. it should be the product of a vibrational moment and a direction cosine matrix element[108] the (Hönl-London factor for a symmetric top). From the spectral simulation of the $2\nu_4 \leftarrow 0$ transition we can determine the rotational intensity factors. Doing so for the rovibrational transitions pumped within a power broadened width of the excitation frequency (944 cm^{-1}) gives their values as being close to unity. Hence we chose to neglect their contribution to the overall Rabi frequency and let ω_R be the same even when different excitation pathways were studied.

The initial supposition that the mode doing most of the ground state absorption at 944 cm^{-1} is $2\nu_4$ turns out, under careful reasoning, not necessarily to be true. Certainly those transitions lying within 0.02 cm^{-1} of this frequency can be expected to be "activated" but these transitions will deplete only a tiny fraction of all rotational ground states (Fig.IV.1) and (in anticipation of the results of our experiments) will not account for the depletion of all (or most) of these

states. For this reason the possibility that other (weak) modes are absorbing infrared laser radiation at 944 cm^{-1} is investigated by carrying out some calculations in which the oscillator strength is much weaker than that of the $2\nu_4 \leftarrow 0$ transition (0.02 cm^{-1}). Only these are displayed in the thesis (Chapter VII). Computer simulations done with a 0.02 cm^{-1} Rabi frequency are shown and discussed in detail, in the companion article to this thesis (Appendix D). As the discussion shall attempt to demonstrate, this possibility provides a very likely explanation for the IR-VIS-DR data so that the use of very small Rabi frequencies is justifiable.

When running the density matrix solution program one needs to input only the Rabi frequency for the first ($0 \rightarrow 1$) transition. The computer code ignores the rotational contribution to line strengths and assumes a harmonic oscillator basis set for the vibrational states. The Rabi frequencies for the higher transitions are automatically computed from the harmonic oscillator expression:

$$\omega_R(n+1 \leftarrow n) = \sqrt{n+1}\ \omega_R(1 \leftarrow 0) \qquad \text{(IV.50)}$$

The relationship between gas pressure and dephasing width is a linear one so that the collision induced dephasing rate ($(1/T_2)_{ij}$) is accepted into the data file as a pressure coefficient ($sec^{-1}mTorr^{-1}$). For testing the hypothesis that the observed pressure dependence of the ground state depletion is due to collisional dephasing the program is run with a trial value for the pressure coefficient for a range of pressure values. The computer output is then plotted in the form of a ground state depopulation vs. pressure curve and is compared with the experimental

results. The coefficient is then varied and the program run again and, hopefully, a better fit between theory and experiment is obtained. This iterative procedure is repeated until satisfactory agreement is obtained.

Rotational relaxation is incorporated into the computer model in exactly the same manner as pure dephasing, so that both collisional phenomena are referred to by the single term--pressure broadening. This is, of course, a simplification--in order to correctly incorporate rotational relaxation into the model we would have to do the following: We would set up several pumped mode ladders, each having the same vibrational level. All of the systems would interact with the light field in a way determined simply by their detunings. Rotational relaxation would transfer population from a state in one ladder to an isoenergetic one in another through the unimolecular reaction term (Γ). In those ladders characterized by an off-resonant $0 \rightarrow 1$ transition, rotational relaxation could then transfer the bottlenecked ground state population to a ladder in which the first transition is resonant. The overall effect--rotational hole filling--would yield a positive pressure effect on the absorption cross section. In those systems of ladders are resonant rotational relaxation would merely exchange population between the ladders. These systems would be affected by pressure only through pressure broadening.

If we were to model the multiphoton absorption process by including m rotational states at each vibrational level, then our computer code would have to solve a system of m (coupled) ladders. This would necessitate the diagonalization of an m^2 X ($N^2 \times N^2$) matrix. For even a two-ladder system the expense of solving the density matrix equations would be prohibitive. This expense is magnified by the number of iterations the model must be put through in order to vary systematically all of the important parameters. The experimental evidence that will soon be presented, moreover, suggests that nearly all rotational states of the vibrationless ground state are pumped through nearly-resonant ladders. From the previous discussion, we can predict that the dominant pressure effect would therefore be pressure broadening. In the absence of rotational resolution of the pumping process, this phenomenon would be experimentally indistinguishable from dephasing and may be modeled through the dephasing rate.

At pressures greater than 1 Torr vibrational relaxation suppresses the infrared pumping efficiency. Incorporating this phenomenon into the computer model is easy--the prescription for doing is laid out in Eqs. (IV.26) and (IV. 28). If we only include V→T transitions between neighboring vibration states (the "dipole-allowed" transitions) then we will have 2(N-1) relaxation rates to specify. Two simplifications can further reduce this number to one: First we can invoke the principle of microscopic reversibility to relate the "up" rates to the corresponding "down" rates:

$$P_{j \leftarrow i} = g_j/g_i \; e^{-(E_i - E_i)/kT} P_{i \leftarrow j} \qquad \text{(IV.51)}$$

(Because of this expression the temperature becomes an input parameter for the model.) Secondly, we can use the Landau-Teller theory to relate all of the rates connecting excited vibrational states to the 0↔1 rate:

$$1/T_1(j \leftrightarrow j+1) = (j+1)1/T_1(0 \leftrightarrow 1) \qquad \text{(IV.51a)}$$

This completes the discussion of the choice and manipulation of input parameters to Copath. All that remains to do in this chapter is to outline the mechanics of the program.

The subroutine that handles all data acquisition--Copath--also serves as one of the two calling subroutines. After it has read in and printed out the input data, it calls upon the second calling subroutine responsible for all of the matrix manipulations--"Eigen". The Hamiltonian matrix for the system under study is set up by a subroutine Eigen calls "LoadH"; this matrix , in turn, is transformed into the corresponding R matrix (Eq. (IV.41)) by the subroutine "LoadR". The appropriate relaxation terms--dephasing rates, vibrational relaxation rates and unimolecular reaction rates--are added on to matrix equations by "LoadDP", which is called by LoadR. Diagonalization of the R matrix is handled by a library routine (from the International Mathematics and Science Library) designed for handling general complex matrices--"EIGCC". Another IMSL routine--"LEQ2C"--inverts the resulting eigenvector matrix $\underset{\approx}{V}$ (Eq. (IV.46)). The density matrix at time zero--$\underset{\sim}{\rho}(0)$--is supplied by the subroutine "Initial" and is a column matrix with the first element being 1 and all others being 0 (or, in the event that the pulse shape option is employed, consists of the final density matrix elements of the previous operation). Multiplication of the matrices a specified in Eq. (IV.46), is carried out by Eigen. Finally,

the subroutine "Prtout" prints out the populations (a_{ii}'s) for as many time intervals as is specified by Copath.

I will conclude this chapter with a description of the ways in which the two shortcomings in the model mentioned earlier--the inability to handle properly rotational relaxation and intramoleculer (V→V) relaxation --can be rectified.

Solution of the former has already been discussed: We only have to set up as many ladders (m) as there are rotational states that either contain or can receive population. The resulting R matrix would then be a sort of super-matrix of rank m×N×N. Solving this gigantic matrix would proceed exactly as before.

The principle behind the above solution is that rotational relaxation is equivalent to intermolecular relaxation by an atomic gas. The same procedure could be used for including, in the model, intramolecular relaxation between the pumped mode states and background states. However, the huge expense involved in diagonalizing the large matrix that would result can be avoided by resorting to the following approximation: Since excitation of the background states is an incoherent process we can model the dynamics in this region with rate equations[127], rather than with the Schrödinger (or density matrix equations). To do so we first consider all of the background states at each energy isoenergetic with a pumped mode state as a single "composite" state. (An explicit discussion of how this is done may be found in Reference 67.) We then set up an R matrix of rank N whose diagonal matrix elements represent the rate of change of population through relaxation (just as in the density matrix).

The off-diagonal elements that are on either side of the diagonal connect the populations of successive levels through radiative transition rates. Coupling the combined background states ladder to the pumped mode ladder is done via gain and loss terms on the diagonals of both matrices. Naturally, one may explicitly take into account the individuality of nonpumped states by writing out as many N×N matrices as there are background modes and connecting them all together with appropriate relaxation terms.

With the above modifications made, modeling the IRMPA process can be carried out without the usual artificial separation of the process into two parts corresponding to the discrete region and the quasicontinuum. Transition from one energy regime to the next is continuous and automatic and the accuracy of such a treatment is limited only by our knowledge of the input parameters. In the case of thiophosgene, this knowledge is incomplete so that nothing can be gained, at present, by resorting to these expensive changes.

V. EXPERIMENTAL

A. Materials

1. Thiophosgene

Thiophosgene was purchased from Aldrich Chemical Company (where it had been analyzed by infrared spectroscopy for impurities). Carbon tetrachloride (boiling point = 76.5°C) and thiophosgene (boiling point = 73°C) form an azeotropic mixture upon distillation of the synthesized product so that the former is present as 15% of the sample. Gas chromatography is required to remove the unwanted CCl_4; however, experiments done with pure $CSCl_2$ (purchased from Aldrich) give the same results as those obtained with the azeotrope. This is not surprising since carbon tetrachloride absorbs neither CO_2 laser radiation nor visible radiation. Furthermore, in a typical molecular beam the number density in the beam is low enough so that collisions between $CSCl_2$ molecules and CCl_4 molecules are rare. In the added gas experiments, the foreign gas is generally present at a much greater pressure than the thiophosgene so that the presence of carbon tetrachloride as a 15% impurity to the thiophosgene sample is inconsequential.

Volatile impurities are removed from the $CSCl_2$-CCl_4 azeotrope by trap-to-trap distillation. A dry ice/acetone mixture is used to trap the thiophosgene but allow the impurities (e.g. CS_2) to pass through the vacuum line. Between experiments, thiophosgene is kept in its ampoule in a refrigerator at approximately 0°C. Prior to experimentation, the ampoule undergoes a minimum of three freeze-thaw cycles in which liquid nitrogen is the freezing agent and water is the thawing agent. By opening the frozen sample to the vacuum line and watching for any pressure rise on a thermocouple gauge one may insure that all gaseous impurities have been removed.

2. Added Gases

All but two of the gases used in the added gas experiments are obtained from lecture bottles and are of >99% purity: helium (Linde/research grade), argon (Matheson/scientific grade), xenon (Liquid Carbonic/research grade), carbon monoxide (Matheson/research grade), nitrogen (Liquid Carbonic/research grade), nitrous oxide (Matheson/99.9%), carbon dioxide (Matheson/Coleman grade) and methyl chloride (Matheson/99.5%). Gases are first transferred to a 3-liter bulb, via the vacuum line, to a pressure of approximately 3 Torr. The bulb is then connected to nylon tubing which enters the beam machine through a shut-off valve on top of the test chamber. The pressure of the added gas in the beam machine is measured with a capacitance manometer (Gould Datametrics).

The other two gases exist as liquids at room temperature: acetonitrile (Aldrich/spectrophotometric grade) and nitromethane (Eastman/reagent ACS grade). Both are trap-to-trap distilled before use in the same manner as that described for thiophosgene. They are fed into the beam machine from warmed ampoules in the same way as the other gases.

B. Delivery System

1. Effusive Beam

Thiophosgene is fed into the beam machine via the vacuum manifold in which the purifications, described above, are carried out. Stainless steel tubing attached to one of the manifold's stopcocks delivers the thiophosgene to the test chamber. The flow rate of the gas into the molecular beam source is controlled by a needle valve located just before the steel tubing. The effusive beam source (see Section V.C) consists of a 3-mm (inner diameter) stainless steel tube capped by a glass capillary

array having 25 μm pores (Galileo, Inc.). This configuration allows a high throughput of molecules into the interaction region ($\sim 10^{11}$ cm^{-3}) while insuring that collisions between them are virtually nonexistent. The pressure inside the test chamber is measured with an ionization gauge located on the top of the machine.

2. Supersonic Beam

In principle, one could use the experimental set-up just described for supersonic beam experiments by merely replacing the thiophosgene ampoule with a bulb containing the appropriate $CSCl_2$/inert gas mixture. However, operating a continuous beam containing seeded thiophosgene would overload the diffusion pump to the detection chamber and raise the background pressures to levels that could no longer insure collisionless conditions.

For this reason, a pulsed valve is used to deliver the $CSCl_2$-Ar mixture in pulses approximately 200 μsec long. The valve (General Valve: model 9-181) is powered by a 180 V power supply and fast switching transistor. The nozzle diameter is 0.75 mm.

Argon/thiophosgene mixtures are prepared as follows: A 10-liter bulb is attached to the vacuum manifold and evacuated. With the manifold closed off from the vacuum pumps, thiophosgene is released into the system (including the bulb) to a final pressure of 2 Torr. The $CSCl_2$ ampoule is closed off and argon (commercial purity) is released, through a needle valve, into the vacuum line. After the mixture has equilibrated, the 10-liter bulb is removed from the manifold and hooked up to a port with a shut-off valve on the bottom of the beam machine.

Experiments were performed to determine the mixture of thiophosgene and argon that would provide the best rotational cooling. Estimating the rotational temperature is done by monitoring the band contour of the

$2_0^1 3_0^1 4_0^1$ transition. To do so we simulate the band at various temperatures and find the synthesized spectrum which most closely matches the experimental one. (Figs.V.1 a,b and c). Using this method we determined the optimum mixture of gases to be: 2 Torr $CSCl_2$ + 700 Torr Ar. This composition gives a rotational temperature of 10-15 K. Decreasing the amount of thiophosgene or changing the carrier gas does not noticeably lower the temperature.

3. Bulb Experiments

In order to do experiments on thiophosgene at pressures greater than 1 mTorr one must replace the molecular beam apparatus with a closed bulb. The easiest way of doing this is simply to close off the gate valves of the beam machine and, effectively, convert it into a giant bulb. This method takes advantage of the superior scattered light rejection and fluorescence detection capabilities of the beam machine. Pressures inside the machine are measured with a capacitance manometer.

C. Molecular Beam Machine

The molecular beam machine is comprised of two units: the source chamber and the detection chamber (Fig.V.2). The former is evacuated by a six-inch diffusion pump and mechanical pump and the latter by a ten-inch diffusion pump and mechanical pump.

In the experiments done by Brenner, Brezinsky and Curtis[85-87] the source chamber housed the beam source, skimmer and aperture. The collimated beam entered the test chamber through an aperture in the steel plate that divides the two chambers. Once through the opening, the beam was collimated by still another aperture before it reached the interaction region.

In all of the collisionless experiments reported here (for uncooled thiophosgene) an effusive flow source was used instead of a true molecular beam. The capillary array sits just 3 cm away from the point of intersection of the two laser beams (Fig.V.3). This so-called interaction region is surrounded on four sides by liquid-nitrogen cooled plates. The bottom baffle has a hole, approximately 2 mm in diameter, less than 1 cm away from the beam source, and partially collimates the effusive, or supersonic, beam. The hole on the top plate is considerably larger (4 cm) to allow viewing by the photomultiplier and the holes on the two side plates are approximately 2 cm wide and allow the dye laser beam to pass through.

To measure the number density of molecules in an effusive beam (at the interaction region) one can measure the fluorescence intensity of a beam of a gas that is excited by the dye laser and then, with the gate valves closed, determine the pressure of the gas needed to yield the same signal. Using the ideal gas law one can then easily calculate the number density in the beam. This was actually done by Brenner[87] who found that the number density inferred from the reading of the ionization gauge was only about 20% lower than the actual (calculated) density. (This implies that the effusive beam is not very well collimated.) I have also verified this surprisingly close agreement in similar measurements. Since we are concerned with knowing the number density of thiophosgene molecules in the effusive or supersonic beam only to the extent of insuring that it is low enough to preclude collisions from being important, reading the ionization gauge for estimating number densities

Figs.V.1 Simulation of the $2_0^1 3_0^1 4_0^1$ absorption spectrum for three rotational temperatures using the computer program "Fastplot"[106].

(a) 5 K
(b) 10K
(c) 15 K

Note that the frequency axes for the three spectra are not at the same scale. The actual spectrum (e.g. Fig. VI.1) is complicated by the overlapping of individual spectra for the three major isotopic species and by contamination with the $1_0^1 4_2^1$ band.

```
35.35-T410PHOSGENE SPECTRUM SIMULATION 2(0.1)3(0.1)4(0.1)

FIGURE  1 PAGE  2

J RANGE   0 TO   90. MAX KA =  50. HALF WIDTH =       .100

                0                    25                   50                   75                  100
             +--------------------+--------------------+--------------------+--------------------+
19439.860 I
19439.800 IX
19439.740 IX
19439.680 IX
19439.620 IX
19439.560 IX
19439.500 IX
19439.440 IX
19439.380 IXX
19439.320 IXX
19439.260 IXX
19439.200 IXXX
19439.140 IXXX
19439.080 IXXXX
19439.020 IXXX
19438.960 IXXXXX
19438.900 IXXXXX
19438.840 IXXXXXX
19438.780 IXXXXXX
19438.720 IXXXXXXX
19438.660 IXXXXXXXX
19438.600 IXXXXXXXXXX
19438.540 IXXXXXXXXXXX
19438.480 IXXXXXXXXXXXXX
19438.420 IXXXXXXXXXXXXXXX
19438.360 IXXXXXXXXXXXXXXXXXXXXXXXX
19438.300 IXXXXXXXXXXXXXXXXXXXXXXXXXXXXXXXXXXXXXX
19438.240 IXXXXXXXXXXXXXXXXXXXXXXXXXXXXXXXXXXXXXXXXXX
19438.180 IXXXXXXXXXXXXXXXXXXXXXXXXXXXXXXXXXXXXXXXXXXXX
19438.120 IXXXXXXXXXXXXXXXXXXXXXXXXXXXXXXXXXXXXXXXXXXXXXXXX
19438.060 IXXXXXXXXXXXXXXXXXXXXXXXXXXXXXXXXXXXXXXXXXXXXXXXXXX
19438.000 IXXXXXXXXXXXXXXXXXXXXXXXXXXXXXXXXXXXXXXXXXXXXXXXXXXXX
19437.940 IXXXXXXXXXXXXXXXXXXXXXXXXXXXXXXXXXXXXXXXXXXXXXXXXXXXXXX
19437.880 IXXXXXXXXXXXXXXXXXXXXXXXXXXXXXXXXXXXXXXXXXXXXXXXXXXXXXXXXX
19437.820 IXXXXXXXXXXXXXXXXXXXXXXXXXXXXXXXXXXXXXXXXXXXXXXXXXXXXXXXXXXXX
19437.760 IXXXXXXXXXXXXXXXXXXXXXXXXXXXXXXXXXXXXXXXXXXXXXXXXXXXXXXXXXXXXX
19437.700 IXXXXXXXXXXXXXXXXXXXXXXXXXXXXXXXXXXXXXXXXXXXXXXXXXXXXXXXXXXXXX
19437.640 IXXXXXXXXXXXXXXXXXXXXXXXXXXXXXXXXXXXXXXXXXXXXXXXXXXXXXXXXXXXXX
19437.580 IXXXXXXXXXXXXXXXXXXXXXXXXXXXXXXXXXXXXXXXXXXXXXXXXXXXXXXXXXXXXX
19437.520 IXXXXXXXXXXXXXXXXXXXXXXXXXXXXXXXXXXXXXXXXXXXXXXXXXXXXXXXXXXXXX
19437.460 IXXXXXXXXXXXXXXXXXXXXXXXXXXXXXXXXXXXXXXXXXXXXXXXXXXXXXXXXXXXXX
19437.400 IXXXXXXXXXXXXXXXXXXXXXXXXXXXXXXXXXXXXXXXXXXXXXXXXXXXXXXXXXXXXX
19437.340 IXXXXXXXXXXXXXXXXXXXXXXXXXXXXXXXXXXXXXXXXXXXXXXXXXXXXXXXXXXXXX
19437.280 IXXXXXXXXXXXXXXXXXXXXXXXXXXXXXXXXXXXXXXXXXXXXXXXXXXXXXXXXXXXXX
19437.220 IXXXXXXXXXXXXXXXXXXXXXXXXXXXXXXXXXXXXXXXXXXXXXXXXXXXXXXXXXXXXX
19437.160 IXXXXXXXXXXXXXXXXXXXXXXXXXXXXXXXXXXXXXXXXXXXXXXXXXXXXXXXXXXXXX
19437.100 IXXXXXXXXXXXXXXXXXXXXXXXXXXXXXXXXXXXXXXXXXXXXXXXXXXXXXXXXXXXXX
19437.040 IXXXXXXXXXXXXXXXXXXXXXXXXXXXXXXXXXXXXXXXXXXXXXXXXXXXXXXXXXXXXX
19436.980 IXXXXXXXXXXXXXXXXXXXXXXXXXXXXXXXXXXXXXXXXXXXXXXXXXXXXXXXXXXXXX
19436.920 IXXXXXXXXXXXXXXXXXXXXXXXXXXXXXXXXXXXXXXXXXXXXXXXXXXXXXXXXXXXXX
19436.860 IXXXXXXXXXXXXXXXXXXXXXXXXXXXXXXXXXXXXXXXXXXXXXXXXXXXXXXXXXXXXX
19436.800 IXXXXXXXXXXXXXXXXXXXXXXXXXXXXXXXXXXXXXXXXXXXXXXXXXXXXXXXXXXXXX
19436.740 IXXXXXXXXXXXXXXXXXXXXXXXXXXXXXXXXXXXXXXXXXXXXXXXXXXXXXXXXXXXXX
19436.680 IXXXXXXXXXXXXXXXXXXXXXXXXXXXXXXXXXXXXXXXXXXXXXXXXXXXXXXXXXXXXX
19436.620 IXXXXXXXXXXXXXXXXXXXXXXXXXXXXXXXXXXXXXXXXXXXXXXXXXXXXXXXXXXXXX


19435.560 IXXXXXXXXXXXXXXXXXXXXXXXXXXXXXXXXXXXXXXXXXXXXXXXXXXXXXXXXXXXXX
19436.500 IXXXXXXXXXXXXXXXXXXXXXXXXXXXXXXXXXXXXXXXXXXXXXXXXXXXXXXXXXXXXX
19436.440 IXXXXXXXXXXXXXXXXXXXXXXXXXXXXXXXXXXXXXXXXXXXXXXXXXXXXXXXXXXXXX
19436.380 IXXXXXXXXXXXXXXXXXXXXXXXXXXXXXXXXXXXXXXXXXXXXXXXXXXXXXXXXXXXXX
19436.320 IXXXXXXXXXXXXXXXXXXXXXXXXXXXXXXXXXXXXXXXXXXXXXXXXXXXXXXXXXXXXX
19436.260 IXXXXXXXXXXXXXXXXXXXXXXXXXXXXXXXXXXXXXXXXXXXXXXXXXXXXXXXXXXXXX
19436.200 IXXXXXXXXXXXXXXXXXXXXXXXXXXXXXXXXXXXXXXXXXXXXXXXXXXXXXXXXXXXXX
19436.140 IXXXXXXXXXXXXXXXXXXXXXXXXXXXXXXXXXXXXXXXXXXXXXXXXXXXXXXXXXXXXX
19436.080 IXXXXXXXXXXXXXXXXXXXXXXXXXXXXXXXXXXXXXXXXXXXXXXXXXXXXXXXXXXXXX
19436.020 IXXXXXXXXXXXXXXXXXXXXXXXXXXXXXXXXXXXXXXXXXXXXXXXXXXXXXXXXXXXXX
19435.960 IXXXXXXXXXXXXXXXXXXXXXXXXXXXXXXXXXXXXXXXXXXXXXXXXXXXXXXXXXXXXX
19435.900 IXXXXXXXXXXXXXXXXXXXXXXXXXXXXXXXXXXXXXXXXXXXXXXXXXXXXXXXXXXXXX
19435.840 IXXXXXXXXXXXXXXXXXXXXXXXXXXXXXXXXXXXXXXXXXXXXXXXXXXXXXXXXXXXXX
19435.780 IXXXXXXXXXXXXXXXXXXXXXXXXXXXXXXXXXXXXXXXXXXXXXXXXXXXXXXXXXXXXX
19435.720 IXXXXXXXXXXXXXXXXXXXXXXXXXXXXXXXXXXXXXXXXXXXXXXXXXXXXXXXXXXXXX
19435.660 IXXXXXXXXXXXXXXXXXXXXXXXXXXXXXXXXXXXXXXXXXXXXXXXXXXXXXXXXXXXXX
19435.600 IXXXXXXXXXXXXXXXXXXXXXXXXXXXXXXXXXXXXXXXXXXXXXXXXXXXXXXXXXXXXX
19435.540 IXXXXXXXXXXXXXXXXXXXXXXXXXXXXXXXXXXXXXXXXXXXXXXXXXXXXXXXXXXXXX
19435.480 IXXXXXXXXXXXXXXXXXXXXXXXXXXXXXXXXXXXXXXXXXXXXXXXXXXXXXXXXXXXXX
19435.420 IXXXXXXXXXXXXXXXXXXXXXXXXXXXXXXXXXXXXXXXXXXXXXXXXXXXXXXXXXXXXX
19435.360 IXXXXXXXXXXXXXXXXXXXXXXXXXXXXXXXXXXXXXXXXXXXXXXXXXXXXXXXXXXXXX
19435.300 IXXXXXXXXXXXXXXXXXXXXXXXXXXXXXXXXXXXXXXXXXXXXXXXXXXXXXXXXXXXXX
19435.240 IXXXXXXXXXXXXXXXXXXXXXXXXXXXXXXXXXXXXXXXXXXXXXXXXXXXXXXXXXXXXX
19435.180 IXXXXXXXXXXXXXXXXXXXXXXXXXXXXXXXXXXXXXXXXXXXXXXXXXXXXXXXXXXXXX
19435.120 IXXXXXXXXXXXXXXXXXXXXXXXXXXXXXXXXXXXXXXXXXXXXXXXXXXXXXXXXXXXXX
19435.060 IXXXXXXXXXXXXXXXXXXXXXXXXXXXXXXXXXXXXXXXXXXXXXXXXXXXXXXXXXXXXX
19435.000 IXXXXXXXXXXXXXXXXXXXXXXXXXXXXXXXXXXXXXXXXXXXXXXXXXXXXXXXXXXXXX
19434.940 IXXXXXXXXXXXXXXXXXXXXXXXXXXXXXXXXXXXXXXXXXXXXXXXXXXXXXXXXXXXXX
19434.880 IXXXXXXXXXXXXXXXXXXXXXXXXXXXXXXXXXXXXXXXXXXXXXXXXXXXXXXXXXXXXX
19434.820 IXXXXXXXXXXXXXXXXXXXXXXXXXXXXXXXXXXXXXXXXXXXXXXXXXXXXXXXXXXXXX
19434.760 IXXXXXXXXXXXXXXXXXXXXXXXXXXXXXXXXXXXXXXXXXXXXXXXXXXXXXXXXXXXXX
19434.700 IXXXXXXXXXXXXXXXXXXXXXXXXXXXXXXXXXXXXXXXXXXXXXXXXXXXXXXXXXXXXX
19434.640 IXXXXXXXXXXXXXXXXXXXXXXXXXXXXXXXXXXXXXXXXXXXXXXXXXXXXXXXXXXXXX
19434.580 IXXXXXXXXXXXXXXXXXXXXXXXXXXXXXXXXXXXXXXXXXXXXXXXXXXXXXXXXXXXXX
19434.520 IXXXXXXXXXXXXXXXXXXXXXXXXXXXXXXXXXXXXXXXXXXXXXXXXXXXXXXXXXXXXX
19434.460 IXXXXXXXXXXXXXXXXXXXXXXXXXXXXXXXXXXXXXXXXXXXXXXXXXXXXXXXXXXXXX
19434.400 IXXXXXXXXXXXXXXXXXXXXXXXXXXXXXXXXXXXXXXXXXXXXXXXXXXXXXXXXXXXXX
19434.340 IXXXXXXXXXXXXXXXXXXXXXXXXXXXXXXXXXXXXXXXXXXXXXXXXXXXXXXXXXXXXX
19434.280 IXXXXXXXXXXXXXXXXXXXXXXXXXXXXXXXXXXXXXXXXXXXXXXXXXXXXXXXXXXXXX
19434.220 IXXXXXXXXXXXXXXXXXXXXXXXXXXXXXXXXXXXXXXXXXXXXXXXXXXXXXXXXXXXXX
19434.160 IXXXXXXXXXXXXXXXXXXXXXXXXXXXXXXXXXXXXXXXXXXXXXXXXXXXXXXXXXXXXX
19434.100 IXXXXXXXXXXXXXXXXXXXXXXXXXXXXXXXXXXXXXXXXXXXXXXXXXXXXXXXXXXXXX
19434.040 IXXXXXXXXXXXXXXXXXXXXXXXXXXXXXXXXXXXXXXXXXXXXXXXXXXXXXXXXXXXXX
19433.980 IXXXXXXXXXXXXXXXXXXXXXXXXXXXXXXXXXXXXXXXXXXXXXXXXXXXXXXXXXXXXX
19433.920 IXXXXXXXXXXXXXXXXXXXXXXXXXXXXXXXXXXXXXXXXXXXXXXXXXXXXXXXXXXXXX
19433.860 IXXXXXXXXXXXXXXXXXXXXXXXXXXXXXXXXXXXXXXXXXXXXXXXXXXXXXXXXXXXXX
19433.800 IXXXXXXXXXXXXXXXXXXXXXXXXXXXXXXXXXXXXXXXXXXXXXXXXXXXXXXXXXXXXX
19433.740 IXXXXXXXXXXXXXXXXXXXXXXXXXXXXXXXXXXXXXXXXXXXXXXXXXXXXXXXXXXXXX
19433.680 IXXXXXXXXXXXXXXXXXXXXXXXXXXXXXXXXXXXXXXXXXXXXXXXXXXXXXXXXXXXXX
19433.620 IXXXXXXXXXXXXXXXXXXXXXXXXXXXXXXXXXXXXXXXXXXXXXXXXXXXXXXXXXXXXX
19433.560 IXXXXXXXXXXXXXXXXXXXXXXXXXXXXXXXXXXXXXXXXXXXXXXXXXXXXXXXXXXXXX
19433.500 IXXXXXXXXXXXXXXXXXXXXXXXXXXXXXXXXXXXXXXXXXXXXXXXXXXXXXXXXXXXXX
19433.440 IXXXXXXXXXXXXXXXXXXXXXXXXXXXXXXXXXXXXXXXXXXXXXXXXXXXXXXXXXXXXX
19433.380 IXXXXXXXXXXXXXXXXXXXXXXXXXXXXXXXXXXXXXXXXXXXXXXXXXXXXXXXXXXXXX
```

Fig. V.1.a.

Fig. V.1.b.

Fig. V.1.c.

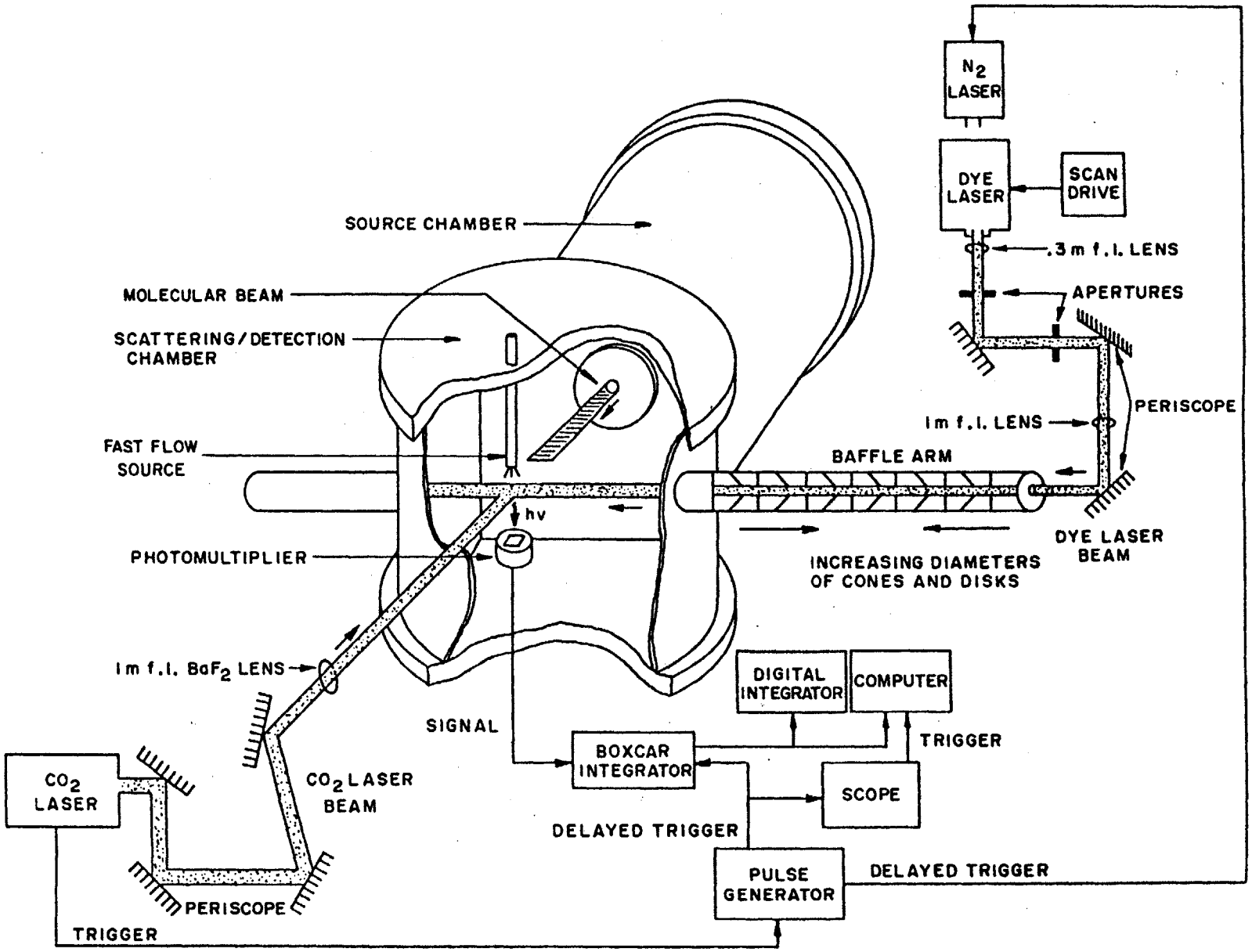


Fig. V.2. Diagram of the molecular beam apparatus used to carry out the infrared-visible double resonance experiments. For performing bulb experiments the gate valves to the beam machine are closed off.

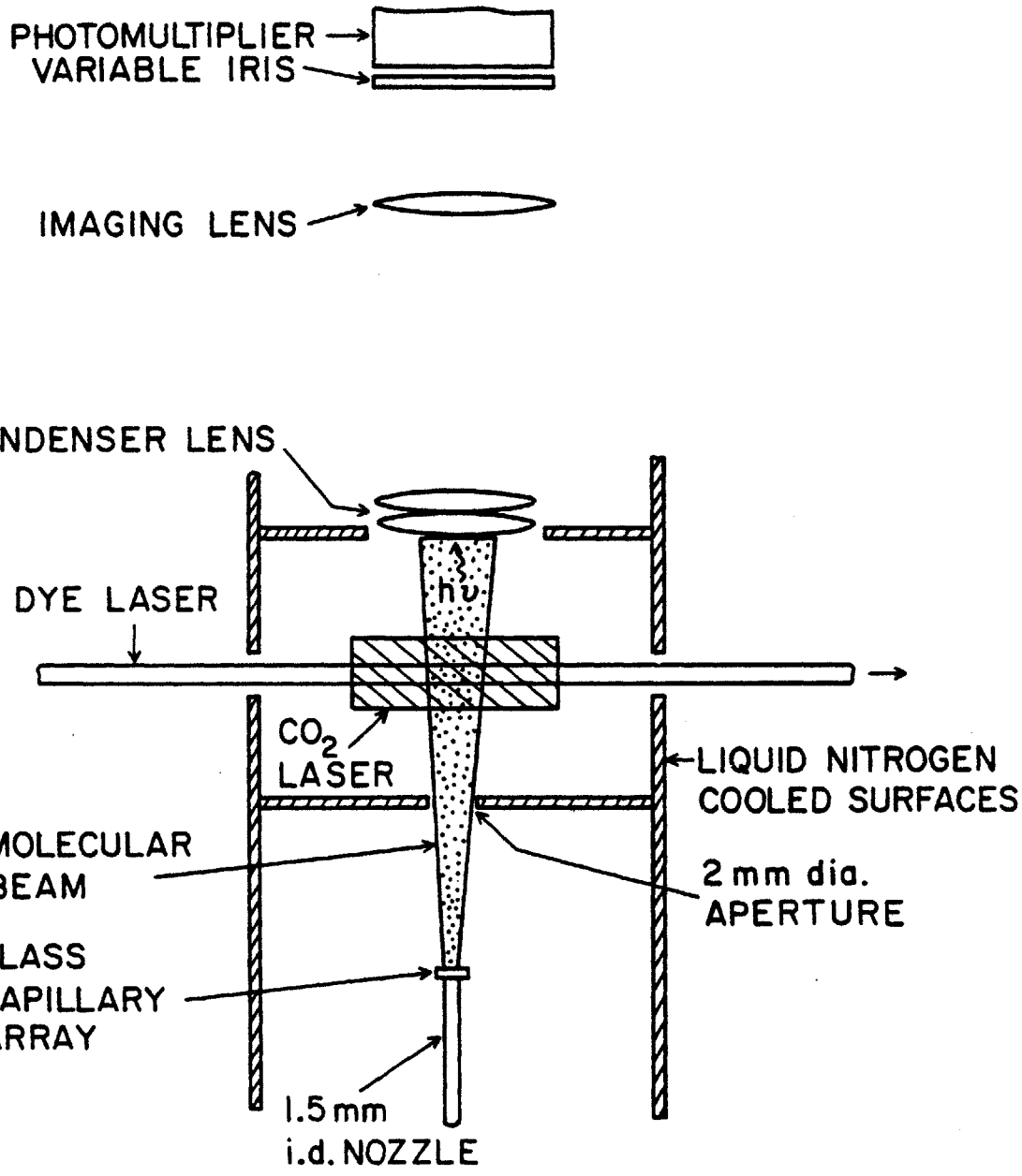


Fig. V.3. Schematic enlargement of the interaction region and fluorescence imaging system. For supersonic cooling of thiophosgene a pulsed valve replaces the effusive beam source.

is quite sufficient. It must be kept in mind, however, that the density inferred this way is always a lower limit to the actual value.

In the effusive beam experiments in which the $2_0^1 3_0^1 4_0^1$ band was used to monitor the ground state depletion the "pressure" of the beam was approximately 1×10^{-4} Torr ($\sim2\times10^{12}$ molecules cm^{-3}). For strong bands the pressure was as low as 5×10^{-5} Torr and for weak bands it was as high as 5×10^{-4} Torr. In the supersonic experiments the pressure of the $CSCl_2$-Ar mixture at the interaction region was adjusted by changing the pulse duration of the valve and varied from 2×10^{-4} Torr to 10^{-3} Torr.

Attached to the sides of the detection chamber and coaxial with the dye laser beam are two baffle arms. Each baffle arm contains eight black disks and cones with varying sized apertures that are designed to reduce scattered dye laser light. With this arrangement the scattered light signal for a 400 μJ pulse (2 V signal) is approximately 200 mV. Using a long wavelength pass filter in front of the imaging system (see Section V.F) further reduces this signal to near zero. (A typical fluorescence signal from thiophosgene excited from the ground state is 1.5 to 2 V.)

D. CO_2 Laser

The CO_2 laser was built by the chemistry machine shop at Brookhaven National Laboratories and was constructed according to the design of Horwitz and Leone[128]. It is a "pin laser" which discharges through six rows of 300 pins. The high voltage is supplied to the pin electrodes through a circulating $CuSO_4$ solution, which is cooled by an air-pump-driven water circulating system.

A master grating (PTR Optics) with 150 grooves/mm is set in an

isolated Lansing mount at one end of the cavity. At the other end is a Germanium output coupler of 69% reflectivity in another isolated Lansing mount. Alignment of the grating and output coupler is accomplished with a He-Ne laser in the usual fashion. To cut down on radio frequency noise generated from the power supply discharge, the entire laser is surrounded by copper shielding. Boxer fans at both ends of the laser circulate air around the cavity and the ventilation system of the building changes the surrounding air and keeps the cavity cool.

The power supply to the laser (Universal Voltronics) is capable of providing up to 50 KV at approximately 100 mA. To produce a P(20), 10.6 μm pulse of 100 mJ energy requires a voltage of approximately 18 KV.

The infrared beam is directed into the beam machine by a set of copper mirrors (Fig.V.2). The first mirror has a 10 meter radius of curvature and sends the laser light to a periscope consisting of two flat molybdenum mirrors, the latter of which translate the beam vertically so that it is at the level of the interaction region. A final flat copper mirror directs the beam through a 1-m focal length BaF_2 lens, a cylindrical lens and into the beam machine itself. The cylindrical lens rotates the rectangular laser beam. In this way maximum overlap between the CO_2 laser beam, dye laser beam and molecular beam is achieved (Fig.IV.3). The final infrared laser image is fairly uniform in intensity although there are hot spots on the two vertical edges.

A beam dump fixed to the dividing plate between the source and test chambers prevents the CO_2 laser beam from reflecting off the inside walls of the beam machine; nonetheless, there is still a small amount of scat-

tered (white) light at higher pulse energies (>100 mJ) which is minimized by adjusting the final copper mirror. Further adjustments of the last mirror are done, when an experiment is in progress, to maximize the overlap between the dye laser and CO_2 laser.

Lasing occurs on most lines (J~10-40) of the P and R branches of the 10.6 μm (00^01 -10^00) and 9.6 μm (00^01 -02^00) transitions. Except for the fluence dependence studies, the pulse energy was kept constant at 100 mJ as measured with a Scientech power meter located just before the final copper mirror. Losses from the mirror, the two lenses and BaF_2 window of the beam machine result in a ~40% loss in pulse energy from the point of its measurement to the interaction zone. This must be remembered when interpreting the fluence variation data presented in the next chapter.

The CO_2 laser gases--He, N_2, and CO_2--are premixed in a glass reservoir before they flow into one end of the laser cavity. A mechanical pump hooked up to the other end draws the gases through. The flow rate, controlled by a bellows valve, is controlled so that the equilibrium pressure of gases inside the cavity is within the range 100-200 Torr. The composition of gases varies according to the pulse shape and energy desired. For a high energy pulse with a (disproportionately) long tail a typical gas mixture is: 45 Torr He, 10 Torr N_2 and 30 Torr CO_2. For a pulse having a short tail (~2 μsec) but less energy, the gas mixture might be: 130 Torr He, 5 Torr N_2 and 30 Torr CO_2. In general, nitrogen lean mixtures yield low energy pulses with short tails.

In an IR-VIS-DR experiment in which the dye laser follows immediately

after the spike of the CO_2 laser pulse (200 nsec) the tail of the pulse only complicates the interpretation of the data. It can contain as much as 50% of the total pulse energy but the only excitation it can create is that of the excited electronic state. For this reason we used short-tail pulses in nearly all of our experiments, even though this entails a sacrifice in pulse energy.

The pulse shape is observed by gently focusing the CO_2 laser beam onto a photo drag detector (Rofin) and displaying the waveform on an oscilloscope (Fig.V.4). The two parameters that are used to characterize the pulse shape are the full-width-at-half-maximum of the spike (100-300 nsec) and the length of the tail (1-5 μsec). For the nitrogen lean mixture described above, the FWHM of the spike is approximately 150 nsec and the tail is 2 μsec long. Thyratron triggering keeps the shot-to-shot jitter to approximately 50 nsec. The pulses are partially mode locked but not so much that individual spikes can be discerned. Finally, the laser operates multimode but just which transverse and longitudinal modes are present is impossible to ascertain due to the lasing pattern created by the pin electrodes.

E. Dye Laser

The visible probe laser consists of a 400 KW pulsed nitrogen laser (Molectron: UV14) which pumps a tunable dye laser equipped with a grating (Molectron DL 200). Lack of amplification limits the pulse energy to less thant 500 μJ with a pulse-to-pulse variation of better than 5%. The pulse width is 10 nsec and the linewidth is 0.3 cm^{-1} as measured with an extra-cavity etalon.

The optical path to the interaction region is configured as follows:

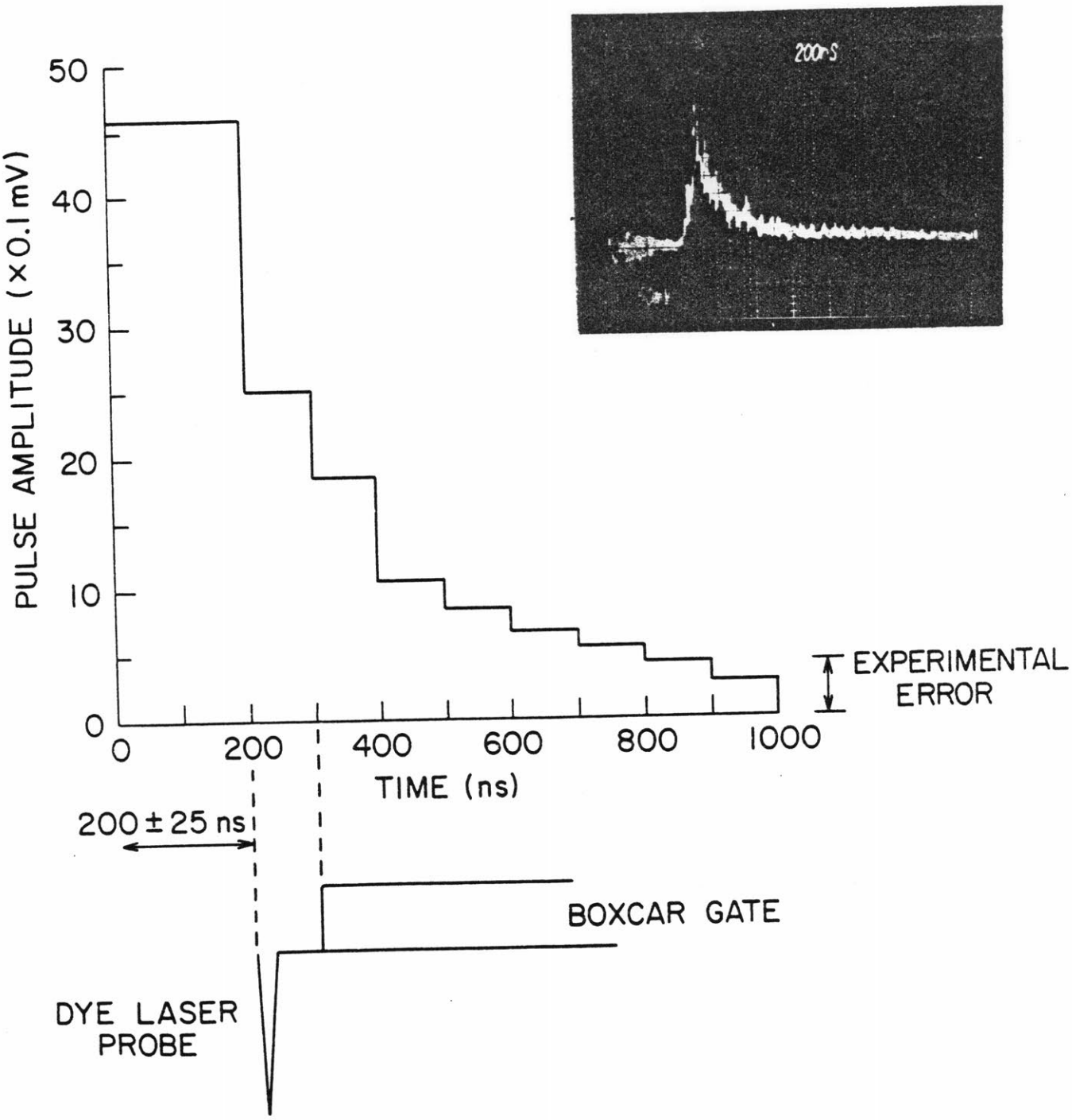


Fig.V.4. Timing of the firing of the CO_2 laser and dye laser and of the opening of the boxcar gate. The histogram at the top shows the temporal energy distribution of the CO_2 laser pulse determined with boxcar averager. The inset shows an oscilloscope display of a typical CO_2 laser pulse. In later experiments, the delay of the gate with respect to the dye laser probe was zero.

The dye laser output is gently focused by a 30-cm focal length lens which then passes through an iris diaphragm with a 3-mm aperture that is designed to select out only the central portion of the beam. A redirecting mirror, second aperture and periscope bring the beam to the level of the interaction region and sends it through the baffle arms. The beam emerges from the second baffle arm and hits a fluorescent card attached to the wall.

Minimizing scattered light is carried out by adjusting the redirecting mirror and/or the periscope mirror. Since the dye laser beam must transverse a much longer distance inside the beam machine than the CO_2 laser, its alignment is more critical and is carried out last before experimentation.

The dyes used are purchased from Exciton and prepared according to the recipes in the company's catalog. Coumarin 485 is used to excite the $2_0^1 3_0^1 4_0^1$ and 4_0^1 bands and gives an output energy or 400-800 μJ/pulse. The 4_2^1 band is excited with Coumarin 540A at 5626 Å (output energy is 150-180 μJ) and the 4_4^1 transition, at 5940 Å, is excited by a solution of Rhodamine 590 with a "pinch" of Rhodamine 610.

F. Detection System

The optical system that detects the fluorescence is configured as follows: At a distance of 2.5 cm. from the dye laser beam a 35-mm focal length condenser lens (Melles Griot) collects the fluorescence and forms an image of it 10 cm away. The enlarged image is refocused onto the photomultiplier cathode by a 100 cm. focal length lens that is situated 36 cm above the condenser lens. The size of the final image of the interaction zone (which is basically the dimensions of the CO_2 laser

spot) is approximately 1 cm. To insure that only this image is seen by the photomultiplier a disk with an aperture with this diameter is fitted against the photocathode. This configuration insures that only those fluorescing molecules that have also absorbed the infrared light are detected. Hence the change in the fluorescence signal following CO_2 laser absorption is equal to the absolute change in population of the absorbing state. Without this optical arrangement the change in the fluorescence signal would be "diluted" by vibrationally unexcited molecules being probed by the dye laser.

In most experiments a cut-off colored glass filter (Hoya) was placed in front of the photomultiplier to exclude scattered dye laser light. For excitation by Coumarin 485, for example, an O-34 filter was used. The only occasions when filters were not used occurred when we monitored the extremely weak 4_4^1 band. The decrease in the fluorescence signal (insignificant in other bands) along with the exclusion of scattered light was considered more of a liability than an asset. In this case the scattered light signal had to be subtracted, manually or electronically, from the fluorescence intensities.

The photomultiplier tube (EMI 9558) is enclosed in a radio frequency noise shield and housed in a light-tight aluminum cylinder. The detected fluorescence signal is sent to a screen room for processing. The screen room is a converted walk-in refrigerator which very effectively shields the experiment's electronics from radio frequency noise generated by the two lasers. In it are the photomultiplier power supply, boxcar averager, strip chart recorder, multichannel analyzer, digital integrator, oscilloscope and dye laser scan drive.

The voltage of the power supply for the photomultiplier (Power Design, Inc.) is typically set at 1600 V but may vary from 100 V to 1900 V according to the strength of the fluorescence signal. In the earlier experiments the PMT signal was amplified inside the screen room by a LeCroy amplifier. In the later experiments it was processed by a homebuilt buffer amplifier located near the photomultiplier (amplification ~10X). This latter arrangement is advantageous since noise picked up by the PMT signal cable does not get amplified inside the screen room.

The photomultiplier signal travels through triaxial cable to a bulkhead in the wall of the screen room, at which point it is transferred to coaxial cable. A gated integrator (Princeton Applied Research 164) receives the signal and feeds it into a boxcar averager Princeton Applied Research) set in the exponential averaging mode. The time constant of the integrator is 50 nsec while that of the averager varies from 0.1 sec (for tracing spectra) to 10 sec (for single wavelength measurement). The duration of the gate is generally set at 35 μsec--the lifetime of the $^1A_2$ state of thiophosgene. For extremely weak fluorescence signals the gate is narrowed to as little as 10 μsec. This gives a greater signal but lower signal-to-noise ratio. Situations prompting this action are probing of the 4_4^1 band and mixed gas experiments in which the added gas quenches the fluorescence.

The boxcar-averaged signal is sent to one or more of four components. A digital voltmeter, located outside the screen room, displays the voltage output from the averager and is used for monitoring the fluorescence

signal. If a recording of the spectrum is desired, the output is sent to a strip chart recorder (Soltec). For measuring the area under a band contour two integrating devices may be used: a Hewlett-Packard 3370B digital integrator or a Tracor Northern multichannel analyzer (TN 1710) operating in the signal averaging and "net integration" modes.

There are two ways of performing an IR-VIS-DR experiment: One can tune the dye laser to the maximum of the electronic probe transition and measure the difference in fluorescence intensity, with and without, CO_2 laser excitation. To do so merely requires reading the voltage of the boxcar averager. Alternatively, one can scan the dye laser frequency over the entire rotational contour of the band while, simultaneously, integrating the area under it. Again, the integrated intensity is measured in the presence and in the absence of the CO_2 laser. Although the latter is strictly the only correct way to measure absorption strength, the former gives a good approximation. This has been checked and verified several times. For those experiments in which the IR-VIS-DR signal is changing in time, thus necessitating the rapid recording of data, "peak height analysis" is preferable. The bulb experiments were all carried out in this fashion since impurities coming off the inside walls of the beam machine and through undetectable leaks from the outside contaminate the sample gas and quickly quench the fluorescence. Also, absorption by highly excited vibrational states ($4\nu_4$) gives such small laser-induced fluorescence signals that the extra accuracy afforded by band integration is lost. Other experiments, especially those involving the pumping of $2\nu_4$, are done using peak height analysis since accuracy

analysis since accuracy is less important than speed of execution.

For those experiments requiring greater accuracy, such as the infrared frequency dependence of the ground state depletion and the fluence dependence of the ground state depletion, integration is the preferred technique. In addition to its greater accuracy this method automatically subtracts the background signal (usually caused by scattered dye laser light) of the boxcar output signal. With peak height analysis one must be careful to subtract the background signal from the LIF signal. This can be done either manually (in the lab notebook) or by zeroing the boxcar output in the absence of thiophosgene in the beam machine.

G. Triggering System

The execution of an IR-VIS-DR experiment requires a complex sequence of events whose timing must be controlled with great precision: The dye laser must fire a specified time after the firing of the CO_2 laser. The gate of the boxcar averager and the oscilloscope must be triggered with a fixed but variable delay after the dye laser pulse. When supersonic experiments are being carried out, the opening of the pulsed valve must precede the triggering of the CO_2 laser by a specified time interval.

The job of synchronizing these events is handled by one or more pulse generators (Fig.V.5). The "sync-output" of the thyratron to the CO_2 laser triggers the pulse generator (Tektronix PG 508), which in turn triggers the dye laser, boxcar averager and oscilloscope with a variable delay. Because of the finite delay it takes for the CO_2 laser to fire after being triggered, the dye laser delay may be set to any value desired. (It may even precede the CO_2 laser.) The gate of the boxcar

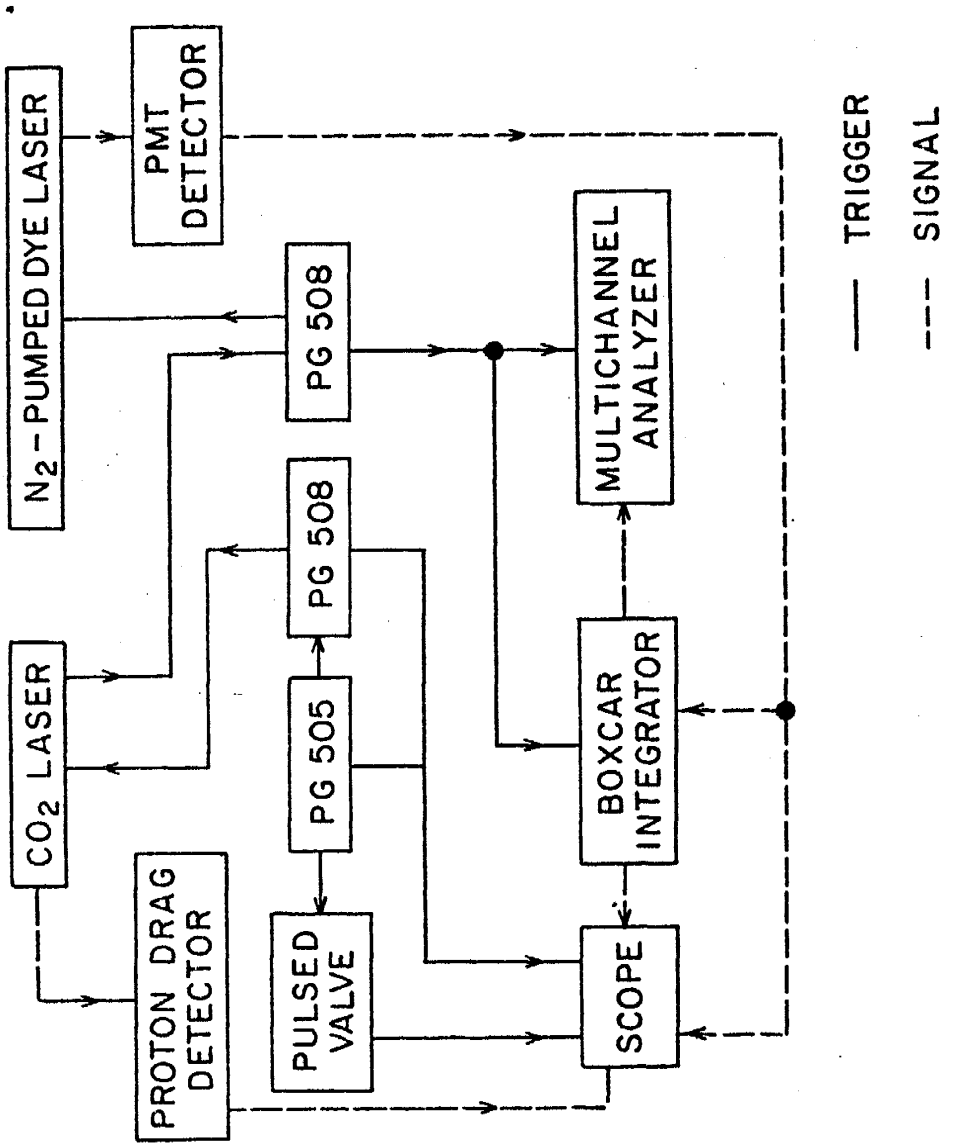


Fig.V.5. Block diagram of the triggering and signal processing system for pulsed valve (supersonic) experiments. The synchronization of effusive beam experiments requires only the right-hand most PG-508 pulse generator.

has its own variable delay and is generally set to coincide with the firing of the dye laser. With the exception of the probe delay experiments, the delay between the two lasers is set to 200 nsec as measured from leading edge of the CO_2 laser pulse to the leading edge of the dye laser pulse. Setting the delays involves displaying both the photon drag detector output and scattered light signal (filter removed) on the oscilloscope and adjusting the delay on the pulse generator accordingly.

For doing supersonic beam experiments two pulse generators must be added. The first (Tektronix PG 505) triggers the pulsed valve and the second pulse generator (Tektronix PG 508). The second generator then triggers the thyratron of the CO_2 laser and the remainder of the scheme is the same as before. Since the second pulse generator indirectly commands the dye laser and boxcar, its delay, with respect to the triggering of the pulsed valve, is set so that the bulk of the supersonic plug of molecules --the "Mach disk"--crosses the interaction region just as the two lasers fire. (Since this time is on the order of 500 μsec the delay between the dye laser and the CO_2 laser is inconsequential.) The delay is set by simply adjusting the delay of the second pulse generator until the fluorescence signal is maximized. The voltage waveform of the pulsed valve can also be displayed on the oscilloscope so that the duration of the pulsed valve opening and the delay between it and the dye laser can be measured.

VI. Results

A. Collisonless Experiments

1. Ground (Vibrationless State)

Depopulation of thiophosgene's ground state by the infrared laser is monitored by changes in the $2_0^1 3_0^1 4_0^1$ fluorescence excitation spectrum. An example of this spectrum--in the absence of and in the presence of the CO_2 laser--is shown in Fig. VI.1. The left half of Fig. VI.1 corresponds to thiophosgene at room temperature (effusive flow) while the right half is for thiophosgene at a rotational temperature of 10-15 K (supersonic beam). The laser CO_2 excitation frequency for both sets of spectra is 944 cm^{-1}. (A slower scan of the room temperature spectrum is shown in Fig. VI.1.c.)

Two unexpected features that these excitation spectra display are: the extent of the ground state depletion and the uniform decrease in absorption over the entire rotational contour. Whether measured by integration or by peak height analysis, the depletion value for a 100 mJ pulse (measured before the final copper mirror) for room temperature thiophosgene, is (66±2%). For cooled thiophosgene the value is (52±2%).

The ground state depletion value can be used as a lower limit to the average number of photons absorbed. For example, a depletion of 66% means that a minimum of .66 photons per molecule (or 66 photons per 100 molecules) are absorbed. If each molecule makes no more than a single quantum transition, i.e. if there are no multiple-photon transitions, and if the excited vibrational states do not absorb, then this minimum becomes an equality. In reality, however, neither of these conditions holds and the actual average photon absorption is many times higher than the fractional ground state depletion.

The uniform depletion over all frequencies in the laser excitation

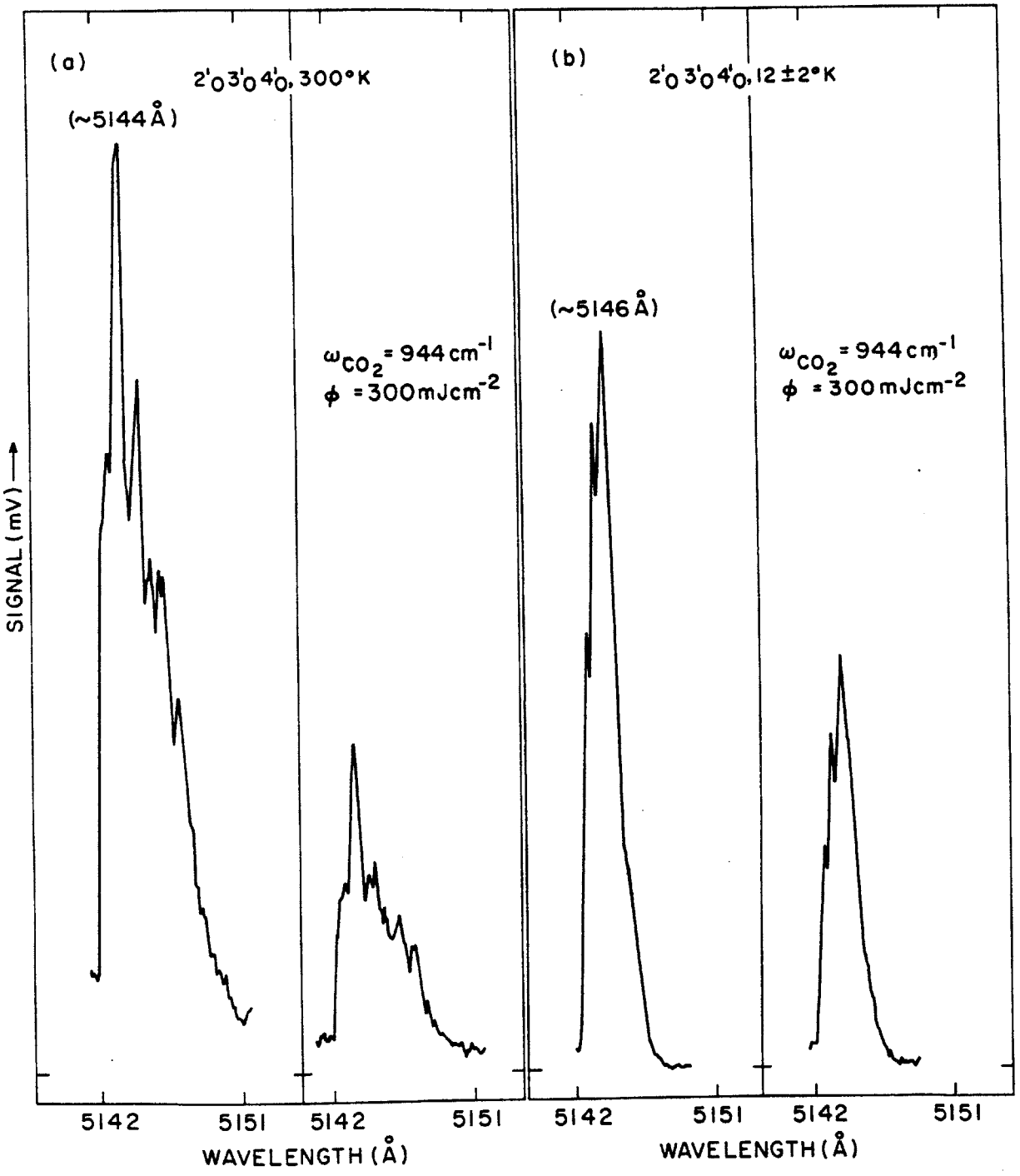


Fig.VI.1. Laser fluorescence excitation spectra of the $2_0^1 3_0^1 4_0^1$ combination band with and without CO_2 laser excitation. Scan speed is 0.6 nm min^{-1}. Infrared fluence is ~300 mJ cm^{-2}.
(a) 298 K (effusive beam).
(b) 12±2 K (supersonic beam).

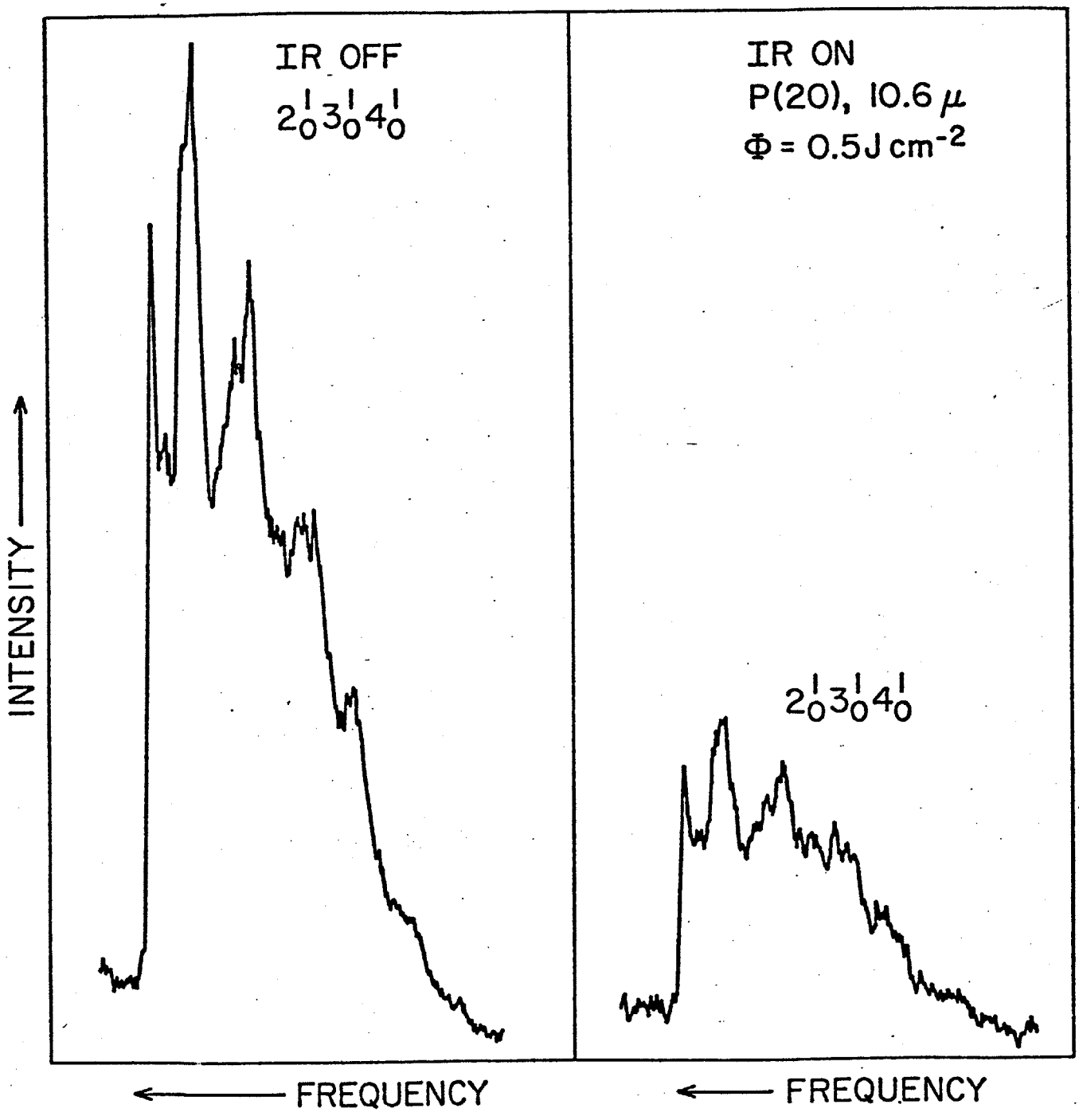


Fig.VI.1. Infrared fluence is ~300 mJ cm^{-2}.
(c) Higher resolution spectra of the $2_0^1 3_0^1 4_0^1$ for thiophosgene at 298 K. scan speed is 0.2 nm min^{-1}.

fluorescence spectrum deserves some comment. Since the linewidth of the dye laser is 0.3 cm^{-1} and the J spacing in the visible (and infrared) spectrum is <0.01 cm^{-1}, we cannot fully resolve the rotational structure of the $2_0^1 3_0^1 4_0^1$ spectrum. Hence, we cannot say with certainty that all transitions in the visible spectrum decrease in intensity when the infrared laser is turned on. Since each transition represents a ground rotational state whose population is proportional to the intensity of that transition, this means we cannot claim that all ground rotational states are depleted by the infrared laser. Nonetheless, many more states do interact with the laser than can be accounted for on the assumption that $2\nu_4$ is the exclusive pumped mode at an excitation frequency of 944 cm^{-1}.

The interpretation of an electronic absorption spectrum perturbed by an infrared laser is complicated by the following factors.

For every rotational state of a symmetric rotor populated or depopulated by the CO_2 laser, the visible (ultraviolet) laser will excite six transitions corresponding to the selection rules:

$\Delta J = 0,\pm 1 \quad \Delta K = \pm 1$ (perpendicular transition)

$\Delta J = 0,\pm 1 \quad \Delta K = 0$ (parallel transition)

For an asymmetric rotor, changes in both K_a and K_c allow even more transitions to take place[108]. At the very least, then, one can expect to see six holes in a symmetric molecule's probe spectrum resulting for every rotational state pumped by the CO_2 laser.

The second factor that makes it difficult to predict whether or not one can expect to see hole-burning in the absorption spectrum subsequent to infrared pumping is the following: The placement of the infrared

pumped rovibrational states in the visible excitation spectrum (in any one of the six sub-bands) may not coincide with their positions in the infrared spectrum of the pumped mode. In order to predict just what changes should be seen in the probe spectrum one does the following analysis:

First, one identifies the pumped mode(s) for the excitation frequency in use and obtains a completely assigned infrared spectrum of the fundamental transition for this mode. With the knowledge of the Rabi frequency for the infrared excitation, one then tabulates all the transitions--and rotational states that these transitions emanate from--that lie within a power-broadened width of the CO_2 laser frequency.

One next looks at a completely assigned visible spectrum for the vibronic band that probes the vibrational state in question and looks, in each branch or sub-branch, for those transitions having, for their absorbing state, the rotational states pumped by the infrared laser. If these visible transitions are bunched together, then a hole-burning effect ought to be observed. If, on the other hand, they are distributed randomly throughout the sub-band, then one will not see this effect. In a rotationally resolved visible spectrum, one would then see decreased intensities in these scattered transitions; in an incompletely resolved spectrum, such as the those shown in Figs. VI.1 and VI.2, one may only see a uniform decrease in intensity over the whole visible band.

Such an analysis has been done for pumping the $2\nu_4$ mode at 944 cm^{-1} and probing the ground state with the $2_0^1 3_0^1 4_0^1$ band. The spectrum

simulation program, Fastplot[106] was used to obtain a listing of spectroscopic transitions in the infrared 4_0^2 band and electronic $2_0^1 3_0^1 4_0^1$ band. A small sample of the output listing is shown in Fig. VI.2. The results of the computer simulation are summarized in Tables VI.1a and 1b. Most of the probe transitions are found in the strong ^RR sub-band in the frequency range 19437 to 19439 cm^{-1}. However, the ^PR and ^RR sub-bands of the R branch overlap extensively so that some of the probe transitions are from the latter system.

Fig.VI.2. Sample portion of the output of "Fastplot" modified to give a listing of transitions in the synthesized spectrum. Spectrum simulated is that for the infrared transition 4_0^2. An arrow indicates the excitation frequency for the P(20),10.6 μm CO_2 laser line.

J"	K_A"	K_c"	J'	K_A'	K_c'	INTENSITY	FREQUENCY
49.00000	30.00000	19.00000	50.00000	32.00000	18.00000	1.54446	94.2295+9E+01
49.00000	31.00000	19.00000	50.00000	33.00000	18.00000	1.54446	.2295+9E+01
35.00000	24.00000	12.00000	36.00000	24.00000	13.00000	8.65912	.2297?8E+01
35.00000	23.00000	12.00000	36.00000	23.00000	13.00000	8.65912	.2297?8E+01
13.00000	9.00000	4.00000	13.00000	11.00000	3.00000	4.79274	.2297+8E+01
11.44707	4.00000	2.00000	6.00000	4.00000	3.00000	2.57888	.2299+9E+01
10.00000	10.00000	1.00000	10.00000	10.00000	0.00000	14.89491	.2300?1E+01
7.00000	7.00000	1.00000	7.00000	5.00000	2.00000	1.86497	.2305?9E+01
14.00000	9.00000	6.00000	14.00000	9.00000	5.00000	5.12680	.2303+6E+01
14.00000	8.00000	6.00000	14.00000	10.00000	6.00000	5.12636	.2307+6E+01
30.00000	17.00000	14.00000	31.00000	17.00000	15.00000	10.66144	.2311?7E+01
30.00000	16.00000	14.00000	31.00000	16.00000	15.00000	10.66144	.2311?7E+01
50.00000	45.00000	5.00000	51.00000	47.00000	4.00000	2.03912	.2311+1E+01
15.00000	7.00000	9.00000	15.00000	7.00000	8.00000	4.40032	.2315+5E+01
15.00000	6.00000	9.00000	15.00000	8.00000	8.00000	4.40032	.2317+5E+01
43.00000	39.00000	4.00000	44.00000	39.00000	5.00000	4.77841	.2313?6E+01
25.00000	10.00000	15.00000	26.00000	10.00000	14.00000	12.38303	.2317+1E+01
25.00000	11.00000	15.00000	26.00000	11.00000	14.00000	12.38303	.2317?1E+01
19.00000	4.00000	15.00000	20.00000	4.00000	14.00000	13.41850	.2325+5E+01
19.00000	5.00000	15.00000	20.00000	5.00000	14.00000	13.41850	.2325?5E+01
50.00000	45.00000	6.00000	51.00000	47.00000	8.00000	2.01519	.2327?7E+01
14.00000	0.00000	14.00000	15.00000	0.00000	14.00000	13.41489	.2325+3E+01
14.00000	1.00000	14.00000	15.00000	1.00000	14.00000	13.41489	.2325+3E+01
48.00000	27.00000	22.00000	49.00000	29.00000	21.00000	1.28807	.2333+0E+01
48.00000	26.00000	22.00000	49.00000	28.00000	21.00000	1.28807	.2333+0E+01
8.00000	7.00000	1.00000	8.00000	7.00000	2.00000	4.36097	.2337+6E+01
49.00000	43.00000	6.00000	50.00000	45.00000	4.00000	2.98559	.2346?1E+01
38.00000	29.00000	10.00000	39.00000	29.00000	11.00000	7.39832	.2346+9E+01
38.00000	28.00000	10.00000	39.00000	28.00000	11.00000	7.39824	.2346+9E+01
24.00000	10.00000	15.00000	25.00000	10.00000	14.00000	12.40191	.2345?1E+01
24.00000	9.00000	15.00000	25.00000	9.00000	14.00000	12.40191	.2345?1E+01
15.00000	6.00000	10.00000	15.00000	6.00000	9.00000	4.15456	.2344+0E+01
15.00000	5.00000	10.00000	15.00000	7.00000	9.00000	4.15456	.2345?0E+01
20.00000	6.00000	15.00000	21.00000	6.00000	14.00000	13.42242	.2350?0E+01
20.00000	5.00000	15.00000	21.00000	5.00000	14.00000	13.42242	.2350?0E+01
49.00000	41.00000	9.00000	50.00000	43.00000	8.00000	3.05375	.2351?5E+01
5.00000	4.00000	2.00000	5.00000	2.00000	3.00000	2.05436	.2356?3E+01
49.00000	32.00000	18.00000	50.00000	34.00000	17.00000	1.63914	.2356+4E+01
49.00000	31.00000	18.00000	50.00000	33.00000	17.00000	1.63914	.2356?4E+01
42.00000	42.00000	1.00000	43.00000	42.00000	2.00000	1.14775	.2356+5E+01
42.00000	42.00000	0.00000	43.00000	42.00000	1.00000	1.14775	.2356?5E+01
5.00000	3.00000	2.00000	5.00000	3.00000	3.00000	2.06909	.2357+6E+01
49.00000	42.00000	8.00000	50.00000	44.00000	7.00000	3.05455	.2357+5E+01
48.00000	41.00000	7.00000	49.00000	43.00000	6.00000	4.60317	.2357+8E+01
42.00000	41.00000	2.00000	43.00000	41.00000	3.00000	2.24427	.2361?1E+01
42.00000	41.00000	1.00000	43.00000	41.00000	2.00000	2.24414	.2361?0E+01
23.00000	8.00000	15.00000	24.00000	8.00000	14.00000	12.41463	.2356?0E+01
23.00000	9.00000	15.00000	24.00000	9.00000	14.00000	12.41463	.2362?0E+01
21.00000	7.00000	15.00000	22.00000	7.00000	14.00000	13.22397	.2356+4E+01
21.00000	6.00000	15.00000	22.00000	6.00000	14.00000	13.22397	.2356+4E+01
22.00000	7.00000	15.00000	23.00000	7.00000	14.00000	13.02173	.2361?0E+01
22.00000	8.00000	15.00000	23.00000	8.00000	14.00000	13.02173	.2360?0E+01
9.00000	9.00000	0.00000	9.00000	9.00000	1.00000	13.00047	.2356+0E+01
49.00000	39.00000	10.00000	50.00000	41.00000	8.00000	2.88458	.2356+7E+01
48.00000	40.00000	8.00000	49.00000	42.00000	7.00000	4.41334	.2370?6E+01
15.00000	4.00000	11.00000	15.00000	6.00000	10.00000	3.44198	.2371?8E+01
15.00000	5.00000	11.00000	15.00000	5.00000	10.00000	3.44198	.2371?8E+01
14.00000	8.00000	7.00000	14.00000	8.00000	6.00000	4.98711	.2371?3E+01
14.00000	7.00000	7.00000	14.00000	9.00000	6.00000	4.98711	.2371?3E+01
13.00000	9.00000	5.00000	13.00000	9.00000	4.00000	4.93927	.2377+3E+01
12.00000	9.00000	3.00000	12.00000	11.00000	2.00000	3.41516	.2377+2E+01
13.00000	8.00000	5.00000	13.00000	10.00000	4.00000	4.93167	.2375+8E+01
51.00000	48.00000	3.00000	52.00000	50.00000	2.00000	1.00775	.2375+2E+01

J"	K_A"	K_c"	J'	K_A'	K_c'	INTENSITY	FREQUENCY
51.00000	48.00000	4.00000	52.00000	50.00000	3.00000	1.00770	94.2375+8E+01
15.00000	1.00000	14.00000	15.00000	3.00000	13.00000	1.47839	.2377?4E+01
15.00000	2.00000	14.00000	15.00000	2.00000	13.00000	1.47439	.2377?4E+01
42.00000	40.00000	3.00000	43.00000	40.00000	4.00000	3.29021	.2381?1E+01
3.00000	0.00000	3.00000	2.00000	0.00000	2.00000	2.30598	.2381+9E+01
3.00000	1.00000	3.00000	2.00000	1.00000	2.00000	2.50514	.2381+9E+01
15.00000	3.00000	12.00000	15.00000	5.00000	11.00000	3.05754	.2384?2E+01
15.00000	4.00000	12.00000	15.00000	4.00000	11.00000	3.05754	.2384?2E+01
10.00000	9.00000	2.00000	10.00000	9.00000	1.00000	4.73754	.2384?4E+01
42.00000	40.00000	2.00000	43.00000	40.00000	3.00000	3.27693	.2384+6E+01
15.00000	2.00000	13.00000	15.00000	4.00000	12.00000	2.40280	.2385?3E+01
15.00000	3.00000	13.00000	15.00000	3.00000	12.00000	2.40280	.2385?3E+01
29.00000	16.00000	14.00000	30.00000	16.00000	15.00000	10.98952	.2387?6E+01
29.00000	15.00000	14.00000	30.00000	15.00000	15.00000	10.98952	.2387?6E+01
42.00000	35.00000	7.00000	43.00000	35.00000	8.00000	5.97515	.2389?7E+01
49.00000	40.00000	10.00000	50.00000	42.00000	9.00000	2.81527	.2389?9E+01
47.00000	24.00000	24.00000	48.00000	25.00000	23.00000	1.11901	.2390?4E+01
47.00000	23.00000	24.00000	48.00000	25.00000	23.00000	1.11901	.2390?4E+01
32.00000	20.00000	13.00000	33.00000	20.00000	14.00000	9.72821	.2392?2E+01
32.00000	19.00000	13.00000	33.00000	19.00000	14.00000	9.72821	.2392?2E+01
6.00000	6.00000	1.00000	6.00000	4.00000	3.00000	1.90403	.2399?4E+01
49.00000	32.00000	17.00000	50.00000	34.00000	16.00000	1.73979	.2393?0E+01
49.00000	33.00000	17.00000	50.00000	35.00000	16.00000	1.73979	.2393?0E+01
15.00000	2.00000	14.00000	16.00000	2.00000	15.00000	13.43595	.2402?4E+01
15.00000	1.00000	14.00000	16.00000	1.00000	15.00000	13.43595	.2402?4E+01
4.00000	3.00000	2.00000	4.00000	1.00000	3.00000	1.49746	.2402?1E+01
4.00000	2.00000	2.00000	4.00000	2.00000	3.00000	1.50185	.2404?7E+01
9.00000	9.00000	1.00000	9.00000	9.00000	0.00000	12.84158	.2402?8E+01
36.00000	26.00000	11.00000	37.00000	26.00000	12.00000	8.10243	.2406?9E+01
36.00000	25.00000	11.00000	37.00000	25.00000	12.00000	8.10242	.2406?9E+01
7.00000	6.00000	1.00000	7.00000	6.00000	2.00000	4.15388	.2406?8E+01
11.00000	9.00000	3.00000	11.00000	9.00000	2.00000	4.69473	.2409?1E+01
39.00000	31.00000	9.00000	40.00000	31.00000	10.00000	5.95684	.2406?2E+01
39.00000	30.00000	9.00000	40.00000	30.00000	10.00000	5.95504	.2406?0E+01
42.00000	37.00000	6.00000	43.00000	37.00000	7.00000	5.76730	.2411?0E+01
12.00000	9.00000	4.00000	12.00000	9.00000	3.00000	4.68598	.2413?2E+01
42.00000	39.00000	4.00000	43.00000	39.00000	4.00000	4.24470	.2413?2E+01
48.00000	28.00000	21.00000	49.00000	30.00000	20.00000	1.37275	.2422?6E+01
48.00000	27.00000	21.00000	49.00000	29.00000	20.00000	1.37276	.2422?6E+01
34.00000	23.00000	12.00000	35.00000	23.00000	13.00000	9.87739	.2423?6E+01
34.00000	22.00000	12.00000	35.00000	22.00000	13.00000	9.87739	.2423?6E+01
14.00000	7.00000	8.00000	14.00000	7.00000	7.00000	4.54967	.2424+7E+01
14.00000	6.00000	8.00000	14.00000	8.00000	7.00000	4.54967	.2424+7E+01
2.00000	1.00000	1.00000	1.00000	1.00000	0.00000	1.49533	.2424?6E+01
12.00000	5.00000	4.00000	12.00000	10.00000	3.00000	4.57833	.2429?3E+01
49.00000	38.00000	11.00000	50.00000	40.00000	10.00000	2.40644	.2427?2E+01
49.00000	39.00000	11.00000	50.00000	41.00000	10.00000	2.40136	.2428+7E+01
49.00000	33.00000	16.00000	50.00000	35.00000	15.00000	1.84769	.2431?9E+01
49.00000	34.00000	16.00000	50.00000	36.00000	15.00000	1.84769	.2431?9E+01
42.00000	39.00000	3.00000	43.00000	39.00000	4.00000	4.20745	.2433?6E+01
49.00000	43.00000	7.00000	50.00000	45.00000	6.00000	2.49022	.2441?6E+01
42.00000	39.00000	5.00000	43.00000	38.00000	6.00000	5.12366	.2441?1E+01
13.00000	9.00000	4.00000	13.00000	8.00000	5.00000	4.76910	.2443+2E+01
13.00000	7.00000	6.00000	13.00000	9.00000	5.00000	4.76891	.2443+6E+01
28.00000	15.00000	14.00000	29.00000	15.00000	14.00000	11.11041	.2445?8E+01
28.00000	14.00000	14.00000	29.00000	14.00000	14.00000	11.11041	.2445?8E+01
8.00000	8.00000	0.00000	8.00000	8.00000	1.00000	11.24353	.2445?3E+01
49.00000	37.00000	12.00000	50.00000	39.00000	11.00000	2.40621	.2450+9E+01
49.00000	34.00000	15.00000	50.00000	36.00000	14.00000	1.94464	.2445?0E+01
49.00000	35.00000	15.00000	50.00000	37.00000	14.00000	1.94464	.2445?0E+01
49.00000	38.00000	12.00000	50.00000	40.00000	11.00000	2.40381	.2445?9E+01
40.00000	33.00000	8.00000	41.00000	33.00000	9.00000	5.57040	.2445+9E+01
16.00000	2.00000	14.00000	17.00000	2.00000	14.00000	13.34719	.2462+8E+01

P(22) 10.6MM

Table VI.1a

Transitions Pumped by 944 cm^{-1} (ω_R=0.02 cm^{-1})

J"	K_a"	K_c"	J'	K_a'	K_c'	Frequency (cm^{-1})	Intensity (Arbitrary Units)
47	29	19	48	31	18	942.824	1.6
47	28	19	48	30	18	942.824	1.6
7	5	3	7	5	2	942.824	3.0
40	38	3	41	38	4	942.824	3.6
18	6	13	19	6	14	942.826	12.1
18	5	13	19	5	14	942.826	12.1
30	19	12	31	19	13	942.827	9.7
30	18	12	30	18	13	942.827	9.7
40	38	2	41	38	3	942.828	3.6
3	3	1	3	3	0	942.831	3.7
9	5	5	9	5	4	942.838	3.3
9	4	5	9	4	4	942.838	3.3
46	39	7	47	41	6	942.838	5.1
7	4	3	7	6	2	942.839	2.9
5	4	2	5	4	1	942.839	2.7
39	33	7	40	33	8	942.840	6.6
46	24	22	47	26	21	942.842	1.3
46	25	22	47	27	21	942.842	1.3
14	3	12	15	3	13	942.843	11.7
14	2	12	15	2	13	942.844	11.7
6	4	2	6	6	1	942.844	1.8
8	5	4	8	5	3	942.844	3.2

Table VI.1a (continued)

J"	K_a"	K_c"	J'	K_a'	K_c'	Frequency (cm^{-1})	Intensity (Arbitrary Units).
8	4	4	8	6	3	942.846	3.2
25	13	13	26	13	14	942.854	11.1
25	13	13	26	13	13	942.854	11.1
11	3	9	11	3	8	942.857	2.4
11	2	9	11	4	8	942.857	2.4
40	37	4	41	37	5	942.859	4.7
19	7	13	20	7	14	942.860	12.0
19	6	13	20	6	13	942.860	12.0
41	35	6	42	35	7	942.861	6.6

Table VI.1b

R Branch $2_0^1 3_0^1 4_0^1$ Transitions Affected by CO_2 Laser Excitation of $2\nu_4$ (ω_R = 0.02 cm^{-1})

J"	Ka"	K_c"	J'	K_a'	K_c'	Frequency (cm^{-1})	Intensity (Arbitrary Units)
47	29	19	48	30	18	19439.2	2.3
47	28	19	48	31	18	19439.2	2.3
7	5	3	8	6	2	1938.8	1.0
40	38	3	41	39	2	19438.3	11.7
18	6	13	19	6	14	19438.5	11.7
18	5	13	19	5	14	19438.5	11.8
30	19	12	31	18	13	19328.2	8.0
30	18	12	31	19	13	19328.2	8.0
40	38	2	4	39	3	19438.3	8.0
3	3	1	4	2	2	19437.7	1.5
3	3	1	4	4	0	19437.9	1.9
9	5	5	10	4	6	19438.2	5.5
9	4	5	10	5	6	19438.2	5.5
46	39	7	47	42	6	19437.6	1.7
7	4	3	8	5	4	19438.1	37
5	4	2	6	3	3	19437.9	2.7
39	33	7	40	34	6	19438.1	3.9
46	24	22	47	25	23	19435.3	7.5
46	24	22	48	27	21	19440.1	1.9
46	25	22	47	26	21	19440.1	1.9
14	3	12	14	4	11	19437.6	2.5
14	3	12	15	2	13	19438.3	11.5
14	2	12	14	3	11	19327.6	2.5

Table VI.1b (continued)

J"	K_a"	K_c"	J'	K_a'	K_c'	Frequency (cm^{-1})	Intensity (Arbitrary Units)
14	2	12	14	3	13	19438.3	11.5
6	4	2	7	5	3	19328.1	2.9
8	5	4	9	4	5	19438.2	4.6
8	4	4	9	5	5	19438.2	4.6
25	13	13	26	14	12	19441.3	1.7
25	12	13	26	15	12	19441.3	1.25
11	3	9	12	2	10	19438.1	9.0
11	2	9	12	3	10	19438.2	9.0
40	37	4	41	38	3	19438.1	9.7
19	7	13	20	6	14	19438.5	11.5
19	6	13	20	7	14	19438.5	11.5
41	35	6	42	38	5	19438.8	1.4
41	35	6	42	36	7	19437.0	2.7

Examination of Table VI.1 shows that the 31 states depleted by pumping $2\nu_4$, with a power broadening of 0.02 cm^{-1}, are distributed over a much larger frequency region (19437.0 cm^{-1} to 19439.2 cm^{-1}) in the $2_0^1 3_0^1 4_0^1$ spectrum than in the 0.02 cm^{-1} region of the $2\nu_4$ infrared spectrum. Most of the R branch transitions which probe these 31 states (18) however are concentrated between 19437.9 cm^{-1} and 19438.3 cm^{-1}. If the resolution of our dye laser were better than the 0.01 cm^{-1} separation between neighboring transitions, then we would see a relatively small region in the R branch where the intensity of the affected transitions decreased. For an incompletely resolved spectrum, such as those recorded here, we might see a localized decrease in intensity in that region. Whether that decrease of 18 transitions would be noticeable against a background of 630 transitions, however, is doubtful. Certainly the extensive bleaching we see in the $2_0^1 3_0^1 4_0^1$ spectrum cannot be due to these few transitions being affected by the CO_2 laser.

The dependence of the ground state depletion on the CO_2 laser excitation frequency has been measured for thiophosgene in an effusive beam and in a supersonic beam. When the depletion values are plotted as a function of frequency the resulting curve can be thought of as a sort of infrared multiphoton absorption spectrum. Superimposed onto the frequency dependence plots (Fig. VI.3) is an enlargement of the same frequency region of a conventional infrared spectrum[129]. One would expect that, at those frequencies where thiophosgene absorbs most strongly, the ground state depletion would also be greatest. However, this is not observed. In fact, the total lack of correlation between the "IRMPA" spectrum and the conventional (one photon, high pressure) infrared spectrum is startling.

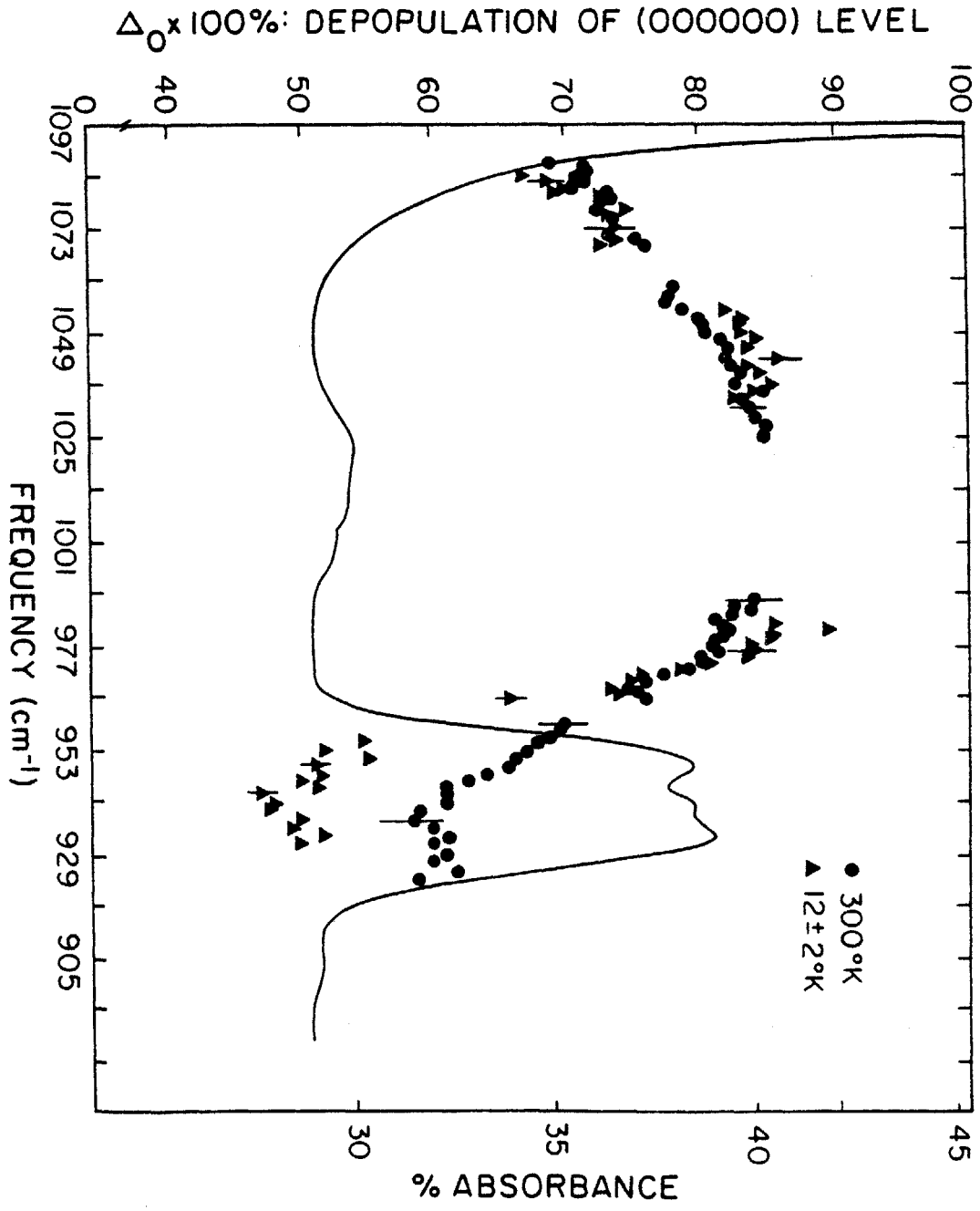


Fig.VI.3. Dependence of the ground state depletion on the CO_2 laser excitation frequency for thiophosgene at two rotational temperatures (300 K and 12±2 K). Infrared fluence is ~300 mJ cm^{-2}. The solid line is an enlarged section of an FTIR spectrum showing the ν_4 overtone.

The frequency dependence of the ground state depletion for cooled thiophosgene differs from that for room temperature thiophosgene only in the 10.6 μm P branch. This indicates that there must be some selectivity to the pumping process, at least in this region, although more experiments need to be done before we can propose more specific explanations.

Figure VI.4 shows the 10.6 μm, P branch section (910 cm^{-1} to 960 cm^{-1}) of the frequency dependence results for room temperature thiophosgene. Superimposed onto this plot is, again, the conventional infrared spectrum of the same wavelength region and photoacoustic data obtained for thiophosgene at 500 mTorr and under the same excitation conditions for which the double resonance data was taken. The data was recorded by D. M. Brenner (at Brookhaven) and is calibrated in terms of average number of photons absorbed. This so-called photoacoustic spectrum has been enlarged in the figure just enough so that it coincides as closely as possible with the infrared spectrum.

The photoacoustic data correlate quite well with the infrared spectrum; neither resemble--even remotely--the double resonance depletion data. When analyzing the depletion data one must remember that the values for the ground state depopulation, expressed as a fraction, represent lower limits to the average number of photons absorbed. With this in mind the reader will notice that there is greater than two orders of magnitude difference between the average photon absorption for the photoacoustic data and the IR-VIS-DR data: At 944 cm^{-1} more than 0.66 photons per thiophosgene molecule are absorbed in the double resonance experiment whereas the photoacoustic measurements give an average absorption of only ~0.01 photons/molecule at this frequency.

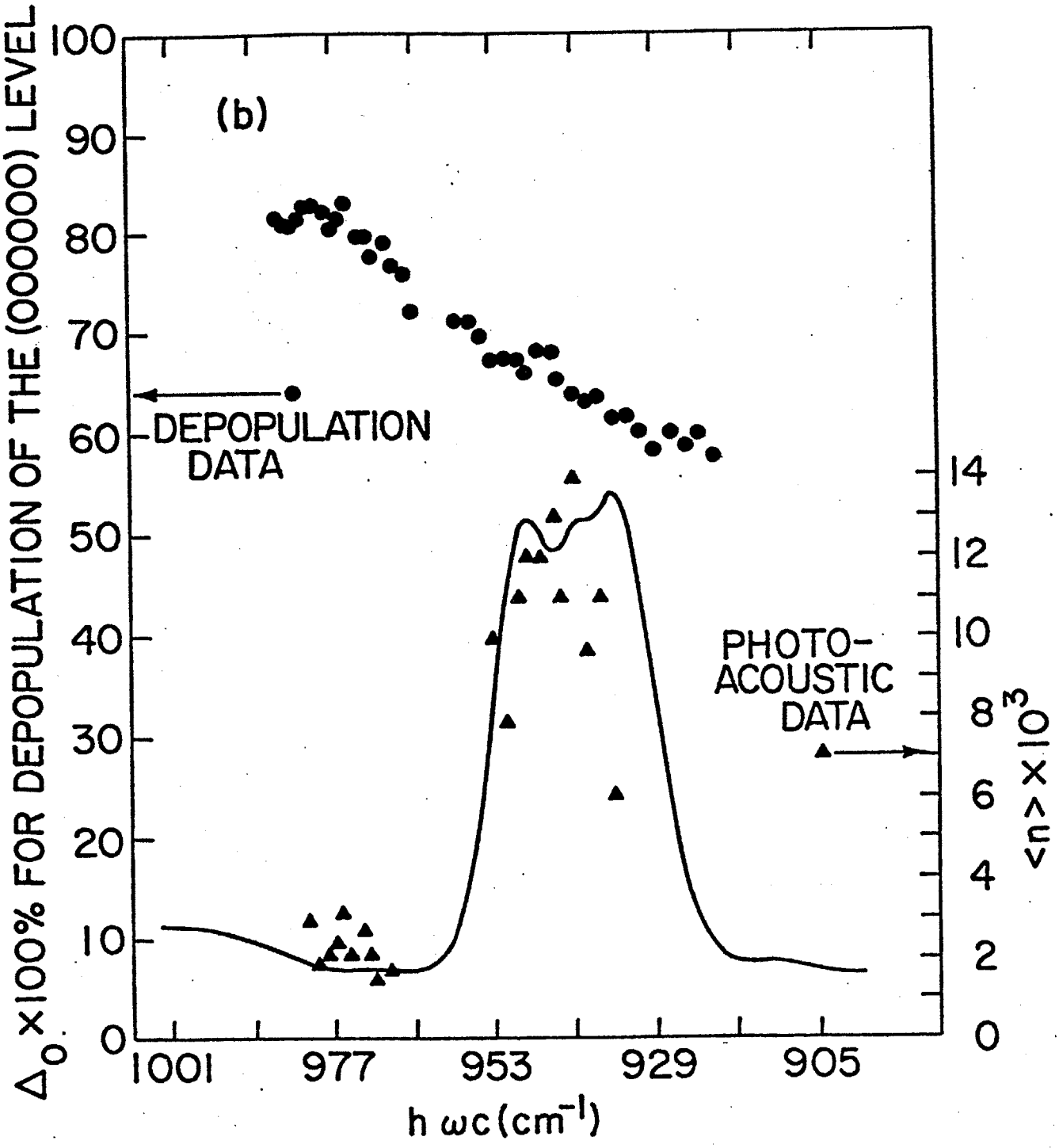


Fig.VI.4. Comparison of CO_2 laser excitation frequency data with photoacoustic data. Data for the former are the same as that in Figure 3 but over a smaller frequency range. Values for the photoacoustic data are given by the right-hand axis. Thiophosgene pressure is 500 mTorr. Solid line is an enlarged section of an FTIR spectrum showing the ν_4 overtone. Infrared fluence for both the photoacoustic and IR-VIS-DR data are ~300 mJ cm^{-2}.

If the infrared spectrum, initially calibrated in transmittance, were recalibrated in terms of average number of photons absorbed, the same discrepancy would be found between this spectrum and the ground state depletion data.

The important point to remember when interpreting these three sets of data is that they are taken for thiophosgene at 3 different pressures (or number densities). The conventional infrared spectrum was recorded for thiophosgene at approximately 30 Torr; the photoacoustic data are for $CSCl_2$ at 500 mTorr and the IR-VIS-DR depletion data were taken of thiophosgene under collisionless conditions in an effusive beam.

Qualitative information about the order of the multiphoton pathway(s) and about the existence of a threshold and saturation intensity for multiphoton absorption can be derived from a fluence dependence study of the ground state depletion. Fluence studies for room temperature thiophosgene excited at four different excitation frequencies (944 cm^{-1}, 978 cm^{-1}, 1043 cm^{-1} and 1081 cm^{-1}) are shown in Figures VI.5a and VI.5b. The corresponding data for rotationally cooled thiophosgene are shown in Figures VI.6a and VI.6b. I must reiterate that the energy/pulse values listed on the absicca of each fluence dependence graph is that measured prior to the last copper mirror and should be multiplied by approximately 0.6 to obtain the energy/pulse at the interaction region. (This correction is made in bulb experiments where knowledge of the exact pulse energy is not critical.) It must also be remembered that, when carrying out these experiments, the variable that is changed is the pulse energy

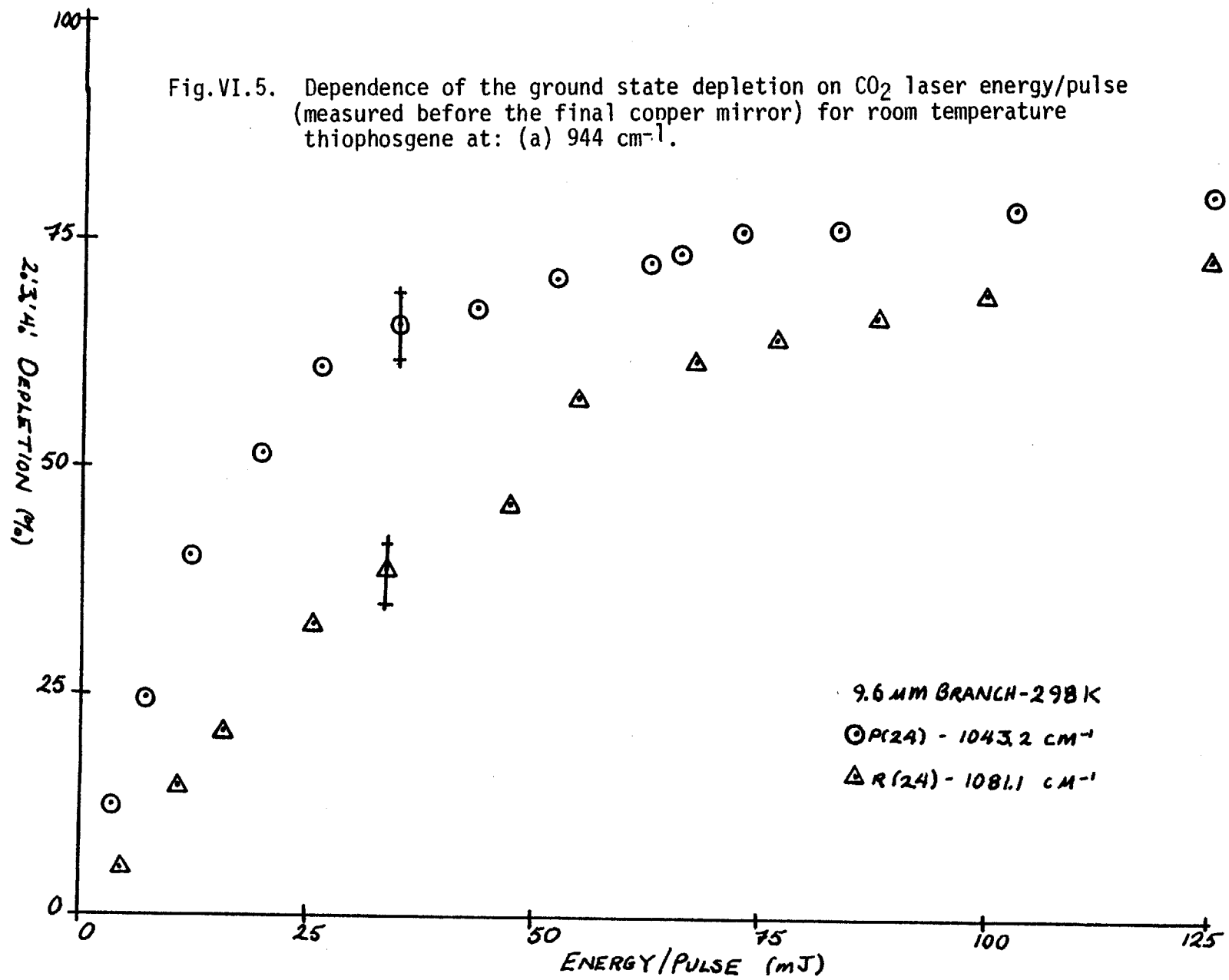


Fig.VI.5. Dependence of the ground state depletion on CO_2 laser energy/pulse (measured before the final copper mirror) for room temperature thiophosgene at: (a) 944 cm^{-1}.

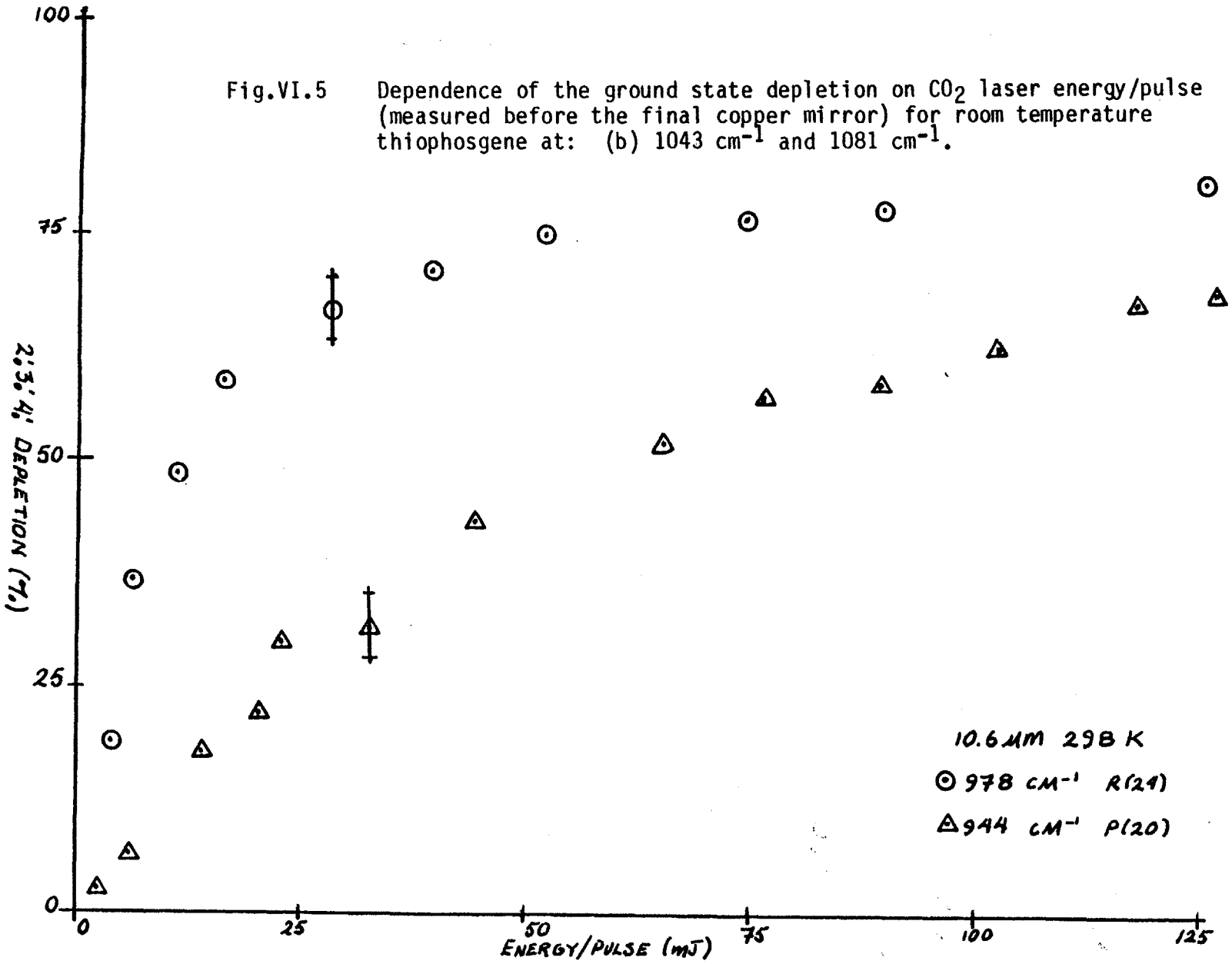


Fig.VI.5 Dependence of the ground state depletion on CO_2 laser energy/pulse (measured before the final copper mirror) for room temperature thiophosgene at: (b) 1043 cm^{-1} and 1081 cm^{-1}.

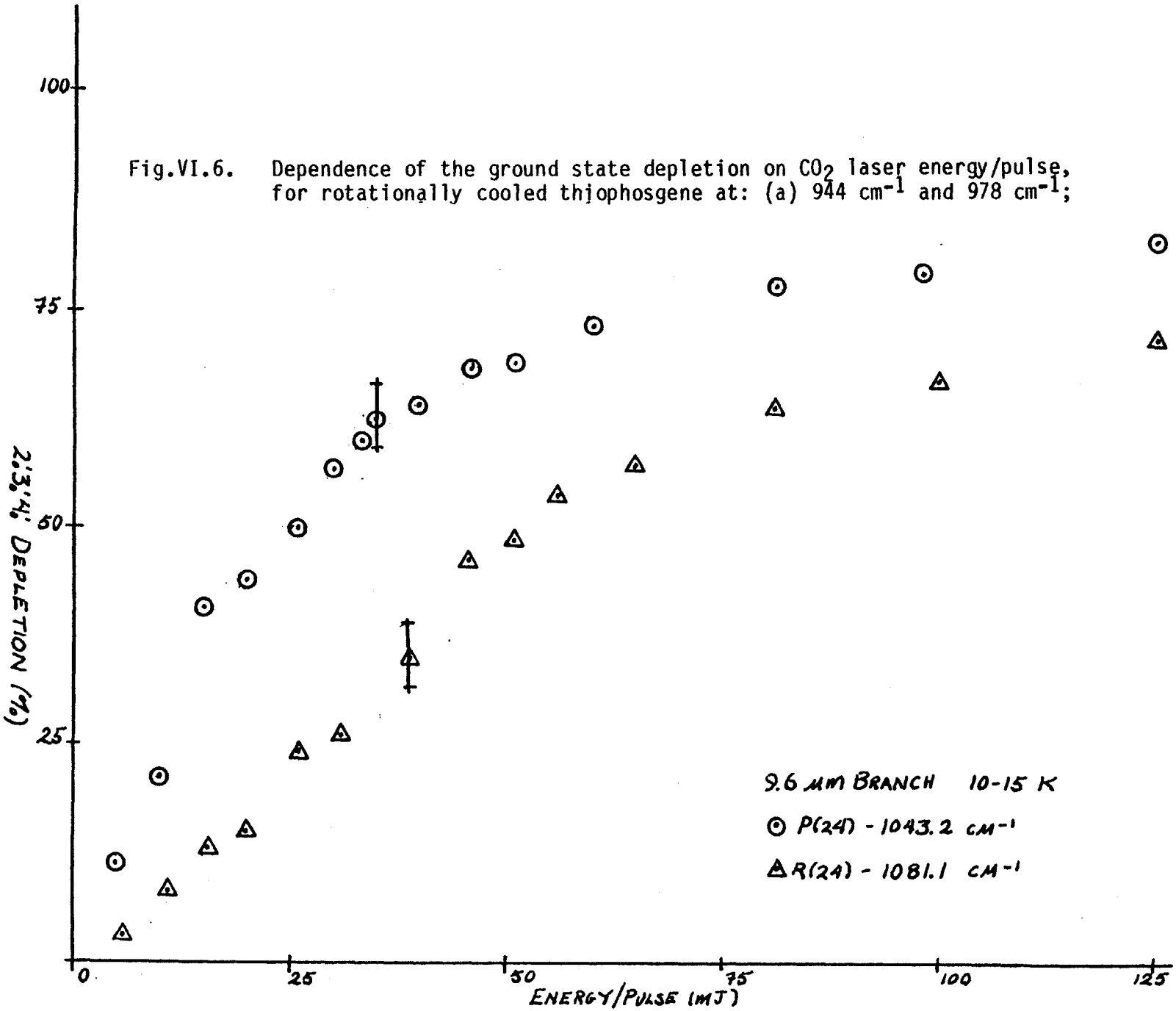


Fig.VI.6. Dependence of the ground state depletion on CO_2 laser energy/pulse, for rotationally cooled thiophosgene at: (a) 944 cm^{-1} and 978 cm^{-1};

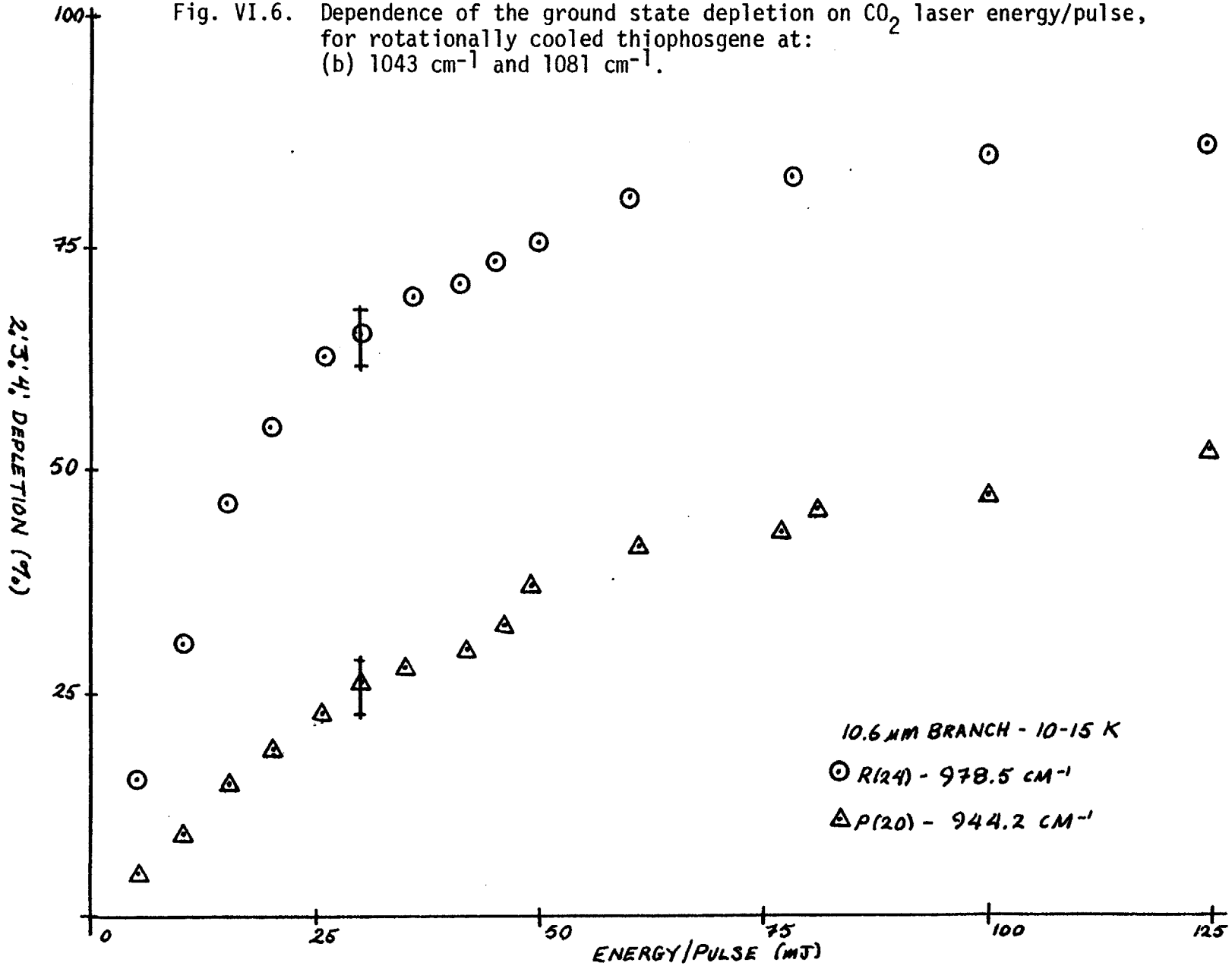


Fig. VI.6. Dependence of the ground state depletion on CO_2 laser energy/pulse, for rotationally cooled thiophosgene at:
(b) 1043 cm^{-1} and 1081 cm^{-1}.

and that this quantity is proportional to both the pulse fluence and pulse intensity. Therefore we are justified in using all three terms interchangeably. (To convert the energy values to intensity values divide by 200 nsec and again by 0.18 cm^2, i.e. divide by 3.6×10^{-8}sec cm^2.)

Several features are immediately apparent upon examination of the data: First, there is no measureable threshold for absorption for excitation at any of the laser frequencies or at either rotational temperature. Second, pumping at the frequencies 978 cm^{-1} and 1043 cm^{-1} is more facile, as evidenced by the earlier onset of saturation, than at the frequencies 944 cm^{-1} and 1081 cm^{-1}. This is in accordance with the frequency dependence studies which showed greater ground state depletion at the two intermediate frequencies than at the other two. Third, the intensities at which saturation occurs is remarkably low--especially when compared with reported saturation values for other systems. For pumping room temperature thiophosgene at 978 cm^{-1} the onset of saturation begins at about 20 mJ pulse, or approximately 3×10^4 W cm^{-2}. Last, supersonically-cooled thiophosgene seems to absorb less efficiently than room temperature thiophosgene as evidenced by the higher onsets of saturation for the former. Again, this agrees with observations made from the frequency dependence data.

In the rate equation formalism of IRMPA, the rate of photon absorption is proportional to the intensity of the light field raised to the nth power, in which N is the order of the multiphoton process. If we make the reasonable approximation that the ground state depletion is proportional to the absorption rate, then we can use the fluence data to extract estimates for N for each excitation frequency and rotational

temperature. To do so we plot the logarithm of the depletion data against the logarithm of the energy/pulse and find the best fit line to the first few data points, i.e. in the fluence region well before saturation. The slope of the line gives N and the intercept gives a number that is proportional to the ground state depletion cross section.

The results of such a least-squares analysis are presented in Table VI.1. The fluence range over which the best fit lines were determined vary from one fluence study to another; it was chosen to be as large as possible without showing saturation effects as manifested by a leveling off of the depopulation. For excitation at 978.5 cm^{-1} (298 K) saturation occurs at a very low fluence so that the range of points chosen is correspondingly very small.

Table VI.2

Least Squares Analysis of Log-Log Plots of Fluence Data

CO_2 Laser Freq.(cm^{-1})	Pressure (mTorr)	Rot'l Temp(K)	Energy/Pulse Range(mJ)	N	ℓn A	Correl. Coef.
944.2	0.1	295	2.5-20	1.12	-0.19	0.997
944.2	0.1	12	5-20	0.95	0.09	0.999
978.5	0.1	295	4-16	0.82	1.87	0.986
978.5	0.1	295	4-11	0.93	1.67	0.994
978.5	0.1	12	2.5-20	1.67	0.77	0.986
978.5	0.1	12	2.5-15	1.80	0.67	0.967
1043.2	0.1	295	3.5-20	0.83	1.54	0.992
1043.2	0.1	12	5-20	1.04	0.74	0.985
1081.1	0.1	29	4.5-26	1.03	0.15	0.999
1081.1	0.1	12	6-26	1.31	-1.10	0.988
978.5	10	295	5-20	0.93	1.02	0.981

$$\%\Delta = AI^N \rightarrow \ell n(\%\Delta) = \ell nA + N\ell nI$$

When reading the table the reader should keep in mind that the value of N (and A) so obtained do not represent the dynamics of a single rovibrational ladder but represent a large number of ladders ensemble-averaged together. Thiophosgene's small rotational constants result in many rotational ground states being populated even at 10 K. If the observation that nearly all rotational states are depleted is true, then can expect many pumped mode ladders to be driven simultaneously at a single excitation frequency. (The incentive for doing supersonic beam experiments was to limit the number of ground rotational states participating in absorption and, hence, to obtain data that would be easier to interpret. However, even the rotational temperatures achieved with supersonic cooling do not seem to significantly affect our results. Boltzmann-type calculations show that a temperature of approximately 3 K is needed to limit ground state population to ~10 states.) Although the values of N so obtained in this manner are only rough estimates to the actual values, it is obvious from Table VI.2 that, under all conditions, N is very close to 1. This is in accord with the hypothesis that thiophosgene absorbs through sequential one-photon absorptions, rather than through true multiphoton absorptions.

2. Excited States

If pumping at 944 cm^{-1} drives the $2\nu_4$ manifold exclusively, as one might think from the known spectroscopy of thiophosgene, then there must be population increases in the excited states of the ladder for some fluence range. The density matrix calculations verify this (Tables VII.1). Regardless of the parameters chosen for the ladder, there is always some Rabi frequency for which there is a net population of any given excited state. With this in mind, we measured the population change of the states, $2\nu_4$ and $4\nu_4$, as a function of energy/pulse. The results are shown in Figs. VI.6 and VI.7. The electronic probe transitions are 4_2^1 and 4_4^1, respectively. The fluence study for $2\nu_4$ shows depopulation of this vibrational state at all energies. The data for the $4\nu_4$ level has a very large uncertainty due to its tiny ($\sim 10^{-4}$) ambient population and, hence, laser-induced fluorescence signal. The population at the second excited state remains more or less constant as we vary the fluence. To appreciate the significance of this latter observation one must remember that, even if only 1% of the ground state population were driven to the $4\nu_4$ level, the resulting change in population would be approximately one hundred-fold!

More highly excited states of the $2\nu_4$ manifold ($6\nu_4$, $8\nu_4$, $10\nu_4$ and $12\nu_4$) were probed at various fluences but population in each of these states--with or without CO_2 laser excitation--was too small to yield a signal.

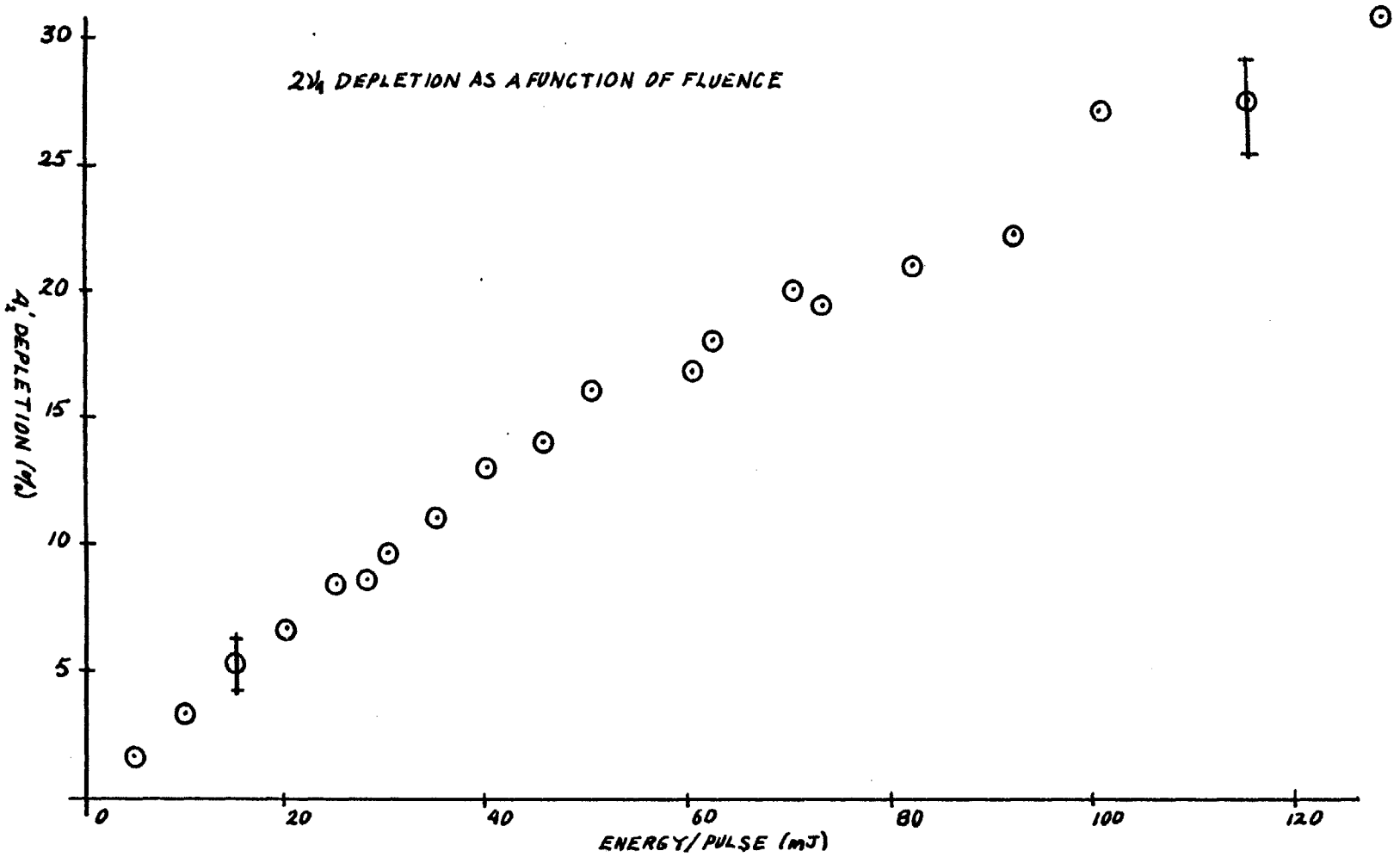


Fig.VI.7. Dependence of the $2\nu_4$ depletion on CO_2 laser energy pulse for room temperature thiophosgene. CO_2 laser excitation frequency is 944 cm^{-1}. Electronic probe transition is 4_2^1.

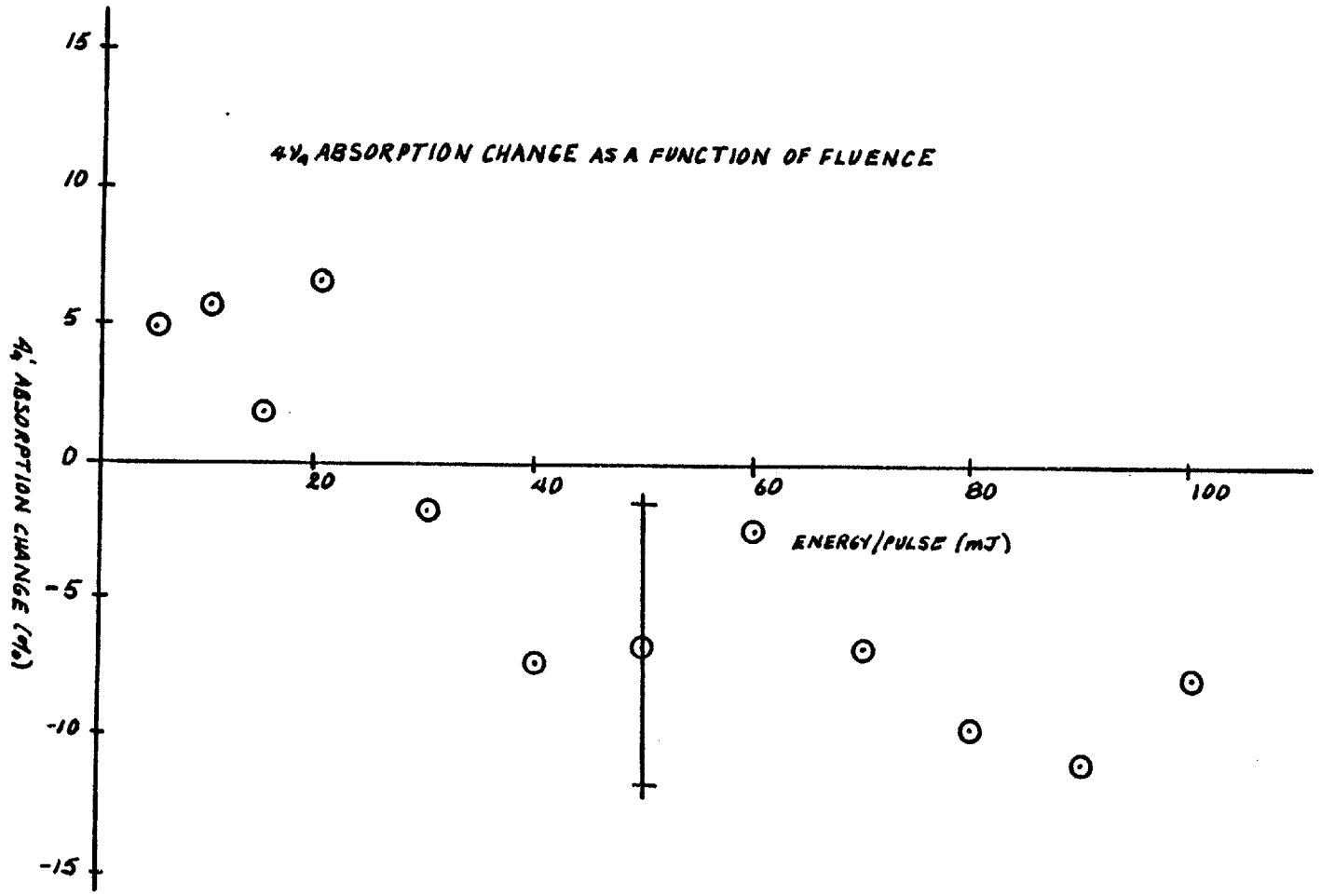


Fig. VI.8. Dependence of the $4\nu_4$ depletion on CO_2 laser energy/pulse for room temperature thiophosgene. Excitation frequency is 944 cm^{-1}. Electronic probe transition is 4_4^1.

B. Static Gas Experiments

1. Vibrationless Ground State

The unanticipated discrepancy between the conventional spectrum of thiophosgene at 30 Torr and the photoacoustic spectrum of the gas at 0.5 Torr, on the one hand, and the effusive beam frequency dependence for the ground state depletion, on the other, suggests that the mechanism for infrared absorption changes as the pressure increases. Accordingly, we measured the ground state depletion as a function of thiophosgene pressure. The resulting pressure dependence study is shown in Fig. VI.9. Except for the lowest pressure point (< 1 mTorr) all the data were obtained in bulb experiments, as described in Chapter V.

The predicted pressure effect is indeed observed. In fact, the ground state depletion begins to decrease at a pressure as low as 5 mTorr. At this pressure the probability of a molecule suffering a hard sphere collision during the 200 nsec laser pulse is only 1 in 500!

Since the pressure effect apparently occurs at a rate that is much faster than gas kinetic, it seems plausible that long-range interactions between absorbing molecules are responsible for it. To test this hypothesis, we next carried out a series of experiments in which a small amount of thiophosgene was mixed with progressively greater amounts of an added gas and the resulting ground state depletion measured. A total of ten gases were used; they represent a wide range of polarizabilities and dipole moments--from helium, having no dipole moment and a tiny polarizability, to acetonitrile, having a very large dipole moment (~3 D) and appreciable polarizability. These pressure studies are shown in Figs. VI.10-VI.13.

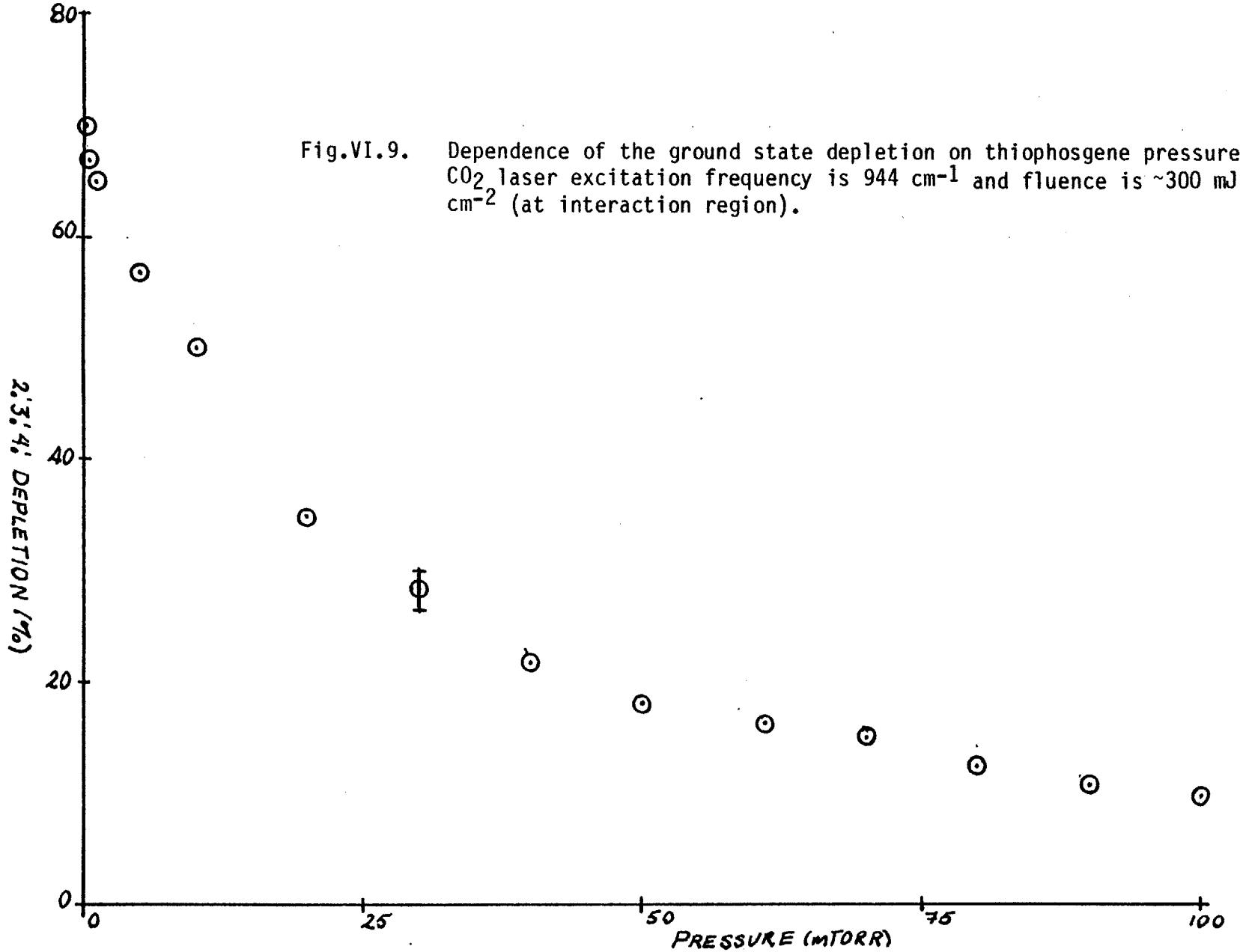


Fig.VI.9. Dependence of the ground state depletion on thiophosgene pressure. CO_2 laser excitation frequency is 944 cm^{-1} and fluence is ~300 mJ cm^{-2} (at interaction region).

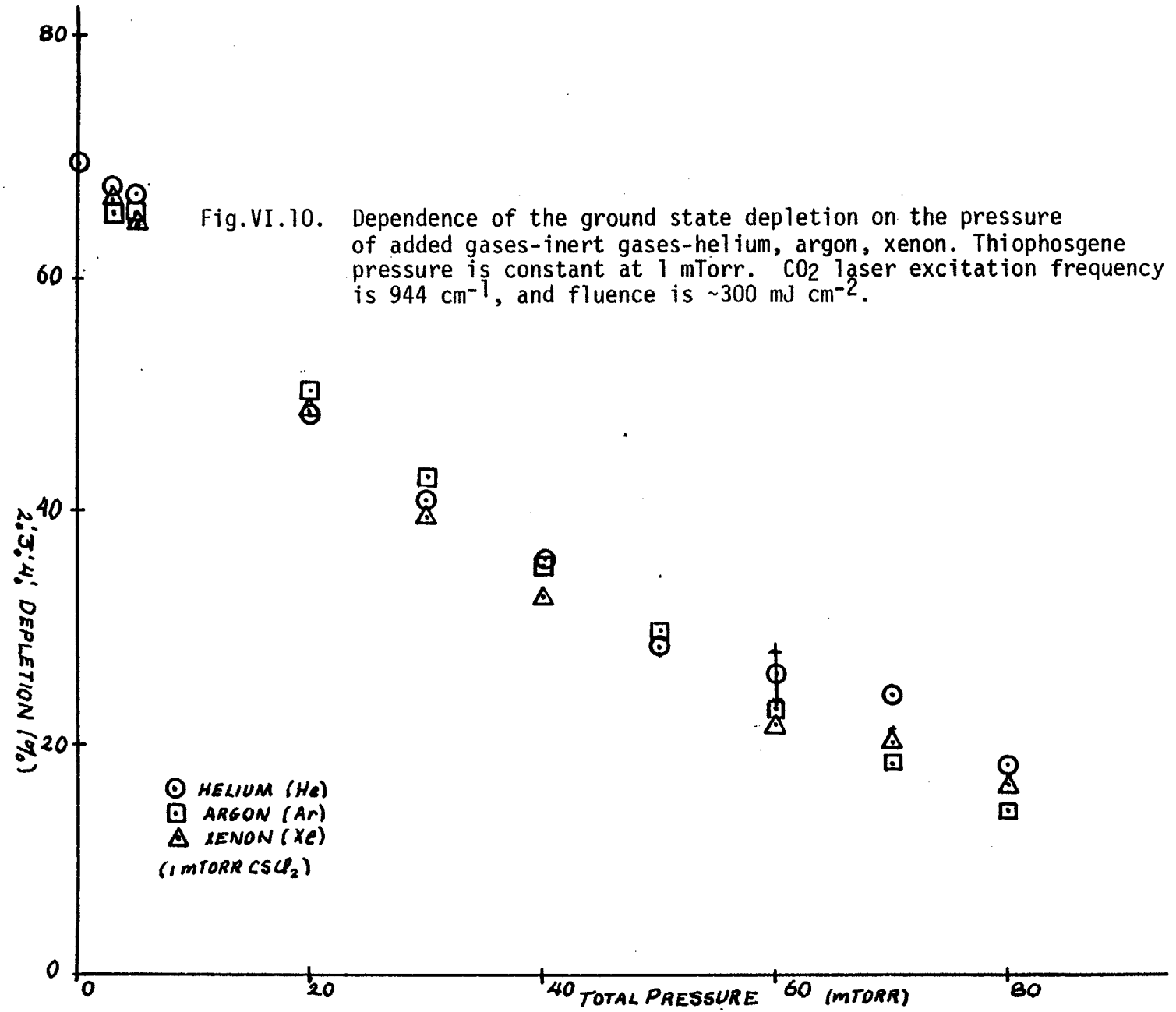


Fig.VI.10. Dependence of the ground state depletion on the pressure of added gases-inert gases-helium, argon, xenon. Thiophosgene pressure is constant at 1 mTorr. CO_2 laser excitation frequency is 944 cm^{-1}, and fluence is ~300 mJ cm^{-2}.

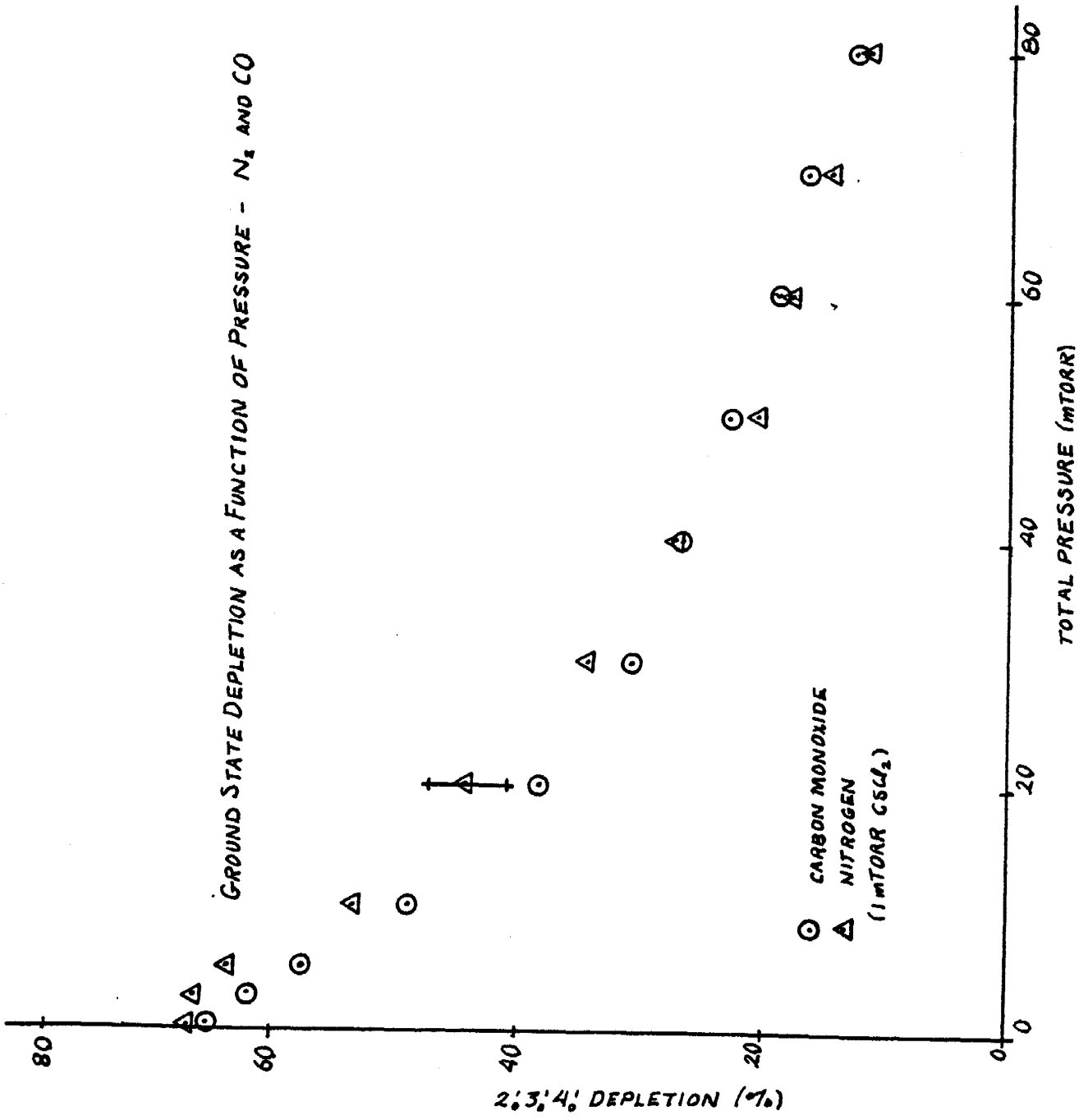


Fig.VI.11. Dependence of the ground state depletion on the pressure of added gases - isoelectronic molecules - nitrogen and carbon monoxide (0.012 D). Thiophosgene pressure is constant at 1 mTorr. CO_2 laser excitation frequency is 944 cm^{-1} and fluence is ~300 mJ cm^{-2}.

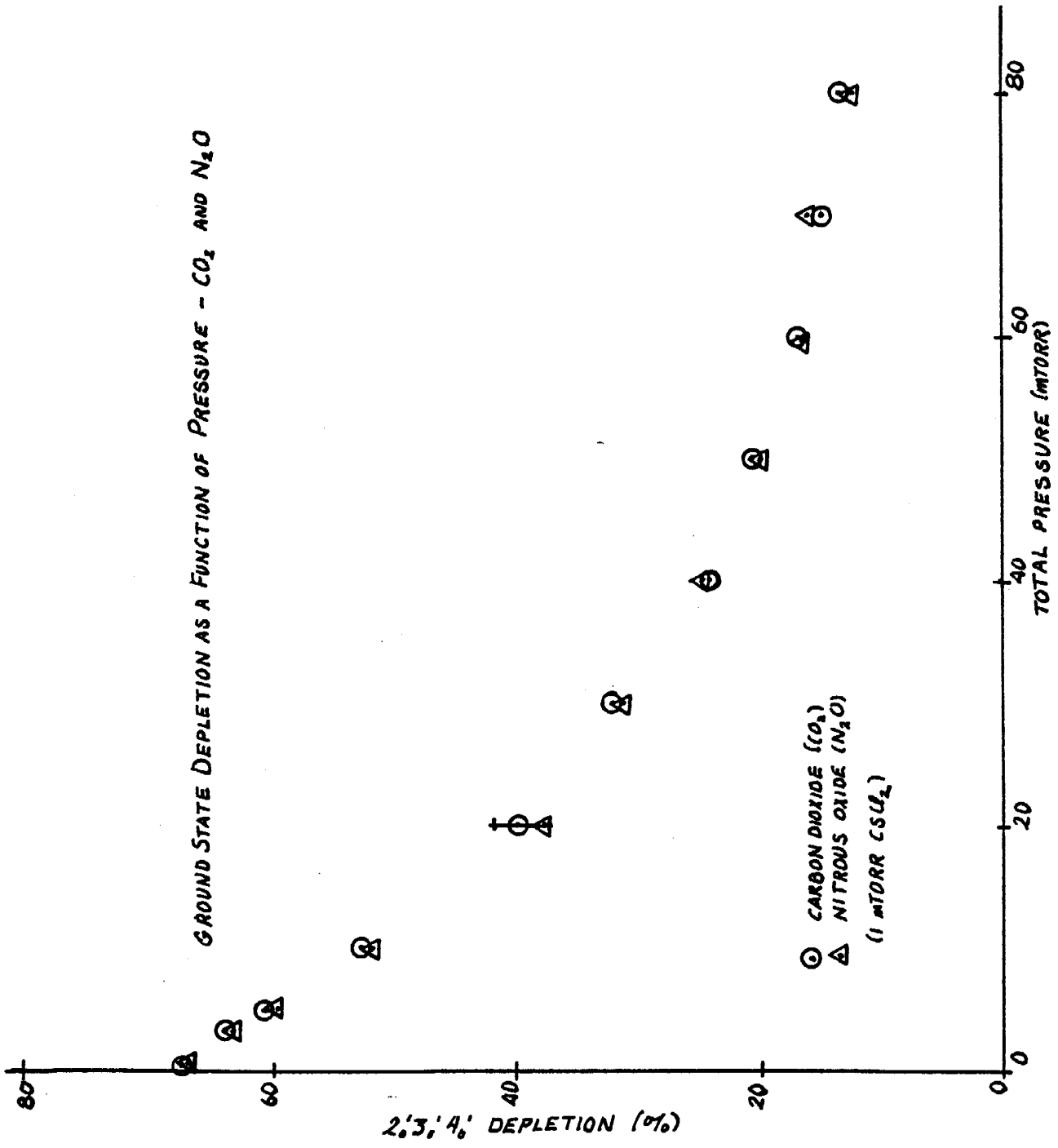


Fig.VI.12. Dependence of the ground state depletion on the pressure of added gases-isoelectronic molecules-carbon dioxide and nitrous oxide (0.167 D). Thiophostene is constant at 1 mTorr. CO_2 laser excitation frequency is 944 cm^{-1} and fluence is ~300 mJ cm^{-2}.

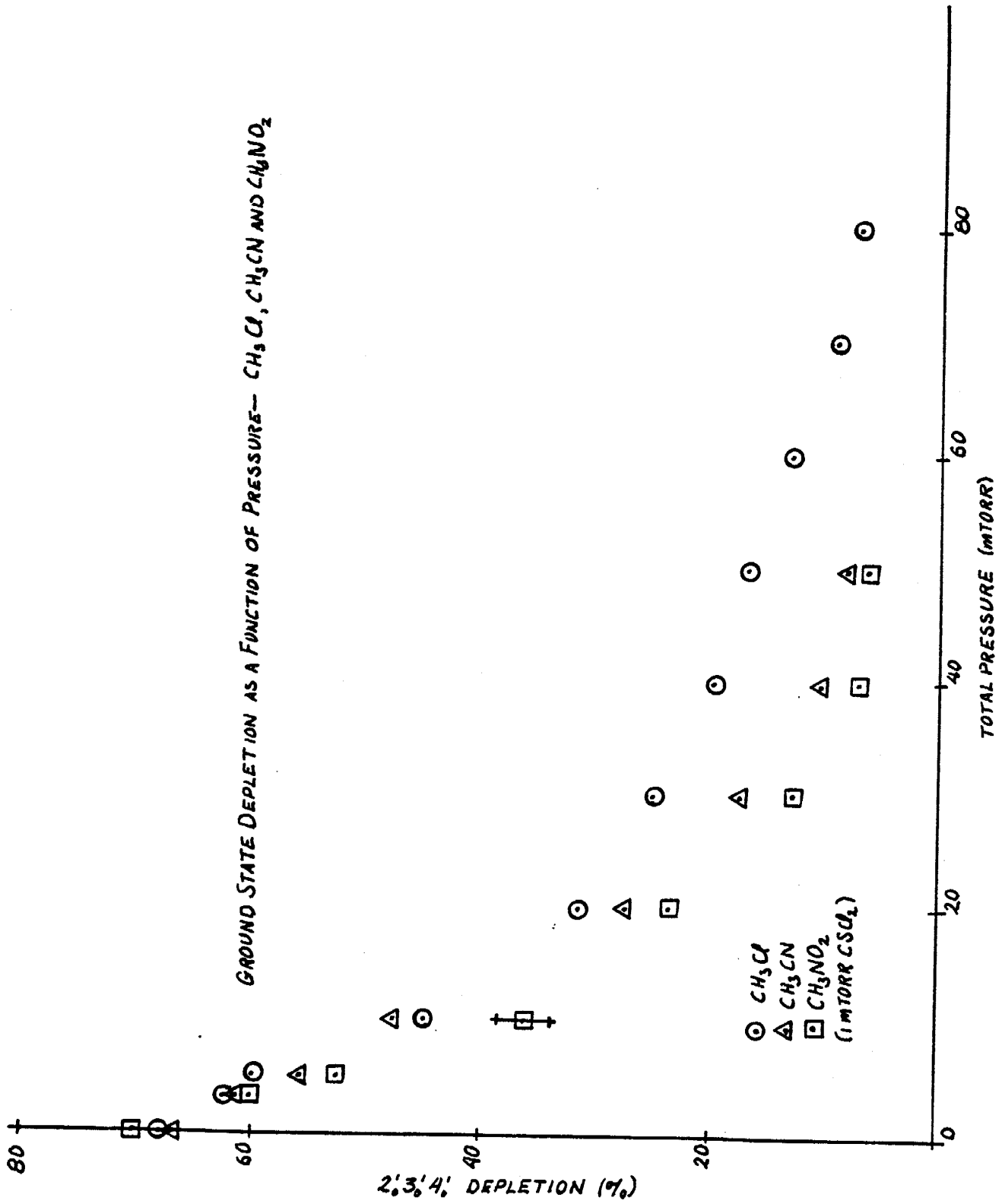


Fig. VI.13. Dependence of the ground state depletion on the pressure of added gases-substituted methanes-methyl chloride (1.87 D), nitromethane (3.4 D), acetonitrile(3.94D). Thiophosgene pressure is constant at 1 mTorr. CO_2 laser excitation frequency is 944 cm^{-1} and fluence is ~300 mJ cm^{-2}.

Since one gas, in general, has a different mass and shape from another, it will also have a different molecular velocity and, consequently, a different collision frequency at any given pressure. In order to compare the efficiency of quenching the ground state depletion between different added gases, we must plot the data as a function of collision frequency rather than pressure. This is done in Figs VI.14-VI.18 using the collision frequency data calculated and displayed in Table VI.3. (Note that, for comparing data for nitrogen with that for carbon monoxide, or for carbon dioxide with nitrous oxide, this conversion is not necessary. This is because both pairs of molecules are, and have, the same isoelectronic masses and collision frequencies.) In converting pressure values to collision frequency values, the van der Waals radii of the molecule were used--when available[130]. When not available the van der Waals radius was approximated by adding bond lengths and van der Waals radii of atoms[131].

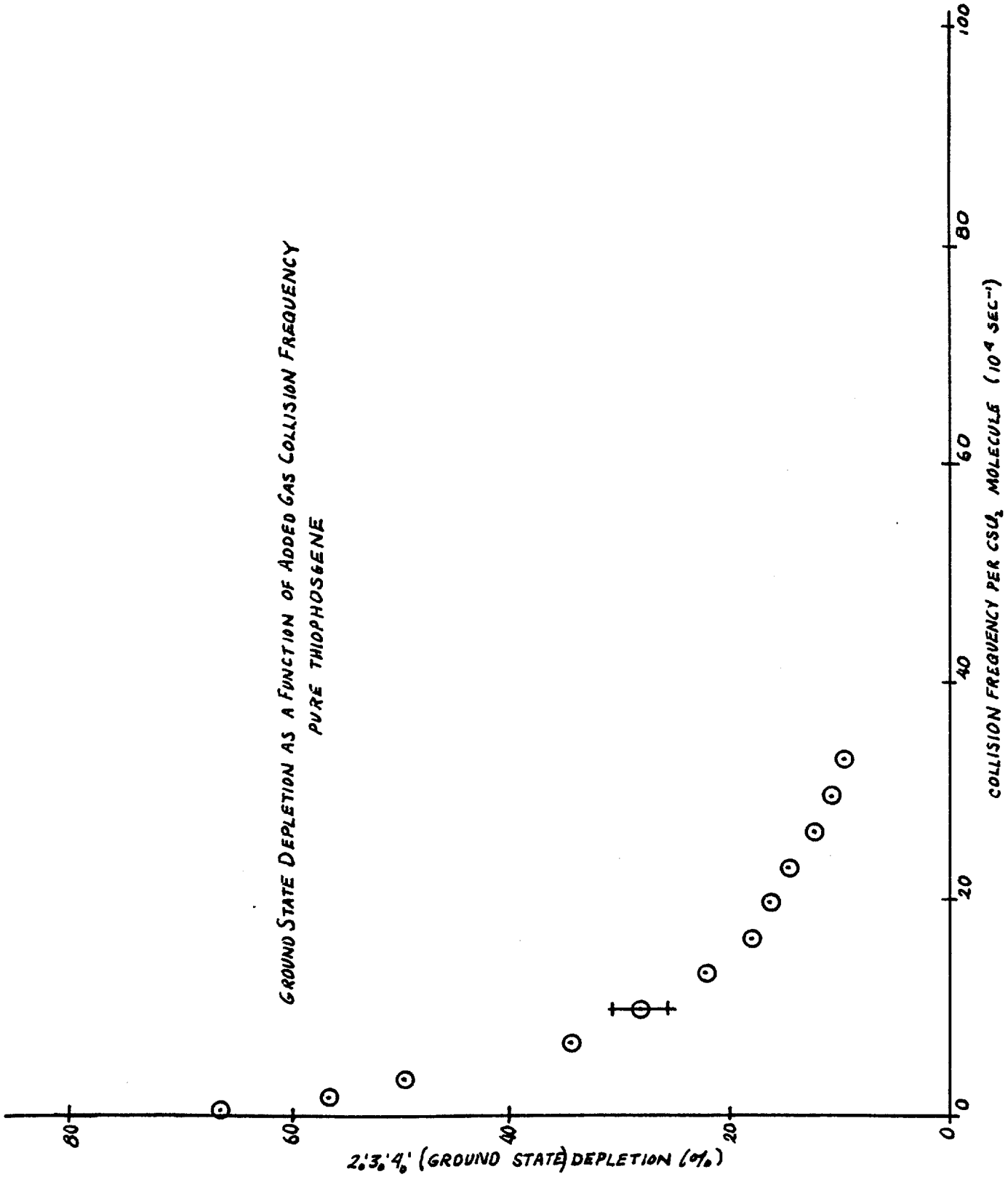


Fig.VI.14. Pressure data (Fig. II.9) replotted against colllision frequency.

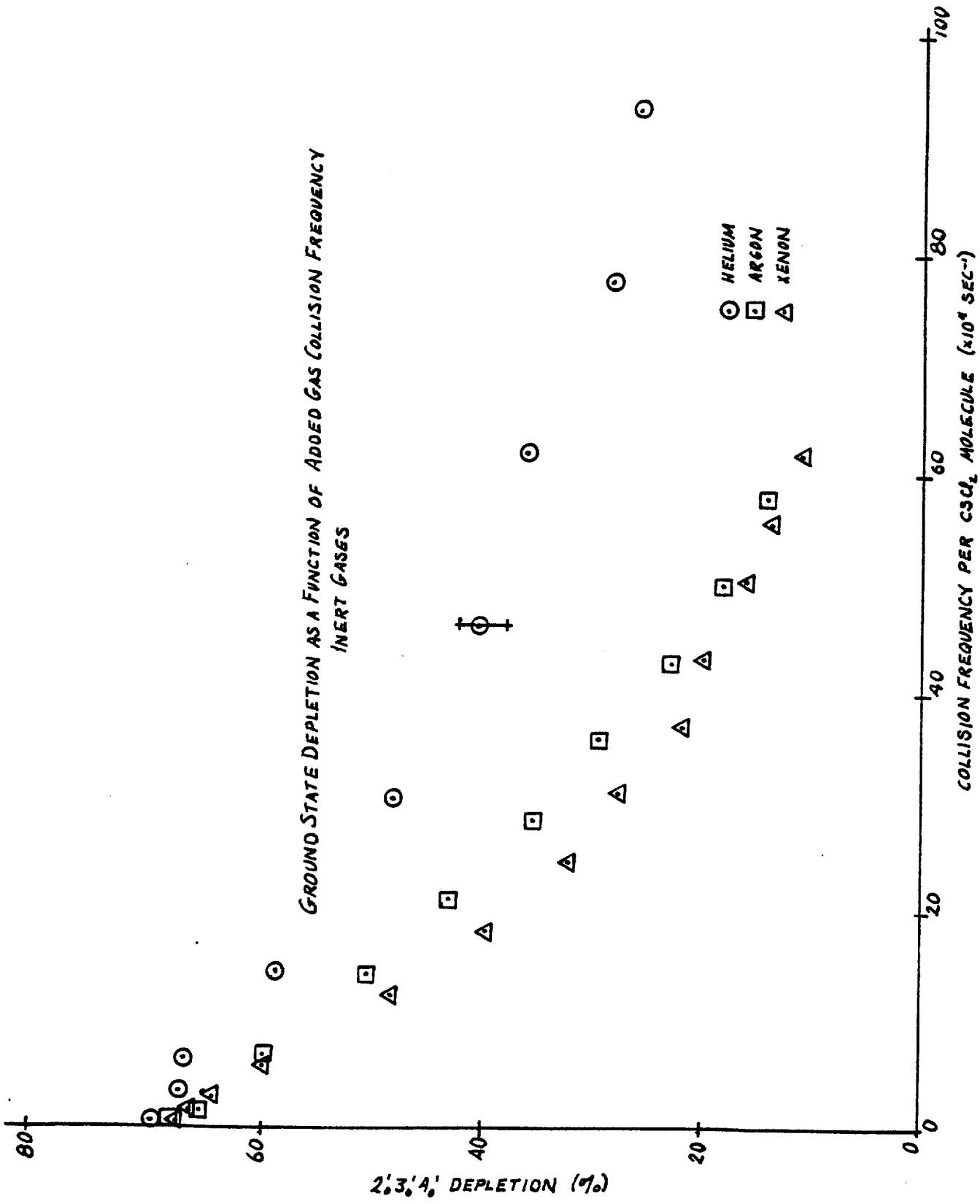


Fig.VI.15. Added gas data (Fig. VI.10) replotted against collision frequency - Inert Gases.

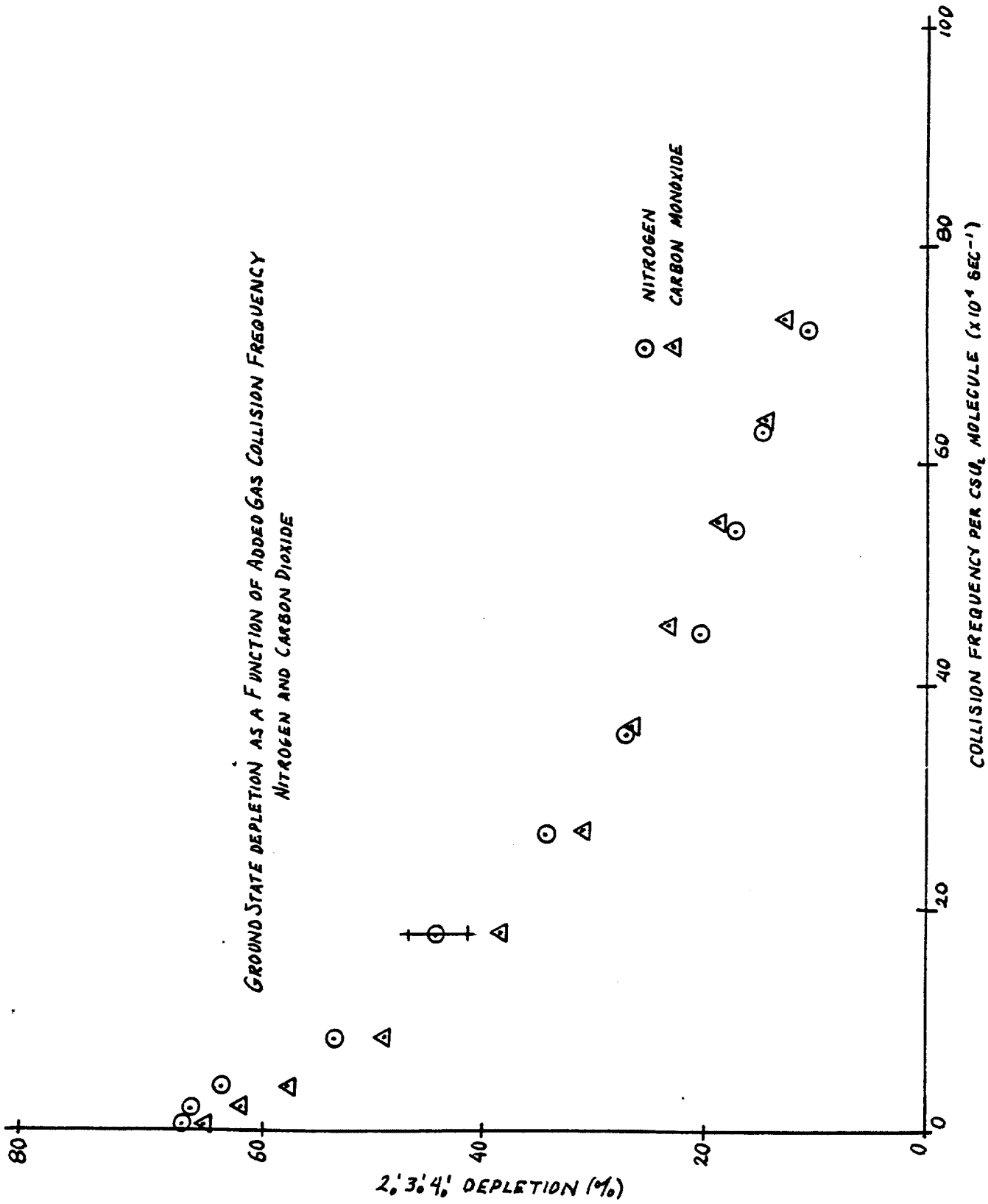


Fig.VI.16. Added gas data (Fig. VI.11) replotted against collision frequency - isoelectric molecules (nitrogen and carbon monoxide).

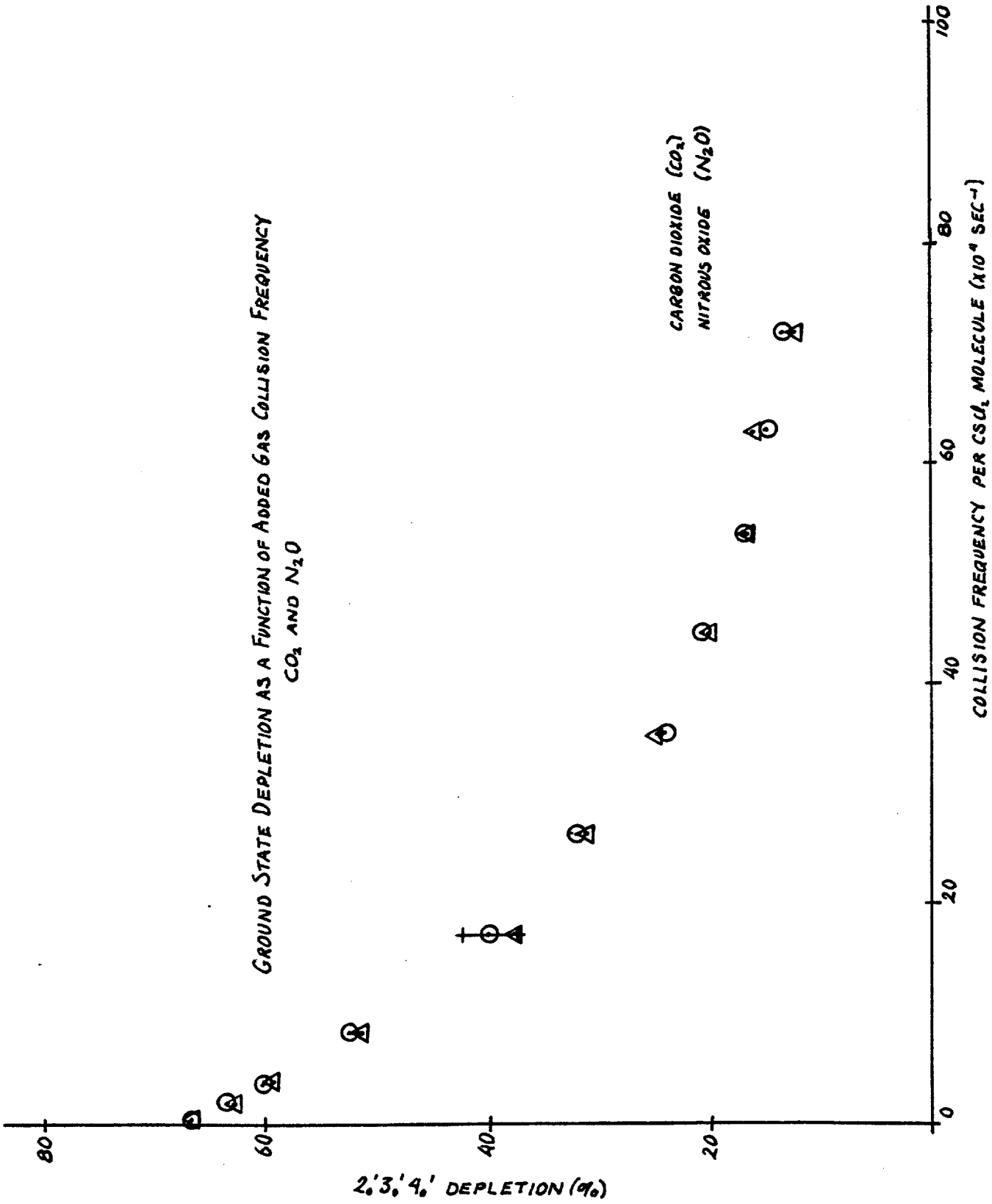


Fig.VI.17. Added gas data (Fig. VI.12) replotted against collision frequency - isoelectronic molecules (carbon dioxide and nitrous oxide).

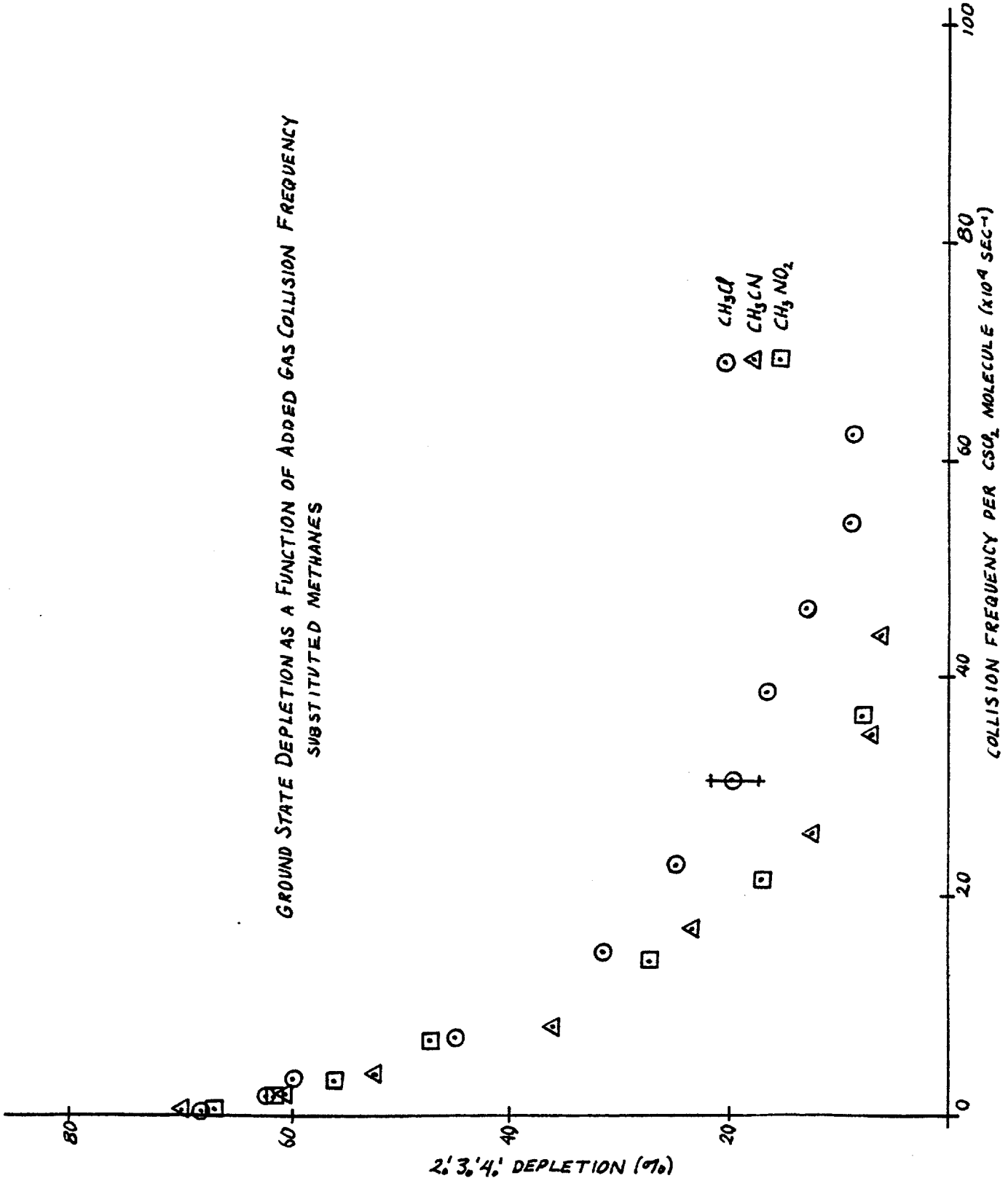


Fig.VI.18. Added gas data (Fig. VI.13) replotted against collision frequency - Substituted Methanes.

Table VI.3

Calculation of Collision Frequencies for Added Gas Experiments

Gas	σ_B (Molecular Diameter)(A)	Mass(a.m.u.)	Collision Frequency* per $CSCl_2$ Molecule per mTorr of Added Gas ($\times 10^4 sec^{-1}$)
$CSCl_2$	4.41	114.981	0.328
He	2.57	4.003	1.58
Ar	3.41	39.948	0.718
Xe	4.31	131.30	0.621
N_2	3.85	28.014	0.919
CO	3.92	28.010	0.935
CO_2	4.55	44.010	0.910
N_2O	4.54	44.013	0.908
CH_3Cl	4.15	50.488	0.791
CH_3CN	4.38	41.053	0.898
CH_3NO_2	4.18	61.040	0.747

*$Z_{AB}/n_B = \pi\sigma_{AB}^2 \sqrt{8kT/\pi\mu}\ (P_B/kT)$; $\sigma_{AB} = 1/2(\sigma_{CSCl_2}+\sigma_B)$

The importance of making this abscissa conversion becomes clear upon examination of the new graphs. Thiophosgene, having a greater mass than any of the added gases, is characterized by a "compressed" plot and, consequently, a greater quenching efficiency than, say, helium, which has the lowest mass and greatest collision frequency at a given pressure. The latter gives an "expanded" pressure plot and shows the smallest collision frequency effect of all the added gases. Table VI.4 summarizes the pressure data with a least squares analysis of exponential fits to the pressure and collision frequency plots.

Table VI.4

Least Squares Analysis of Added Gas Experiments

Added Gas	ℓnA	B	$\frac{1}{B}$ (mTorr)	ℓn C	D	$\frac{1}{D}$ ($\times 10^4 sec^{-1}$)	Correlation Coefficient
$CSCl_2$	4.02	0.0190	52.8	3.01	0.0578	17.3	-0.981
He	4.24	0.0167	60.1	4.23	0.0105	95.1	-0.995
Ar	4.29	0.0194	51.4	4.27	0.0271	36.9	-0.997
Xe	4.24	0.0183	54.7	4.23	0.0295	33.9	-0.999
N_2	4.22	0.224	44.6	4.20	0.0244	40.9	-0.998
CO	4.12	0.0195	51.2	4.10	0.0209	47.8	-0.994
CO_2	4.17	0.214	46.7	4.15	0.0236	42.4	-0.992
N_2O	4.15	0.214	46.8	4.13	0.0236	42.4	-0.992
CH_3Cl	4.12	0.0261	38.4	4.10	0.0330	30.3	-0.989
CH_3Cl	4.20	0.0515	19.4	4.15	0.0575	17.4	-0.990
CH_3CN	4.25	0.0452	22.1	4.21	0.0608	16.5	-0.997

$$\%\Delta = A \exp[-B \cdot \text{pressure}] = C \exp[-D \cdot \text{coll} \cdot \text{freq}]$$

$$\ell n(\%\Delta) = \ell nA - B \cdot \text{pressure} = \ell nC - D \cdot \text{coll} \cdot \text{freq}$$

$$A = C = \%\Delta \ (1 MTorr)$$

The dependence of collision-induced state changes on long range interactions has been treated theoretically by Lin et al.[132]. In their work they derive the following correlation between the intermolecular potential between added gas molecules and the cross section of the resulting change of state:

$$\ell n\ \sigma_M = \ell n(\ \sigma_{gas\text{-}kinetic}) + \beta(\varepsilon_{MM}/k)^{1/2} \qquad (VI.1)$$

in which σ_M is the cross section of the state change induced by an added gas M, $\sigma_{gas\text{-}kinetic}$ is the gas-kinetic collision cross section, $(\varepsilon_{MM}/k)^{1/2}$ is the Lennard-Jones well depth in degrees Kelvin for the interaction between two added gas molecules (M) and β is a parameter to be determined experimentally for each foreign gas. Values of $(\varepsilon_{MM}/k)^{1/2}$ for all of the added gases used in our experiments are found in Table I of Lin's paper and are determined from either virial coefficients, transport parameters, Stockmayer values or boiling points.

In order to determine whether or not the collision-induced effect we were observing could be described by Lin's theory, we plotted the results of the added gas experiments in the form of Eq. (VI.1). For pure thiophosgene $(\varepsilon_{MM}/k)^{1/2}$ was calculated using the empirical formula $\varepsilon_{MM}/k = 1.15\ T_b$. Since we did not know the absolute value of the cross section for suppressing the ground state depopulation by each added gas, we took it to be the collision frequency required to reduce the ground state depletion value to 1/e of the collisionless value, divided by the 1/e collision frequency for helium.

Since we are plotting the results in log-log form this procedure gives exactly the same plot as if we were to use the actual values for the cross sections. The gas kinetic collision cross sections have already been determined (Table IV.3). Strictly speaking they are somewhat larger than gas kinetic since they are calculated from van der Waals sizes. They are also expressed relative to that of helium. The resulting plot is shown in Fig. VI.19; the correlation between quenching efficiency and long range attractive forces is quite good.

In order to determine whether the efficiency of the pressure effect depends on the infrared excitation frequency the pressure dependence of the ground state depletion was measured at a second frequency, 978.5 cm^{-1}. The pressure dependence is shown in Fig. VI.20a along with the previous pressure dependence curve obtained from pumping at 944.2 cm^{-1}. Since different collisionless depletion values are observed at the two excitation frequencies, the curves are replotted in Fig. VI.20b in which the data are normalized with respect to the 1 mTorr value. This plot shows that pumping at 978.5 cm^{-1}, which is more efficient under collisionless conditions, is less affected by collisions than pumping at 944.2 cm^{-1}.

In all of the added gas experiments reported so far, we have implicitly assumed that, at a pressure of 1 mTorr, thiophosgene suffers no collisions during the duration of the CO_2 laser (200 nsec). This seems plausible since the collision effect does not begin to manifest itself until the pressure is increased beyond 2 mTorr. To verify this supposition, we performed fluence and probe delay measurements on

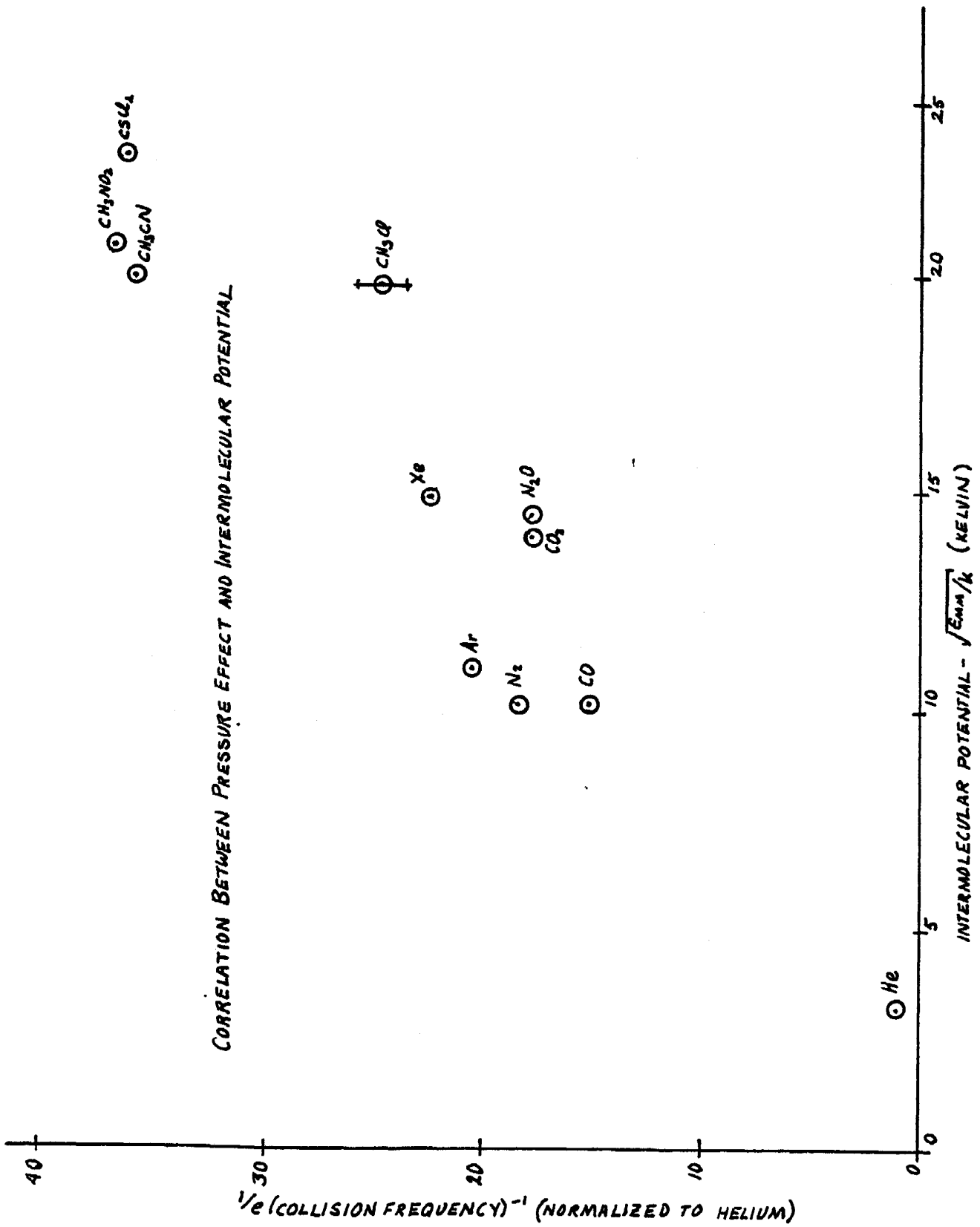


Fig.VI.19. Dependence of the quenching efficiency of the ground state depletion normalized to helium, on intermolecular well depth $(\epsilon_{mm}/2)^{1/2}$, between added gas molecules. Quenching efficiency is taken to be the collision frequency per thiophosgene molecule needed to reduce the ground state depletion to 1/e of the collisionless value and normalized to helium.

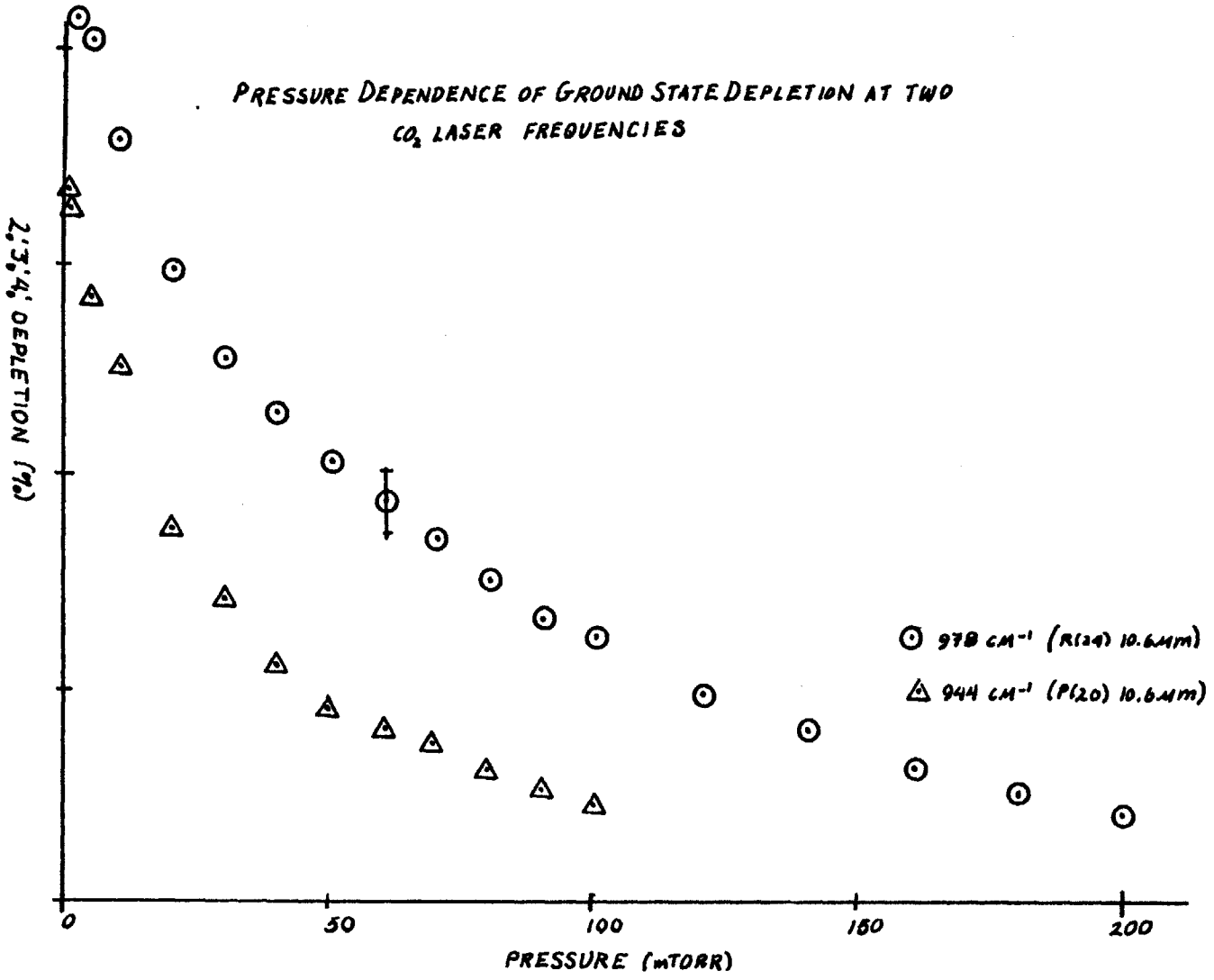


Fig.VI.20. (a)Dependence of the ground state depletion on the pressure at two CO_2 laser excitation frequencies. Infrared fluence is ~300 mJ cm^{-2}.

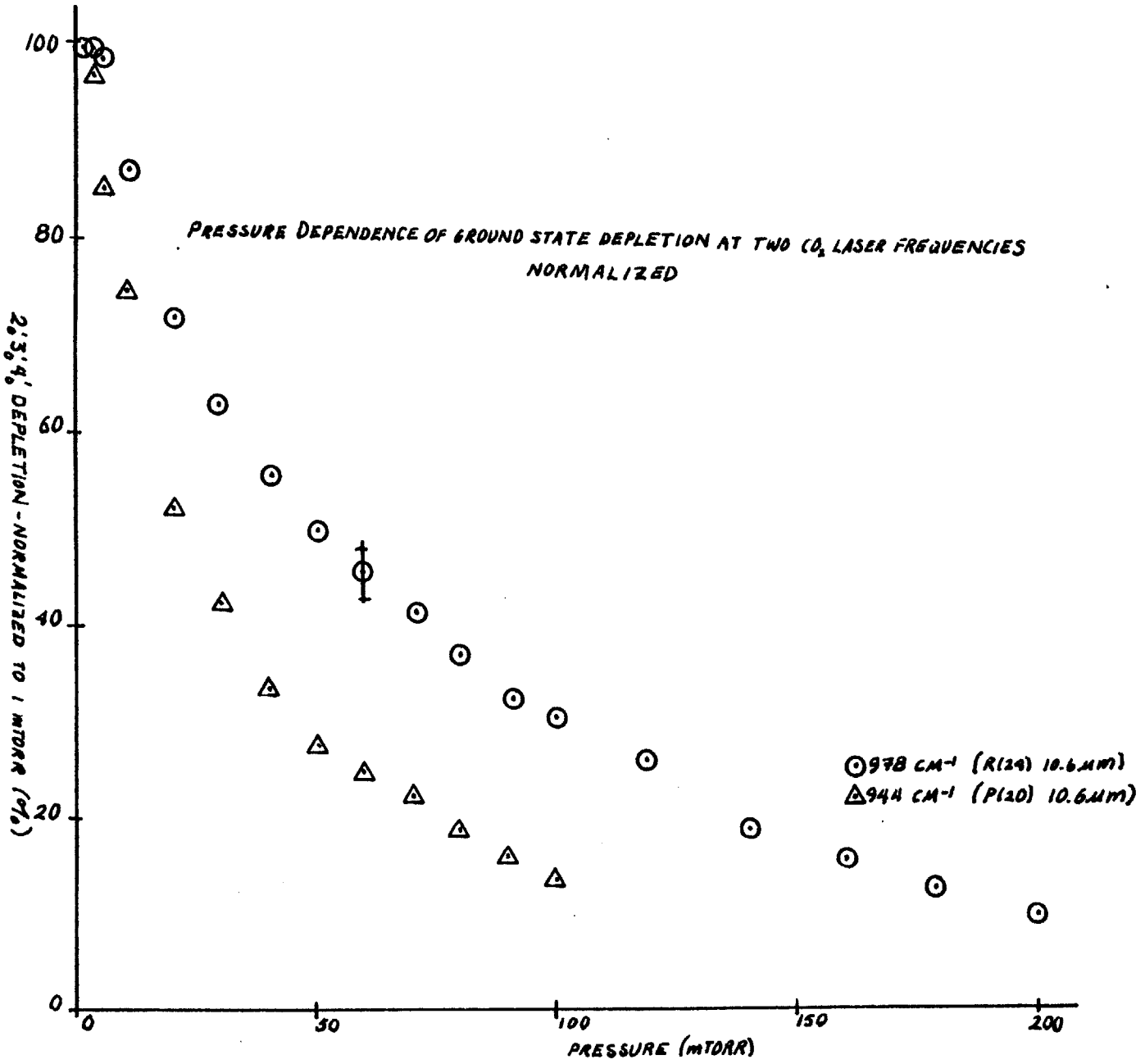


Fig. VI.20. (b)Pressure data of Fig. VI.20 (a) normalized to collisionless ground state depletion value.

thiophosgene at three pressures: 6×10^{-5} Torr (effusive beam), 1 mTorr and 10 mTorr. (For an explanation of the probe delay study see Section VI.B.2.) As Figs. VI.21 and VI.22 show, the data for 1 mTorr are identical to the collisionless data but quite different from the 10 mTorr data.

Fluence studies at 3 pressures (10 mTorr, 20 mTorr and 50 mTorr) were done for an excitation frequency of 978.5 cm^{-1}. The results are shown in Fig. VI.23, along with the data taken for thiophosgene in an effusive beam. One can observe a decreasing initial slope and larger saturation pulse energy as the pressure increases. This confirms our intuition that, as the collision frequency increases, the collision induced interactions interfere more with the absorption and make it more difficult for thiophosgene to move out of the vibrationless ground state. A more precise formulation of this explanation will be given in the discussion.

2. Excited Vibrational States

Under collisionless conditions the vibrationless ground state loses 50% to 90% of its population to higher lying vibrational states depending on the excitation wavelength and rotational temperature. However, even when the CO_2 laser is tuned to excite the $2\nu_4$ mode at 944 cm^{-1}, we cannot find any population increases in the excited states of the $2\nu_4$ ladder--at any fluence. Just where the missing ground state population goes is the question we next turned to answer.

Increasing the pressure of thiophosgene, or an added gas, decreases the pumping efficiency; therefore, it should be possible to observe a

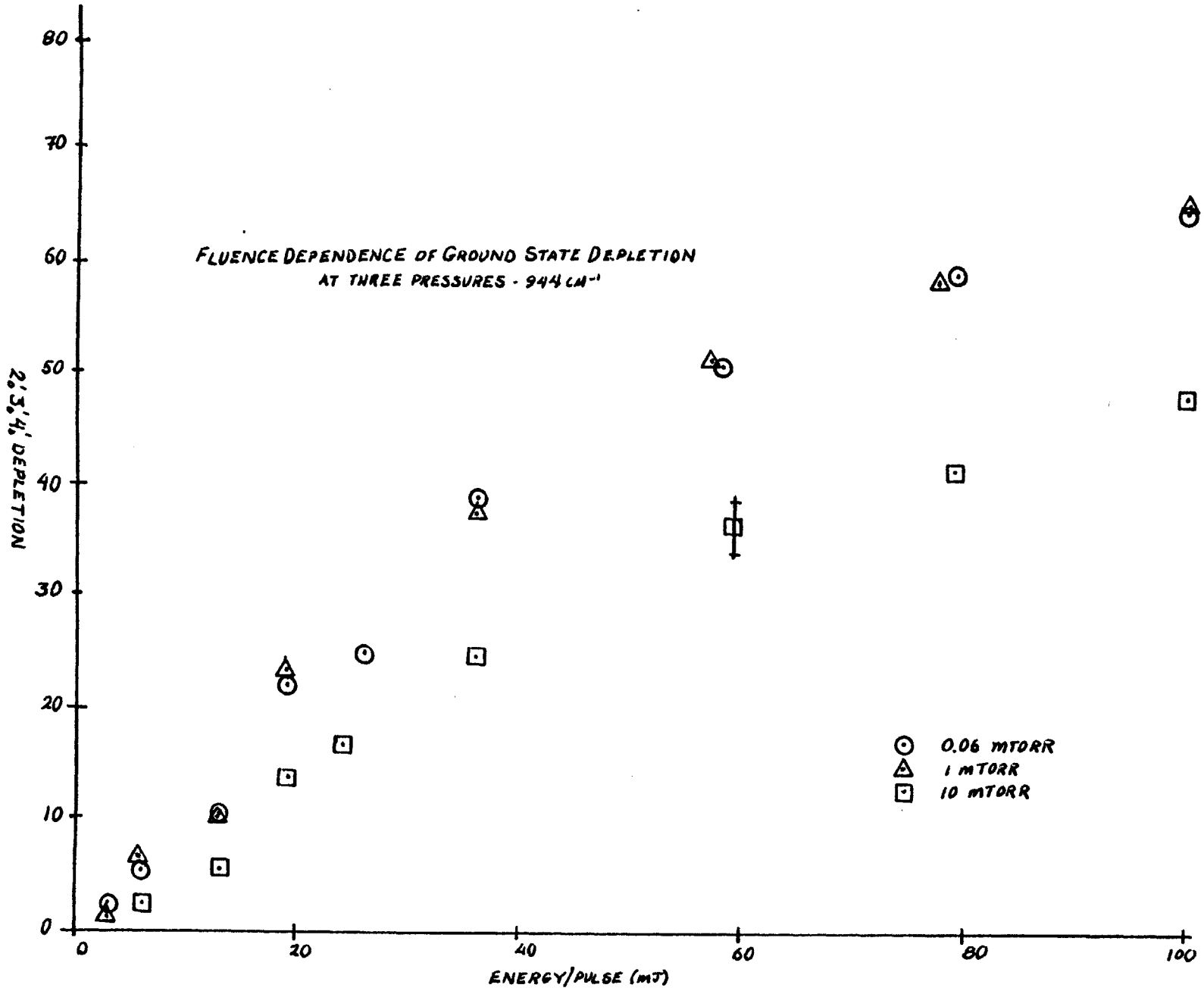


Fig.VI.21. Dependence of the ground state depletion on CO_2 laser energy/pulse at three pressures. CO_2 laser excitation frequency is 944 cm^{-1}.

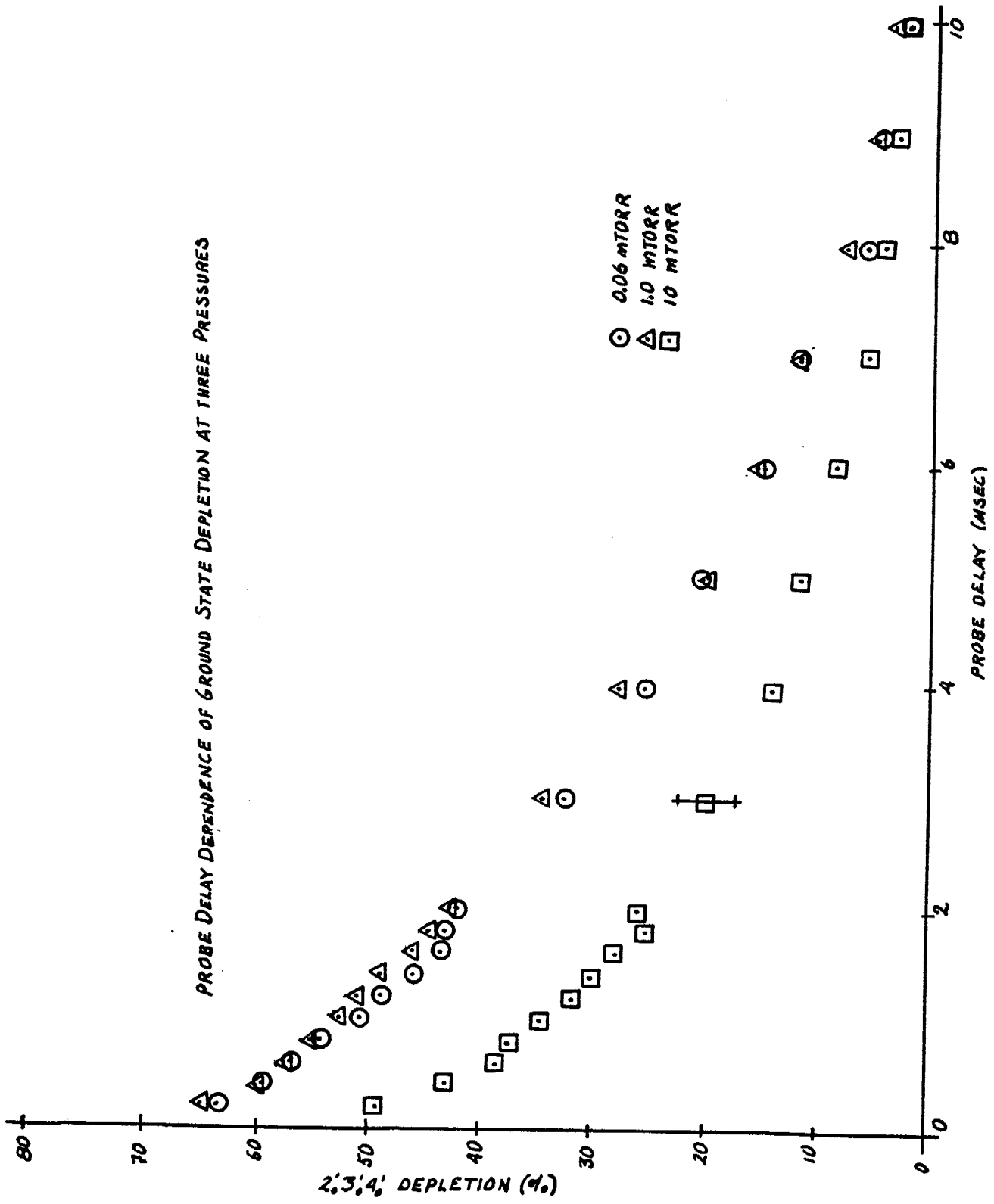


Fig.VI.22. Dependence of ground state depletion on dye laser delay at three pressures. (CO_2 laser excitation frequency is 944 cm^{-1} and fluence is ~300 $mJcm^{-2}$

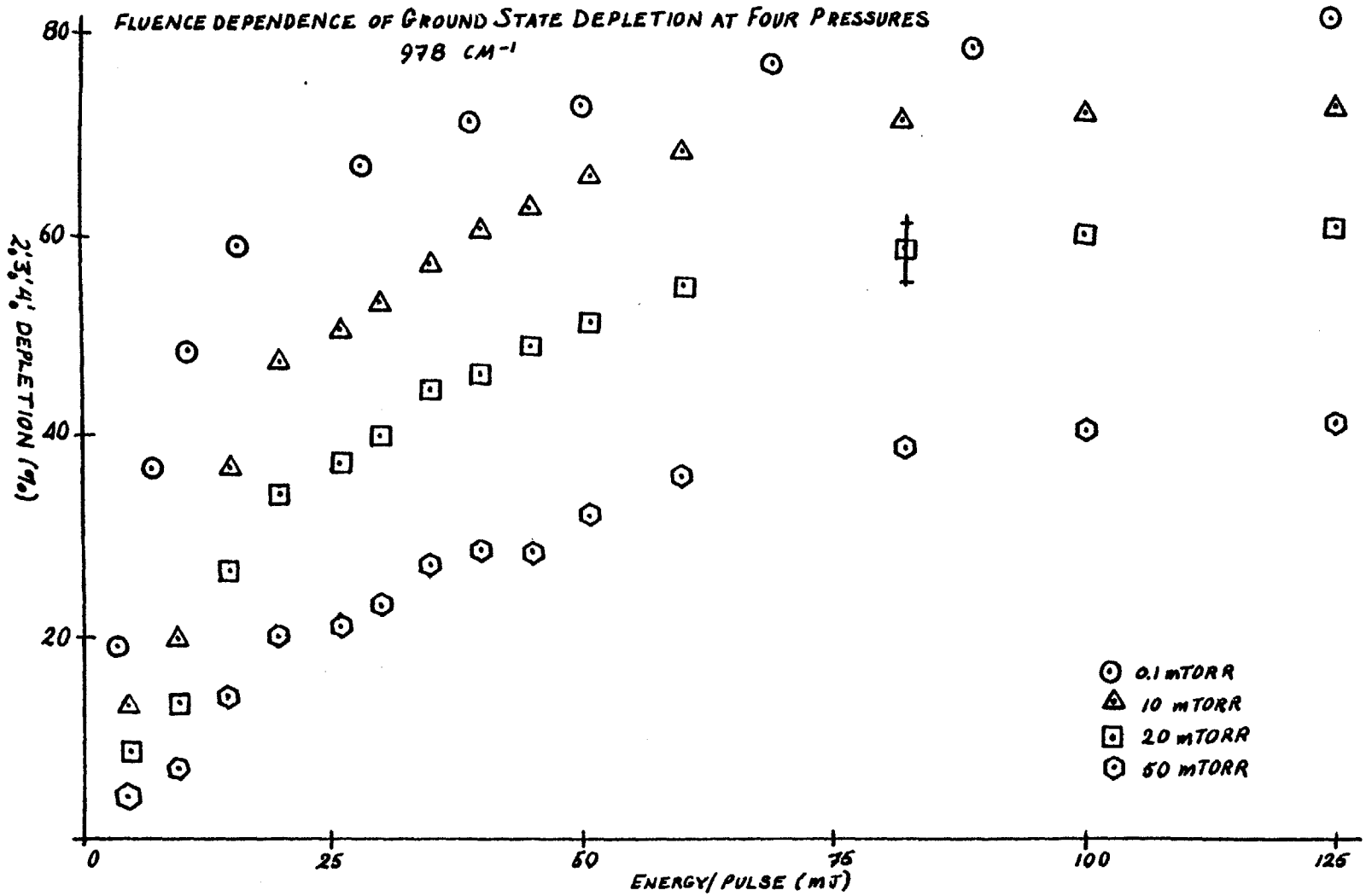


Fig.VI.23. Dependence of ground state depletion on CO_2 laser energy/pulse at 4 pressures. CO_2 laser excitation frequency is 978.5 cm^{-1}.

build-up of population at the intermediate levels by increasing the pressure. Furthermore, it seems plausible that, if one waits long enough after the pulse of infrared excitation to probe the excited states' population, one will observe thiophosgene "falling" back down toward the ground state as a result of vibrational relaxation.

Both of these ideas were incorporated into a set of experiments in which the population change of the ground state and first two excited states of the $2\nu_4$ ladder was measured as a function of the dye laser delay at various pressures (excitation frequency=944 cm^{-1}). The results for the probe delay/pressure experiments are displayed in Figs. VI.24-26.

Including ground state depletion measurements in this series of experiments is necessary for the following reason: As the dye laser delay increases, infrared pumped molecules drift out of the interaction region and are replaced by vibrationally "cold" molecules. This results in the population change of any level measured after a delay from the CO_2 laser pulse being reduced from what it would be if we could keep track of all vibrationally excited molecules. For the ground vibrationless state, this dilution effect is the predominant physical process which changes the IR-VIS-DR signal as the delay increases. Therefore, a measurement of the fractional decrease of the ground state depletion as a function of pressure and delay can be used to give correction factors for the population changes measured for the excited vibrational states.

As shown in Table VI.5 the decrease in the ground state depopulation as a function of probe delay follows a falling exponential with a high degree of correlation at all pressures. We can, therefore,

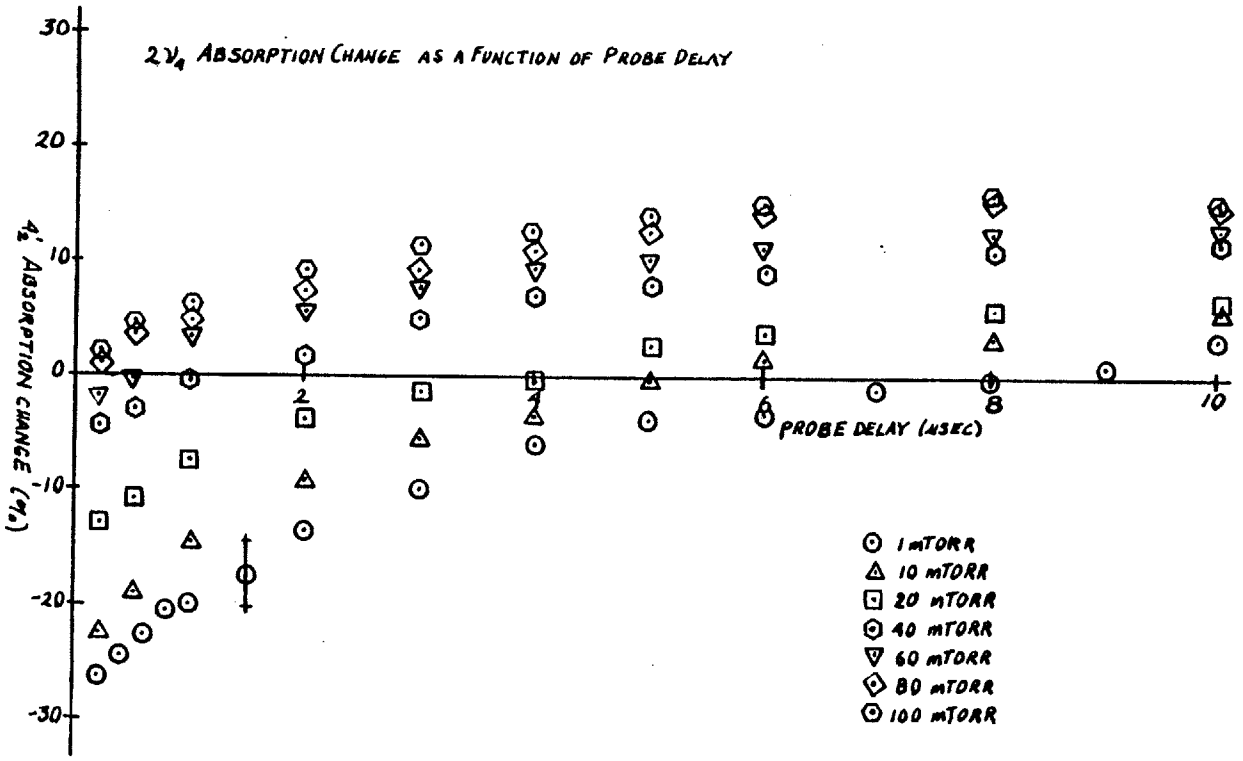


Fig.VI.25. Dependence of population change of $2\nu_4$ on dye laser delay at 7 pressures. CO_2 laser excitation frequency is 944 cm^{-1} and fluence is ~300 mJ cm^{-2}.

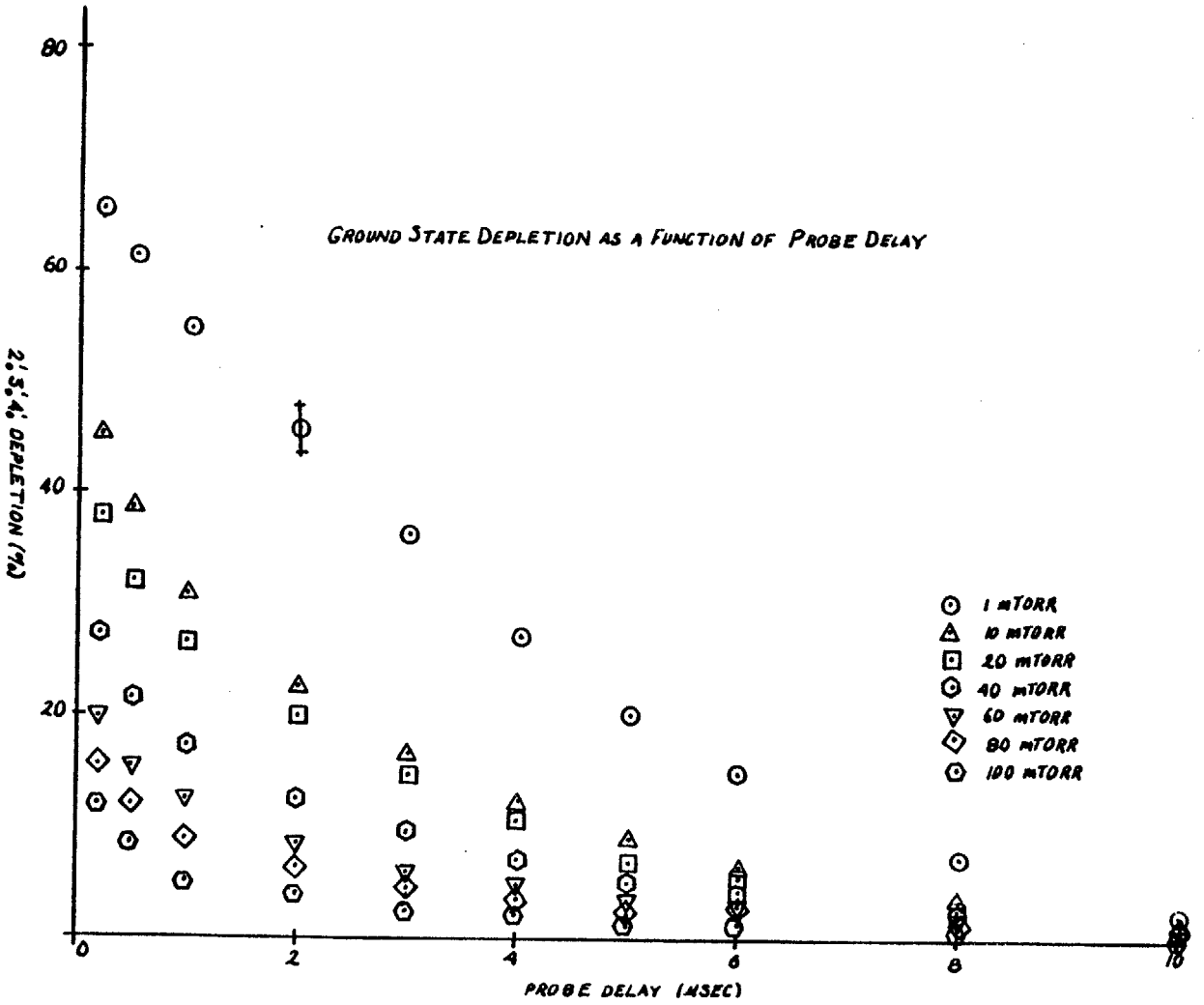


Fig.VI.24. Dependence of ground state depletion on dye laser delay at 7 pressures. CO_2 laser excitation frequency is 944 cm^{-1} and fluence is ~300 mJ cm^{-2}.

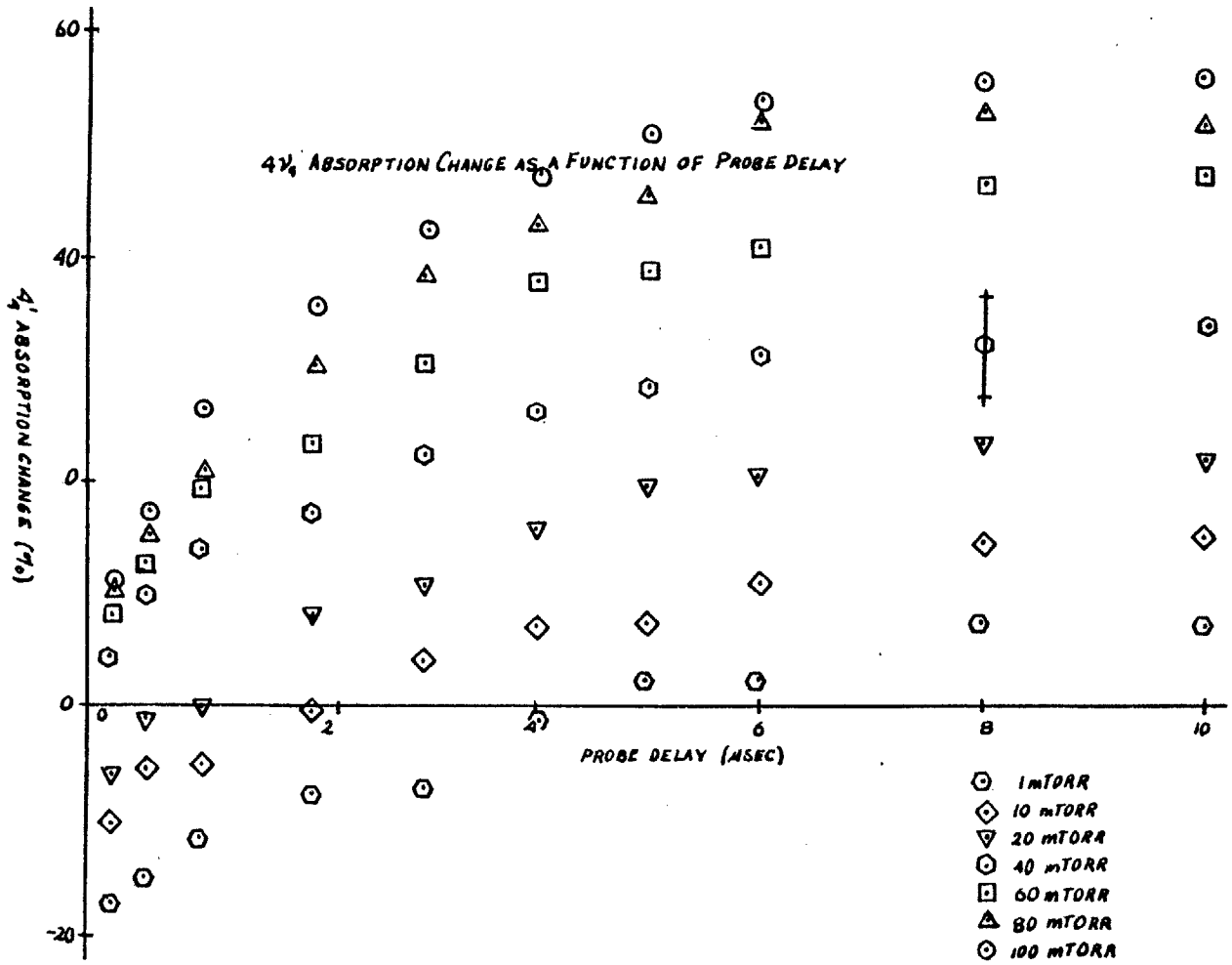


Fig.VI.26. Dependence of population change of $4\nu_4$ on dye laser delay at 7 pressures. CO_2 laser excitation frequency is 944 cm^{-1} and fluence is ~300 mJ cm^{-2}.

extract parameters to the exponential fitting function:

$$\%\Delta(t_D) = \%\Delta(0.2\ \mu sec)\ e^{-Bt} \qquad (VI.2)$$

and use the parameterized formulae to correct the excited state data (Fig. VI 27,28). Although this treatment is valid for short delays, at long delays, the exponential correction factor becomes tremendously large and must be treated with caution.

Table VI.5

Least Squares Analysis of Pressure/Probe Delay Data for the Vibrationless Ground State

Pressure (mTorr)	$\ell nA(\mu sec^{-1})$	B	Correlation Coefficient
1	-0.253	0.0913	-0.996
10	-0.324	-0.0086	-0.998
20	-0.332	0.0188	-0.998
40	-0.311	-0.0772	-0.995
60	-0.315	-0.1075	-0.990
80	-0.348	-0.0955	-0.991
100	-0.373	-0.235	-0.972

$$\%\Delta = A\exp[-B \cdot t_D]$$

$$\ell n(\%\Delta) = \ell nA - Bt_D$$

$$A = \%\Delta(0.2\ \mu sec)$$

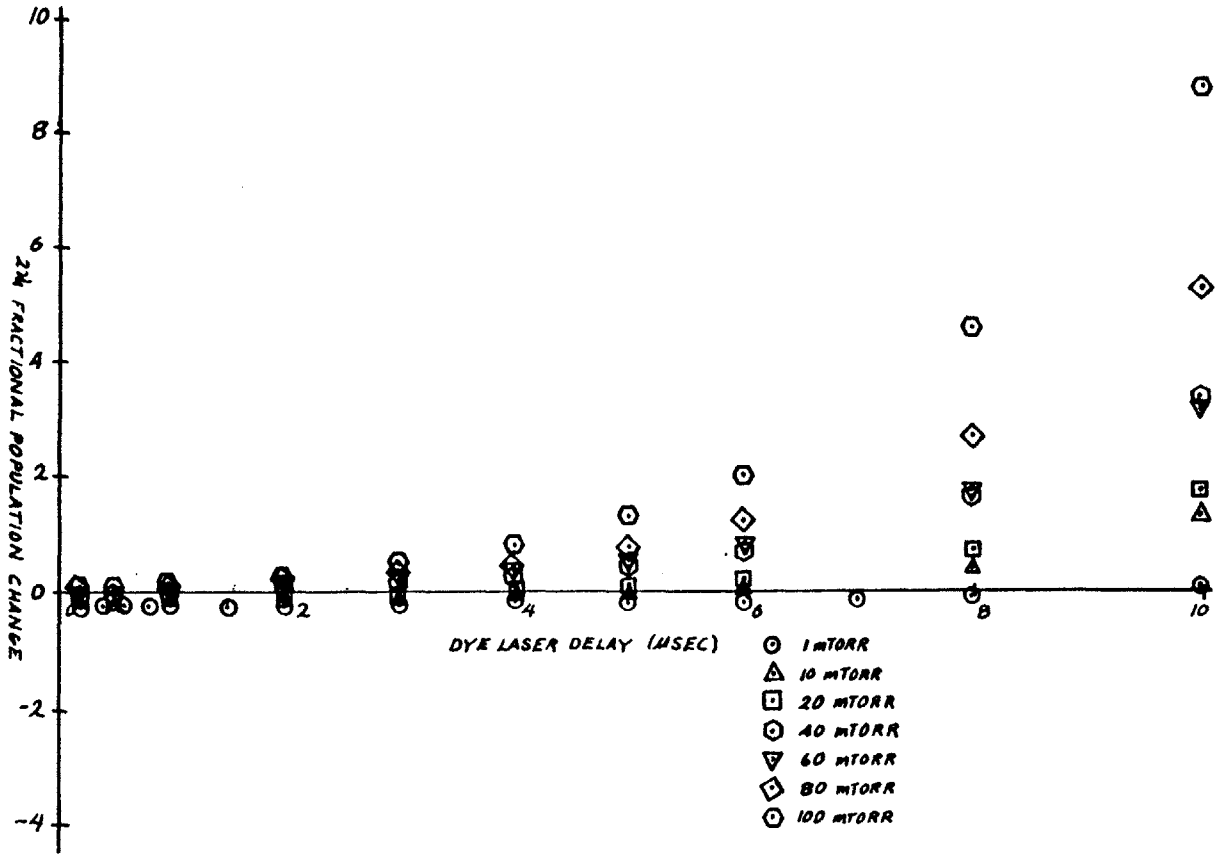


Fig.VI.27. Dependence of population change of $2\nu_4$ on dye laser delay at 7 pressures. (Fig. 25) - Corrected for expansion of vibrationally excited molecules out of the viewing region using data from Table VI.5.

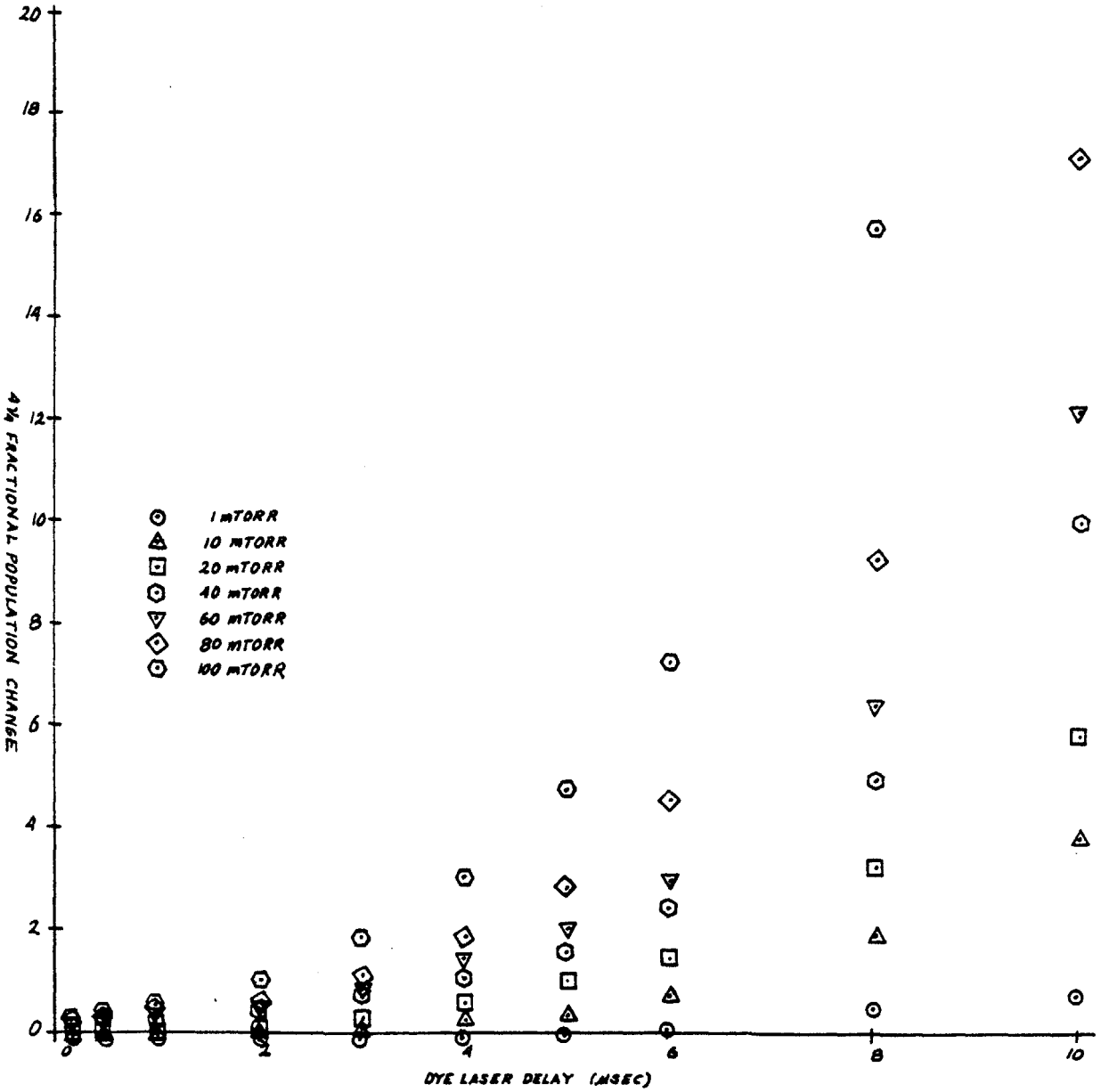


Fig.VI.28. Dependence of $4\nu_4$ population change on dye laser delay at 7 pressures (Fig. 26) - corrected for expansion of vibrationally excited molecules out of the viewing region using data from Table VI.5.

Table VI.6

Number of Gas Kinetic* Collisions Occurring between Thiophosgene Molecules as a function of pressure and delay

Pressure (mTorr)

Delay (μsec)	1	10	20	40	60	80	100
0.2	0.001	0.0065	0.013	0.026	0.039	0.052	0.066
0.5	0.002	0.016	0.033	-.066	0.098	0.131	0.164
1.0	0.003	0.033	0.066	0.131	0.197	0.262	0.328
2.0	0.007	0.066	0.131	0.262	0.394	0.525	0.656
3.0	0.010	0.098	0.197	0.394	0.590	0.787	0.984
4.0	0.013	0.131	0.262	0.525	01787	1.04	1.31
5.0	0.016	0.164	0.328	0.656	0.984	1.31	1.64
6.0	0.020	0.192	0.394	0.788	1.18	1.57	1.97
8.0	0.026	0.262	0.525	1.05	1.57	2.10	2.62
10.0	0.033	0.328	0.656	1.31	1.97	2.62	3.28
15.0	0.049	0.492	0.984	1.97	2.95	3.94	4.92

*Calculated using van der Waals Radii

Lower right-hand figures separated by the solid line indicate range of pressures and delays in which collisions become important.

Drawn in Figs. VI.27 and VI.28 are the population changes for the $2\nu_4$ and $4\nu_4$ states, respectively, when the correction factor calculated from Table VI.5 are applied. For long delays and high pressure[5], the population increases in $2\nu_4$ and $4\nu_4$ are calculated to be between 1 and 2 orders of magnitude, respectively, greater than observed. However, even under these conditions, not all of the population driven out of the ground state is accounted for. For instance, at a delay of 10 μsec and a pressure of 100 mTorr, the population in the first two excited vibrational states of the $2\nu_4$ ladder is calculated to increase by factors of 8.8 and 33.4, respectively. While these are large numbers the ambient population in these two levels is only about 10^{-2} and 10^{-4} so that the population found in both of these levels under these most advantageous circumstances is still less than 10%. This is another piece of evidence that argues against $2\nu_4$ being the pumped mode at an excitation frequency of 944 cm^{-1}.

Table VI.6 lists the number of collisions (assuming van der Waals radii) that take place between thiophosgene molecules at various times and pressures. Examination of Table VI.6 shows that only at the higher pressures and longer delays, as denoted in the table, does diffusion contribute to the equilibration of "hot" and "cold" molecules. (The proper treatment of the data for this pressure and delay regime requires a random walk approach rather than diffusion equations.) For all other pressures and delays the exiting of vibrationally excited molecules out of the viewing region can be described as free expansion.

Sodickson[133] has worked out explicit expressions for the free expansion of a cylindrical plug of molecules into a vacuum. Although they are, in general, impossible to evaluate analytically, they simplify considerably when one examines the change in density as a function of time at the axis of the cylinder:

$$\rho(t_D) = \rho(0)[1-e^{-(r_0/c)^2 t^2}] \qquad \text{(VI.3)}$$

in which r_0 is the radius of the cylinder and c is the mean molecular velocity. The interaction region, defined as the interaction of the dye laser and CO_2 laser beams, can be approximated by a cylinder.

If we accept three approximations, we can use Eq. (VI.3) to calculate the change in the excited state populations as a function of delay and compare the results with the experimentally obtained delay data. The first approximation is to let the population change at the axis represent the change integrated over the entire dye laser volume. The second one is the implicit assumption that vibrationally hot molecules are replaced only by room temperature molecules; in reality, the CO_2 laser focal region extends horizontally beyond the dye laser boundary and allows some hot molecules to be replaced by other hot molecules. Both of these approximations will have the effect of decreasing the calculated population change, from the actual change. Third, we may assume, when we use this expression, that the expansion of originally separated gases into each other is equivalent to the expansion of one gas into a vacuum. As long as there are no collisions in the system this assumption is valid.

Notice that since we are using a free expansion model to simulate the time delay studies, the pressure of the thiophosgene does not enter as a parameter. If the escape of excited molecules were due to diffusion then we would describe their motion with the diffusion equations which contain pressure-dependent constants[134]. Examination of Table VI.5 indeed shows that the pressure coefficients to the exponential correction formulae are roughly constant throughout the 10 to 80 mTorr pressure range.

With these approximations in mind we can now use Eq. (VI.3) to calculate the curve for the ground state depletion vs. probe delay and compare this to the experimentally determined curve. As Fig. VI.29 shows, the agreement between the calculated curve and the experimental (1mTorr) curve is good at intermediate delays. At short and long delays, however, the fall-off of the experimental curve is faster than predicted from the simplified model. A possible explanation for this will be given in the discussion.

The last set of experiments I shall describe were done to verify that the increases observed in $2\nu_4$, as a result of raising the pressure and increasing the delay, are affected by long range forces. Pressure/delay studies for $2\nu_4$ were carried out in which 5 mTorr of thiophosgene was mixed with 35 mTorr and 75 mTorr of an added gas--helium, argon, nitromethane and thiophosgene, itself. When interpreting the results, shown in Figs. VI.30-33, it is important to remember the point made earlier concerning the differing collision frequencies for two gases at the same pressure. To allow the reader to compare on mixed gas experiment with another, I have listed, in each

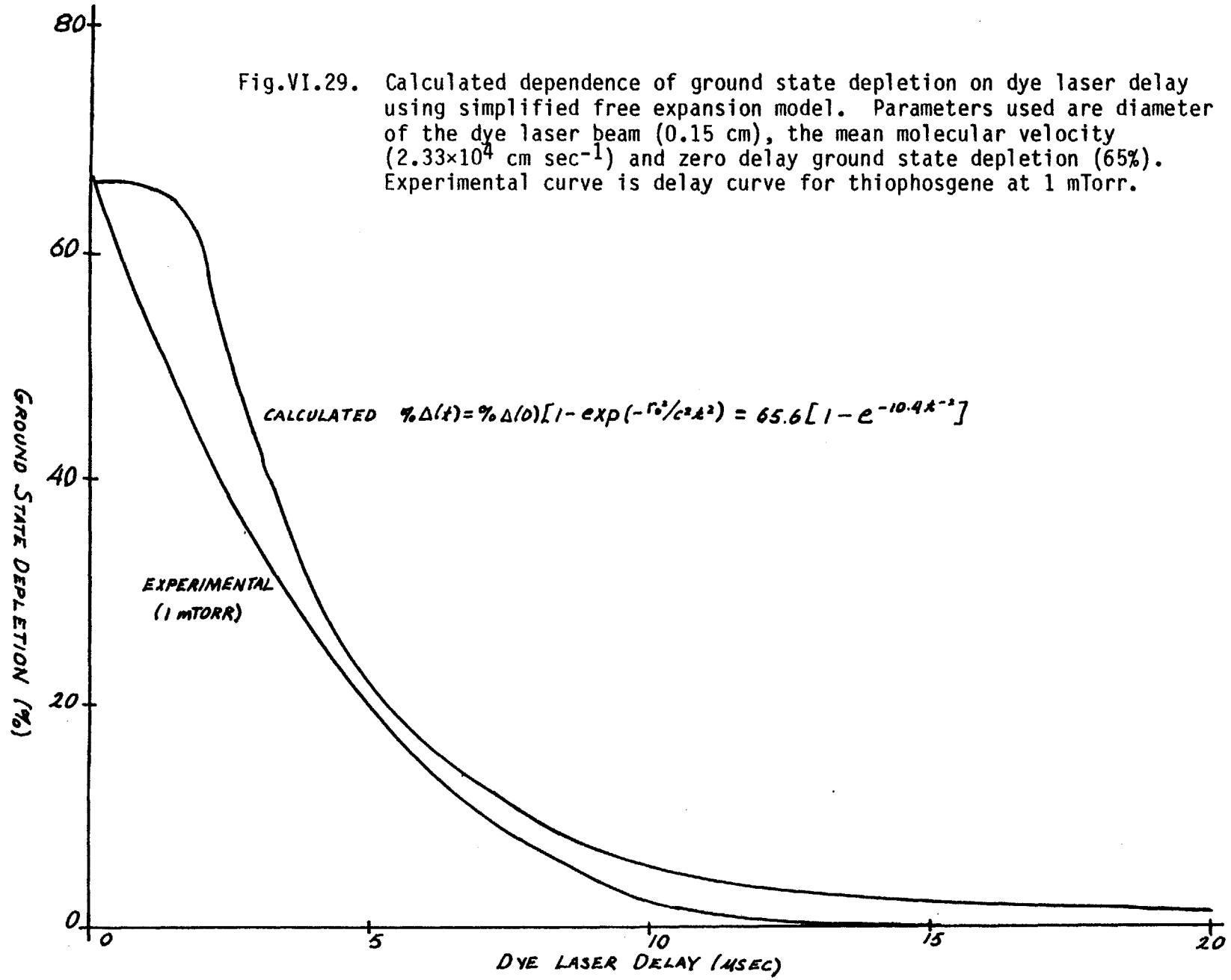


Fig.VI.29. Calculated dependence of ground state depletion on dye laser delay using simplified free expansion model. Parameters used are diameter of the dye laser beam (0.15 cm), the mean molecular velocity (2.33×10^4 cm sec^{-1}) and zero delay ground state depletion (65%). Experimental curve is delay curve for thiophosgene at 1 mTorr.

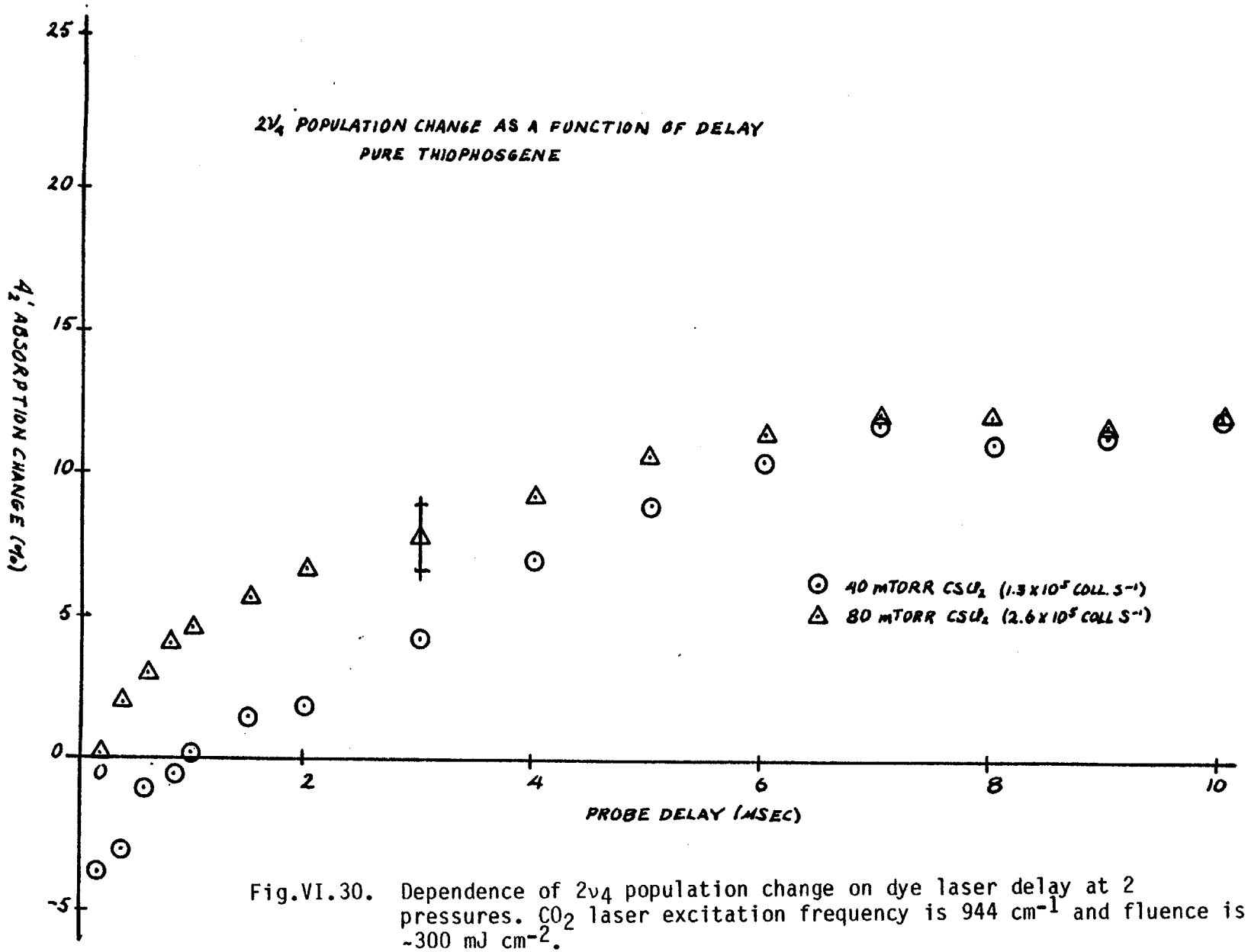


Fig.VI.30. Dependence of $2\nu_4$ population change on dye laser delay at 2 pressures. CO_2 laser excitation frequency is 944 cm^{-1} and fluence is ~300 mJ cm^{-2}.

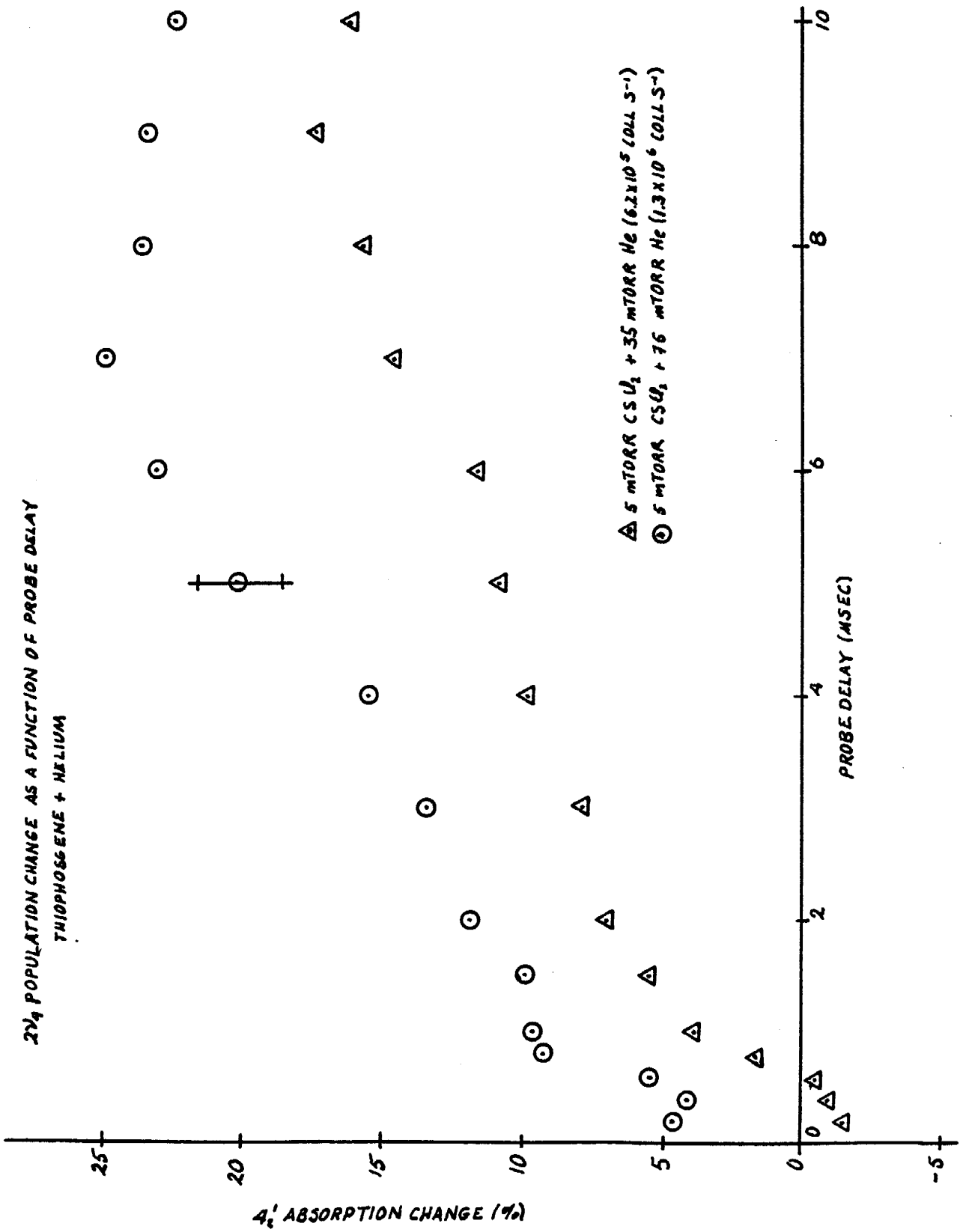


Fig.VI.31. Dependence of ν_4 population change on dye laser delay for added gas mixtures - thiophosgene and helium. CO_2 laser excitation frequency is 944 cm^{-1} and fluence is ~300 mJ cm^{-2}.

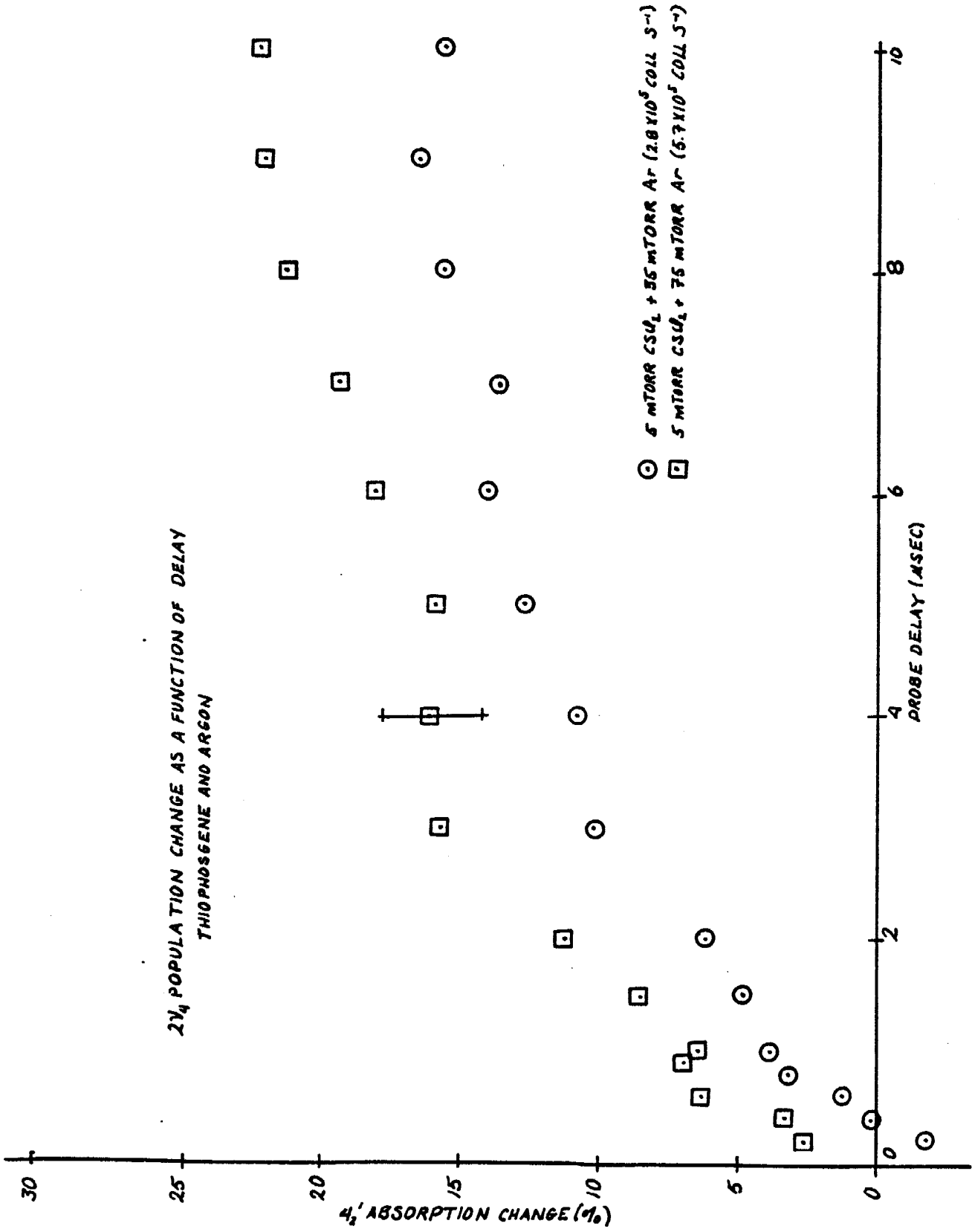


Fig.VI.32. Dependence of $2\nu_4$ population change on dye laser delay of two added gas mixtures - thiophosgene and argon. CO_2 laser excitation frequency is 944 cm^{-1} and fluence is ~300 mJ cm^{-2}.

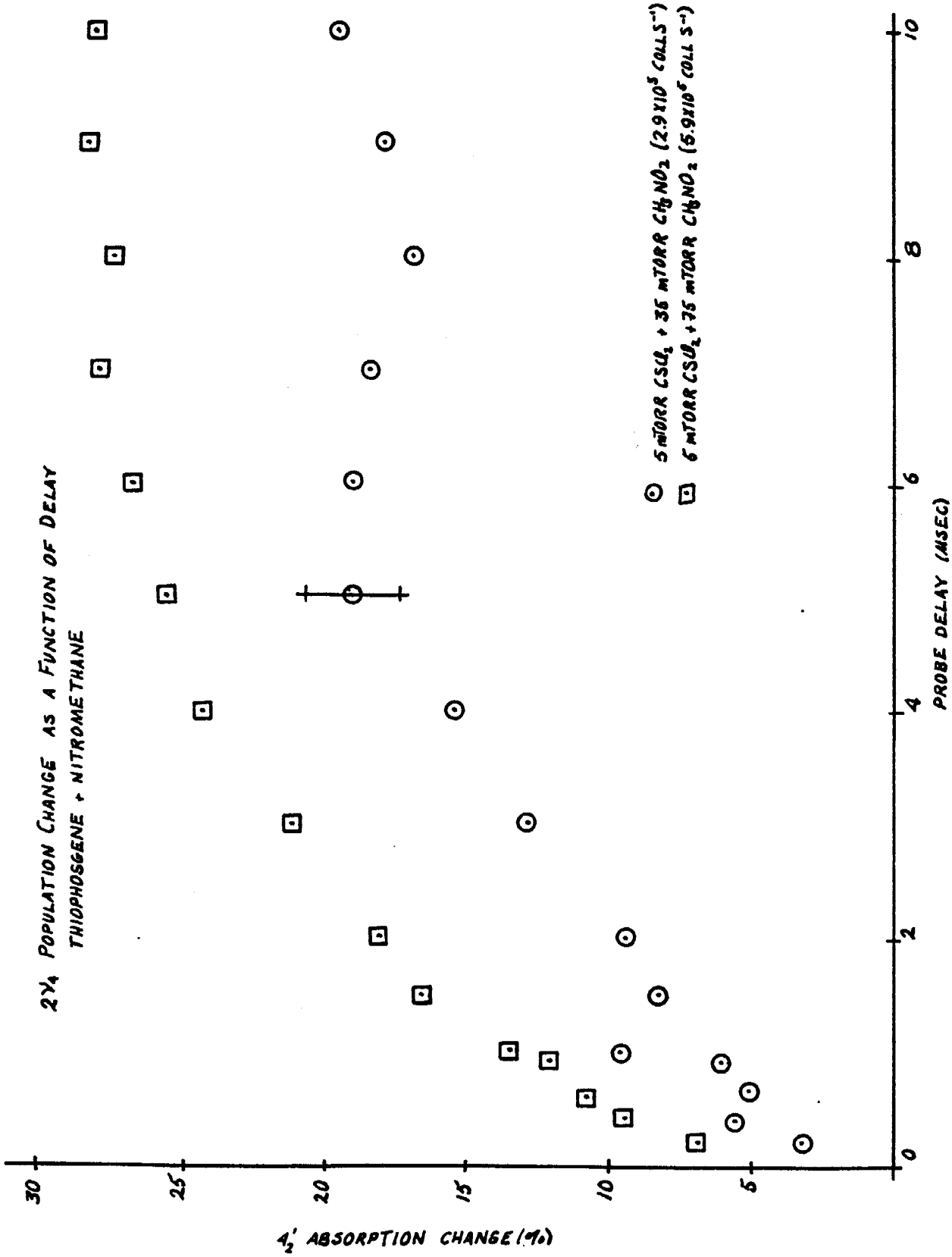


Fig.VI.33. Dependence of $4\nu_4$ population change on dye laser delay at two added gas mixtures - Thiophosgene and nitromethane. CO_2 laser excitation frequency is 944 cm^{-1} and fluence is ~300 mJ cm^{-2}.

figure, the collision frequency for each gas mixture. For example, we may compare directly the data for 5 mTorr $CSCl_2$ + 35 mTorr Ar (collision frequency = $2.8\times10^{-5}sec^{-1}$), 5 mTorr $CSCl_2$ + 35 mTorr CH_3NO_2 ($2.9\times10^{-5}sec^{-1}$) and 80 mTorr $CSCl_2$ ($2.8\times10^{-5}sec^{-1}$). As expected, nitromethane shows a greater pressure effect than argon, which, in turn, shows a greater effect than helium. Unexpectedly, thiophosgene colliding with thiophosgene is less effective in promoting population to $2\nu_4$ than all the added gases except, perhaps, helium.

VII. Discussion

The experimental results presented in the previous chapter exemplify the anomalous characteristics of thiophosgene's response to an intense and monochromatic infrared field. In this final chapter I shall present possible explanations for this molecule's unique behavior. In the process of doing so I shall draw on the results of the density matrix calculations; as I mentioned in Chapter IV, they will allow us to accept or reject hypotheses on the basis of the values of the parameters needed to make them work.

Before proceeding, let us enumerate the thiophosgene's distinctive characteristics when it undergoes IRMPA.

First, let us list the experimental observations made on thiophosgene under collisionless conditions.

1. The fraction of rotational states in the ground vibrationless state that is depleted by the CO_2 laser, at any excitation frequency, is many times larger than can be accounted for by the known infrared spectroscopy of thiophosgene. At CO_2 laser frequencies around 944 cm^{-1}, for instance, the assumption that $2\nu_4$ is the predominant pumped mode cannot explain the observed depletion, over the entire rotational envelope, of 66% (298 K). The apparent lack of rotational specificity in the ground state depletion is also observed in the first excited state of the $2\nu_4$ ladder.

2. There is no correlation between a conventional infrared spectrum of thiophosgene and a plot of the ground state depletion as a function of CO_2 laser frequency. Inspection of the infrared spectrum

shown in Fig. VI.3 shows significant absorption only by the ν_4 overtone in the region around 942 cm^{-1}. However, ground state depletion is greatest where the conventional infrared spectrum is virtually transparent. The extent of the ground state depletion also implies a far greater absorption efficiency than one derives from the infrared spectrum. On the other hand, photoacoustic measurements taken of thiophosgene at 500 mTorr correlate well with the infrared spectrum in both the frequency dependence of the infrared absorption and the average photon absorption.

3. There is no evidence for true multiphoton processes. In fact, the fluence dependence studies suggest that IRMPA proceeds through sequential one photon transitions.

4. For pumping at 944 cm^{-1}, no population increases in the excited states of the $2\nu_4$ ladder are observed. This is true regardless of the energy of the CO_2 laser pulse.

When collisions are allowed to take place with thiophosgene molecules, the following observations are made:

5. The ground state depletion is rapidly suppressed as the pressure is increased. This inverse pressure effect is observed at pressures as low as 5 mTorr and, therefore, occurs much faster than gas kinetic rate.

6. Mixed gas experiments show that the efficiency of the collisional effect is proportional to the long range forces between thiophosgene and colliding gas molecules.

For the remainder of this thesis, I will present hypotheses that, I believe, explain all of the anomalous results. The explanations are very conventional in origin but, as we shall see, require unconventional parameters to make them work. The discussion is separated into two sections: The first part is devoted to explaining the collisionless results and the second part deals with the bulb experiments.

A. Collisionless Experiments

The first unexpected observation made in the IR-VIS-DR experiments was the depletion of many more rotational states than could be explained on the basis of the known spectroscopy of thiophosgene. One hypothesis that has been proposed in the past to explain this phenomenon for thiophosgene, and other molecules, is the existence of multiphoton transitions. We have already discarded the possibility of true multiphoton transitions involving virtual intermediate states. Resonance-enhanced transitions, however, might conceivably connect rotational states in the vibrationless ground state to excited rovibrational states ($v>1$) through off-resonant intermediate states. For instance, population in those ground rotational states that could not make one-photon transitions to, say, $2\nu_4$ could perhaps find a two-photon transition to $4\nu_4$ using a resonant enhanced intermediate state at $2\nu_4$. These multiphoton transitions would allow more ground rotational states to be added to the list of states that can be pumped by a CO_2 laser at any given frequency. This mechanism has been proposed to explain similar observations on SF_6[135,136].

For explaining thiophosgene's behavior, however, this hypothesis is unsatisfactory. The $2_0^1 3_0^1 4_0^1$ spectrum for thiophosgene contains approximately 32,000 rovibronic transitions, which represent ~5400 unique ground rotational states. (For a symmetric top, each absorbing state gives rise to six transitions.) Pumping at 944 cm^{-1} with a 0.02 cm^{-1} Rabi frequency depletes 20 of these states. It is difficult to conceive that resonantly enhanced multiphoton transitions could account for the majority of the other 5380 states being depopulated. Furthermore, multiphoton transitions generally require higher electric fields or dipole moments[122] than resonant one-photon transitions and, hence, have a larger intensity threshold. The fluence studies, however, show that no appreciable threshold intensity is needed to depopulate the ground state at any CO_2 laser excitation frequency.

The extent of the ground state depletion, the fluence studies of the $2\nu_4$ and $4\nu_4$ states,the probe delay studies and the strong ground state depletion observed at frequencies where thiophosgene is transparent in an infrared spectrophotometer all point to one conclusion: Under collisionless conditions, the CO_2 laser excites vibrational transitions that are not observable in the conventional (i.e. high pressure, incoherent) infrared spectrum. More specifically, I propose that absorption is due to the pumping of combination and overtone bands that are too weak in oscillator strength to be observed in an infrared spectrum but, under collisionless conditions, are still strong enough to deplete the ground state.

Table III.2 lists the frequencies of all possible combination and

overtone bands that can conceivably be constructed out of the four lowest frequency fundamental modes. One will notice from this table that only three of these bands have been observed: The strongest of these modes is the $2\nu_4$ overtone, which has a dipole moment of 0.012 D (corresponding to a Rabi frequency of 0.02 cm^{-1} for the CO_2 laser used in these experiments). However, as the density matrix calculations show, a Rabi frequency as low as 10^{-4} cm^{-1} is sufficient to drive a resonant ladder to saturation.

This is illustrated in Tables VII.3-VII.9 in which the pressure effect is simulated using various values of detunings, Rabi frequencies, laser dephasing rates, pressure broadening coefficients and top level decay rates. For now we are only concerned with the 1 mTorr entries in each of the tables, since these points represent nearly collisionless conditions. (Other collisionless data can be found in the fluence dependence simulations but the parameters used in them are not appropriate for this part of the discussion.)

Before proceeding further with a discussion of the computer model one important point is in order. The reader will notice, when viewing the tables and graphs displaying the intensity and pressure dependence simulations, that varying parameters for the Rabi frequency have been used. This has necessitated the need for adjusting the value for the pressure broadening coefficient, accordingly, in order to simulate the pressure effect. In some cases (Tables VII.6-VII.9) the "large" Rabi frequency ($>10^{-4}$ cm^{-1}) required pressure broadening coefficients (or dephasing rates) that turn out to be unrealistically large. However, the important observation to make in each of these tables or plots is how the simulated pressure dependence changes with certain parameters--the top level

decay rate (Γ_5), the dephasing rate, and the detuning (Δ). It is just as easy to carry out all of the simulations using the lower bound Rabi frequency of 10^{-4} cm^{-1} along with the more believable dephasing rates of $<10^{10}$ sec^{-1} $Torr^{-1}$ but we chose, instead, to present the computer calculations using a range of ω_R's ($10^{-4} \rightarrow 1.5\times10^{-3}$). In in the article reproduced in Appendix D one can find simulations, which use a Rabi frequency of 0.02 cm^{-1}, and which show the effects of detunings at one or more levels in the ladder. This is fine for illustrative purposes although, as already discussed, it is doubtful that pumping at 944 cm^{-1} is characterized by this Rabi frequency.

Notice that the choice of the laser dephasing rate is critical to the absorption efficiency. For instance, for a dephasing rate and detuning of zero and a top level decay of 10^8 sec^{-1} (Table VII.3d) the ground state depletion is 92.6% whereas, for a dephasing rate $2\times10^{-9}sec^{-1}$ the ground state depletion is only 6.6%. (Since the dephasing rate is simply equal to the sum of the laser dephasing rate and the collisional dephasing rate, we may use the pressure data to determine the effects of the laser coherence.) For larger Rabi frequencies the absorption rate would not be as sensitive to the value of $1/T_2$ (laser) which acts as a base (zero pressure) broadening coefficient. This underscores the motivation, as mentioned in Chapter IV, of letting the laser dephasing rate be zero. A realistic $1/T_2$(laser) of $10^8 sec^{-1}$ would put a lower limit on the ground state depletion value of 68.1% but this difference would not affect the validity of the preceding argument.

Combination bands typically have very wide infrared band envelopes (>20 cm^{-1})[137]. Since there are eleven of them postulated to exist in a 150 cm^{-1} region, I hypothesize that they form a virtual continuum of very

weak oscillator strength throughout the CO_2 laser frequency range. Furthermore, examination of Table III.2 shows that they are most concentrated around 1000 cm^{-1}--where the ground state depletion peaks.

Absorption at frequencies around 944 cm^{-1} was previously believed to occur exclusively in the $2\nu_4$ manifold. While we still may be certain that those rovibrational transitions lying within 0.02 cm^{-1} of the CO_2 laser excitation frequency will be pumped, it now appears that the depletion of the greater than 99% of the unaffected ground states proceeds through these other modes ($2\nu_3 + \nu_6$, $\nu_2+\nu_4$, $2\nu_2$). In addition, as was mentioned in Chapter IV, there is no assurance that pumping of the $2\nu_4$ ladder proceeds beyond $2\nu_4$. Since the density matrix solutions are presented for "prototypical" rovibrational ladders, they were carried out under the assumption that pumping at 944 cm^{-1} does proceed through combination bands other than $2\nu_4$ and with a much lower Rabi frequency than 0.02 cm^{-1}.

Although this explanation is unique it is not unprecedented. Several other workers have invoked previously-unobserved combination bands to explain multiphoton absorption in molecules that were supposedly transparent to the exciting infrared radiation.

Isenor et al.[11] credited absorption in SiF_4 at 946 cm to the combination modes $2\nu_2+\nu_4$ at 925 cm-1 and $\nu_1+2\nu_2-\nu_4$ at 947 cm^{-1}. In another observation reminiscent of thiophosgene, they were unable to find an intensity threshold to absorption (dissociation) as would certainly be required if true multiphoton absorption was taking place.

Campbell et al.[138] studied the low pressure (1 Torr) multiphoton dissociation of ammonia to form NH_2 fragments. At infrared excitation

wavelengths where ammonia was transparent, dissociation was observed. In fact, like thiophosgene, the frequency dependence of the dissociation did not correlate at all with the conventional infrared spectrum. When one also considers also the unusually efficient absorption efficiency by ammonia, as reported by Tablas et al.[72] and discussed in Chapter II, it is reasonable to propose combination band pumping for this molecule as well.

Brenner et al.[86] measured the ground state depletion of propynal for several CO_2 laser frequencies and found no correlation of the values with a photoacoustic spectrum recorded in the same frequency range. Like thiophosgene, more rotational states were depopulated than could be accounted for by power broadening. For this molecule, combination bands (e.g. $\nu_4+\nu_9$), were assumed to be responsible for pumping at certain frequencies.

These three examples demonstrate that thiophosgene is not singular in its behavior when irradiated with a CO_2 laser. Still, this molecule is unrivaled in the degree with which it displays these excitation frequency effects. This I believe, is due to the following two characteristics that are unique to thiophosgene: First, there are eleven known and postulated combination bands in the 150 cm^{-1} range of the CO_2 laser that, I propose, provide a very weak, continuous absorption continuum. (If there were a fundamental vibrational mode in this region infrared pumping through this strong absorption feature might compete with and mask the effects of combination band pumping.) Second, thiophosgene's very small rotational constants give rise to an exceedingly dense manifold of rotational states. This characteristic,

together with the proliferation of combination modes, seems to guarantee that at any CO_2 laser frequency there is a set of rovibrational transitions resonant with the light field.

The earlier onset of saturation at the excitation frequencies 978 cm^{-1} and 1043 cm^{-1} than at the frequencies 944 cm^{-1} and 1081 cm^{-1} (Figs. VII.1 and VII.2) might also reflect the greater prevalence of resonant transition at the two intermediate frequencies. This same explanation can also be used to explain the greater ground state depletions observed at room temperature than at 10-15 K.

Computer simulations of fluence dependence of the ground state depletion (Tables VII.1 and VII.2 and Figs. VII.1 and VII.2) support this hypothesis. Fig. VII. shows the fluence dependence of the ground state depletion for a resonant ladder whereas Fig. VII.2 shows the fluence dependene for a ladder having detunings at each of the intermediate levels of 0.02 cm^{-1}. The resonant ladder, as expected, saturates much more quickly than the nonresonant one. Since I have postulated that the ground state depletion value measured in an IR-VIS-DR experiment represents the excitation of many ladders ensemble-averaged together, the more gradual rise in depletion with fluence for excitation at 944 cm^{-1} may be due to the greater number of off-resonant ladders driven by the laser frequency than at 978 cm^{-1}.

B. Bulb Experiments

Thiophosgene's response to collisions during infrared excitation has no precedent in the IRMPA literature. To appreciate the novelty of the results discussed in the last chapter let us review the effects collisions are known to have on other molecules undergoing infrared multiphoton absorption.

In the absence of collisions--or any other relaxtion processes--a molecule will Rabi precess through all radiation coupled states. Collisions affect this precession (nutation) of molecules up and down the pumped mode ladder in various ways:

1. Dephasing, or velocity-changing, collisions destroy the coherence of the excitation and permit the vibrational levels to acquire "steady state" populations. (Any relaxation phenomenon will also destroy the molecule's optical nutation.)

2. In what is really a by-product of all four other effects, pressure broadening spreads oscillator strength into a finite width of transitions. Those transitions that are on resonance with the infrared field lose oscillation strength while those that are off resonance generally, but not always, gain.

3. Rotational relaxation refills rotational states that have been initially depleted by the CO laser or populates states that have not been radiatively populated. In the former case, rotational relaxation enhances IRMPA by insuring a steady supply of molecules in the resonantly pumped states.

4. Collision-induced V→V relaxation spreads vibrational energy into nonpumped modes. This destroys the mode-selectivity of the pumping process but its effect on the efficiency of absorption depends on various parameters: the vibrational density of states, the relaxation rates at each pumped mode level and the oscillator strength in the pumped mode ladder and in the background states[67].

5. For very high pressures (>10 Torr) vibrational relaxation (V→T) drives population back toward the ground state.

Let us briefly review the literature to see how these collisional phenomena have affected the course of IRMPA in other molecules:

The theory of dephasing collisions is derived from the theory of $1/T_2$ relaxation in two level systems[139]. Dephasing, as was just pointed out, need not occur through collisions; any sort of perturbation (e.g. anharmonic) that couples a radiatively populated state to another state will dephase the system. In fact, coherent excitation of a vibrational manifold rarely persists for more than a few states before coupling between states totally destroys the phase relationship between the molecule and the radiation field[140]. For an excellent discussion of coherence effects in a two level system absorbing infrared light see Shoemaker's review article[68]. For a treatment of N level vibrational systems see references [125,126,141-145].

Dephasing collisions occur with the greatest cross section of all the five pressure effects mentioned and are influenced strongly by long range forces. Nonpolar SF_6, for example, has a cross section that has been measured to be $180Å^2$ [146] (approximately 9 times gas kinetic), whereas for polar methyl fluoride it is $380Å^2$ [146] (approximately 15 times gas

kinetic).

$1/T_2$ collisions have been postulated by Stone, Goodman and Thiele[125-126] as a means of reducing the unimolecular reaction rate from the top level of a coherently driven harmonic oscillator. However, no experimental investigations, to date, have implicated this phenomenon in an explanation of pressure data (perhaps because a coherently driven harmonic oscillator does not exist in nature).

Pressure broadening, like $1/T_2$ relaxationis actually a by-product of all relaxation processes--collisional or noncollisional. Nonetheless, it affects the absorption in a vibrational manifold in a fundamentally different way from the principal effects of the other pressure phenomena. Collision broadening parameters are, of course, of the same order as the pressure effect that gives rise to them. Typically, they are larger than gas kinetic reflecting the predominant contribution to them from rotational relaxation or dephasing collisions.

For formaldehyde the pressure broadening coefficient has been measured by Dyksterhuis and Heckenberg[147] and is (20.5±0.6) $MHz^{-1}Torr$ in pure formaldehyde and (3.3±0.3) MHz $torr^{-1}$ for formaldehyde in a bath of helium. These two workers also determined the broadening coefficient for OCS to be (5.9±0.2) MHz $Torr^{-1}$.

Instances of pressure broadening influencing the dynamics of infrared multiphoton absorption are rare[12,30,59,82]. Only in the first and last of the references do the authors explicitly implicate collisional broadening as the likely cause for an enhancement of absorption with pressure. References 30 and 59 describe pressure effects

that I have ascribed to this effect: the increase in the isotope enrichment factor of $^{13}CF_3Br$ with pressure[30] and increasing cross section for CF_2CHCl at low pressures. Orr et al.[82] actually used the IR-UV-DR technique to extract an estimate for pressure broadening of formaldehyde--(27±7) MHz $Torr^{-1}$.

Reports of rotational relaxation in the IRMPA literature are far more numerous[11,25-27,32,35,36,55,59,72,78,79,82,138,148]. In all instances the effect of this phenomenon has been to increase the fraction of molecules able to interact with the field by filling the rotational states depleted by the laser (See, especially, reference 33.) The pressure range over which rotational relaxation has been observed to have an effect varies between molecules. Some examples are: CF_2HCl, 0.5 to 1.5 Torr[36]; CH_3CHF_2 0.1 to 2 Torr[32]; $H_2C{=}CF$, 0.1 to 10 Torr[32]; $H_2C{=}CHF$, 0 to 15 Torr[32]; HDCO and D_2CO, 0.1 to 10 Torr[26], SF_6 0 to 100 Torr of added xenon[59]; CDF_3 0.1 to 15 Torr[25]. Mixed gas experiments on SF_6[55] showed that the absorption cross section increases linearly with the collision cross section. The most detailed investigations of rotational relaxation rate constants in a CO_2 laser driven molecule has been done by Orr et al.[11-13]. (See Chapter II on D_2CO.) From these experiments they concluded that most of the rotational relaxation in D_2CO molecules undergoing infrared absorption followed electric dipole rules and occurred in a time scale of ~10 μsec Torr.

Exchange of vibrational energy between different vibrational states --V↔V relaxation--may be easily induced by collisions. In general, when the vibrational energy change resulting from the collisional transfer (ΔE) is approximately zero and when both colliding

partners have allowed dipole moments, the V→V rate is approximately gas-kinetic. When one partner undergoes a quadrupole-allowed transition, there is little dependence of the rate on ΔE and it is roughly 1/300 of the gas kinetic frequency[149].

Collision-induced V→V relaxation, occurring during infrared excitation, has been observed mainly in isotope enrichment experiments in which it manifests itself through a decrease in the enrichment factor with an increase in pressure[15,16,24,42,44,47,48,150]. In most cases[15,16,42,44,48,150] the enrichment factor dropped to near unity (no selectivity) when the pressure reached approximately 1 Torr. Other investigations in which a positive pressure effect has been attributed to V→V relaxation include those measuring absorption cross sections[52,59], IR-UV-DR experiments[15,52,81,85-87] and experiments which monitor dissociation[25,26]. In some experiments, molecules having a fundamental frequency of vibration roughly equal to that of the pumped mode fundamental (or overtone), were used in added gas experiments[85,87,150]. In detailed investigations of relaxation of propynal by a variety of added gases, Brenner *et al.*[85,87] confirmed that energy transfer for an "allowed" transition takes place in a single collision, as predicted[149].

For pressures exceeding ~10 Torr most molecules undergoing IRMPA show a decreasing absorption cross section with pressure as a result of vibrational relaxation (V→T or V→R)[11,22,25,33,36,44,47,69,70,151]. Ambartzumian *et al.*[69] used infrared-ultraviolet double resonance to obtain estimates of the V→T time constant of ammonia. In pure ammonia it was 2.5 nsec atm (between 10 and 15 Torr). For ammonia molecules colliding with added gases, the time constant was 120±10 nsec atm

(oxygen), 188±5 nsec atm (argon) and 240±20 nsec atm (xenon).

The foregoing summary represents a wide sampling of experiments that have measured the effects of collisions on the dynamics of infrared multiphoton absorption. In none of them--or any other--has any collisional effect been observed at a pressure less than 100 mTorr. In the double resonance experiments we have done, however, the quenching of the ground state depletion "turns on" at less than 5 mTorr!

When comparing the results for thiophosgene with those for other molecules, one must remember that (with the exception of SiF_4) only thiophosgene lacks a fundamental frequency of vibration in the range of the CO_2 laser. Its weak oscillator strength in the infrared region means a small Rabi frequency and, accordingly, an unusual sensitivity to processes that interfere with the very slow rate of absorption. Therefore, it is not surprising that thiophosgene is affected more easily by collisions when it is undergoing IRMPA than other studied molecules--especially if absorption is proceeding through the combination bands postulated in the previous section.

Of the mechanisms by which collisions change the course of infrared multiphoton absorption, the one that has been implicated the least in producing a pressure effect is pressure broadening. Ordinarily, one thinks of pressure broadening as a means of distributing oscillator strength over a frequency range in such a way that a Lorentzian profile of absorption results (Eq.IV.56). Since the oscillator strength over the absorption profile is conserved, the enhancement of absorption for an off-resonant transition is always at the expense of a resonant one.

However, time constraints imposed by the pulsed CO_2 laser may not permit population to be driven out of the pressure broadened off-resonant rotational ground states. In fact, for very weakly driven systems, the broadening may be extensive enough so that none of the ladders brought into resonance are able to attain saturation by the time the 200 nanosecond CO_2 laser pulse is over. The overall result will then be a decreasing ground state depopulation as pressure broadening envelopes more and more transitions.

The plausibility of both of these latter mechanisms is supported by density matrix calculations as illustrated in Figs. VII.3-VII.6 and Tables VII.3-VII.9. Pressure broadening is incorporated in the model, as mentioned earlier, through the collisional dephasing term.

Fig. VI.5 shows the effect of detunings on the simulated ground state depletion vs. pressure curves.

Again, we must remember that different Rabi frequencies are used throughout the pressure simulation tables and plots. For the lower limit Rabi frequency--the smallest ω_R value needed to deplete the ground state within 200 nsec (10^{-4} cm^{-1}) the corresponding dephasing rate needed to suppress the pumping is 5×10^9 sec^{-1} $Torr^{-1}$. All other Rabi frequencies used in the simulations are higher and require higher values for the pressure broadening coefficient.

One can see the expected enhancement of the ground state depletion for detuned ladders as the pressure increases--but only for a low range of pressures. At pressures greater than 20 mTorr <u>all</u> ladders show a decreased absorption efficiency as the collision frequency increases. (If the infrared field were on long enough for the pressure-broadened,

off-resonant transitions to achieve saturation, one would not observe this apparent violation of oscillator strength conservation.)

Additional computer simulations show the pressure dependence of the ground state depletion for various values of the top level decay rate (Figs. VII.3 and 4) and the dephasing rate (Fig. VII.6). Notice the relative insensitivity of ground state depletion to the choice of Γ_5. This is because suppression of the radiatively driven population is more pronounced at higher vibrational states than at lower ones. Since the top level is the first state, then, to be "shut off" from infrared pumping, it makes little difference what decay routes exist for it. No juxtaposition of the experimental and computer calculated pressure curves is shown since this would imply greater knowledge of the parameters used in the density matrix program than is actually possessed. All we are striving for with these computer simulations is qualitative agreement with experiment.

For a Rabi frequency of 10^{-4} cm^{-1}, Fig. VII.3 shows that a broadening coefficient of 5×10^{9} sec^{-1} $Torr^{-1}$ is required to yield the experimentally observed pressure effect. This, I repeat, is the lower limit to the coefficient for a five-level resonant ladder undergoing IRMPA. If we use a larger Rabi frequency, then, as Fig. VII.6 shows, the dephasing width required to yield the same pressure effect increases. For purposes of comparison, the gas kinetic collision frequency for thiophosgene is 3.3×10^{6} sec^{-1} $Torr^{-1}$. Therefore, a factor of no less than 1000 separates the frequency of dephasing collisions and the hard-sphere collision frequency. The pressure experiments discussed in the last chapter told us that the pressure effect was long-range in

nature but this discrepancy between the gas-kinetic and the $1/T_2$-type collision frequencies still comes as quite a surprise. Only future experimental and theoretical investigations can decide whether or not the proposed explanation for the pressure effect is valid in light of these startling numbers. If it is, these IR-VIS-DR experiments will have provided one of the most impressive demonstration of collisional effects.

Although we have modeled the bulb experiments by varying the dephasing rate, we would have achieved similar results by varying the rate of rotational relaxation in a suitably modified density matrix program (See Chapter IV). At this time it is impossible to say whether the observed collisional effects are due to $1/T_2$ relaxation or rotational relaxation. Both phenomena occur at a rate that is influenced strongly by long range forces and both are known to occur many times faster than gas kinetic so that both are equally possible. More IR-VIS-DR experiments, in which rotational structure is clearly resolved, are needed to resolve this point.

If we accept the explanation of collision broadening of very weak but resonant ladders, we are still left with the problem of explaining the dynamics of absorption when the excitation frequency is 944 cm^{-1} and we are supposedly exciting a mode that has a Rabi frequency of 0.02 cm^{-1}. Certainly, with a Rabi frequency as large as this, pressure broadening should result in a positive pressure effect for excited states in the $2\nu_4$ ladder. This is precisely what is observed. As Figs. VII.25 and VII.26 show (even at zero probe delay), as the pressure of thiophosgene increases population buildup is observed in $2\nu_4$ and $4\nu_4$. The only reason we don't see an overall population increase in the ground state

state depletion, for CO_2 laser excitation at 944 cm^{-1} , when we raise the pressure is, I believe, because of the dominating influence of the other combination modes that are also excited at this frequency. Although they are much weaker than the overtone, I propose they allow thiophosgene to be pumped resonantly from more ground rotational states and through more vibrational levels.

The discrepancy between the experimentally measured probe delay dependence of the ground state depletion and the calculated dependence deserves some comment. It is doubtful that the approximations mentioned in the previous chapter are responsible for the discrepancy at short delays; introducing them should give an artificially fast decrease rather than a slow one, as is observed. Also, vibrational relaxation cannot be the reason since the difference between the two curves persists for pressures as low as 1 mTorr (as shown) where vibrational relaxation is inconsequential.

The most likely explanation for this discrepancy lies in the choice of the diameter of the dye laser beam (0.15 cm). A smaller value would increase the drop in the ground state depletion. This might be due to a nonuniform intensity across the beam cross section which might then result in only the central portion of the beam exciting ground state molecules to excited electronic state.

Whatever the explanation, I believe that the experimental probe delay curves are adequate for correcting the delay curves for the excited vibrational state at low to moderate delays. At long delays, however, the empirical correction factors are unusually large and yield corrected population increases that must be treated with suspicion.

One last set of data that remains to be explained is that for the probe delay/pressure experiments done with added gases (Figs. VII.30-33). When one takes into account the differing collision frequencies for each mixture of gases (indicated in each plot) one is able to verify that the pressure effect is proportional to long range forces, as expected. However, for thiophosgene molecules colliding with thiophosgene molecules, the population increases in the first excited state of the $2\nu_4$ ladder are smaller than in the argon or nitromethane experiments. Whether or not these data contradict the earlier added gas experiments is difficult to say. It is quite possible that the unexpectedly small increase in $2\nu_4$ for pure thiophosgene simply reflects an efficiency of suppression that is so great that population remains bottlenecked in the ground state. It is also possible, that, with thiophosgene molecules colliding with each other, V→V processes must be taken into account and that these somehow will change the dynamics of absorption.

This concludes my hypothesized explanation of thiophosgene's anomalous behavior when irradiated with a CO_2 laser and when undergoing collisions. At the heart of this explanation is the proposed existence of a closely packed set of combination bands lying in the frequency region of the CO_2 laser. Although the oscillator strength for each of these modes is undoubtedly very weak, they give rise, I suggest, to a "continuum" of rovibrational ladders of which, at any given excitation frequency, many are able to absorb resonantly. Density matrix calculations on 5-level protypical ladders add plausibility to this argument: A Rabi frequency of only 10^{-4} cm^{-1} is sufficient to drive a resonant ladder to saturation. These weakly driven systems are,

accordingly, easily influenced by perturbations, such as collisions, to the absorption process.

In explaining the unique collisional effects on the absorption process, I have set forth the simplest and most conventional explanation possible--pressure broadening. The range of pressure broadening coefficients that the density matrix calculations yield in order to obtain agreement with experiment is unusually large--greater than 1000 times gas kinetic. Among studies of collision-induced interactions this sensitivity to pressure is unprecedented but more experiments are needed to confirm or reject this explanation.

Future workers who wish to gain more insight into these newly discovered phenomena should pursue the following experimental and theoretical investigations:

Of highest priority, is the normal coordination analysis of each of the postulated overtone and combination bands listed in Table IV.2 From these calculations will come a determination of the frequencies, anharmonicities and dipole moments for each mode. If, in addition, high resolution spectra of these modes could possibly be recorded and assigned, then we would possess all the necessary vibrational and rotational parameters needed to model the dynamics of absorption using the density matrix equation solution program. Hopefully, we could also measure pressure broadening coefficients for these modes. This essential information would allow us to modify the program to include such effects as intramolecular relaxation and rotational relaxation. The resulting computer model would be spectroscopically complete and enable us to model, quantitatively, thiophosgene's response to an intense infrared

field, as we change the excitation frequency, vary the field intensity, and increase the pressure.

One modification of the experimental apparatus that can be implemented immediately and that might answer the question of how rotationally selective IRMPA by thiophosgene is the replacement of the current dye laser probe with one of much higher resolution. For the future other double resonance schemes could be employed which would allow us to probe vibrational states that we could not access with our infrared-visible experiment. Infrared-infrared double resonance or IR-UV-DR employing, perhaps, the second excited singlet state might give a more complete picture of the vibrational distribution set up by the CO_2 laser.

Lastly, it is imperative that we determine whether thiophosgene responds to an infrared field and to collisions in a totally unique way or whether other molecules share its unexpected properties. Because of its many low frequency vibrational modes and very dense rotational structure, I believe that the number of molecules that might be found to possess these unusual characteristics will be very few. Ammonia and silicon tetrafluoride are two candidates that have already shown a faint resemblence to thiophosgene and ought to be studied more thoroughly.

As a means of modeling infrared absorption more quantitatively, I suggest that diatomic molecules, such as several of the metal hydrides, be used in an IR-UV-DR experiment. Even if absorption proceeds only through two quanta of the vibrational mode, the rotationally resolved data that would be obtained would provide an excellent test for the ability of the density matrix formalism to simulate infrared multiphoton

absorption.

Perhaps the most intriguing experiment of all that could be done immediately would be to try to find a molecule that is totally transparent in the CO_2 laser frequency but which has fundamental frequencies of vibration less than 100 cm^{-1} and which has a well-resolved visible absorption spectrum. If our explanation of thiophosgene's behavior is correct then this molecule should behave in the same way. If so, then these experiments will have shown that weak interactions between radiation and matter are of far more consequence than once believed and their study will take on a new importance.

Simulations of Intensity Dependence of CO_2 Laser Induced Population Changes in a Five-Level Ladder

Tables (VII.1) Resonant Ladders (Δ's = 0)

$1/T_2(\text{LASER}) = 10^9\ \text{sec}^{-1}$ $\quad$ $1/T_2 = 10^{12}\ \text{sec}^{-1}/\text{Torr}$

(a) $\Gamma_5 = 10^7\ \text{sec}^{-1}$

$\omega_R(\text{cm}^{-1})$	Level 1	2	3	4	5
10^{-4}	.934	.062	.004	.000	.000
2×10^{-4}	.779	.172	.038	.007	.002
4×10^{-4}	.468	.250	.134	.074	.042
6×10^{-4}	.286	.212	.162	.127	.104
8×10^{-4}	.204	.180	.160	.144	.131
10^{-3}	.173	.163	.153	.145	.137
1.25×10^{-3}	.158	.152	.147	.142	.137
1.5×10^{-3}	.156	.147	.143	.140	.136
2×10^{-3}	.143	.141	.139	.137	.135

(b) $\Gamma_5 = 10^8\ \text{sec}^{-1}$

ω_R ($\times10^{-4}$ cm^{-1})	Level 1	2	3	4	5
1	.9434	.062	.004	.000	.000
2	.779	.172	.038	.008	.006
4	.468	.247	.127	.057	.010
6	.275	.188	.120	.067	.011
8	.161	.119	.083	.042	.025
10	.094	.073	.054	.037	.022
12.5	.051	.041	.032	.025	.017
15	.030	.025	.021	.017	.013
20	.015	.013	.012	.010	.009

(c) $\Gamma_5 = 10^{10}$ sec^{-1}

ω_R(cm^{-1})	Level 1	2	3	4	5
1	.934	.062	.004	.000	.000
2	.229	.172	.038	.010	.000
4	.469	.253	.142	.087	.000
6	.288	.213	.157	.115	.000
8	.186	.149	.117	.088	.000
10	.114	.092	.073	.055	.000
12.5	.021	.017	.014	.010	.000
20	.002	.002	.001	.001	.000

Tables VII.2 - Off-Resonant Ladders ($\Delta_2 = \Delta_3 = \Delta_4 = 0.02$ cm^{-1})

(a) $\Gamma_6 = 10^7$ sec^{-1}

ω_R ($\times 10^{-4}$ cm^{-1})	Level 1	2	3	4	5
1	.985	.014	.001	.000	.000
2	.941	.047	.010	.002	.000
4	.794	.108	.054	.033	.007
6	.616	.146	.101	.079	.033
8	.453	.164	.133	.116	.059
10	.330	.169	.150	.138	.101
12.5	.237	.166	.156	.149	.125
15	.191	.160	.155	.151	.134
20	.160	.150	.148	.146	.137

(b) $\Gamma^5 = 10^8$ sec^{-1}

ω_R ($\times 10^{-4}$ cm^{-1})	Level 1	2	3	4	5
1	.985	.014	.001	.000	.000
2	.941	.047	.010	.002	.000
4	.794	.108	.054	.032	.001
6	.616	.143	.096	.071	.007
8	.450	.149	.114	.091	.015
10	.318	.134	.109	.090	.022
12.5	.202	.103	.087	.074	.026
15	.128	.074	.065	.056	.025
20	.056	.038	.034	.031	.018

(c) $\Gamma_5 = 10^{10}$ sec^{-1}

ω_R ($\times 10^{-4}$ cm^{-1})	Level 1	2	3	4	5
1	.985	.014	.001	.000	.000
2	.941	.047	.010	.002	.000
4	.794	.108	.053	.032	.000
6	.615	.142	.095	.069	.000
8	.448	.144	.107	.083	.000
10	.312	.121	.094	.074	.000
12.5	.086	.080	.064	.051	.000
15	.101	.045	.036	.029	.000
20	.022	.010	.008	.006	.000

Simulations of Pressure Dependence of CO_2 Laser-Induced Population Changes in a Five-Level Ladder

Tables VII.3

$\omega_R = 10^{-4}$ cm^{-1} Δ's = 0 $1/T_2$(LASER) = 0 $1/T_2 = 10^{10}$ sec^{-1} Torr^{-1}

(a) $\Gamma_5 = 0$

Pressure (mTorr)	Level 1	2	3	4	5
1	.224	.250	.191	.164	.170
5	.271	.217	.183	.163	.166
10	.419	.248	.151	.099	.083
20	.588	.244	.101	.043	.024
40	.740	.193	.050	.013	.004
60	.810	.154	.029	.006	.001
80	.850	.128	.019	.003	.000
100	.876	.109	.013	.002	.000
200	.934	.062	.004	.000	.000

(b) $\Gamma_5 = 10^6$ sec^{-1}

Pressure (mTorr)	Level 1	2	3	4	5
1	.216	.241	.184	.158	.163
5	.270	.216	.181	.160	.159
10	.419	.248	.150	.098	.080
20	.588	.249	.101	.043	.023
40	.740	.193	.050	.013	.004
60	.810	.154	.029	.006	.001
80	.850	.128	.019	.003	.000
100	.876	.109	.013	.002	.000
200	.934	.062	.004	.000	.000

c) $\Gamma_5 = 10^7$ sec^{-1}

Pressure (mTorr)	Level 1	2	3	4	5
1	.160	.175	.136	.116	.118
5	.268	.208	.164	.133	.116
10	.418	.247	.146	.088	.058
20	.588	.244	.100	.041	.017
40	.740	.193	.050	.013	.003
60	.810	.154	.029	.006	.001
80	.850	.128	.019	.003	.000
100	.876	.109	.013	.002	.001
200	.934	.062	.004	.000	.000

(d) $\Gamma_5 = 10^8$ sec^{-1}

Pressure (mTorr)	Level 1	2	3	4	5
1	.074	.061	.056	.054	.021
5	.265	.197	.141	.098	.023
10	.418	.246	.141	.077	.012
20	.588	.244	.100	.039	.004
40	.740	.193	.050	.013	.001
60	.810	.154	.029	.005	.000
80	.850	.128	.019	.003	.000
100	.876	.109	.013	.002	.000
200	.934	.062	.004	0	0

Tables VII.4

$\omega_R = 10^{-4}$ cm^{-1} Δ's=0 $1/T_2$(LASER) = 0 $1/T_2 = 5\times10^9$ sec^{-1} mTorr^{-1}

(a) $\Gamma_5 = 0$

Pressure (mTorr)	Level 1	2	3	4	5
1	.308	.299	.162	.115	.117
5	.189	.204	.202	.197	.208
10	.271	.217	.193	.163	.166
20	.419	.248	.151	.099	.083
40	.588	.244	.101	.043	.024
60	.681	.218	.069	.022	.009
80	.740	.172	.038	.008	.002
100	.780	.172	.038	.008	.002
200	.876	.109	.013	.002	.000

(b) $\Gamma^5 = 10^8$ sec^{-1}

Pressure (mTorr)	Level 1	2	3	4	5
1	.047	.032	.032	.032	.014
5	.154	.129	.106	.088	.027
10	.265	.197	.141	.098	.023
20	.418	.246	.141	.077	.012
40	.588	.244	.100	.039	.004
60	.681	.218	.069	.021	.001
80	.740	.193	.050	.013	.001
100	.780	.172	.038	.008	.000
200	.876	.109	.013	.002	.000

Tables VII.5

$\omega R = 10^{-4}$ cm^{-1} $\quad \Delta = 0 \quad 1/T_2(\text{LASER}) = 0 \quad \Gamma_5 = 10^8$ sec^{-1}

(a) $1/T_2(1) = 10^{10}$ sec^{-1} Torr^{-1} $\quad 1/T_2(2 \to 5) = 0$

Pressure (mTorr)	Level 1	2	3	4	5
1	.022	.004	.004	.005	.006
5	.030	.018	.016	.026	.018
10	.060	.033	.032	.044	.026
20	.149	.055	.046	.060	.0231
40	.320	.066	.049	.059	.028
60	.444	.064	.045	.052	.024
80	.532	.059	.039	.046	.021
100	.597	.054	.035	.040	.018

(b) $1/T_2(1) = 0 \quad 1/T_2(2 \to \sigma) = 10^{10}$ sec^{-1} Torr^{-1}s

Pressure (mTorr)	Level 1	2	3	4	5
1	.046	.028	.031	.028	.011
5	.131	.118	.099	.080	.024
10	.211	.188	.141	.099	.023
20	.319	.262	.164	.094	.015
40	.451	.307	.139	.057	.005
60	.537	.305	.106	.034	.002
80	.601	.289	.081	.021	.001
100	.649	.270	.063	.014	.001

(c) $1/T_2(1\rightarrow4) = 0$ $\quad 1/T_2(5) = 10^{10}\ \text{sec}^{-1}\ \text{Torr}^{-1}$

Pressure (mTorr)	Level 1	2	3	4	5
1	.033	.003	.005	.001	.002
5	.072	.012	.008	.004	.002
10	.118	.022	.010	.005	.003
20	.201	.036	.011	.007	.003
40	.326	.055	.009	.008	.002
60	.413	.067	.007	.008	.002
80	.476	.075	.006	.008	.002
100	.524	.081	.005	.008	.002

(d) $1/T_2(1\rightarrow3) = 0$ $\quad 1/T_2(4,5) = 10^{10}\ \text{sec}^{-1}\ \text{torr}^{-1}$

Pressure (mTorr)	Level 1	2	3	4	5
1	.039	.014	.012	.006	.003
5	.098	.059	.037	.022	.006
10	.162	.093	.053	.036	.009
20	.269	.120	.065	.057	.011
40	.420	.114	.064	.091	.011
60	.519	.095	.055	.114	.010
80	.588	.079	.046	.127	.009
100	.639	.066	.039	.133	.002

(e) $1/T_2(1 \rightarrow 2) = 0$ $\quad 1/T_2(3 \rightarrow 5) = 10^{10}\ \text{sec}^{-1}\ \text{Torr}^{-1}$

Pressure (mTorr)	Level 1	2	3	4	5
1	.047	.022	.021	.012	.005
5	.127	.084	.069	.042	.012
10	.197	.131	.101	.065	.016
20	.285	.178	.133	.094	.017
40	.378	.216	.160	.106	.011
60	.427	.234	.169	.095	.007
80	.460	.246	.170	.080	.005
100	.483	.255	.167	.067	.003

Tables VII.6

$\omega_R = 10^{-3}$ cm^{-1} Δ's = 0 $1/T_2$(LASER) = 1.59×10^{8} sec^{-1}

(a) $1/T_2 = 1.59\times10^{10}$ sec^{-2} Torr^{-1} $\Gamma_5 = 0$

Pressure (mTorr)	Level 1	2	3	4	5
1	.040	.034	.027	.021	.016
5	.063	.051	.039	.029	.019
10	.094	.073	.054	.037	.022
20	.153	.114	.080	.051	.025
40	.252	.175	.114	.064	.024
60	.327	.211	.129	.067	.019
80	.386	.232	.133	.065	.015
100	.436	.243	.130	.060	.012
200	.596	.240	.096	.035	.004

(b) $1/T_2 = 1.59\times10^{10}$ sec^{-1} Torr^{-1} $\Gamma_5 = 1.59\times10^{7}$ sec^{-1}

Pressure (mTorr)	Level 1	2	3	4	5
1	.063	.051	.039	.029	.019
5	.181	.132	.090	.055	.025
10	.292	.196	.123	.067	.022
20	.436	.243	.130	.060	.012
40	.596	.240	.096	.035	.004
60	.686	.215	.067	.020	.002
80	.743	.191	.049	.012	.001
100	.782	.170	.037	.008	.000
200	.887	.108	.013	.002	.000

(c) $1/T_2 = 7.95\times10^{10}$ xec^{-1} Torr^{-1} $\quad \Gamma_5 = 1.59\times10^{8}$ sec^{-1}

Pressure (mTorr)	Level 1	2	3	4	5
1	.063	.051	.039	.029	.019
5	.169	.117	.073	.037	.002
10	.288	.189	.113	.054	.002
20	.435	.242	.127	.055	.001
40	.596	.240	.095	.033	.000
60	.686	.215	.067	.019	.000
80	.743	.191	.049	.012	.000
100	.782	.170	.037	.008	.000
200	.887	.108	.013	.002	.000

(d) $1/T_2 = 7.95\times10^{10}$ sec^{-1} Torr^{-1} $\quad \Gamma_5 = 1.59\times10^{9}$ sec^{-1}

Pressure (mTorr)	Level 1	2	3	4	5
1	.086	.072	.059	.047	.000
5	.192	.145	.106	.072	.000
10	.295	.202	.132	.079	.000
20	.436	.244	.134	.066	.000
40	.596	.241	.096	.036	.000
60	.686	.215	.068	.020	.000
80	.643	.191	.049	.012	.000
100	.782	.170	.037	.008	.000
200	.877	.108	.013	.002	.000

(e) $1/T_2 = 1.59\times10^{11}$ sec^{-1} Torr^{-1} $\quad \Gamma_5 = 1.59\times10^{8}$ sec^{-1}

Pressure (mTorr)	Level 1	2	3	4	5
1	.094	.073	.054	.037	.022
5	.292	.196	.123	.067	.022
10	.436	.243	.130	.060	.012
20	.596	.240	.096	.035	.004
40	.743	.191	.049	.012	.001
60	.811	.153	.029	.005	.002
80	.851	.127	.019	.003	.000
100	.877	.108	.013	.002	.000
200	.934	.062	.004	.000	.000

Table VII.7

$\omega_R = 10^{-3}$ cm^{-1} $\quad \Delta_2 = \Delta_3 = \Delta_4 = 0.02$ cm^{-1}

$1/T_2$(LASER) $= 1.59\times10^{8}$ sec^{-1} Torr^{-1} $\quad \Gamma^5 = 1.59\times10^{7}$ sec^{-1}

Pressure (mTorr)	Level 1	2	3	4	5
1	.318	.134	.109	.090	.022
5	.348	.198	.126	.075	.019
10	.459	.237	.127	.061	.011
20	.603	.237	.094	.034	.004
40	.744	.190	.049	.012	.001
60	.812	.153	.029	.005	.000
80	.851	.127	.019	.003	.000
100	.877	.108	.013	.002	.000
200	.934	.062	.004	.000	.000

Tables VII.8

$\omega_R = 1.5\times10^{-3}$ cm^{-1} Δ's = 0 $1/T_2$(LASER) = 1.59×10^{11} sec^{-1} Torr^{-1}

(a) $\Gamma_5 = 1.59\times10^{6}$ sec^{-1}

Pressure (mTorr)	Level 1	2	3	4	5
1	.150	.147	.143	.140	.136
5	.190	.173	.158	.145	.134
10	.263	.204	.162	.133	.112
20	.397	.241	.149	.095	.064
40	.562	.246	.108	.048	.022
60	.656	.226	.078	.027	.009
80	.717	.203	.057	.016	.004
100	.760	.182	.044	.011	.002
200	.863	.118	.016	.002	.000

(b) $\Gamma_5 = 1.59\times10^{7}$ sec^{-1}

Pressure (mTorr)	Level 1	2	3	4	5
1	.030	.024	.021	.017	.013
5	.134	.101	.072	,046	.025
10	.247	.172	.112	.064	.024
20	.395	.234	.133	.064	.015
40	.562	.246	.106	.041	.005
60	.656	.226	.077	.024	.002
80	.717	.203	.057	.015	.001
100	.760	.183	.044	.010	.001
200	.853	.118	.016	.002	.000

(c) $\Gamma_5 = 1.59\times10^9\ sec^{-1}$

Pressure (mTorr)	Level 1	2	3	4	5
1	.021	.017	.014	.010	.000
5	.130	.095	.066	.040	.000
10	.246	.170	.109	.059	.000
20	.395	.234	.132	.063	.000
40	.562	.246	.106	.040	.000
60	.656	.226	.077	.024	.000
80	.717	.203	.057	.015	.000
100	.760	.183	.044	.010	.000
200	.863	.118	.016	.002	.000

Tables VII.9

$\omega_R = 1.5\times10^{-3}cm^{-1}$ $1/T_2(LASER) = 1.59\times10^8sec^{-1}$ $1/T_2 = 1.59\times10^{11}sec^{-1}Torr^{-1}$

(a) $\Delta = 0$ $(\Gamma_5 = 1.59\times10^7\ sec^{-1}$

Pressure (mTorr)	Level 1	2	3	4	5
1	.091	.077	.064	.052	.040
5	.134	.101	.072	.046	.025
10	.247	.172	.112	.064	.024
20	.395	.234	.133	.064	.015
40	.562	.246	.106	.041	.005
60	.656	.226	.077	.024	.002
80	.717	.203	.057	.015	.001
100	.760	.183	.044	.010	.000
200	.863	.118	.016	.002	.000

(b) Δ=0.01 cm^{-1} (Γ_5 - 1.59×10^7 sec^{-1})

Pressure (mTorr)	Level 1	2	3	4	5
1	.050	.038	.032	.026	.017
5	.142	.104	.075	.049	.025
10	.251	.173	.113	.065	.024
20	.397	.234	.132	.064	.015
40	.562	.245	.106	.041	.005
60	.656	.225	.077	.024	.002
80	.717	.203	.057	.015	.001
100	.760	.183	.044	.010	.001
200	.863	.118	.016	.002	.000

(c) Δ = 0.02 cm^{-1} (Γ_5 = 1.59×10^7 sec^{-1})

Pressure (mTorr)	Level 1	2	3	4	5
1	.198	.161	.154	.148	.000
5	.221	.186	.166	.148	.000
10	.283	.214	.171	.139	.000
20	.404	.244	.155	.103	.000
40	.564	.246	.110	.052	.000
60	.657	.225	.078	.028	.000
80	.717	.203	.058	.017	.000
100	.760	.182	.044	.011	.000
200	.863	.118	.016	.002	.000

(d) $\Delta = 0.05\ cm^{-1}$ ($\Gamma_5 = 1.59\times10^8\ sec^{-1}$)

Pressure (mTorr)	Level 1	2	3	4	5
1	.542	.110	.101	.095	.012
5	.332	.146	.113	.089	.021
10	.339	.182	.122	.079	.020
20	.432	.228	.129	.066	.013
40	.573	.240	.103	.040	.005
60	.661	.222	.076	.024	.002
80	.720	.201	.057	.015	.001
100	.761	.181	.044	.010	.001
200	.863	.118	.016	.002	.000

(e) $\Delta = 0.10\ cm^{-1}$ ($\Gamma_5 = 1.59\times10^8\ sec^{-1}$)

Pressure (mTorr)	Level 1	2	3	4	5
1	.841	.050	.047	.045	.001
5	.643	.111	.090	.078	.007
10	.543	.155	.108	.080	.010
20	.525	.203	.115	.065	.009
40	.605	.225	.096	.039	.004
60	.675	.214	.073	.024	.002
80	.727	.196	.055	.015	.001
100	.766	.178	.047	.010	.001
200	.864	.118	.016	.002	.000

Tables VII.10

Simulation of CO_2 Laser-Induced Population Changes in a Five Level Ladder Calculated Using a Realistic Pulse Shape

For all simulations:

Rectangular Pulse No.	τ(nsec)	$\omega_R(cm^{-1})$
1	0-25	2.5×10^{-4}
2	25-50	5.0×10^{-4}
3	50-75	1.75×10^{-3}
4	75-100	1.25×10^{-3}
5	100-130	7.5×10^{-4}
6	130-165	5.0×10^{-4}
7	165-205	4.0×10^{-4}
8	205-250	2.5×10^{-4}
9	250-2250	2.0×10^{-5}

$\sum\omega_R\Delta\tau = 0.2\ cm^{-1}\ nsec$

(a) Δ's=0 $1/T_2$=0 $1/T_2$(LASER)=0 Γ_5 = 0 1mTorr

Pressure (mTorr)	Level 1	2	3	4	5
1	.254	.345	.243	.099	.059
2	.271	.371	.222	.074	.062
3	.467	.025	.220	.027	.262
4	.291	.324	.159	.101	.124
5	.330	.248	.172	.084	.166
6	.398	.123	.197	.051	.232
7	.350	.205	.181	.073	.190
8	.347	.204	.181	.075	.192
9	.237	.199	.194	.167	.203

(b) Δ's = 0 $1/T_2$(LASER) = 10^8 sec^{-1} $1/T_2$'s = 10^{12} sec^{-1}/Torr

Γ's=0 1mTorr

Pressure (mTorr)	Level 1	2	3	4	5
1	.911	.081	.007	.001	.000
2	.671	.222	.073	.024	.010
3	.209	.202	.198	.196	.195
4	.201	.200	.200	.199	.199
5	.201	.200	.200	.200	.200
6	.200	.200	.200	.200	.200
7	.200	.200	.200	.200	.200
8	.200	.200	.200	.200	.200
9	.200	.200	.200	.200	.200

(c) Δ's = 0 $1/T_2$(LASER) = 0 $1/T_2 = 10^{11}$ sec^{-1} Γ's = 0 100 mTorr

Pressure (mTorr)	Level 1	2	3	4	5
1	.545	.281	.119	.038	.016
2	.201	.201	.198	.175	.225
3	.206	.200	.197	.195	.202
4	.202	.201	.200	.199	.198
5	.200	.200	.200	.200	.200
6	.200	.200	.200	.200	.200
7	.200	.200	.200	.200	.200
8	.200	.200	.200	.200	.200
9	.200	.200	.200	.200	.200

(d) Δ's = 0 $1/T_2$(LASER) = 0 $1/T_2 = 10^{12}$ sec^{-1} Γ's = 0 100 mTorr

Pressure (mTorr)	Level 1	2	3	4	5
1	.903	.088	.008	.001	.000
2	.650	.229	.080	.028	.013
3	.205	.201	.100	.197	.197
4	.201	.200	.200	.200	.200
5	.200	.200	.200	.200	.200
6	.200	.200	.200	.200	.200
7	.200	.200	.200	.200	.200
8	.200	.200	.200	.200	.200
9	.200	.200	.200	.200	.200

REFERENCES

1. J. I. Steinfeld, Molecules and Radiation, M.I.T. Press, Cambridge, MA, 1974.
2. S. Druet, J. Taran, Chemical and Biocheimical Applicatons of Lasers, Vol. 4, Edited by C. B. Moore, Academic Press, 1979, 182-252.
3. A. Yariv, Quantum Electronics, second edition, J. Wiley, New York, New York, 1975.
4. M. Sargent III, M. O. Scully, W. E. Lamb, Jr., Laser Physics, Addison Wesley, Reading, MA 1974.
5. W. C. Peticolas, "Multiphoton Spectroscopy", Ann. Rev. Phys. Chem. 18, 233-260 (1967).
6. M. C. Borde, A. H. Henry, M. C. Henry, C. R. Acad. Sci. Paris, B262, 1389-1390 (1969).
7. N. V. Karlov, Y. N. Petrov, A. M. Prokhorov, O. M. Stel'makh, Zhetf. Pis. Red. 11, 220-222, (1970).
8. S. S. Alimpiev, N. V. Karlov, Sov. Phys. JETP 39, 260-264 (1974).
9. V. S. Letokhov, N. V. Chekalin, V. S. Dojikov, V. S. Letokhov, E. A. Ryabov, Chem. Phys. Lett. 25, 515-518 (1974).
10. N. R. Isenor, V. Merchant, R. S. Hallsworth, M. C. Richardson, Can. J. Phys 51, 1281-1287 (1973).
11. N. R. Isenor, M. C. Richardson, Appl. Phys. Lett. 18, 224-226 (1971).
12. V. S. Letokhov, E. A. Ryabov, O. A. Tumanov, Opt. Commun. 5, 168-169 (1972).
13. V. S. Letokhov, E. A. Ryabov, O. A. Tumanov, Sov. Phys. JETP 36, 1069-1073 (1973).

14. R. V. Ambartzumian, V. S. Letokhov, E. A. Ryabov, N. V. Chekalin, JETP Lett. 20, 273-27 (1974).

15. R. V. Ambartzumian, Y. A. Gorokov, V. S. Letokhov, G. N. Makarov, JETP Lett. 21, 171-172 (1975).

16. J. L. Lyman, R. J. Jensen, J. Rink, C. P. Robinson, S. D. Rockwood, Appl. Phys. Lett. 27, 87-89 (1975).

17. J. L. Lyman, R. J. Jensen, J. Phys. Chem. 77, 883-888 (1973).

18. J. I. Steinfeld, Laser Induced Chemical Processes, Ed. by J. I. Steinfeld, Plenum, Cambridge, MA, 1981, Ch. 4.

19. R. V. Ambartzumian, Y. A. Gorokhov, V. S. Letokhov, C. N. Makarov, A. A. Puretsii, JETP Lett. 23, 22-25 (1976).

20. R. V. Ambartzumian, N. P. Furzikov, Y. A. Gorokhov, V. S. Letokhov, G. N. Makarov, A. A. Puretskii, Opt. Commun. 18, 517-521 (1976).

21. R. V. Ambartzumian, Y. A. Gorokhov, V. S. Letokhov, G. N. Makarov, N. P. Furzikov, JETP Lett. 23, 194-197 (1976).

22. R. V. Ambartzumian, N. V. Chekalin, V. S. Doljikov, V. S. Letokhov, V. N. Lokhman, Opt. Commun. 18, 400-402 (1976).

23. P. Kolodner, C. Winterfeld, E. Yablonovitch, Opt. Commun. 20, 119-122 (1977).

24. D. Tal, U. P. Oppenheim, G. Koren, M. Okon, Chem. Phys. Lett. 48, 67-71 (1977).

25. R. Corkum, C. Willis, R. A. Back, Chem. Phys. 24, 13-23 (1977).

26. I. P. Herman, J. B. Marling, Chem. Phys. Lett. 64, 75-80 (1979).

27. G. Koren, M. Okon, U. P. Oppenheim, Opt. Commun. 22, 13-23 (1977).

28. G. Koren, U. P. Oppenheim, Opt. Commun. 26, 449-452 (1978).

29. G. Koren, Appl. Phys. 21, 65-75 (1980).

30. P. A. Hackett, M. Gauthier, C. Willis, R. Pilon, J. Chem. Phys. 71, 3613-3619 (1979).

31. P. A. Schultz, A. S. Sudbo, E. R. Grant, Y. R. Shen, Y. T. Lee, J. Chem. Phys. 72, 4985-4995 (1980).

32. C. R. Quick, Jr., C. Wittig, J. Chem. Phys. 69, 4201-4205 (1978).

33. J. Stone, E. Thiele, M. F. Goodman, J. C. Stephenson, D. S. King, J. Chem. Phys. 73, 2259-2270 (1980).

34. J. C. Stephenson, D. S. King, J. Chem. Phys. 69, 1485-1492 (1978).

35. J. C. Stephenson, D. S. King, M.F. Goodman, J. Stone, J. Chem. Phys. 70, 4496-4508 (1979).

36. R. Duperrex, H. Van den Bergh, J. Chem. Phys. 71, 3613-3619 (1979),

37. Y. Haas, G. Yahav, Chem. Phys. Lett. 48, 63-66 (1977).

38. M. N. R. Ashfold, M. A. Fullstone, G. Hancock, G. W. Ketley, Chem. Phys. 55, 245-257 (1981).

39. M. N. R. Ashfold, G. Hancock, G. W. Ketley, Farad. Disc. Chem. Soc. 67, 204-211 (1979).

40. M. N. R. Ashfold, G. Hancock, M. L. Hardaker, J. Photochem. 10, 85-88 (1980).

41. G. Hancock, R. J. Hennesy, T. Villis, J. Photochem. 10, 305-314 (1979).

42. R. V. Ambartzumian, Y. A. Gorokhov, V. S. Letokhov, G. N. Makarov, Sov. Phys. JETP 42, 993-1000 (1976).

43. S. M. Freund, J. J. Ritter, Chem. Phys. Lett. 32, 255-260 (1975).

44. R. V. Ambartzumian, Y. A. Gorokhov, V. S. Letokhov, G. N. Makarov, E. A. Ryabov, N. V. Chekalin, Sov. J. Quant. Electron. 6, 437-441 (1976).

45. R. V. Ambartzumian, N. P. Furzikov, Y. A. Gorokhov, V. S. Letokhov, G. N. Makarov, A. A. Puretskii, Opt. Lett. 1, 22-24 (1977).

46. M. C. Gowler, K. W. Billman, Opt. Commun. 20, 123-129 (1977).

47. S. Bittenson, P. L. Houston, J. Chem. Phys. 67, 4819-4824 (1977).

48. M. Gauthier, W. S. Nip, P. A. Hackett, C. Willis, Chem. Phys. Lett. 69, 372-374 (1980).

49. V. S. Doljikov, Y. R. Kolomisky, E. A. Ryabov, Chem. Phys. Lett. 80, 433-438 (1981).

50. S. S. Alimpiev, V. N. Bagratshvii, N. V. Karlov, V. S. Letokhov, V. V. Lobko, G. N. Makarov, B. G. Sartakov, E. M. Khokhlov, JETP Lett. 25, 547-550 (1978).

51. R. V. Ambartzumian, G. N. Makarov, A. A. Puretskii, Opt. Lett. 3, 103-105 (1978).

52. D. O. Ham, M. Rothschild, Opt. Lett. 1, 28-30 (1977).

53. T. F. Deutsch, Opt. Lett. 1, 25-27 (1977).

54. D. Tal, U. P. Oppenheim, G. Koren, M. Okon, Chem. Phys. Lett. 48, 67-71 (1977).

55. G. P. Quigley, Opt. Lett. 3, 106-108 (1978).

56. J. G. Black, E. Yablonovitch, N. Bloembergen, S. Mukamel, Phys. Rev. Lett. 38, 1131-1134 (1977).

57. H. S. Kwok, E. Yablonovitch, Phys. Rev. Lett. 41, 745-749 (1978).

58. J. G. Black, P. Kolodner, M. J. Shulz, E. Yablonovitch, N. Bloembergen, Phys. Rev. A 19, 704-716 (1979).

59. S. L. Chin, G. Boisclair, Opt. Lett. 4, 340-341 (1979).

60. W. Fuss, J. Hartmann, J. Chem. Phys. 70, 5468-5476 (1979).

61. W. Tsay, C. Riley, D. O. Ham, J. Chem. Phys. 70, 3558-3560 (1979).

62. N. Bloembergen, C. D. Cantrell, D. M. Larsen, Tunable Lasers and Their Applications, Ed. by A. Mooradian, T. Jaeger, P. Stokseth, (Springer-Verlag, Berlin, 1976) 162-252.

63. S. C. Lin, J. H. Morris, J. Quant. Spect. Radiat. Transfer 17, 577-593 (1977).

64. C. D. Cantrell, H. W. Galbraith, Opt. Commun. 18, 513-516 (1976).

65. C. W. Patterson, B. J. Krohn, A. S. Pine, Opt. Lett. 6, 39-41 (1981).

66. C. W. Patterson, Conference on Intramolecular Relaxation of Polyatomic Molecules, Los Alamos National Laboratories, 1982.

67. R. V. Ambartzumian, V. S. Letokhov, G. N. Makarov, A. A. Puretsky, Chem. Phys. Lett. 16, 252-254 (1972).

68. H. W. Galbraith, J. R. Ackerhalt, "Vibrational Excitation in Polyatomic Molecules", Laser Induced Chemical Processes, Ed. by J. I. Steinfeld, Plenum, Cambridge, MA 1980, Ch. 1.

69. J. I. Steinfeld, "Double Resonance Spectroscopy", Laser and Coherence Spectroscopy, Ed. by J. I. Steinfeld, Plenum Press, Cambridge, MA 1976.

70. R. V. Ambartzumian, V. S. Letokhov, G. N. Makarov, A. A. Puretsky, O. A. Tumanov, Sov. Phys. JETP 37, 392-398 (1973).

71. R. V. Ambartzumian, V. S. Letokhov, G. N. Makarov, A. A. Puretsky, Sov. Phys. JETP 41, 871-876 (1976).

72. F. G. Tablas, W. E. Schmid, K. L. Kompa, Opt. Commun. 16, 136-140 (1976).

73. R. V. Ambartzumian, Y. A. Gorokhov, V. S. Letokhov, G. N. Makarov, JETP Lett. 22, 43-44 (1975).

74. R. Campargue, B. Soep, Chem. Phys. Lett. 46, 469-472 (1979).

75. A. Yogev, Y. Haas, Chem. Phys. Lett. 21, 544-548 (1973).

76. B. J. Orr, Chem. Phys. Lett. 93, 446-450 (1976).

77. I. Burak, T. J. Quelley, J. I. Steinfeld, J. Chem. Phys. 70, 334-343 (1979).

78. B. J. Orr, G. F. Nutt, Opt. Lett. 5, 12-14 (1980).

79. B. J. Orr, G. F. Nutt, J. Mol. Spec. 84, 272-287 (1980).

80. B. J. Orr, G. F. Nutt, Talk presented at the XI International Quantum Electronics Conference, (1980).

81. B. J. Orr, J. G. Haub, Opt. Lett. 6, 236-238 (1981).

82. B. J. Orr, J. G. Haub, G. F. Nutt, J. L. Steward, O. Vozzo, Chem. Phys. Lett. 78, 621-625 (1981).

83. R. G. Gordon, J. Chem. Phys. 46, 4399-4403 (1967).

84. M. L. Lesiecki, G. R. Smith, J. A. Stewart, W. A. Guillory, J. Mol. Struct. 59, 237-247 (1980).

85. D. M. Brenner, K. Brezinsky, Chem. Phys. Lett. 67, 36-40 (1979).

86. D. M. Brenner, K. Brezinsky, P. Curtis, Chem. Phys. Lett. 72, 202-208 (1980).

87. D. M. Brenner, J. Chem. Phys. 74, 494-507 (1981).

88. L. O. Brockway, J. Y. Beach, L. Pauling, J. Am. Chem. Soc. 57, 2693-2704 (1935).

89. L. Pauling, L. O. Brockway, J. Y. Beach, J. Am. Chem. Soc. 57, 2705-2709 (1935).

90. I. E. Coop, L. E. Sutton, Trans. Faraday Soc. 35, 505 (1939).

91. J. H. Carpenter, D. F. Rimmer, J. G. Smith, D. H. Whiffen, J. Chem. Soc. Faraday Trans II, 71, 1752-1762 (1975).

92. J. C. D. Brand, J. H. Callomon, D. C. Moule, J. Tyrell, T. H. Goodwin, Trans. Faraday Soc., 2365-2381 (1965).

93. C. A. Frenzel, K. E. Blick, C. R. Bennet, K. Niedenzu, J. Chem. Phys. 53, 198-204 (1970).

94. I. S. Butler, A. M. English, Spectrochimica Acta 33A, 545-547 (1977).

95. V. Henri and J. Duchesne, Nature 143, 28-29 (1939).

96. L. Burnell, J. Chem. Phys. 24, 620 (1956).

97. D. J. Clouthier, D. C. Moule, J. Mol. Spectrosc. 60, 471-481 (1981).

98. R. Vasudev, Y. Hirata, E. C. Lim, W. M. McClain, Chem. Phys. Lett. 76, 249-253 (1980).

99. J. H. Meal, S. R. Polo, J. Chem. Phys. 24, 1119-1138 (1956).

100. G. Viswanath, M. Kasha, J. Chem. Phys. 24, 574-577 (1956).

101. D. Huppert, J. Jortner, P. M. Rentzepis, Chem. Phys. Lett. 13, 225-228 (1972).

102. J. Fabian, H. Viola, R. Mayer, Tetrahedron 23, 4323-4329 (1967).

103. M. Kasha, Discuss. Faraday Soc. 9, 14 (1950).

104. D. J. Clouthier, F. W. Birss, J. Mol. Spectrosc. 86, 389-391 (1982).

105. J. R. Lombardi, J. Chem. Phys. 52, 6126-6129 (1970).

106. F. W. Birss, S. D. Colson, D. A. Ramsay, Can. J. Phys. 51, 1031-1038 (1973).

107. J. C. D. Brand, J. L. Hardwick, K. E. Teo, J. Mol. Spectrosc. 57, 215-220 (1975).

108. H. C. Allen, P. C. Cross, Molecular Vib-rotors, John Wiley, New York, (1963).

109. J. R. McDonald, L. E. Brus, Chem. Phys. Lett. 16, 587-589 (1972).

110. Stern-Volmer relation is:

$$1/\tau = 1/\tau_0 + kp$$

where $1/\tau$ is the inverse lifetime at a pressure p, $1/\tau_0$ is the zero pressure (extrapolated) inverse lifetime and k is the quenching rate constant.

111. The relationship between oscillator strength ($f\tau$), excited state lifetime (τ) and wavelength of maximum fluorescence (λ_0) is:

$$f\tau = \frac{mc}{8\pi e^2} \frac{g_2}{g_1} \lambda_0^2 = 1.51 \frac{g_2}{g_1} \lambda_0^2 \quad (\lambda_0 \text{ in cm; in nanoseconds}).$$

where g_1 and g_2 are the degeneracies for the lower and upper states, respectively.

112. S. Z. Levine, K. A. R. Knight, R. P. Steer, Chem. Phys. Lett. 29, 73-76 (1974).

113. T. Oka, A. R. Knight, R. P. Steer, J. Chem. Phys. 63, 699-706 (1977).

114. T. Oka, A. R. Knight, R. P. Steer, J. Chem. Phys. 63, 2414-2420 (1975).

115. D. J. Clouthier, A. R. Knight, R. P. Steer, P. A. Hackett, J. Chem. Phys. 72, 1560-1568 (1980).

116. D. C. Moule, C. R. Subramainiam, J. Mol. Spectrosc. 48, 336-345 (1973).

117. J. R. Lombardi, J. Koffend, R. A. Gottscho, R. W. Field, J. Mol. Spectrosc. 65, 446-454 (1977).

118. P. F. Bernath, P. G. Cummins, J. R. Lombardi, R. W. Field, J. Mol. Spectrosc. 69, 166-167 (1978).

119. D. J. Clouthier, D. C. Moule, J. Mol. Spectrosc. 81, 471-481 (1981).

120. D. J. Clouthier, A. R. Knight, R. P. Steer, P. A. Hackett, Chem. Phys. 48, 1-11 (1980).

121. C. Cohen-Tannoudji, B. Diu, F. Laloe, Quantum Mechanics, John Wiley and Sons, New York, (1977).

122. V. S. Letokhov, V. P. Chebotayev, Nonlinear Laser Spectroscopy, Chs. 4,5, Springer-Verlag, Berlin (1977).

123. Yu. P. Raizer, Sov. Phys. Uspekhi 8, 650-673 (1966) (From Usp. Fiz. Nauk. 87, 29-64, 1951).

124. R. Wallace, Molecular Physics 11, 457-470 (1966).

125. M. F. goodman, J. Stone, E. Thiele, J. Chem. Phys. 59, 2919-2928 (1973).

126. M. F. Goodman, J. Stone, E. Thiele, J. Chem. Phys. 63, 2929-2935 (1975).

127. For a two-level system the rate for (incoherent) absorption is:

$$R = \frac{\omega_R^2 \gamma/4}{\Delta^2+\gamma/4}$$

where ω_R is the transition Rabi frequency, γ is the dephasing rate and Δ is the detuning.

128. A. B. Horwitz, S. R. Leone, Rev. Sci. Instruments 50, 811-816 (1979).

129. Fourier transform infrared spectrum taken at the Chemical Spectrometry Laboratory at M.I.T. on a Nicolet spectrometer.

130. Van der Waals radii for the added gases: helium, argon, xenon, nitrogen, carbon monoxide, carbon dioxide, nitrous oxide and methyl

chloride were obtained from Hirschfelder, Curtiss and Bird, Molecular Theory of Gases and Liquids, pages 1110-1113 and 1212-1215.

131. Van der Waals radii for acetonitrile, nitromethane and thiophosgene were estimated by adding bond distances and atomic van der Waals radii. Both were obtained from the Handbook of Chemistry and Physics, Chemical Rubber Company, Cleveland, (1972).

132. H. M. Lin, M. Seaver, K. Y. Tang, A. E. W. Knight, C. S. Parmenter, J. Chem. Phys. 70, 5442-5462 (1978).

133. L. Sodickson, Phys. Fluids 9, 1252-1254 (1966).

134. The solutions for the diffusion equations can be found in any physical chemistry textbook. In one dimension it is:

$$C(x,t) = N/2(\pi Dt)^{1/2}\exp[-x^2/4Dt]$$

where D is the diffusion coefficient and N is the number density of diffusing molecules at time zero.

135. S. S. Alimpiev, V. N. Bagratashvili, N. V. Karlov, V. S. Letokhov, V. V. Lobko, A. A. Makarov, B. G. Sartakov, E. M. Khoklov, JETP Lett. 25, 547-550 (1978).

136. C. W. Patterson, R. S. McDowell, P. F. Moulton, A. Mooradian, Opt. Lett. 6, 93-95 (1981).

137. G. Herzberg, Molecular Spectra and Molecular Structure, II. Infrared and Raman Spectra of Polyatomic Molecules, Van Nostrand Reinhold, Ltd., New York (1945).

138. J. D. Campbell, G. Hancock, J. B. Halpern, K. H. Welge, Chem. Phys. 44, 404-410 (1976).

139. C. P. Slichter, Principles of Magnetic Resonance, Springer-Verlag, Berlin (1976).

140. A. H. Zewail, Acc. Chem. Research 13, 360-368 (1980).

141. J. Stone, E. Thiele, M. F. Goodman, J. Chem. Phys. 63, 2936-2948 (1975).

142. M. F. Goodman, J. Stone, D. A. Dows, J. Chem. Phys. 65, 5052-5061 (1976).

143. J. Stone, M. F. Goodman, J. Chem. Phys. 71, 408-414 (1979).

144. J. Stone, E. Thiele, M. F. Goodman, Chem. Phys. Lett. 71, 171-176 (1980).

145. J. Stone, E. Thiele, M. F. Goodman, J. Chem. Phys. 75, 1712-1727 (1980).

146. B. Comaskey, R. E. Scotti, R. L. Shoemaker, Opt. Lett. 6, 45-47 (1981).

147. F. H. Dyksterhuis, N. R. Heckenber, J. Mol. Spectrosc. 77, 147-148 (1979).

148. H. Stafast, W. E. Schmid, K. L. Kompa, Opt. Commun. 21, 121-126 (1976).

149. E. Weitz, G. W. Flynn, Ann. Rev. Phys. Chem. 25, 275-315 (1974).

150. D. S. Doljikov, Y. R. Kolomisky, E. A. Ryabov, Chem. Phys. Lett. 80, 433-438 (1981).

151. R. V. Ambartzumian, N. V. Chekalin, D. S. Doljikov, V. S. Letokhov, E. A. Ryabov, Chem. Phys. Lett. 25, 515-518 (1974).

152. J. R. Anderson, J. Chem. Phys. 44, 3496-3500 (1966).

153. R. Stair, W. E. Schneider, J. K. Jackson, Appl. Opt. 2, 1151-1154 (1963).

Appendix A

Measurement of Branching Ratios for the $2_0^1 3_0^1 4_{2n}^1$ Progression

The ultimate goal of infrared-visible double resonance is to determine the population distribution in a vibrational manifold interacting with an infrared laser. Once the measurement of visible absorption intensities for each of the vibrational states undergoing absorption has been completed the data can then be transformed into population data.

Two methods are available for doing this: In the first, one calculates the population of the state in question in the absence of the field simply by using the Boltzmann Equation. The change in population induced by the CO_2 laser is then equal to the fractional change in the fluorescence excitation signal emanating from that state. In the second method, one determines the Franck-Condon factors of the electronic transitions that probe the vibrational distribution. Once these are known, one can immediately determine the new population distribution set up by the CO_2 laser by measuring only the IR-on fluorescence excitation intensities and using the folowing expression:

$$I_{abs}(e'v' \leftarrow e"v") = 8\pi^3/3hc \; I_0 \Delta x N_{e"v"} \overline{R}_e^2 \nu |\langle \psi_{e'v'} | \psi_{e"v"} \rangle|^2$$

where I is the intensity of the incident radiation

Δx is the thickness of the absorbing layer

$N_{e"v"}$ is the population of absorbing state

$\overline{R}_e$ is the average electronic transition moment

and $\langle e"v" | e'v' \rangle$ is the Franck-Condon factor for the vibronic transition.

In accordance with this second method of determining vibrational state populations, we decided to measure the Franck-Condon factors for

the progression $2_0^1 3_0^1 4_{2n}^1$=1,2,3,4,5,6 of the $\tilde{A}(^1A_2) \leftarrow \tilde{X}(^1A_1)$ electronic transition.

Before I describe the determination of these factors I must emphasize a point made in Chapter III: Since the $^1A_2 \leftarrow ^1A_1$ transition is electric dipole forbidden the moment matrix element $\langle e''v''|\mu|e'v'\rangle$ cannot be separated into an electronic dipole moment matrix element ($\langle e'|\mu|e''\rangle$) and a vibrational overlap integral ($\langle v''|v'\rangle$)--the Franck-Condon factor. However, by including vibronic (Herzberg-Teller) coupling in the transition matrix element, one obtains integrals of the form $\langle v''|\partial H_{ev}/\partial Q|v\rangle$ where H_{ev} is the perturbation potential which mixes electronic states through the normal mode Q[116,152]. These can be used in the expression above just as if they were actual Franck-Condon factors themselves. Nonetheless, it would be inaccurate to use the term "Franck-Condon factor" when describing electronic absorption that is dipole-forbidden. For this reason I shall use, instead, the terms absorption branching ratio and emission branching ratio.

Experimental

The emission spectra from which we obtained the branching ratios for the $2_0^1 3_0^1 4_{2n}^1$ progression has been previously recorded and assigned by Brand, Hardwick and Teo[107]. (Had they made calibrated intensity measurements in addition to the frequency measurements our recording of the spectrum would have been unnecessary.) Since we used the same excitation frequency (5145 Å) we were able to use their assignments to find the six bands in the progression. Unfortunately, we

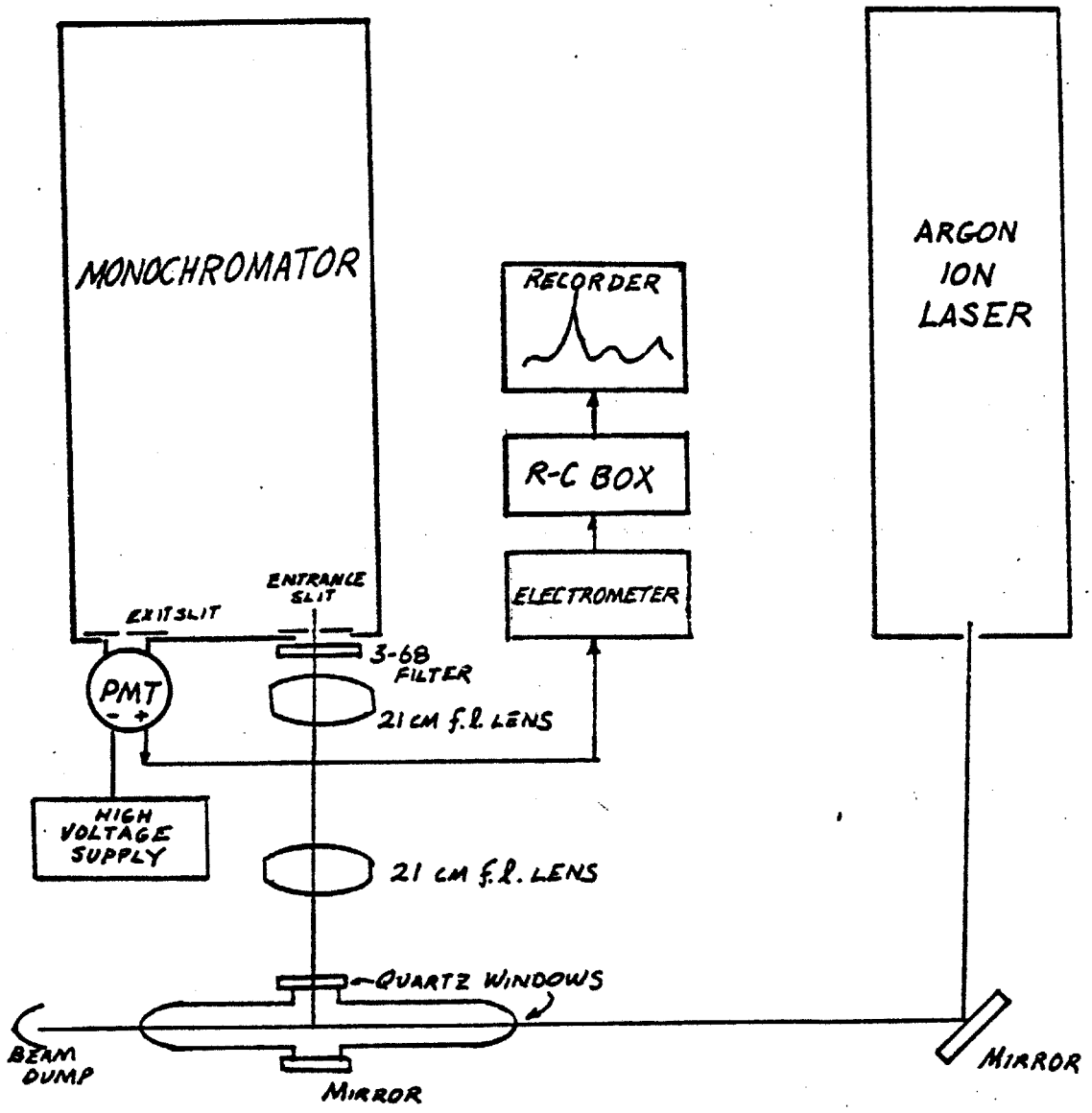


Fig. A.1. Schematic Design of Apparatus used to record laser-induced fluorescence spectra of thiophosgene excited with 5145 Å Argon Ion laser light.

were unable to measure the fluorescence intensity of the $2_0^1 3_0^1 4_{0n}^1$ band since scattered laser light interfered with the fluorescence.

The experimental set up is shown in Fig. A-1. The laser source is a c.w. Spectra Physics Argon ion laser having an operating range of 1 to 4 watts at 5145 Å. Since the excitation transition ($2_0^1 3_0^1 4_0^1$) saturates at approximately 1 W, there was no need to operate the laser at a higher power than this.

Thiophosgene was purified and degassed in the manner described in Chapter V. Since the $^1A_2$ state has a very long lifetime (35 μsec), at pressures greater than approximately 5 mTorr collisional quenching of the excited state decreases the fluorescence quantum yield faster than the increase in total fluorescence (due to the greater number of thiophosgene molecules). For this reason the pressure of thiophosgene in the absorption cell was kept as low as possible--between 35 and 300 mTorr. (Adsorption of thiophosgene onto the cell walls and leakage of air into the cell prevented us from using lower pressures.) Pressures were measured with an MKS Baratron capacitance manometer with a 10 Torr head. We refilled the absorption cell with fresh sample prior to each run.

The entrance and exit windows and viewing window of the cell are quartz flats. The former are set at Brewster's angle to reduce scattered light. Opposite the viewing window is a flat mirror whose purpose is to redirect some of the fluorescence back through the viewing window.

A telescope assembly consisting of two 21-cm focal length, 2-inch diameter, coated lenses collects and focuses the fluorescence onto the entrance slit of the monochromator. To eliminate most of the scattered laser light a 3-68 (yellow) colored glass filter was placed in front of the slit.

A 1-meter Spex monochromator (1700 II) was used to disperse the emission. It contains a holographic grating having 1800 lines/mm and driven by a digital scan drive.

To detect the fluorescence we used a side-arm, uncooled Hamamatsu R-95 photomultiplier which is characterized by an enhanced red sensitivity and low dark current. The operating voltage was 900 V and was delivered by a Northeast Scientific high voltage supply. A Kiethly electrometer (910 BR) detected the PMT signal with a sensitivity limited only by the dark current (~10^{-9} amp). An RC filter with a time constant of ~1 sec smoothed the signal. Fluorescence spectra were recorded with a strip chart recorder.

For recording of the entire wavelength region (5400 Å to 7500 Å) of the $2^1 3^1 4^1$ emission the scan speed was set at 1/3 Å sec^{-1}. For slow scans the scan rate was reduced to 2/15 Å sec^{-1}. Since fluorescence intensity was a far more important consideration than resolution, the entrance and exit slits were opened to ~1 mm.

Band areas were measured with a planimeter (A. Ott, Keuffel and Esser). When the band of interest overlapped with another band, a Lorentzian lineshape was assumed and the appropriate band shape drawn in. Naturally, as we went higher in the progression the intensity of the bands decreased and the uncertainty of the integrated areas increased. A very large uncertainty (±30%) is associated with $2_0^1 3_0^1 4_{12}^1$. In order to complete the measurement of branching ratios for the entire band progression, we attempted to measure the absorption branching ratios for the $2_0^1 3_0^1 4_0^1$ and $2_0^1 3_0^1 4_2^1$ bands from an excitation spectrum. Unfortunately, contamination of the $2_0^1 3_0^1 4_0^1$ band with the $2_0^1 4_0^3$ and

$3_0^1 4_0^1$ bands prevented us from actually doing so.

In order to obtain accurate branching ratios correction must be made for the varying response of the photomultiplier and grating to wavelength. Intensity calibration was carried out by recording the spectrum of a 6.6 A, 200 W quartz-iodine lamp and comparing it to a published, calibrated spectrum[154]. With the two response curves set equal at 5407 A ($2_0^1 3_0^1 4_2^1$) the ratio of an intensity on the experimental curve was taken as the correction factor for that wavelength. The integrated intensities of the bands in the progression were then multiplied by the appropriate factor to obtain their true fluorescence intensities.

Branching Ratios

$I_{mn}^{emission} \alpha R_{mn} \nu^3 \quad I_{mn}^{abs} \alpha R_{mn} \nu$

$\alpha R_{mn} 1/\lambda^3 \quad \alpha R_{mn} 1/\lambda$

Band	λ(Å)	Emission Branching Ratio	F-C.Factor	Absorption Branching Ratio
$2_0^1 3_0^1 4_2^1$	5407.5	1.000	1.000	1.000
$2_0^1 3_0^1 4_4^1$	5697.0	0.398±.023	0.465±.027	0.442±.026
$2_0^1 3_0^1 4_6^1$	6018.7	0.157±.011	0.216±.015	0.195±.014
$2_0^1 3_0^1 4_8^1$	6378.8	0.316±.025	0.519±.041	0.440±.035
$2_0^1 3_0^1 4_{10}^1$	6782.9	0.170±.040	0.336±.079	0.268±.063
$2_0^1 3_0^1 4_{12}^1$	7242	0.065±.021	0.156±.050	0.117±.038

Appendix B.

Listing of the computer program "Copath" used to solve the density matrix equations of motion for a general N level system. The two subroutines that diagonalize and invert matrices (E1GCC and L EQ2C, respectively) are called from the International Mathematics and Science Library.

```
      PROGRAM COPATH(INPUT,OUTPUT,TAPE=INPUT,TAPE9=OUTPUT)                MAR00010
      COMPLEX R,RHO,RHOI,VEC,EV                                           MAR00020
      COMMON/A/R(64,64),RHO(64,100),RHOI(64),VEC(64,64),EV(64)            MAR00030
     2,RHOEND(10,64)                                                      MAR00040
      COMMON/B/RABI(10),TIMLZR(10),FREQL,WO,XPP,TEMP,PRES(10)             MAR00050
      COMMON/C/T2(8),T2P(8),T2LZR,T1GND(10),T1(8,8),UNI(10,8),UNIP(8),PUMAR00060
     2NIP(8)                                                              MAR00070
      COMMON/D/POP(100,8)                                                 MAR00080
      COMMON/E/IHAM,H(8,8),HROT(10,8),REDUC(7),PREDUC(7)                  MAR00090
C                                                                         MAR00100
C     IF YOU WANT THE OPTION OF ADDING ROTATIONAL ENERGY CORRECTIONS TO    MAR00110
C     THE ANHARMONIC OSCILLATOR ENERGY LEVELS SET IHAM EQUAL TO 1.        MAR00120
C     IF YOU WANT THE OPTION OF CONVOLUTING POPULATIONS OVER AN           MAR00130
C     ARBITRARY PULSE SHAPE SET ICON EQUAL TO 1.  THIS OPTION WORKS       MAR00140
C     BY APPROXIMATING THE PULSE SHAPE BY A SERIES OF SQUARE PULSES       MAR00150
C     EACH OF WHICH HAS A DIFFERENT INTENSITY AND USES THE POPULATION     MAR00160
C     FROM THE LAST SQUARE PULSE FOR ITS INITIAL POPULATION.              MAR00170
C     IF YOU WANT THE OPTION OF REDUCING THE RABI FREQUENCY FROM LEVEL    MAR00180
C     N TO LEVEL N+1 BY A PRESSURE DEPENDENT MIXING OF STATES  SET IMIX   MAR00190
C     EQUAL TO 1.                                                         MAR00200
C     IF YOU WANT THE OPTION OF ADDING PRESSURE DEPENDENT V TO V          MAR00210
C     RELAXATION RATES TO THE UNIMOLECULAR REACTION RATES SET IUNIP       MAR00220
C     EQUAL TO 1.                                                         MAR00230
C                                                                         MAR00240
      READ (10,100) (IHAM,ICON,IMIX,IUNIP)                               MAR00250
C                                                                         MAR00260
C     NL IS THE NUMBER OF LADDERS TO BE SOLVED.                           MAR00270
C     N IS THE NUMBER OF LEVELS IN EACH LADDER.                           MAR00280
C     NTIME IS THE NUMBER OF TIME INTERVALS TO BE SOLVED FOR.             MAR00290
C                                                                         MAR00300
      READ (10,105) (NL,N,NTIME)                                          MAR00310
C                                                                         MAR00320
C     WO, THE HARMONIC OSCILLATOR FREQUENCY, IS READ IN AS CM-1,S.        MAR00330
C     XPP, THE ANHARMONICITY, IS READ IN AS CM-1,S.                       MAR00340
C     T2 AND T2LZR, THE DEPHASING RATE OF THE LASER, ARE READ IN AS       MAR00350
C     NSEC-1,S.                                                           MAR00360
C     FREQL, THE FREQUENCY OF THE LASER, IS READ IN AS CM-1,S.            MAR00370
C     TEMP, THE VIBRATIONAL TEMPERATURE, IS READ IN AS DEGEES KELVIN.     MAR00380
C                                                                         MAR00390
      READ(10,110) (WO,XPP,T2LZR,FREQL,TEMP)                              MAR00400
      READ (10,120) (T2(I),I=1,N)                                         MAR00410
C                                                                         MAR00420
C     IF IMIX WAS SET EQUAL TO 1 THE PRESSURE DEPENDENT FACTORS BY WHICHMAR00430
C     THE RABI FREQUENCIES FOR EACH OF THE N-1 TRANSITIONS IS REDUCED     MAR00440
C     MUST BE READ IN (IN UNITS OF INVERSE MTORR).                        MAR00450
C                                                                         MAR00460
      NM=N-1                                                              MAR00470
      IF (IMIX.EQ.1) READ (10,115)(REDUC(I),I=1,NM)                       MAR00480
C                                                                         MAR00490
C     THE ELEMENTS OF UNIP REPRESENT COLLSION INDUCED V TO V RELAXATION.MAR00500
C     THEY ARE READ IN (IN UNITS OF INVERSE NSEC/MTORR) ONLY IF IUNIP ISMAR00510
C     SET EQUAL TO 1.                                                     MAR00520
C                                                                         MAR00530
      IF (IUNIP.EQ.1) READ (10,120) (UNIP(I),I=1,N)                       MAR00540
C                                                                         MAR00550
```

```
C     RABI, THE BARE RABI FREQUENCY, IS READ IN AS CM-1,S.                  MAR00560
C     TIMLZR, THE PULSE DURATION OF THE LASER, IS READ IN AS NSECS.         MAR00570
C     TIGND, THE V TO T TRANSITION RATE FOR THE 1 TO 0 TRANSITION IS        MAR00580
C     READ IN AS NSEC-1/MTORR.                                              MAR00590
C     PRES, THE PRESSURE OF THE GAS, IS READ IN AS MTORR.                   MAR00600
C                                                                           MAR00610
      DO 2 I=1,NL                                                           MAR00620
      READ (10,130) (RABI(I),TIMLZR(I),T1GND(I),PRES(I))                    MAR00630
C                                                                           MAR00640
C     THE ELEMENTS OF UNI REPRESENT COLLISION-FREE RELAXATION OUT OF        MAR00650
C     THE PUMPED MODE LADDER.  THEY ARE READ IN AS UNITS OF NSECS.          MAR00660
C                                                                           MAR00670
      READ(10,120)((UNI(I,J),J=1,N))                                        MAR00680
C                                                                           MAR00690
C     IF IHAM WAS SET EQUAL TO 1 THE ROTATIONAL ENERGY CORRECTIONS FOR      MAR00700
C     THE N LEVELS MUST NOW BE READ IN (IN CM-1).                           MAR00710
C                                                                           MAR00720
      IF (IHAM.EQ.1) READ (10,120) ((HROT(I,J),J=1,N))                      MAR00730
    2 CONTINUE                                                              MAR00740
      DO 90 IL=1,NL                                                         MAR00750
      DO 3 I=1,100                                                          MAR00760
      DO 3 J=1,8                                                            MAR00770
    3 POP(I,J)=0.                                                           MAR00780
      NN=N*N                                                                MAR00790
C                                                                           MAR00800
C     FILL UP THE T1 MATRIX                                                 MAR00810
C     THE MATRIX ELEMENT T1(I,J) REPRESENTS THE COLLISION-INDUCED V TO TMAR00820
C     TRANSITION FROM STATE J TO STATE I.                                   MAR00830
C     FOR THE T1 MATRIX-                                                    MAR00840
C     THE DIAGNOL MATRIX ELEMENTS REPRESENT TRANSITIONS FROM THE            MAR00850
C     RESPECTIVE LEVELS INTO ALL OTHER LEVELS.  FROM THE CONSTRAINT OF      MAR00860
C     POPULATION CONSERVATION EACH DIAGNOL ELEMENT IS EQUAL TO THE          MAR00870
C     OPPOSITE OF THE SUM OF ALL OTHER ELEMENTS IN ITS COLUMN.              MAR00880
C     FROM THE PRINCIPLE OF MICROSCOPIC REVERSIBILITY THE T(I,J)'S ARE      MAR00890
C     OBTAINED FROM THE T(J,I)'S.                                           MAR00900
C     IN THIS PROGRAM THE LANDAU-TELLER THEORY IS USED TO OBTAIN THE        MAR00910
C     T1(I,I+1)'S FROM T1(1,2).  ALL T1(I,J)'S WHERE J DIFFERS FROM I       MAR00920
C     BY MORE THAN ONE VIBRATIONAL QUANTUM ARE SET EQUAL TO ZERO IN         MAR00930
C     ACCORDANCE WITH THE PROPENSITY RULE--DELTA V=+/-1.  THUS ONLY         MAR00940
C     T(2,1) NEEDS TO BE SPECIFIED--THE COMPUTER DOES THE REST.             MAR00950
C                                                                           MAR00960
      DO 10 I=1,N                                                           MAR00970
      DO 10 J=1,N                                                           MAR00980
   10 T1(I,J)=0.                                                            MAR00990
      IMAX = N-1                                                            MAR01000
      DO 20 I = 1,IMAX                                                      MAR01010
      J = I+1                                                               MAR01020
      T1(I,J)=I*T1GND(IL)                                                   MAR01030
   20 CONTINUE                                                              MAR01040
      DO 30 I = 2,N                                                         MAR01050
      J = I-1                                                               MAR01060
      EDIF = (J-I)*WO + (I*I-J*J+2*(J-I))*XPP                               MAR01070
      T1(I,J) = T1(J,I)*EXP(EDIF/(.69494*TEMP))                             MAR01080
   30 CONTINUE                                                              MAR01090
      DO 50 J=1,N                                                           MAR01100
```

```
      TSUM=0.                                                                  MARO1110
      DO 40 I=1,N                                                              MARO1120
      TSUM = TSUM+T1(I,J)                                                      MARO1130
   40 CONTINUE                                                                 MARO1140
      T1(J,J) = -TSUM                                                          MARO1150
   50 CONTINUE                                                                 MARO1160
      WRITE (9,200)                                                            MARO1170
      WRITE (9,202)                                                            MARO1180
       IF (ICON.NE.1) WRITE (.,205) (IL)                                       MARO1190
      IF (ICON.EQ.1) WRITE (9,206) (IL,NL)                                     MARO1200
      WRITE (9,210) (N,WO,XPP,FREQL,RABI(IL),TIMLZR(IL),NTIME)                 MARO1210
      WRITE (9,215)                                                            MARO1220
      DO 60 I=1,N                                                              MARO1230
      T2P(I)=T2(I)*PRES(IL)                                                    MARO1240
      WRITE (9,220) (I,T2P(I))                                                 MARO1250
   60 CONTINUE                                                                 MARO1260
      WRITE (9,225) (T2LZR)                                                    MARO1270
      WRITE (9,230)                                                            MARO1280
      DO 70 I=1,N                                                              MARO1290
      JMIN=MAXO(I-1,1)                                                         MARO1300
      JMAX=MINO(I+1,N)                                                         MARO1310
      DO 70 J=JMIN,JMAX                                                        MARO1320
      WRITE (9,240) (I,J,T1(I,J))                                              MARO1330
   70 CONTINUE                                                                 MARO1340
      WRITE (9,250)                                                            MARO1350
      WRITE (9,260) (I,UNI(IL,I),I=1,N)                                        MARO1360
      IF (IMIX.NE.1) GO TO 4                                                   MARO1370
      WRITE (9,261)                                                            MARO1380
      DO 75 I=1,NM                                                             MARO1390
      PREDUC(I)=EXP(-(REDUC(I)*PRES(IL)))                                      MARO1400
   75 WRITE (9,262) (I,PREDUC(I))                                              MARO1410
    4 IF (IUNIP.NE.1) GO TO 5                                                  MARO1420
      WRITE (9,263)                                                            MARO1430
      DO 80 I=1,N                                                              MARO1440
      PUNIP(I)=UNIP(I)*PRES(IL)                                                MARO1450
   80 WRITE (9,264) (I,PUNIP(I))                                               MARO1460
    5 IF (IHAM.EQ.1) WRITE (9,265)                                             MARO1470
      IF (IHAM.EQ.1) WRITE (9,266) (I,HROT(IL,I),I=1,N)                        MARO1480
      WRITE (9,270) (TEMP)                                                     MARO1490
      WRITE (9,280) (PRES(IL))                                                 MARO1500
      CALL EIGEN(IL,NN,N,NTIME,ICON,IMIX,IUNIP)                                MARO1510
   90 CONTINUE                                                                 MARO1520
  100 FORMAT (4I10)                                                            MARO1530
  105 FORMAT(3I10)                                                             MARO1540
  110 FORMAT (6F10.5)                                                          MARO1550
  115 FORMAT (7F10.5)                                                          MARO1560
  120 FORMAT (8F10.5)                                                          MARO1570
  130 FORMAT (F10.8,3F10.5)                                                    MARO1580
  200 FORMAT (*1*5X,114HBLOCH EQUATION MODEL FOR THE INTERACTION BETWEENMARO1590
     2 AN ANHARMONIC OSCILLATOR AND A MONOCHROMATIC COHERENT LIGHT FIELDMARO1600
     3)                                                                        MARO1610
  202 FORMAT (2(/))                                                            MARO1620
  205 FORMAT (*0*13HLADDER NUMBERI3)                                           MARO1630
  206 FORMAT(*0*20HTIME INTERVAL NUMBERI3,33H OF A PULSE SHAPE APPROXIMAMARO1640
     2TED BYI3,19H RECTANGULAR PULSES)                                         MARO1650
```

```
  210 FORMAT (*O*18HNUMBER OF LEVELS =I2/*O*34HHARMONIC OSCILLATOR LEVELMARO1660
     2 SPACING=F10.5,7H CM-1'S/*O*32HANHARMONIC CORRECTION CONSTANT =F6.MARO1670
     34,7H CM-1'S/*O*17HLASER FREQUENCY =F10.5,7H CM-1'S/*O*16HRABI FREQMARO1680
     4UENCY =E12.5,7H CM-1'S/*O*16HLASER DURATION =F8.3,6HNSECS./*O*53HNMARO1690
     5UMBER OF TIME INTERVALS STUDIED DURING LASER PULSE =I4)           MARO1700
  215 FORMAT (*O*29HT2 RELAXATION RATES (NSEC-1)-)                     MARO1710
  220 FORMAT(* *5X,3HT2(I1,4H) = F10.2,7H NSEC-1)                      MARO1720
  225 FORMAT (*O*30HDEPHASING RATE OF THE LASER = F8.2,8H NSEC-1.)     MARO1730
  230 FORMAT (*O*105HINTERMOLECULAR RELAXATION RATES EXPRESSED AS T1(I,JMARO1740
     2) (TRANSITION FROM STATE J TO STATE I) (NSEC-1/MTORR)-)          MARO1750
  240 FORMAT (* *5X,3HT1(I1,1H,I1,4H) = F10.5)                         MARO1760
  250 FORMAT (*O*37HUNIMOLECULAR REACTION RATES (NSEC-1)-)             MARO1770
  260 FORMAT (* *5X,4HURR(I1,4H) = F9.5)                               MARO1780
  261 FORMAT(*O*72HCOLLISION INDUCED REDUCTION OF RABI FREQUENCIES THROUMARO1790
     2GH MIXING OF STATES)                                             MARO1800
  262 FORMAT(* *5X,30HREDUCTION FACTOR OF TRANSITIONI2,3H = F9.5)      MARO1810
  263 FORMAT (*O*51HCOLLISION INDUCED V TO V RELAXATION RATES (NSEC-1)-)MARO1820
  264 FORMAT (* *5X,4HVRR(I1,4H) = F9.5)                               MARO1830
  265 FORMAT (*O*72HROTATIONAL ENERGY CORRECTIONS ADDED TO VIBRATIONAL EMARO1840
     2NERGY LEVELS (CM-1)-)                                            MARO1850
  266 FORMAT (* *5X,5HEROT(I1,4H) = F10.5)                             MARO1860
  270 FORMAT (*O*14HTEMPERATURE = F6.2,15H DEGREES KELVIN)             MARO1870
  280 FORMAT (*O*11HPRESSURE = F5.1,6H MTORR)                          MARO1880
      END                                                              MARO1890
      SUBROUTINE EIGEN(IL,NN,N,NTIME,ICON,IMIX,IUNIP)                  MARO1900
      COMPLEX R,RHO,RHOI,VEC,VECINV(64,64),EV,WA(4300),WK(150),ZZ      MARO1910
      COMMON/A/R(64,64),RHO(64,100),RHOI(64),VEC(64,64),EV(64)         MARO1920
     2,RHOEND(10,64)                                                   MARO1930
      COMMON/B/RABI(10),TIMLZR(10),FREQL,WO,XPP,TEMP,PRES(10)          MARO1940
      COMMON/D/POP(100,8)                                              MARO1950
      COMMON/E/IHAM,H(8,8),HROT(10,8),REDUC(7),PREDUC(7)               MARO1960
      CALL LOADH(N,IL,IMIX)                                            MARO1970
      CALL LOADR(N,NN,IL,IUNIP)                                        MARO1980
      CALL INITIAL(NN,ICON,IL)                                         MARO1990
      IJOB=1                                                           MARO2000
      CALL EIGCC(R,NN,64,IJOB,EV,VEC,64,WK,IER)                        MARO2010
      WRITE (9,200)                                                    MARO2020
      WRITE (9,210) (I,REAL(EV(I)),AIMAG(EV(I)),I=1,NN)                MARO2030
      DO 80 I=1,NN                                                     MARO2040
      DO 80 J=1,NN                                                     MARO2050
      VECINV(I,J)=CMPLX(0.,0.)                                         MARO2060
      IF (I.EQ.J) VECINV(I,J) = CMPLX(1.,0.)                           MARO2070
   80 CONTINUE                                                         MARO2080
      IJOB=0                                                           MARO2090
      CALL LEQ2C(VEC,NN,64,VECINV,NN,64,IJOB,WA,WK,IER)                MARO2100
      WRITE (9,220) (IER)                                              MARO2110
      DO 120 IT=1,NTIME                                                MARO2120
      T=(TIMLZR(IL)/FLOAT(NTIME))*IT                                   MARO2130
      DO 110 K=1,NN                                                    MARO2140
      RHO(K,IT) = CMPLX(0.,0.)                                         MARO2150
      DO 100 M=1,NN                                                    MARO2160
      DO 100 L=1,NN                                                    MARO2170
      ZZ=EV(L)*T                                                       MARO2180
      IF (REAL(ZZ).LT.-675.) GO TO 100                                 MARO2190
      RHO(K,IT) = RHO(K,IT) + VEC(K,L)*CEXP(ZZ)*VECINV(L,M)*RHOI(M)    MARO2200
```

```
      IF (IT.EQ.NTIME) RHOEND(IL,K)=RHO(K,NTIME)                        MAR02210
  100 CONTINUE                                                          MAR02220
  110 CONTINUE                                                          MAR02230
  120 CONTINUE                                                          MAR02240
  200 FORMAT (*0*,79HCALCULATED COMPLEX EIGENVALUES (WRITTEN AS (REAL PAMAR02250
     2RT,IMAGINARY PART)) (NSEC-1))                                     MAR02260
  210 FORMAT (* *5X,3HEV(I2,5H) = (F12.6,1H,F12.6,1H))                  MAR02270
  220 FORMAT (*0*28HERROR PARAMETER FOR LEQ2C ISI4)                     MAR02280
      CALL PRTOUT(IL,N,NTIME)                                           MAR02290
  230 RETURN                                                            MAR02300
      END                                                               MAR02310
      SUBROUTINE LOADH(N,IL,IMIX)                                       MAR02320
      COMMON/B/RABI(10),TIMLZR(10),FREQL,WO,XPP,TEMP,PRES(10)           MAR02330
      COMMON/E/IHAM,H(8,8),HROT(10,8),REDUC(7),PREDUC(7)                MAR02340
      DO 100 I=1,N                                                      MAR02350
      DO 100 J=1,N                                                      MAR02360
      H(I,J) = 0.0                                                      MAR02370
  100 CONTINUE                                                          MAR02380
      NM = N-1                                                          MAR02390
      DO 110 I=2,N                                                      MAR02400
      H(I,I) = (I-1)*(WO-FREQL) - (I-1)*(I-1)*XPP                       MAR02410
  110 IF (IHAM.EQ.1) H(I,I)=H(I,I)+HROT(IL,I)                           MAR02420
      DO 120 IR=1,NM                                                    MAR02430
      IC=IR+1                                                           MAR02440
      XIR=IR                                                            MAR02450
      H(IR,IC) = SQRT(XIR)*RABI(IL)                                     MAR02460
      IF (IMIX.EQ.1) H(IR,IC)=H(IR,IC)*PREDUC(IR)                       MAR02470
  120 CONTINUE                                                          MAR02480
      DO 130 I=2,N                                                      MAR02490
      II = I-1                                                          MAR02500
      H(I,II)=H(II,I)                                                   MAR02510
  130 CONTINUE                                                          MAR02520
      WRITE (9,200)                                                     MAR02530
      DO 140 I=1,N                                                      MAR02540
      WRITE (9,210) (H(I,J),J=1,N)                                      MAR02550
  140 CONTINUE                                                          MAR02560
C     NOW CONVERT THE ELEMENTS OF THE HAMILTONIAN INTO UNITS OF NSEC-1. MAR02570
      DO 150 J=1,N                                                      MAR02580
      DO 150 I=1,N                                                      MAR02590
  150 H(I,J)=29.998*H(I,J)                                              MAR02600
  200 FORMAT (*0*48HRESULTING ROTATING FRAME HAMILTONIAN (IN CM-1.)-)   MAR02610
  210 FORMAT (* *2X,8(F10.5,4X)/)                                       MAR02620
      RETURN                                                            MAR02630
      END                                                               MAR02640
      SUBROUTINE LOADR(N,NN,IL,IUNIP)                                   MAR02650
      COMPLEX R,RHO,RHOI,VEC,EV                                         MAR02660
      COMMON/A/R(64,64),RHO(64,100),RHOI(64),VEC(64,64),EV(64)          MAR02670
     2,RHOEND(10,64)                                                    MAR02680
      COMMON/E/IHAM,H(8,8),HROT(10,8),REDUC(7),PREDUC(7)                MAR02690
C     ZERO COEF MATRIX                                                  MAR02700
      DO 100 I=1,NN                                                     MAR02710
      DO 100 J=1,NN                                                     MAR02720
      R(I,J)=CMPLX(0.,0.)                                               MAR02730
  100 CONTINUE                                                          MAR02740
C     CREATE COEFFICIENT MATRIX                                         MAR02750
```

```
      DO 120 I=1,N                                                          MARO2760
      DO 120 J=1,N                                                          MARO2770
      DO 120 K=1,N                                                          MARO2780
      LTDC=N*(I-1)+J                                                        MARO2790
      LRCP=N*(K-1)+J                                                        MARO2800
      LRCM=N*(I-1)+K                                                        MARO2810
      R(LTDC,LRCP)= R(LTDC,LRCP) +   H(I,K)*CMPLX(0.,-1.)                   MARO2820
      R(LTDC,LRCM) = R(LTDC,LRCM) +   H(K,J)  *CMPLX(0.,1.)                 MARO2830
  120 CONTINUE                                                              MARO2840
C     NOW CONVERT THE UNITS OF THE R MATRIX TO UNITS OF RADIANS/SEC.        MARO2850
      DO 130 I=1,NN                                                         MARO2860
      DO 130 J=1,NN                                                         MARO2870
  130 R(I,J)=6.28318*R(I,J)                                                 MARO2880
C     LOADDP WILL LOAD T2, T1 AND UNIMOLECULAR DECAY RATES INTO THE         MARO2890
C     COEFFECIENT MATRIX (R).                                               MARO2900
      CALL LOADDP(N,NN,IL,IUNIP)                                            MARO2910
      RETURN                                                                MARO2920
      END                                                                   MARO2930
      SUBROUTINE LOADDP(N,NN,IL,IUNIP)                                      MARO2940
      COMPLEX R,RHO,RHOI,VEC,EV                                             MARO2950
      COMMON/A/R(64,64),RHO(64,100),RHOI(64),VEC(64,64),EV(64)              MARO2960
     2,RHOEND(10,64)                                                        MARO2970
      COMMON/B/RABI(10),TIMLZR(10),FREQL,WO,XPP,TEMP,PRES(10)               MARO2980
      COMMON/C/T2(8),T2P(8),T2LZR,T1GND(10),T1(8,8),UNI(10,8),UNIP(8),PUMARO2990
     2NIP(8)                                                                MARO3000
      DO 100 II=1,NN                                                        MARO3010
      K = (II+N-1)/N                                                        MARO3020
      L = II-(K-1)*N                                                        MARO3030
      R(II,II) = R(II,II) - 0.5*(UNI(IL,K) + UNI(IL,L))                     MARO3040
      IF(IUNIP.EQ.1) R(II,II)=R(II,II)-0.5*(PUNIP(K)+PUNIP(L))              MARO3050
      IF (K.EQ.L) GO TO 100                                                 MARO3060
      R(II,II) = R(II,II) - 0.5*(T2P(K) +T2P(L)) -T2LZR                     MARO3070
  100 CONTINUE                                                              MARO3080
      DO 70 L=1,N                                                           MARO3090
      I=(L-1)*N+L                                                           MARO3100
      DO 70 M=1,N                                                           MARO3110
      J=(M-1)*N+M                                                           MARO3120
      R(I,J) = R(I,J) + T1(L,M)*PRES(IL)                                    MARO3130
   70 CONTINUE                                                              MARO3140
      RETURN                                                                MARO3150
      END                                                                   MARO3160
      SUBROUTINE INITIAL(NN,ICON,IL)                                        MARO3170
      COMPLEX R,RHO,RHOI,VEC,EV                                             MARO3180
      COMMON/A/R(64,64),RHO(64,100),RHOI(64),VEC(64,64),EV(64)              MARO3190
     2,RHOEND(10,64)                                                        MARO3200
      IF(ICON.NE.1) GO TO 90                                                MARO3210
      IF (IL.EQ.1) GO TO 90                                                 MARO3220
      DO 50 I=1,NN                                                          MARO3230
      M=IL-1                                                                MARO3240
   50 RHOI(I)=RHOEND(M,I)                                                   MARO3250
      IF (ICON.EQ.1) GO TO 200                                              MARO3260
   90 DO 100 I=1,NN                                                         MARO3270
  100 RHOI(I)=CMPLX(0.,0.)                                                  MARO3280
      RHOI(1)=CMPLX(1.,0.)                                                  MARO3290
  200 RETURN                                                                MARO3300
```

```
      END                                                                   MARO3310
      SUBROUTINE PRTOUT(IL,N,NTIME)                                         MARO3320
      COMPLEX R,RHO,RHOI,VEC,EV                                             MARO3330
      COMMON/A/R(64,64),RHO(64,100),RHOI(64),VEC(64,64),EV(64)              MARO3340
     2,RHOEND(10,64)                                                        MARO3350
      COMMON/B/RABI(10),TIMLZR(10),FREQL,WO,XPP,TEMP,PRES(10)               MARO3360
      COMMON/D/POP(100,8)                                                   MARO3370
      DO 100 IT=1,NTIME                                                     MARO3380
      DO 100 I=1,N                                                          MARO3390
      IND = (I-1)*N+I                                                       MARO3400
      POP(IT,I)=REAL(RHO(IND,IT))                                           MARO3410
  100 CONTINUE                                                              MARO3420
      WRITE (9,220) (IL)                                                    MARO3430
      WRITE (9,230) (I,I=1,N)                                               MARO3440
      WRITE (9,240)                                                         MARO3450
      DO 110 IT = 1,NTIME                                                   MARO3460
      TL=(TIMLZR(IL)/FLOAT(NTIME))*IT                                       MARO3470
      WRITE (9,250) (TL,(POP(IT,I),I=1,N))                                  MARO3480
  110 CONTINUE                                                              MARO3490
  220 FORMAT (*1*32X,46HFRACTION OF POPULATION IN EACH LEVEL OF LADDERI2MARO3500
     2,//)                                                                  MARO3510
  230 FORMAT (*0*3X,18HTIME (NANOSECONDS)5X,5HLEVEL7(I2,5X,5HLEVEL),I2) MARO3520
  240 FORMAT (* *3X,120(1H-))                                               MARO3530
  250 FORMAT (*0*8X,F6.2,11X,F8.6,7(4X,F8.6)/)                              MARO3540
      RETURN                                                                MARO3550
      END                                                                   MARO3560
```

Appendix C

Reprint of letter of communication printed in the Journal of Chemical Physics. This article constitutes the first announcement of the anomalous pressure effect observed in thiophosgene.

Influence of collisions on coherent IR multiphoton absorption in thiophosgene

D. M. Brenner

Department of Chemistry, Brookhaven National Laboratory, Upton, New York 11973

M. Spencer and J. I. Steinfeld

Department of Chemistry, Massachusetts Institute of Technology, Cambridge, Massachusetts 02138

(Received 26 May 1981; accepted 14 July 1981)

Collisionless IR multiphoton absorption (IRMPA) in the pumped-mode ladder is postulated to involve coherent pumping with anharmonic defects compensated by rotational and/or vibrational splittings.[1] Previously it has been shown that the effects of this interaction on the rovibronic populations of the pumped mode can be monitored by IR–visible double resonance under molecular beam conditions.[2] In particular, experimental evidence on thiophosgene (Cl_2CS) suggests that pumping from the vibrationless level (000000) at all CO_2 laser frequencies results in the depopulation of a large fraction of the total number of rotational states.[3] In this communication, it is shown that the absolute change in the total rotational population induced by IR pumping (1) decreases with increasing pressure (10^{-5}–0.3 Torr) from 65% (collisionless) to 0% (300 mTorr), and (2) is unrelated to the photoacoustic and low energy IR spectra.

The apparatus for IR–visible double resonance has been described previously.[4] In this experiment, modifications have been made which allow absolute changes in the integrated intensity of the vibrationless level due to IR pumping to be monitored. These include focusing the CO_2 laser beam with a cylindrical lens to increase the interaction region of the CO_2 laser, cryogenic pumping under beam conditions, and an imaging system[5] between the fluorescence zone and the photomultiplier detector to limit the field of view to the interaction region Measurements in the 10^{-4} Torr range have been made under fast flow conditions and those in the $\geq 10^{-3}$ Torr range, under bulb conditions in which the gate valves of the beam machine have been closed. To be certain that under all conditions the fraction probed is not larger than that pumped, the invariance of the results with aperture size in the imaging system was checked and verified.

Figure 1(a) shows the pressure dependence of the absolute change, $\Delta = 1 - I_{IR\ ON}/I_{IR\ OFF}$, where I is the integrated fluorescence intensity, in the population of the vibrationless level due to IR pumping. The conditions of the CO_2 laser are $h\nu_{CO_2} = 944\ cm^{-1}$, Φ (fluence) $= 0.56\ J\,cm^{-2}$, t_p (pulse duration) = 200 ns (FWHM), and t_d (delay time between leading edges of pump and probe) = 300 ns. *With increasing pressure the total depopulatio of the vibrationless level decreases and at* $p \geq 300$ mTorr *no depopulation occurs within experimental error.* This is in sharp contrast to the behavior of other small mole-

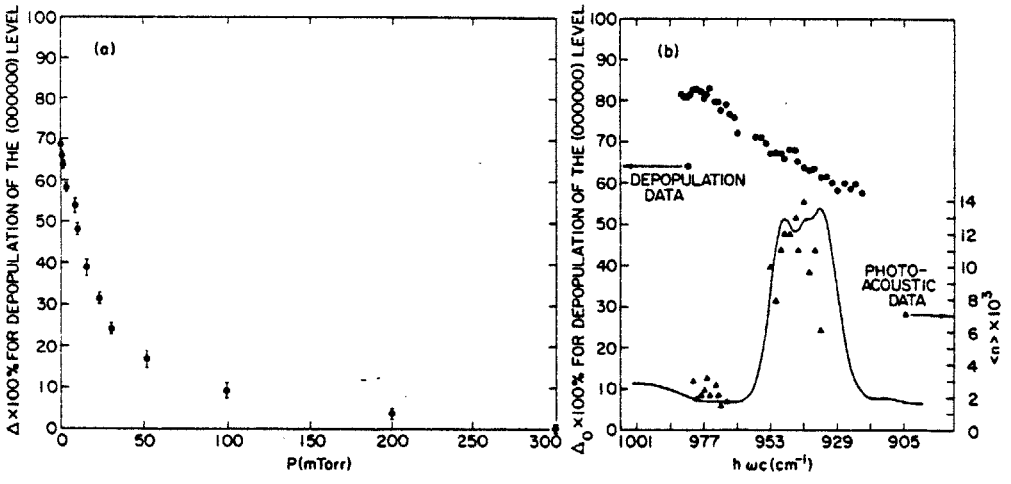


FIG. 1. (a) Plot of the absolute, IR-induced change $\Delta(\times 100\%)$ in the vibrationless level of thiophosgene vs pressure. (b) Comparison of the absolute, IR-induced change Δ_0 ($\times 100\%$) in the vibrationless level under collisionless conditions with (1) the average number of photons absorbed $\langle n \rangle$ under bulb conditions (500 mTorr) at different CO_2 laser frequencies, and (2) the low energy IR absorption spectrum of $2\nu_4$. Errors in Δ_0 are < 3% and in $\langle n \rangle$, < 15%.

 0021-9606/81/183153-02$01.00 © 1981 American Institute of Physics

cules (e.g., CDF_3[6]) in which an increase in pressure results in increased IR energy deposition. Variation of t_d establishes that pumping of the electronically excited state is unimportant.[7]

The results of Fig. 1(a) indicate that under collisional conditions ($p \geq 300$ mTorr), the average number of photons absorbed per molecule $\langle n \rangle$ will be ≤ 0.03, the experimental uncertainty at $p = 300$ mTorr. This is to be contrasted with Δ_0 which represents for collisionless conditions a lower bound[8] for $\langle n \rangle$. Figure 1(b) compares $\langle n \rangle$ measured in a calibrated photoacoustic cell[9] with both the low energy IR spectrum of $2\nu_4$ and Δ_0 for $h\nu_{CO_2} = 953-933$ cm^{-1} at constant $\phi = 0.56$ J cm^{-2}. At 944 cm^{-1}, $\langle n \rangle$ measured photoacoustically ($p = 500$ mTorr) is 0.013 ± 0.001 in agreement with the fluorescence measurements. The similarity of the low energy IR and photo-acoustic spectra and the observation that $\Delta = 0$ for $p \geq 300$ mTorr provide evidence that IR pumping under collisional conditions is incoherent and involves only the $1 - 0$ transition.

Figure 1(b) reveals that the probability of IRMPA under collisionless conditions is much greater than that under collisional conditions. Moreover, it has been observed by monitoring the combination bands $2^1_0 3^1_0 4^1_n$, $n = 2, 4, 6, 8$, that the "pumped mode" $2\nu_4$ [see the low energy IR spectrum in Fig. 1(b)] is *not* populated at higher levels up to $8\nu_4$ ($4h\nu_{CO_2}$ absorbed)[3] when the CO_2 laser frequency is 942–951 cm^{-1}. At 944 cm^{-1}, for example, this means $\langle n \rangle_{\text{collisionless}} > 2.7$ compared to $\langle n \rangle_{\text{collisional}} = 0.012$. It can therefore be concluded that at these CO_2 laser frequencies there is a $>10^2$ difference in the absorption cross section for pumping to levels $> 4h\nu_{CO_2}$ compared to that for the incoherent, one photon transition.

Figure 1(b) also demonstrates that IRMPA causes efficient depopulation of the vibrationless level under beam conditions at frequencies where the intensity of the low energy IR absorption is extremely weak. An incoherent process which causes an 80% decrease in the total number of states in the absence of collisions would have to have an improbably large dipole moment for the $1 - 0$ transition.

These results (1) demonstrate the existence of a collision induced, long range interaction which reduces the probability of IRMPA in thiophosgene, and (2) suggest that pumping in the ladder is coherent. Recently a prominent feature in the SF_6 IRMPA spectrum has been assigned as a coherent two-photon excitation on the basis of spectroscopic evidence.[10]

The long range perturbation observed in these experiments occurs during the laser pulse and would be described as collision-induced dephasing if pumping is indeed coherent.[11] Its origin is probably similar to rotational relaxation.[12] The implication of these experiments is that IRMPA in thiophosgene involves a change in mechanism in going from the collisionless to the collisional regime. The nature of this interaction and its occurrence in other small molecules is under investigation.

This work was carried out at Brookhaven National Laboratory and supported in part (DMB) by the U. S. Department of Energy and in part (MS and JIS) by the Air Force Office of Research, grant AFOSR-78-3725.

[1]Overviews can be found in R. V. Ambartzumian and V. S. Letokhov, in *Chemical and Biochemical Applications of Lasers*, edited by C. B. Moore (Academic, New York, 1977), Vol. III; M. F. Goodman, J. Stone, and E. Thiele in *Multiple-Photon Excitation and Dissociation of Polyatomic Molecules*, Topics in Current Physics, edited by C. Cantrell (Springer, Heidelberg, 1980); J. Ackeralt and H. Galbraith, in *Laser-Induced Chemical Processes*, edited by J. I. Steinfeld (Plenum, New York, 1981).

[2]D. M. Brenner and K. Brezinsky, Chem. Phys. Lett. 67, 36 (1979); D. M. Brenner, K. Brezinsky, and P. M. Curtis, *ibid.* 72, 202 (1980).

[3]D. M. Brenner, J. Chem. Phys. 74, 2293 (1981); D. M. Brenner, M. Spencer, and J. I. Steinfeld (to be published).

[4]D. M. Brenner, J. Chem. Phys. 74, 494 (1981). The home-built TE CO_2 laser used in these studies is multimode, but the pulse shape shows only a minimal degree of mode beating.

[5]R. E. Smalley, D. H. Levy, and L. Wharton, J. Chem. Phys. 64, 3266 (1976).

[6]I. P. Herman and J. B. Marling, Chem. Phys. Lett. 64, 75 (1979).

[7]D. M. Brenner, J. Phys. Chem. 84, 3341 (1980).

[8]The pumped mode ladder under the conditions of this experiment is not populated up to at least $v = 4$. See Ref. 3.

[9]D. M. Brenner (in preparation).

[10]C. W. Patterson, B. J. Krohn, and A. S. Pine, Opt. Lett. 6, 39 (1981).

[11]Theoretical treatment of this effect can be found in J. Stone, E. Thiele, and M. F. Goodman, J. Chem. Phys. 63, 2936 (1975).

[12]For a general discussion, see J. T. Yardley, *Introduction to Molecular Energy Transfer* (Academic, New York, 1980), pp. 274–302.

Appendix D

Preprint of companion article to this thesis ~~accepted for publication~~ printed in the Journal of Chemical Physics ~~(January 1, 1983)~~. In it the reader will find summaries of density matrix calculations done with different parameter values from those described in this thesis as well as an alternative explanation to the one presented here for the static gas experiments.

Photophysics of infrared multiphoton excitation in thiophosgene

D. M. Brenner[a)]

Brookhaven National Laboratory, Department of Chemistry, Upton, New York 11973

M. N. Spencer and J. I. Steinfeld

Massachusetts Institute of Technology, Department of Chemistry, Cambridge, Massachusetts 02139
(Received 19 July 1982; accepted 20 September 1982)

IR multiphoton absorption (IRMPA) in thiophosgene has been studied by IR-visible double resonance. In particular, the probability of absorption has been measured in both collision-free (molecular beam) and collision-perturbed environments by monitoring the depopulation of the ground state level (000000). Although no evidence for true multiphoton absorption is found, a number of important observations have been made. (1) No correlation exists between the IRMPA spectrum under collision-free conditions and the low energy IR absorption spectrum. (2) Homogeneous depletion of rotational populations occurs at all CO_2-laser frequencies. (3) Bottlenecks to absorption do not occur in the pumped-mode ladder. (4) The probability of absorption depends inversely on pressure and is affected dramatically by long-range collisions. These results are interpreted in the framework of an optical Bloch equation model.

I. INTRODUCTION

The properties of polyatomic molecules at high levels of vibrational excitation are currently the subject of considerable interest. One approach to preparing such systems is infrared multiphoton absorption (IRMPA).[1-3] While versatile and efficient, IRMPA involves a complex interplay of photon absorption and emission, intramolecular vibrational relaxation, and irreversible decay processes at sufficiently high energies. As a consequence, measurements of highly averaged properties of the distribution of excited molecules, such as total yield of a dissociation product or total infrared energy deposited in the sample, cannot by themselves uniquely specify the distribution function, especially in the discrete levels characteristic of low to intermediate vibrational energies. Properties of the quasicontinuum, such as the averaged infrared absorption cross-section $\sigma(E)$, can be extracted from such data[4] using deconvolution[5] and master-equation modeling[6] techniques, but do not reveal much information concerning the dynamics. However, it is possible to elucidate the absorption dynamics in the discrete "ladder" of vibrational levels in small polyatomic molecules by employing spectroscopic probes which are responsive to populations in individual vibrational levels.

A number of such double-resonance methods have been applied to the IRMPA problem. Both infrared emission[7] and transient absorption[8-10] have been used to probe vibrational distributions in SF_6 pumped in its ν_3 mode by a CO_2 laser. Changes in UV photoabsorption cross sections can be used to monitor infrared photon absorption, e.g., in ozone.[11] Both spontaneous[12] and stimulated[13] Raman scattering have been employed as probes of vibrational excitation following IRMPA. When IR-visible double resonance via laser-induced fluorescence (LIF) excitation spectroscopy can be employed, however, its superior sensitivity and resolution make it the method of choice. The greatest limitation on this method is that the molecule under study must possess a strongly fluorescing visible or near-UV transition. This requirement can be satisfied for systems such as formaldehyde[14] and propynal[15]; in this study, we report on LIF spectroscopy of thiophosgene ($Cl_2C=S$) pumped by a CO_2 laser. The spectroscopy of the $\tilde{X}\,^1A_1$ and $\tilde{A}\,^1A_2$ states have been studied extensively for this system.[16]

Theoretical models of the dynamics for IRMPA[1,17] generally involve transitions between Rabi-broadened "pumped-mode" levels in the discrete region and coupling to a dense set of background levels at higher vibrational energies. In these models, both stepwise excitation via a sequence of near-resonant one-photon transitions between pumped-mode levels and multiphoton excitation to a resonant n-quantum final state (with $n \geq 2$) may contribute to the excitation process. There is as yet little clear-cut evidence for the multiphoton process, however. Alimpiev *et al.*[18] have found structure in the IRMPA spectrum of SF_6, part of which has been assigned to direct two photon $2\nu_{3-0}$ transitions.[19]

In general, the effect of gas collisions on IRMPA in small molecules such as CDF_3,[20] CF_2HCl,[21] NH_3,[22] SF_6,[23] and CF_3Cl[24] is to increase the net dissociation yield; eventually, at higher pressures, the yield may decrease as a result of deactivating collisions. Measurements of infrared energy deposition in ozone, by IR-UV double resonance,[11] also show a linear increase in energy deposition with pressure. The basis for this pressure effect is best described as a combination of "hole filling" due to rotational relaxation, which relieves the saturation of specific resonant transitions, and pressure broadening of off-resonant absorption features. These effects have, in general, *not* been incorporated into current theoretical models for IRMPA because of the complexity they would add to the equations describing the process.

[a)]Present address: Occidental Research Corporation, P.O. Box 19601, Irvine, California 92713.

 0021-9606/83/010136-14$02.10 © 1983 American Institute of Physics

In earlier work on thiophosgene,[25] it was found that population was pumped out of the ground vibrational state by several CO_2 laser lines near the one-photon $2\nu_4 - 0$ absorption at 942 cm^{-1} without appearing in $v = 2$, 4, 6, or 8 of the ν_4 mode. We also noted[26] that infrared pumping out of the vibrational ground state became much less efficient as the pressure of thiophosgene increased, and that infrared energy deposition, measured photoacoustically at moderate pressures, differed both in magnitude and in infrared frequency dependence from IRMPA under collision-free conditions.

In this paper, we report results on the dependence of ground-state depletion on infrared frequency, laser influence, and rotational temperature of the thiophosgene molecules. We also report on the pressure dependence of the ground state depletion for a variety of collision partners; in the present case, we find that the effect of collisions is not to enhance, but rather to reduce the probability of the IRMPA process. Following a presentation of the experimental data, we discuss an optical Bloch equation (OBE) model for this process, and propose as a possible explanation for the effect of collisions, mixing of the pumped-mode states with infrared-inactive background states, whenever the magnitude of the collisional perturbation is larger than the effective Rabi-frequency.

The IRMPA of thiophosgene in the $\tilde{A}\,^1A_2$ state, prepared by optical excitation prior to the CO_2 laser pulse, has also been investigated and reported elsewhere.[27,28] Infrared pumping of the $\tilde{A}$ state is a possible source of interference in these experiments, and is considered in greater detail below.

II. EXPERIMENTAL

The apparatus for these experiments has been described previously[28,29] and will be mentioned here only briefly. An effusive molecular beam, formed from a 2 mm diam nozzle terminated in a 25 μm capillary array and collimated with a liquid nitrogen (LN_2) cooled aperture, intersects the beam axes of a homebuilt CO_2 laser and a N_2-pumped dye laser (Molectron UV14/DL200) at right angles. The interaction region is surrounded with LN_2-cooled baffles and viewed through an imaging system with a photomultiplier. The photomultiplier only detects fluorescence from a region defined by the intersection of the dye laser and CO_2 laser (see Fig. 1). Scattered light in the system is eliminated by the combination of imaging system and cut-off filters (Hoya). The fluorescence signal is amplified (LeCroy, model VV100B), averaged in a boxcar integrator (PAR model 162 mainframe with either model 164 or model 165 plug-in), and stored in a multichannel analyzer (Tracor Nothern, model 1710 with model 1710-30 plug-in) for integration.

Experiments involving rotational cooling are carried out with a supersonic jet. The source, located 3 cm from the interaction zone, is a pulsed valve (General Valve, model 9-181) operated with a 180 V power supply and fast-switching transistor. The valve terminates in a nozzle ~0.75 mm in diam and is routinely operated to produce pulses ~200 μs (FWHM) in duration

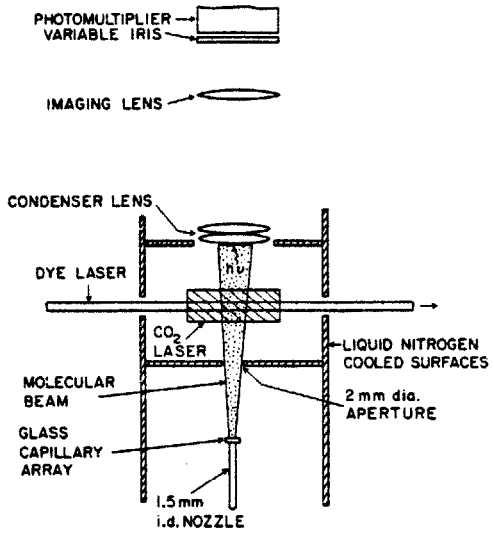


FIG. 1. Schematic representation of imaging system and interaction zone. A similar configuration is used in pulsed-valve experiments, except that a free jet is used instead of a beam.

determined spectroscopically. Rotational cooling is accomplished by the expansion of 800 Torr of argon containing 0.25% of thiophosgene. Based on computer simulation of the $2_0^1 3_0^1 4_0^1$ band, an upper bound to the rotational temperature of thiophosgene under these conditions is 12 ± 2 K. The electronic gating of pulsed valve, laser, boxcar integrator, and multichannel analyzer is accomplished by means of a master oscillator.

The CO_2 laser pulse used in these experiments is multimode but shows only a minor degree of mode beating. The temporal energy distribution of the laser pulse is measured with a photon drag detector (Rofin, model 7400), the signal from which is amplified (Ortec, model 9301) and averaged with a boxcar integrator. The energy of the pulse is measured in 50 ns intervals and the result is displayed as a histogram in 100 ns intervals in Fig. 2. Also shown in Fig. 2 are the time delays between pump and probe, and between probe and boxcar gate. Since the dye laser probe interrogates populations after 200 ± 25 ns, only ~60% of the total energy per pulse is used in the experimental measurements. Appropriate corrections, therefore, have been made in determining the fluence. Varying the delay time between pump and probe up to 600 ns has at most a 10% *attenuating* effect on the signal; at later times, diffusion out of the viewing region begins to be a significant loss process.

Experiments at higher pressure (> 5 mTorr) are carried out in the same beam apparatus, but with the gate valves closed, thereby converting it into a bulb. Since the imaging system rigorously limits the viewing region, only molecules within the interaction zone are detected under these conditions as well. Pressures in

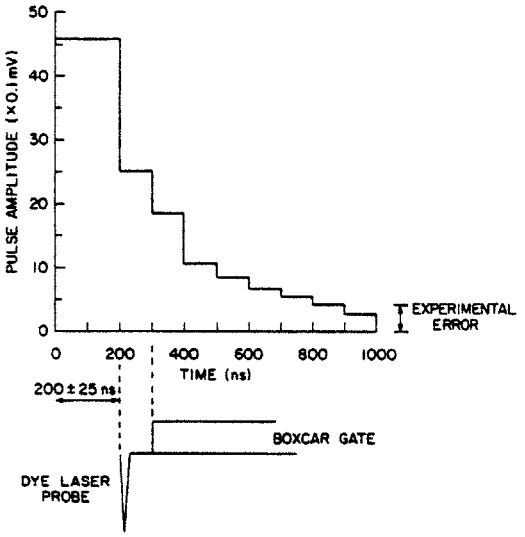


FIG. 2. Temporal energy distribution of the CO_2-laser pulse and gating diagram. Pressure-dependence studies are carried out with a 200 ns delay between pump and probe, the results of which are invariant with changes in the delay time. The magnitude of the ground state depletion does decrease at times >600 ns due to diffusion out of the interaction zone.

these experiments are measured with a capacitance manometer (Datametrics model 1173 electrometer with model 570 A Barocel) having a precision of ±0.5 mTorr. In studies involving mixed quenchers, 1 mTorr of $CSCl_2$ is first added to the bulb and the appropriate pressure of quencher gas is added subsequently. This procedure gives results reproducible to better than 10% measured on separate days.

Thiophosgene stabilized with 15% CCl_4 (Aldrich Co.) is purified by low temperature, trap-to-trap distillation at reduced pressure. The first fraction typically contains the bulk of volatile impurities and is discarded. Purified thiophosgene used in these experiments contains CCl_4 as an impurity. This impurity can be eliminated by gas chromatographic separation, but the experimental results obtained with high purity $CSCl_2$ (>99.9%) are identical to those obtained when CCl_4 is present as an impurity. Therefore, trap-to-trap distillation has been used as the purification method throughout.

Quencher gases are used without further purification and are in all cases of >> 99% purity: He, Research Grade (Linde); Ar, Scientific Grade (Matheson); Xe, Research Grade (Liquid Carbonic); CO, Research Grade (Matheson); N_2O, 99.9% (Matheson); CO_2, Coleman Grade (Matheson); CH_3Cl, 99.5% (Matheson); CH_3NO_2, Reagent ACS Grade (Eastman); CH_3CN, Spectrophotometric Grade (Aldrich).

III. RESULTS

Previous IR-visible double resonance experiments on $CSCl_2$[25] demonstrated that depletion of the ground-state-level (000000) by IRMPA is characterized by a homogeneous bleaching of rotational states (within the resolution limits of the dye-laser probe). However, in those experiments only a lower bound for the actual depletion could be measured because an imaging system was not used to limit the field of view. Figure 3(a) is a laser-excitation spectrum of the $2_0^1 3_0^1 4_0^1$ combination band obtained with the improved detection (imaging) system described above. The decrease in intensity from IR pumping at $\omega_{CO_2} = 944$ cm^{-1} is directly proportional to the change in rovibronic population of the (000000) level since $I = FN$ where I is the integrated signal intensity, F is the Franck–Condon factor for the transition, and N is the integrated population of that level of the ground state from which the electronic transition originates [in this case (000000)]. Since the extent of depletion is much larger than that previously measured, the sensitivity to inhomogeneities should be much greater. In fact, only homogeneous depletions are observed at all CO_2 laser frequencies which supports the earlier result. This observation indicates that a substantial fraction of the total rotational state population is able to interact with the IR radiation field at all CO_2-laser frequencies. This is in contrast to results of IR–UV double resonance studies on formaldehyde[14] and propynal[15,30] in which rotational hole burning has been observed.

The extent of depletion of the ground state population is measured by integrating over the entire rotational contour. This is accomplished with a digital integrator[29] or by storing the averaged signal of the boxcar integrator in the multichannel analyzer and integrating. The result of these integrations at different CO_2-laser frequencies, which is effectively an IRMPA spectrum, is given in Fig. 4. This IRMPA spectrum obtained under collision-free conditions, indicates that depletion of the ground state is extremely efficient; between 80% and 85% of the (000000) thiophosgene molecules have absorbed *at least one* IR photon. This range represents a lower bound to the average number of photons absorbed, since more than one IR photon may be absorbed per ground-state molecule lost. Thus, Fig. 4 is a spectrum of the average minimum number of photons absorbed per molecule. This number $\langle p \rangle$ ranges from 0.6 to 0.85 and is associated with IR pumping of a Boltzmann population of states at 300 K under collision-free conditions.

Comparison of the collision-free IRMPA spectrum with the low resolution (1 cm^{-1}) infrared absorption spectrum indicates a very unexpected result. Although depletion of the ground state is efficient, there is no correlation with the low energy IR absorption spectrum. This suggests that the probability for multiphoton absorption is not derived primarily from the oscillator strength for the one-photon transitions in the 900–1100 cm^{-1} frequency range. In view of the magnitude of the depletions, however, this result is not totally unexpected; absorption in the 900–1100 cm^{-1} range corresponds in $CSCl_2$ only to weak overtone ($2\nu_4$, $2\nu_3$) and combina-

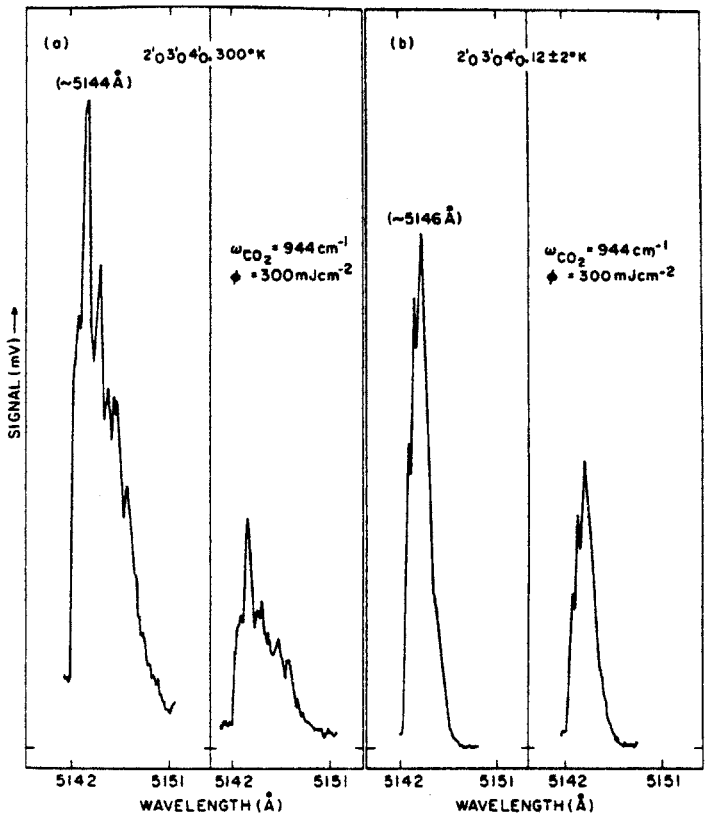


FIG. 3. Laser-induced fluorescence excitation spectrum of the $2^1_0 3^1_0 4^1_0$ combination band before and after IRMPA. The rotational temperature is (a) 300 K and (b) 12 ± 2 K. The signal-intensity scales of (a) and (b) are different. In both (a) and (b), $\omega_{CO_2} = 944$ cm^{-1} and $\Phi \sim 300$ mJ cm^{-2}.

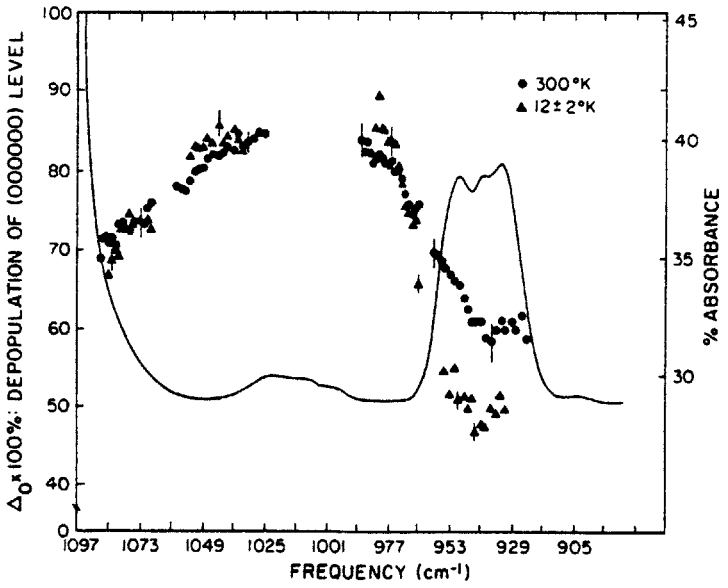


FIG. 4. IRMPA spectrum under collision-free conditions measured from the magnitude of the ground state depletion $\Delta_0 \times 100\%$ at a fluence of ~ 300 mJ cm^{-2} and at rotational temperatures (●) 300 K and (▲) 12 ± 2 K.

TABLE I. Vibrational and rotational constants of ground state $CSCl_2$.

Mode (symmetry)	Frequency[a] (cm^{-1})	Anharmonicity (cm^{-1})
Fundamentals		
$\nu_1(a_1)$	1137.7 ± 3.0	−4.0 ± 1.2
$\nu_2(a_1)$	497 ± 2.4	
$\nu_3(a_1)$	288.5 ± 2.5	1.5 ± 1.1
$\nu_4(b_1)$	471.5 ± 0.7	−0.23 ± 0.02
$\nu_5(b_2)$	818[b]	
$\nu_6(b_2)$	286[b]	
Overtones and combinations		
$2\nu_4$	941.9[b]	
$2\nu_2$	994	
$\nu_2+\nu_4$	963	
$2\nu_3+\nu_4$		
$2\nu_6+\nu_4$	1048	
$\nu_3+\nu_6+\nu_4$		
$\nu_2+2\nu_3$		
$\nu_2+2\nu_6$	1074	
$\nu_2+\nu_3+\nu_6$		
Rotational constants (MHz)[c]		
A_0	3557.3089(3)	
B_0	3464.1108(3)	
C_0	1753.1000(2)	

[a]Taken from Ref. 16(d).
[b]Taken from Ref. 16(a).
[c]Taken from Ref. 33. The standard deviations are given in parentheses and refer to the least significant digit quoted.

tion bands (see Table I). The largest oscillator strength for these transitions is associated with $2\nu_4$ and has a value of 0.012 D (~4% of the static dipole moment)[31] corresponding to an absorption cross section of 5.65×10^{-20} cm^2. (The oscillator strength from which the cross section is determined is measured by integration of the FTIR spectrum). As a reference, the cross section for ν_3 in SF_6 is ~100 times larger than that of $2\nu_4$ in $CSCl_2$.

Previous studies of population changes of the $2\nu_4$ ladder indicated that when the laser frequency is 944 cm^{-1}, no population increases are observed[25] when the intensities of the $2_0^1 3_0^1 4_n^1$ bands with $n = 2, 4, 6, 8, 10$ are monitored. These results have been corroborated in the present set of experiments. Moreover, significant depletions of both the 4_2 and 4_4 levels have been observed. These results imply one of two possible interpretations: either the $2\nu_4$ ladder is not the only pumped mode and therefore is unperturbed by laser excitation at 944 cm^{-1} (see Fig 4) or anharmonic bottlenecks in the $2\nu_4$ ladder are absent up to at least ~6000 cm^{-1} when $2\nu_4$ is the pumped mode. The latter is plausible in view of the small anharmonicity of (0.2 cm^{-1}) of the $2\nu_4$ mode[16(b),16(d)] and the significant role rotational compensation mechanisms would be expected to play in IR pumping of an asymmetric top (*vide infra*).

If indeed anharmonic bottlenecks are unimportant in pumping the "sparse" region of $CSCl_2$, then the absence of population increases in the $2\nu_4$ ladder concurrent with large depletions of the (000000) level would be strong evidence for a multiphoton process. If indeed, this were a true multiphoton phenomenon involving virtual state intermediates, one might expect intensity dependences I^n, where $n \gg 1$. Figure 5 shows the dependence of the depletion of the ground state on laser energy per pulse at several CO_2 laser frequencies. The beam is gently focused to a cylinder in the interaction region, the cross sectional area of which is ~0.18 cm^2. To convert energy per pulse to intensity, these values should be multiplied by 1.85×10^7 s^{-1} cm^{-2}. It should be noted that the error limits of the experimental method preclude reliable measurements of depletions < 5%; therefore, any threshold for depletion would not be observable.

Figure 5 shows that the dependence of the depletion of the (000000) level on laser energy at low intensity is $n = 1$ to 1.5 at the indicated CO_2 laser frequencies. This result clearly indicates that the probability of absorption is not dominated by true multiphoton pathways involving virtual state intermediates. It must also be interpreted as an average intensity dependence, averaged over a large number of many rotational ladders, each of which has its own intensity dependence. The predominant pathway is approximately linear with laser intensity; in view of the multiphoton nature of the absorption, this suggests that resonantly enhanced transitions are the most important. In addition, there is no indication of a threshold for depletion. This is not unexpected because the lower limit to depletion in these experiments, given by Beer's Law for resonant $1 - 0$ absorption, is on the order of a few percent.

Figure 5 also shows that the relative probability of absorption reaches a constant value as the laser energy increases, suggesting saturation-like behavior. This

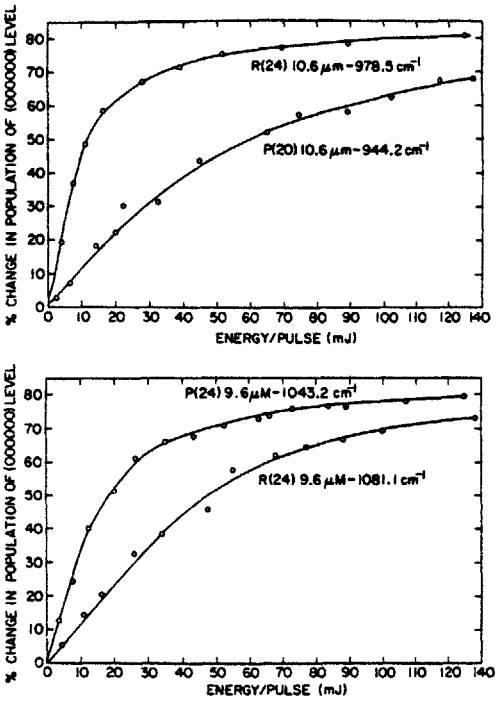


FIG. 5. Dependence of the population change of the ground state on laser energy/pulse at (a) $\omega = 978.5$ and 944.2 cm^{-1}, and (b) 1043.2 and 1081.1 cm^{-1}.

trend toward "saturation" indicates that the interaction linewidth is increasing more slowly than the probability of pumping states within that linewidth. Hence, at higher fluences, the increment of states which can absorb IR photons is decreasing relative to the absorption probability of those states that are accessible. In the collision free regime, this means that the Rabi frequency $\omega_R = \mu \cdot E/2\hbar$ is increasing more slowly than the detunings $\Delta\omega$ between laser frequency and pumped mode frequency. As a consequence of this trade off between ω_R and $\Delta\omega$, the dependence of the depletion on laser energy is also sensitive to CO_2-laser frequency as is shown in Fig. 5.

Since the probability of absorption in $CSCl_2$ and its dependence on laser intensity depends in part on how many rotational states are within the power broadened linewidth, a shift in Boltzmann populations to different J, K values at lower rotational temperatures could have positive or negative effects on the depletion experiments, depending on the resonance conditions established at the lower temperature. Figure 3(b) shows a laser excitation spectrum of the $2_0^1 3_0^1 4_0^1$ combination band, rotationally cooled to 12 ± 2 K. The rotational temperature is estimated by comparing computer simulated spectra of $2_0^1 3_0^1 4_0^1$ and 4_0^1 bands at different rotational temperatures to their experimental spectra. Computer simulations are carried out with the program Fastplot[32] on a CDC 7600 computer with known spectroscopic constants from microwave[33] and visible absorption data.[16(a)] Figure 3(b), compared to Fig. 3(a), shows that the effect of rotational cooling on the depletion of the ground state level is to reduce slightly the probability of IRMPA when $\omega_{CO_2} = 944$ cm^{-1}. This can be interpreted as a shift of Boltzmann populations of rotational states to states for which the off-resonant contributions are larger in the sum of IRMPA pathways. As a result, the probability of IRMPA at this particular CO_2-laser frequency is reduced.

The IRMPA spectrum of rotationally cooled $CSCl_2$ is shown in Fig. 4 in comparison with the room temperature results. Only in the frequency range 900–1000 cm^{-1} are there any substantial differences. The data clearly indicate that when the laser frequency overlaps that of the $2\nu_4$ mode, pumping is less efficient. There may even be a slight increase in the probability of absorption at 983 cm^{-1}. Nevertheless, the similarities are very striking and consequently do not at this level of resolution permit a detailed analysis of the role that specific rotational pathways play in IRMPA of $CSCl_2$. Furthermore, the intensity dependence under rotationally cooled supersonic conditions is experimentally nearly indistinguishable from results at room temperature. This suggests that the proportion of off-resonant to resonant transitions *vis á vis* the power broadened linewidth at a particular laser energy is independent of rotational temperature over the range ~12 to 300 K.

Previously[28] it was reported that the probability of IRMPA depends inversely on pressure, in contrast with other studies of IRMPA.[20–24] In addition, photoacoustic studies were shown to be consistent with lower probability of IRMPA at higher pressures (0.5 Torr) compared to lower pressures (<5 mTorr). This inverse pressure dependence occurs independent of CO_2 laser frequency as is shown in Fig. 6 for two representative

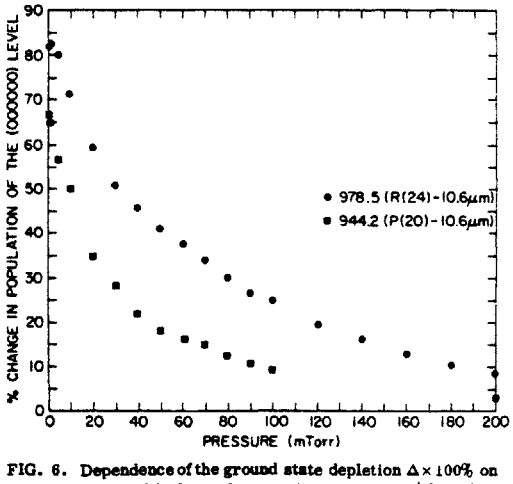


FIG. 6. Dependence of the ground state depletion $\Delta \times 100\%$ on pressure at two CO_2-laser frequencies, 978.5 cm^{-1} [R(24), 10.6 μm] and 944.2 cm^{-1} [P(20), 10.6 μm].

frequencies. However, the dependence of the depletions on laser energy does vary depending on the presence or absence of long range collisions. In Fig. 7 we show a comparison of the fluence dependence at four pressures. Although in each case the value of the depletion at saturation varies, the slopes of these curves at low laser energies are also different. Figure 7 shows that as the pressure increases, it is more difficult to pump the (000000) level and the number of absorbing states that are pumped decreases, especially at lower laser energies. Since the delay time between pump and probe is 200 ± 25 ns, at these pressures collisional perturbations can affect the mechanism of absorption only through long range terms in the potential. The net effect appears to be a reduction in the effective pumping rate. Several possible explanations exist for this effect which will be discussed in the following section.

Because IR pumping of the $\tilde{A}\,^1A_2$ state causes a reduction in its fluorescence quantum yield,[27,28] it is important to exclude the possibility that the inverse pressure dependence of IRMPA in $CSCl_2$ is not due to IR pumping of the $\tilde{A}$ state. This can be ruled out from results of time-delay experiments.

Under collision-free conditions when the delay time t_d between pump and probe is scanned over the duration of the CO_2-laser pulse (see Fig. 2) the ground-state depletion is constant (within ~10%) for $200 \leq t_d < 600$ ns and then decreases at longer delay times because of diffusion out of the viewing region. For example, at a delay time of 1 μs compared to 200 ns, the collision-free ground-state depletion ot $\omega_{CO_2} = 944$ cm^{-1}, $\phi \approx 300$ mJ cm^{-2}, is 55% compared to 65%.

If IR pumping of the $\tilde{A}$ state after the probe pulse is off were to explain the observed inverse pressure dependence, then the depletion of the ground state should not be inversely proportional to pressure when the probe occurs after the IR pulse ($t_d \geq 1$ μs). Figure 8 shows the dependence of the ground state population on pressure at different delay times t_d when $\omega_{CO_2} = 944$ cm^{-2}. Regardless of the delay time, an inverse pressure dependence is observed. Collisional quenching of the $\tilde{A}$ state can also be ruled out as an explanation because the data are normalized to the fluorescence intensity of the $2_0^1 3_0^1 4_0^1$ band when the CO_2 laser is off. Complications from overlap of other bands are rigorously ruled out by the known spectroscopy of the $\tilde{A}$ state.[16(a)]

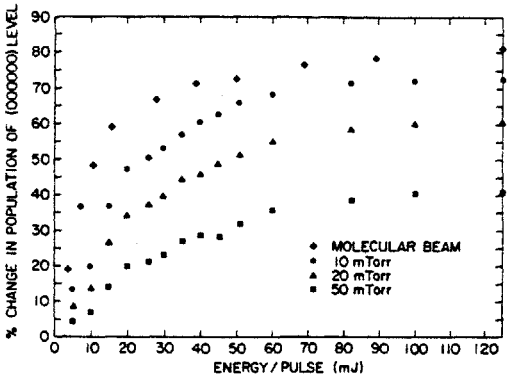


FIG. 7. Dependence of the population change of the ground state on laser energy at $\omega_{CO_2} = 978.5$ cm^{-1} for four pressures—collision free, 10, 20, and 50 mTorr. Note that for a given ground-state depletion, there is a nonlinear relationship to (pressure/energy) per pulse.

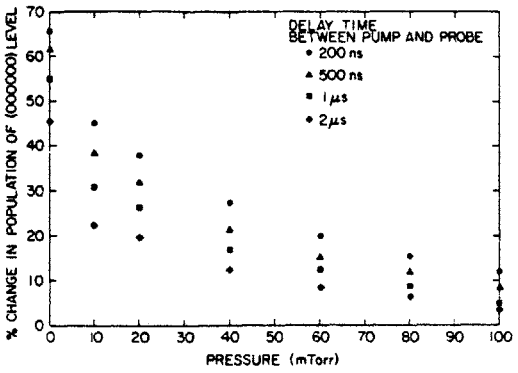


FIG. 8. Dependence of the ground-state depletion on pressure at four delay times—(●) 200 ns, (▲) 500 ns, (■) 1 μs, (◆) 2 μs; $\omega_{CO_2} = 944$ cm^{-1}, $\Phi \sim 300$ mJ cm^{-2}.

Not only do collisions of thiophosgene with itself reduce the overall probability of IRMPA, but also collisions with other gases have been observed to have a similar effect. Experiments conducted under bulb conditions with 1 mTorr of $CSCl_2$, diluted with a quencher gas up to a total pressure of ~100 mTorr, show that collisions in general reduce the probability of IRMPA. These quenching curves, similar to the ones shown in Fig. 6, have been fit to an exponential and the pressures required to reduce the depletion of the ground-state depopulation to $1/e$ of its collision-free value are given in Table II for a variety of polar and nonpolar collision

TABLE II. Characteristic quenching pressures and collision frequencies for ground-state depopulation.

Collision partner	$P(1/e)$ (mTorr)	$Z(1/e)$ (collisions molecule^{-1} s^{-1})
He	60	73×10^4
Ar	51	25
Xe	55	25
N_2	51	30
CO	45	26
CO_2	46	24
N_2O	47	24
CH_3Cl	36	16
CH_3NO_2	22	11
CH_3CN	19	11
$CSCl_2$	51	10

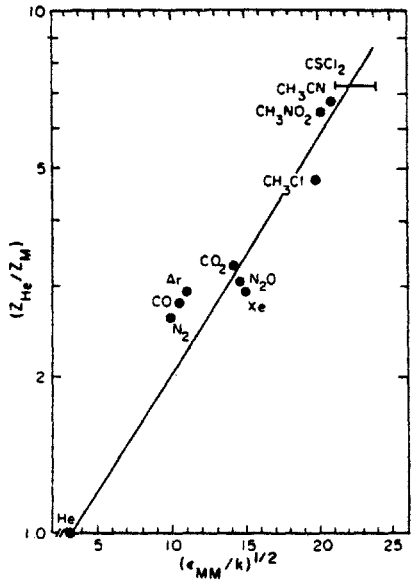


FIG. 9. Dependence of the "quenching efficiency" Z_{He}/Z_M, normalized to helium, on Lennard-Jones attraction parameter of quencher $(\epsilon_{MM}/k)^{1/2}$. The values Z_{He}/Z_M are obtained from the $1/e$ points of Table II (Z_M) and normalized to helium (Z_{He}).

partners. The data are also given in terms of gas-kinetic collision frequency per thiophosgene molecule, which factors out the hard-sphere cross section of the collision pair and the mean relative thermal velocity at 300 K. This representation displays more clearly the variation in "quenching" efficiency with interaction potential. While this efficiency does vary markedly in going from the rare gases (e.g., He) to polar molecules (CH_3NO_2, or thiophosgene itself), what is striking is the extremely rapid decrease in pumping efficiency; most of the depopulation is suppressed at gas-kinetic collision frequencies of only a few $\times 10^5$ per second. The implications of this will be discussed further in the following section.

Lin *et al.*[34] have proposed a correlation for the efficiency of collision-induced state changes, such as rotational relaxation or intersystem crossing, with intermolecular potential well depth. This correlation can be expressed as

$$\ln\sigma_M = \ln(\sigma_{\text{gas-kinetic}}) + \beta(\epsilon_{MM}/k)^{1/2}, \quad (1)$$

where σ_M is the cross section for the process induced by collision partner M, (ϵ_{MM}/k) is the Lennard-Jones well depth in degree K for the interaction of species M with itself, and β is a parameter characteristic only of the process. From the data of Table II, *relative* efficiencies can be found simply by taking the reciprocal collision frequency required to reduce ground-state depopulation by a factor of $1/e$. Values of $(\epsilon_{MM}/k)^{1/2}$ may be found in Table I of Ref. 34 for all collision partners studied here, with the exception of thiophosgene itself. The resulting correlation is shown in Fig. 9; the data clearly are of the form given by Eq. (1), confirming that it is the long-range interaction between the thiophosgene molecule and the collision partner which influences the IRMPA process.

IV. MODEL CALCULATIONS

The population dynamics of a pumped-mode ladder interacting with an intense IR radiation field is given by a formalism analogous to the Bloch equations.[35] This formalism describes the time evolution of the complete density matrix of a system absorbing light from a monochromatic source. It takes into account the dephasing time of the coherent light source, phase-changing (T_2) and energy-changing (T_1) collisions, and irreversible intramolecular decay of the pumped mode into a high density of background states, the quasicontinuum. Analytical solutions are tractable only for two- and three-level systems,[36] but approximate methods (generalized master equation[37]) have been developed for N-level systems. The modeling described below is the result of a numerical computer calculation for an N-level system.

According to quantum mechanics, the time rate of change of populations of a pumped-mode ladder interacting with a coherent light source is given by the time-dependent Schrödinger equation

$$\dot{\rho} = (-i/\hbar)[\mathcal{H}, \rho],$$

where $\mathcal{H}$ is the total Hamiltonian of the system and ρ the density matrix. For optically allowed transition, the Hamiltonian can be represented as

$$\mathcal{H} = \mathcal{H}_0 - \mu \cdot \mathbf{E},$$

where $\mathcal{H}_0$ is the unperturbed Hamiltonian from spectroscopy and $\mu \cdot \mathbf{E}$ the perturbation Hamiltonian which describes the interaction of the off-diagonal matrix elements of the dipole moment μ with the radiation field E. In these calculations, the amplitude of the radiation field initially was chosen to duplicate temporally the laser pulse (see Fig. 2). These results were found to be the same (within 20%) as those for a 200 ns square-wave pulse having the same integrated amplitude; therefore the latter pulse shape was used for most of these calculations.

For a dilute gas undergoing thermalizing collisions with a heat bath, the time evolution of the density matrix must also include T_1- and T_2- type collisional relaxation. In addition, populations can be lost from the pumped-mode ladder if there is an irreversible decay channel such as intramolecular relaxation into a high density of background states. The population dynamics for this model system is, then, given by Eq. (2),

$$\frac{d\rho}{dt} = \frac{i}{\hbar}[\rho, \mathcal{H}] + \left(\frac{1}{\tau}\mathrm{K}\rho - \frac{1}{\tau}\rho\right) - \frac{i}{\hbar}\sum_{n=0}^{N-1}\Gamma_n(\rho\mathrm{P}_n + \mathrm{P}_n\rho), \quad (2)$$

which has been discussed in detail by Stone, Thiele, and Goodman[37] (see Fig. 10). This equation represents the dynamical evolution of the density matrix in the presence of energy changing collisions with a relaxation

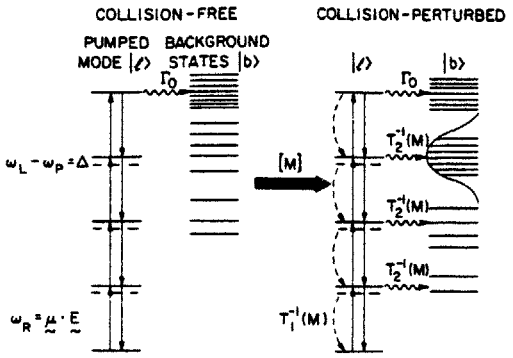


FIG. 10 Schematic representation of the optical Bloch equation model (a) in the absence of collisions and (b) in the presence of collisional perturbations.

time T_1, represented by the term $\tau^{-1}K\rho$, phase changing collisions with a relaxation time T_2, represented by the term $\tau^{-1}\rho$, and irreversible intramolecular relaxation represented by the term in $\Gamma_n\rho$. It has been shown that dephasing due to the laser field can be incorporated into this equation by summing its effect with that due to phase changing collisions.[38]

For an N-level system, Eq. (2) describes a set of N^2 coupled differential equations for the time dependence of population and driving terms. The N-level system can be solved in the standard way by writing the coupled equations in matrix notation and finding the eigenvectors V and eigenvalues λ,

$$\rho(t) = \mathbf{V}e^{t\lambda}\mathbf{V}^{-1}\rho(o) ,$$

in the harmonic oscillator basis $\rho(o)$. However, for $N > 3$ analytical solutions are intractable and numerical methods are necessary. The computer code used in numerical solutions was furnished to us by Dr. H. W. Galbraith, of Los Alamos National Laboratory and extensively modified by us. Matrix diagonalization is accomplished with standard programs available for a CDC 7600.

Numerical solution of Eq. (2) requires a number of inputs. In the absence of collision, these include the Rabi frequency $\omega_R = \mu \cdot E/2\hbar$; the energy spacing in the ladder specified by the detuning of the laser frequency with respect to the pumped mode frequency, Δ(Δ is determined from the anharmonicity and rotational energy); the dephasing rate associated with the laser source $(T_2)^{-1}_{\text{laser}} \propto (\Delta\nu)_{\text{laser}}$; and the rate of irreversible intramolecular decay Γ. In reality, intramolecular decay will be irreversible only if $2\pi\rho(E) \gg \omega_R$, where $\rho(E)$ is the density of coupled background states,[1] which varies from only 0.1 state/cm^{-1} at the one-photon energy of 1000 cm^{-1} to about 20 states/cm^{-1} at 7000 cm^{-1}. In principle, all of these inputs could be obtained and an exact calculation carried out as has been done recently for SF_6.[39] However, because of more limited resources, we have investigated the behavior of a small number of prototypical, five-level ladders, specified by a detuning Δ at each level, to determine qualitatively the expected overall experimental behavior. For each of these ladders, an upper bound to $\omega_R(1 \leftarrow 0)$ is 2×10^{-2} cm^{-1} at 0.5 J cm^{-2}; the value of μ is obtained from integration of the $2\nu_4$ band in the FTIR spectrum; $(T_2)^{-1}_{\text{laser}}$ is determined from the estimated laser bandwidth (≤ 0.04 cm^{-1}); and Γ is varied from 10^6 to 10^{10} s^{-1} and affects population only at the uppermost level. The latter is a simplification, assumed to be reasonable based on the density of states given above. Although additional relaxation pathways or a more complicated ladder involving competitive pumping of background states (see Galbraith and Ackerhalt[1]) could be included, the lack of experimentally determined molecular parameters does not warrant these additional complications.

Insight into how the OBE model behaves in the absence of collisions can be obtained by varying Δ, ω_R, and Γ. In pumping $2\nu_4$ at 944 cm^{-1}, $\omega_R = 0.02$ cm^{-1} and the dependence of populations on Δ is shown in Table III for $\Gamma = 0$. In these simulations $(T_2)^{-1}_{\text{laser}} = 10^9$ s^{-1} (estimated from the laser bandwith) and the population distribution appears to be insensitive to coherent effects. For the coherent process, the population distribution is typically skewed to the higher levels. These results show that when $\Delta > 50\omega_R$, the absorption probability becomes small. However, when $\Gamma = 10^9$–10^{10} s^{-1}, the dynamic range of Δ relative to ω_R is slightly larger, but more importantly, the population distribution changes markedly. In particular, as shown in Fig. 11, when $\Gamma \geq 10^9$ s^{-1} population in the pumped-mode ladder is rapidly lost to the quasicontinuum from levels above the detuned level. Therefore, population will be observed in the ground state and in the quasicontinuum after the laser probe is off, but essentially not in-between. This observation is consistent with the experimental observation.

The experimental data measure an average, over-all population of rotational ladders. Therefore, in modeling, for example, the fluence dependence (Fig. 5), some ladders will be pumped more efficiently and others less efficiently. Table IV shows the fluence dependence for a typical ladder. The overall behavior parallels that

TABLE III. Effect of detunings (Δ_n) at various levels (n) of the pumped-mode ladder on populations in the ladder for a five-level system.[a]

Detunings (cm^{-1})			Populations at levels				
Δ_2	Δ_3	Δ_4	1	2	3	4	5
0	0	0	0.2	0.2	0.2	0.2	0.2
0.25	0.25	0.25	0.232	0.193	0.193	0.193	0.189
0.5	0.5	0.5	0.561	0.119	0.118	0.118	0.084
1.0	1.0	1.0	0.855	0.045	0.044	0.044	0.012
1.5	1.5	1.5	0.932	0.022	0.022	0.022	0.003
1.5	0	1.5	0.336	0.068	0.264	0.073	0.259
1.5	0	0	0.384	0.055	0.187	0.187	0.187
0	0	1.5	0.230	0.230	0.230	0.086	0.223
0	2	0	0.453	0.453	0.036	0.036	0.029

[a]The Rabi frequency for the $0 \rightarrow 1$ transition, $\omega_R(o) = 0.02$ cm^{-1} and $\omega_R(n) = \sqrt{n}\,\omega_R(o)$; $(T_2)^{-1}_{\text{laser}} = 1$ ns^{-1}; $(T_1)^{-1} = 0$; $\Gamma = 0$; laser pulse duration = 200 ns; $\omega_{\text{laser}} = 942$ cm^{-1}; population in level 1 (ground state) = 1.0 at $t = 0$.

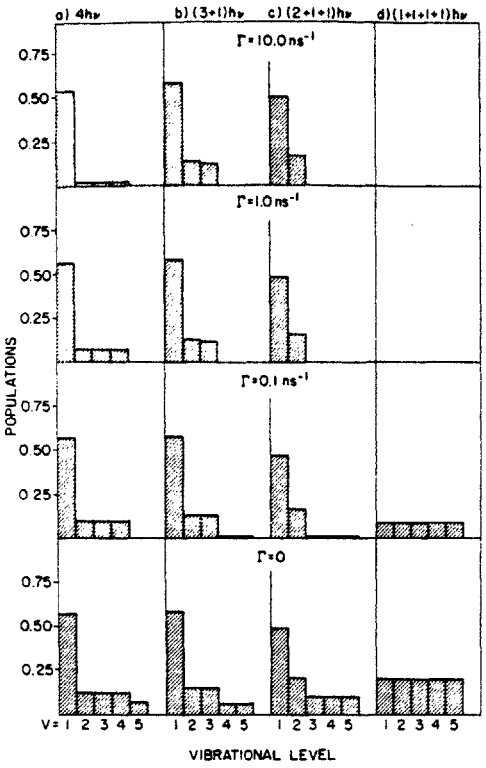


FIG. 11. Effect of Γ at $v = 5$ of the ladder for four ladders having detunings Δ as follows: (a) $\Delta_2 = \Delta_3 = \Delta_4 = 0.25$, (b) $\Delta_2 = \Delta_3 = 0.25$, $\Delta_4 = 0$, (c) $\Delta_2 = 0.25$, $\Delta_3 = \Delta_4 = 0$, (d) $\Delta_2 = \Delta_3 = \Delta_4 = 0$. In each case, $\omega_R = 0.015$ cm^{-1}, $(T_2)^{-1}_{\text{laser}} = 1$ ns^{-1}, $(T_2)^{-1} = 0$, laser pulse duration = 200 ns, population in level 1 (ground state) = 1.0 at $t = 0$.

observed experimentally. Although all ladders that are pumped show this behavior, the absolute magnitudes are different. However, the experimental observations will reflect a sum over a very large number of such ladders, weighted by their respective Boltzmann factors.

When collisions become important, as indicated by the experimental data for pressures > 5 mTorr, the optical Bloch equations can accommodate these perturbations, in principle, directly through T_1 and T_2 relaxation. T_1 or energy changing collisions preserve population in the ladder, but cause suppression of population to lower vibrational levels. Vibration to translation relaxation is a typical type of mechanism for this process and would be expected to have a rate constant, $T_1^{-1} \leq 10^7$ s^{-1} Torr^{-1}. Because $\omega_R \gg 10^7$ s^{-1}, conventional T_1- collisions have no effect on the population dynamics of quenching observed experimentally. Only if $T_1^{-1} \geq 10^9$ s^{-1} Torr^{-1} ($\omega_R = 0.02$ cm^{-1}) can the quenching data be accounted for. However such large rate constants have no precedent for any known intermolecular, energy changing process.

TABLE IV. Effect of laser intensity expressed as $\omega_R = \mu \cdot I^{1/2}/2k$, (a) on the population (N_0) of the ground state for ladders with $\Delta = 0$ (resonant at each level) and $\Delta = 0.02$ cm^{-1} (detuned at each level),[a] and (b) on populations of the ladder when $\Delta = 0.25$ cm^{-1}.[b]

ω_R(cm^{-1})	N_0 ($\Delta = 0$)	N_0 ($\Delta = 0.02$ cm^{-1})
0.0001	0.933	0.985
0.0002	0.779	0.941
0.0004	0.468	0.794
0.0006	0.275	0.616
0.0008	0.161	0.450
0.0010	0.094	0.318
0.00125	0.051	0.202
0.0015	0.030	0.128
0.002	0.015	0.056

	Population at levels				
ω_R(cm^{-1})	1	2	3	4	5
0.001	0.994	0.002	0.002	0.002	0.000
0.004	0.903	0.022	0.022	0.022	0.000
0.008	0.671	0.030	0.029	0.029	0.000
0.012	0.410	0.020	0.019	0.019	0.000
0.016	0.204	0.011	0.009	0.010	0.000
0.025	0.019	0.001	0.001	0.001	0.000

[a] In both cases, $(T_2)^{-1}_{\text{laser}} = 1$ ns^{-1}, $\Gamma_5 = 0.1$ ns^{-1}, $(T_1)^{-1} = 0$, laser pulse duration = 200 ns, $N_0 = 1$ at $t = 0$.
[b] $(T_2)^{-1}_{\text{laser}} = 1$ ns^{-1}, $\Gamma_5 = 10$ ns^{-1}, $(T_1)^{-1} = 0$, laser pulse duration = 200 ns, $N_0 = 1$ at $t = 0$.

Dephasing, or T_2-type collisions, are analogous to pressure-broadening collisions and therefore affect the pumping rate through the linewidth. Intermolecular rate constants for dephasing-type collisions are known for a limited number of examples such as photon echoes and transient nutation and have values typically $\sim 10^7$ s^{-1} Torr^{-1}.[40] Computer results from the OBE model indicate, however, that suppression of population by dephasing requires $(T_2)^{-1} \geq 1 \times 10^{10}$ s^{-1} Torr^{-1} ($\omega_R = 10^{-3}$ cm^{-1}) or 10^3 times larger then $(T_2)^{-1}$ from previously reported experiments (see Table V). Moreover,

TABLE V. Effect of collision-induced dephasing $(pT_2)^{-1} = 1$ ns^{-1} mTorr^{-1} on populations of the pumped-mode ladder for a resonant ladder ($\Delta = 0$) and an off-resonant ladder ($\Delta = 0.02$ for levels 2, 3, 4) with $\omega_R = 0.02$ cm^{-1}.

Pressure (mTorr)	Δ (cm^{-1})	Populations at levels 1	2	3	4	5
1	0	0.030	0.025	0.021	0.017	0.013
	0.02	0.151	0.079	0.071	0.064	0.025
5	0	0.134	0.101	0.072	0.046	0.025
	0.02	0.125	0.081	0.066	0.051	0.025
10	0	0.247	0.172	0.112	0.064	0.024
	0.02	0.167	0.115	0.084	0.057	0.026
20	0	0.395	0.234	0.133	0.064	0.015
	0.02	0.262	0.175	0.115	0.067	0.023
40	0	0.562	0.246	0.106	0.041	0.005
	0.02	0.401	0.233	0.132	0.065	0.015
80	0	0.717	0.203	0.057	0.015	0.001
	0.02	0.564	0.245	0.105	0.041	0.005
200	0	0.863	0.118	0.016	0.002	0.000
	0.02	0.760	0.182	0.043	0.010	0.001

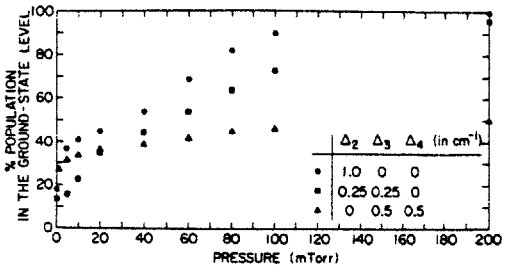


FIG. 12. Effect of a reduced Rabi frequency $R \cdot \omega_R(n)$ on populations in the ground-state level. The reduction factor is $R = \exp[-p\gamma\rho(E)]$ (see the text) and has values $R(n)$ for levels n, $R(1) = 0.01$, $R(2) = 0.01$, $R(3) = 0.06$, $R(4) = 0.26$, where γ is assumed constant and has been chosen arbitrarily. The same result is obtained for either $\omega_R(n) = \omega_R(0)$ or $\omega_R(n) = \sqrt{n}\,\omega_R(0)$. $\omega_R = 0.02$ cm^{-1}, $(T_2)^{-1} = 1$ ns^{-1}, $(T_1)^{-1} = 0$, $\Gamma_5 = 10$ ns^{-1}; detunings are as shown in the figure.

the $1/e$ points reported in Table II occur at pressures between 20 and 60 mTorr, which translates into a rate constant no greater than 10^9 s^{-1} Torr^{-1}. These observations suggest that either the model is oversimplified in its treatment of T_2, the cross section is $\gg 100$ times gas kinetic (which is not credible) or the $(T_2)^{-1}$ measured in this process cannot be related to the standard kinetic expression $k = N\sigma v$.

A third parameter which affects population in the ladder is the Rabi frequency. If we assume resonant pumping ($\Delta = 0$), then ω_R must be $\geq 10^{-5}$ cm^{-1} for pumping out of the ground state to occur. In general, a detuning $\Delta \gtrsim 50\omega_R$ appears to be sufficient to suppress depopulation of the ground state on the 200 ns time scale of the laser pulse, as was shown in Table III. Therefore, a decrease in ω_R for constant Δ also has the same effect as increasing $(T_1)^{-1}$ or $(T_2)^{-1}$. This is demonstrated in Fig. 12 where ω_R has been decreased using a phenomenological weighting factor $\exp[-p\gamma\rho(E)]$ where p is the pressure; γ a pressure dependent coupling parameter; and ρ the density of states at vibrational energy E. Although no theoretical justification exists for such a weighting factor, an exponential form was chosen because the data on pressure dependence fit exponential functions with a very high degree of correlation (> 0.99). The result shows that for a particular ladder, suppression of population occurs if ω_R depends indirectly on pressure through coupling (γ) of the pumped mode to the background states. This is equivalent to dilution and loss of oscillator strength through intramolecular relaxation, which can be described as a T_1- or T_2-type process depending on which basis set is chosen.

In summary, our attempts to model the pressure dependence of ground-state depopulation and IRMPA in thiophosgene by means of computer modeling of the OBE always result in inconsistencies. In order to avoid invoking physically unreasonable collision cross sections, we must either admit that the theoretical basis for this phenomenon is considerably more complex than is embodied in our model, or that a hitherto unsuspected interaction exists which influences the magnitude of the oscillator strength, and thus the effective Rabi frequency, for level-to-level transitions. In the following section, we suggest a possible explanation which intuitively seems reasonable but will require considerable further theoretical development.

V. DISCUSSION

The experimental observations reported in these studies indicate that the characteristics of IRMPA in $CSCl_2$ are somewhat anomalous compared to other systems. These characteristics, in the collision-free regime, include (1) homogeneous depletion of a large fraction of rotational states at all CO_2-laser frequencies; (2) no correlation between the IRMPA- and low energy IR absorption spectra; (3) no obvious indication of true multiphoton resonances based on the intensity dependence; (4) no population increases in the intermediate levels of the ladder, suggesting no anharmonic bottlenecks. When collisions are important, additional, unexpected results are observed and include (5) long range interactions; (6) an inverse dependence of the IRMPA probability on pressure; (7) correlations of the pressure dependence involving mixed quenchers with polarizability and dipole moment. This discussion will address each of these observations and is presented in the order given above.

Although the results of photophysical measurements of IRMPA in $CSCl_2$ do not appear to fit easily within the accepted theoretical framework,[1,16,35,37] the most reasonable approach to an understanding of this problem is to assume that the OBE formalism can explain the details of pumping in the ladder and that the anomalous properties can be attributed to the complicated spectroscopy of the $\tilde{X}^1A_1$ state.[16] Unfortunately, only the basic spectroscopic parameters of this system are known; the spectroscopy of higher order overtone and combination bands remains to be understood. The discussion will make use of the qualitative features of the IR spectroscopy which are summarized below.

Table I summarizes the frequencies of fundamentals of the $\tilde{X}$ state and the values of the ground-state rotational constants. In the 900–1100 cm^{-1} region, absorption occurs only through overtone and combination bands. The combination bands listed in Table I are based on fundamentals, but have not been identified spectroscopically. Although the transition moments for the combination bands are predicted to be very weak, these transitions are expected to provide additional pathways for IRMPA because of the high intensity of the radiation field.

The rotational constants of $CSCl_2$ (Table I) are quite small and lead to a very dense manifold of rotational transitions as shown in the microwave spectrum.[33] Recently, an attempt has been made to analyze the rotational spectrum of the $2\nu_4$ band.[41] Because of the small (> 0.01 cm^{-1}) rotational spacings, the analysis requires very high resolution. Preliminary assignment of a diode laser scan near the band origin (~ 942 cm^{-1}) gives values for the rotational constants (in cm^{-1}) of $2\nu_4$ as A

$=0.118\,555_6$, $B=0.115\,820_9$, $C=0.047\,821_4$, $\Delta_J=(0.6\pm0.1)\times10^{-7}$, $\Delta_{JK}=-(1.6\pm0.5)\times10^{-7}$, $\Delta_K=(1.6\pm0.8)\times10^{-7}$, $\delta_J=-(1.8\pm0.6)\times10^{-8}$, $\delta_K=(1.4\pm0.2)\times10^{-7}$. Based on these constants, there are ~2500 rotational transitions per wave number for a Boltzmann distribution at 300 K for which $J<150$, $K<50$. Of these ~2500 states, a large fraction (~60%) are unique rotational states. Thus not only is there a number of possible vibrational ladders involved in IRMPA, but also there are within each ladder many rotational pathways by which population of the ground state can be moved to higher vibrational energies.

The results of IR-visible double resonance show that IRMPA causes a large decrease in the LIF spectral intensity, integrated over all rotational states (Fig. 3), at all CO_2-laser frequencies (Fig. 4). The laser frequency dependence is reminiscent of that found for dissociation of ethylene dimers with a high-power pulsed CO_2 laser[42]; all lines between 9 and 11 μm were effective. With a low-power cw CO_2 laser, however, a much narrower photodissociation spectrum, corresponding to an ethylene fundamental vibration, was found.[43] In both cases, the high-power laser pulse appears to be saturating the very weak overtone and combination bands, thus washing out details of the vibrational fine structure. The uniform depletion of rotational states can similarly be interpreted to mean that within a frequency range equal to $\pm50\omega_R$ (see Table III and Fig. 11), the average extent of depletion of all rotational states is equal to the fractional decrease in intensity. In reality some states will be pumped more strongly than others depending on the detunings. When more than one vibrational transition is available, the probability of IRMPA is enhanced because a larger fraction of rotational transitions can be involved (assuming different rotational constants for each vibrational band). Thus, homogeneous depletion of the rotational manifold is probably the result of the rich rotational spectroscopy of $CSCl_2$; the quantitative proof, however, must await detailed spectroscopic analysis.

The lack of correlation between the low energy IR absorption spectrum and the IRMPA spectrum (Fig. 4) suggests that the predominating mechanism involves absorption pathways not strongly dependent on the transition moment for the 0–1 transition. For example, true multiphoton processes via virtual state intermediates is consistent with the experimental IRMPA spectrum. However, the intensity dependence suggests that the dominant rate limiting step in absorption involves one or at most two photons ($I^{1.0-1.7}$); at some CO_2-laser frequencies there are clearly higher order processes involved ($I^{1.7}$) but these do not predominate. The IRMPA spectrum and intensity dependence when taken together appear to rule out an explanation in which true multiphoton absorption is important. Instead, the data imply that IRMPA in $CSCl_2$ is a resonantly enhanced process at the $v=1$ level; the lack of correlation in the spectra may be attributed to the high density of rovibronic transitions in the 900–1100 cm^{-1} frequency range.

When the intermediate levels of the $2n\nu_4$ pumped-mode ladder are probed by LIF spectroscopy (with $\omega_{CO_2}=944$ cm^{-1}) in the absence of collisions, population increases are not observed up to vibrational energies of ~6000 cm^{-1} implying that there are no significant anharmonic bottlenecks. However, in the presence of collisions levels at ~944 ($2\nu_4$) and 1888 cm^{-1} ($4\nu_4$) are observed to increase in population; at sufficiently high pressures (> 50 mTorr) these increases do not require T_1- type collisions.[44] Instead, these increases can be attributed to pressure broadening T_2- type collisions which bring off-resonant ladders into resonance. These observations suggest that in the collision-free regime, population is moved irreversibly from the ground vibrational level to much higher vibrational levels in the quasicontinuum. In order for this to occur, coupling of the pumped-mode ladder to the background states must have a rate constant $\Gamma\geq10^9\,s^{-1}$ (when $\omega_R=0.02$ cm^{-1}). This conclusion is derived from model calculations in the OBE formalism (see Fig. 16). These calculations show that population in the ladder which would have been present if $\Gamma=0$ is more directly coupled to the background states and therefore is lost more rapidly than that of the ground state. Consequently, the experimentally observed population remaining in the ground state represents the result of overall anharmonic bottlenecks which in turn reflect the relative values of the detunings at each level of the ladder compared to the Rabi frequency for the "unpumped" rotational ladders.

Perhaps the most dramatic results reported here on the photophysics of IRMPA in $CSCl_2$ involve the effect of collisions. In all cases involving either pure $CSCl_2$ or mixed quenchers, the effect of collisions is observed initially at very low pressure (~5 mTorr). If the data are fit to exponentials (correlation coefficients are > 0.99 in all cases), the $1/e$ points lie in a pressure range of 20–60 mTorr for the gases studied.

This pressure range represents a cross section that ranges from 60 times gas kinetic to approximately gas kinetic. However, it should be noted that these observations are made 200 ns after the leading edge of the CO_2 laser pulse and are invariant if the delay time is reduced to 50 ns. Therefore, these cross-section estimates can only represent a lower bound. For pure thiophosgene, the quenching rate constant must be $>5\times10^8$ $s^{-1}\,Torr^{-1}$, but an exact measure can be obtained only if a time-resolved experiment is carried out in the < 50 ns time regime.

In examining the effect of collisions on the behavior of the OBE model, it was noted that only abnormally large T_1- or T_2- type relaxation rate constants could account for the experimental data. Although values of $(pT_1)^{-1}$ of 10^8–10^9 $s^{-1}\,Torr^{-1}$ do suppress IR pumping, this T_1-process is a vibration to translation relaxation pathway (V-T) for which known rate constants are typically more than two orders of magnitude smaller. Therefore, if T_1 relaxation is the phenomenological basis for the experimental observations, it is probably an intramolecular process. Figure 13 is one possible scheme that would, in effect, mimic the behavior of an intermolecular relaxation process. In this model, coupling of the background states to the pumped mode is pressure dependent and reversible. Pumping of background states is slower

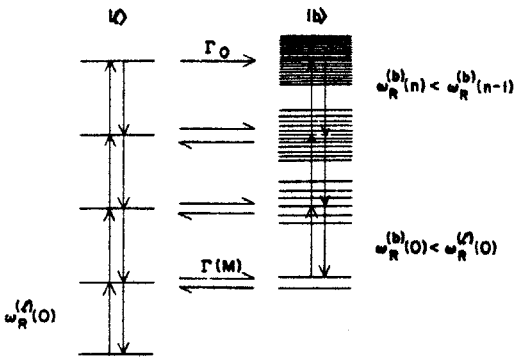


FIG. 13. A possible scheme by which collision-induced rovibronic mixing of background states $|b\rangle$ would have a similar effect on the dynamics of pumping of the ladder $|\ell\rangle$ as V-T relaxation, an intermolecular T_1 process. Because there is a number of rovibronic states at an energy $1\ h\nu \sim 1000\ cm^{-1}$, the background states in principle could also be connected directly to the vibrationless level. Intramolecular coupling below the uppermost levels depends on pressure $\Gamma(M)$; the Rabi frequency in pumping $|b\rangle$, $\omega_R^{(b)}$ is smaller than $\omega_R^{(\ell)}$ because of dilution of oscillator strength and small detunings resulting from collision-induced perturbations.

than pumping in the ladder and the Rabi frequency depends inversely on vibrational quantum number. The overall mechanism, then, has nearly the same effect as intermolecular V-T relaxation, but the validity of the model depends on the spectroscopy.

Dynamically, such a quenching scheme influences the vibrational manifold through an intramolecular, T_1-type relaxation process, but would enter the OBE model through both diagonal and off-diagonal matrix elements. Therefore, this type of process also affects the linewidth in much the same way as T_2. However, as has been previously discussed, the value for $(T_2)^{-1}$ that by itself has a marked effect on the population dynamics is 10^{11} $s^{-1}\,Torr^{-1}$ when $\omega_R = 10^{-3}\ cm^{-1}$. This value is not credible and suggests that T_2 alone is probably not the entire explanation for the observed effects of collision.

An explanation for the effect of collisions in suppressing IRMPA in $CSCl_2$ is not immediately obvious from the OBE modeling. The experimental data suggest that IRMPA in $CSCl_2$ is extremely facile and therefore occurs nearly resonantly. Interpretation of these observations in the OBE framework without regard to actual cross sections suggests as the simplest explanation for the pressure dependence, collision-induced dephasing. Such a mechanism is similar to that observed in SO_2[45] and is plausible only if the long-range part of the potential $\mu^2/r^3 \gg \omega_R$; this condition can be easily met for $r \sim 40$ Å since $\mu^2/r^3 \sim 1\ cm^{-1}$ and $\omega_R < 10^{-2}\ cm^{-1}$. However, the spectroscopic evidence to justify all rotational levels being pumped near resonance is lacking and the magnitudes of $(T_2)^{-1}$ from model calculations are considerably larger than what is justifiable experimentally. This suggests that an explanation for the pressure dependence is considerably more complex than dephasing induced by long range collisions.

A model involving background states, such as that used by Galbraith and Ackerhalt,[1] is plausible, for a number of reasons, as a basis for developing a qualitative hypothesis for the pressure dependence. The density of pure vibrational levels rises rapidly in $CSCl_2$. Associated with each vibrational level is a large rotational manifold of states through which rovibronic coupling can occur. A small perturbation, as would be characteristic of a long range interaction, could have the effect of mixing two or more vibrational manifolds through rotation-vibration interaction. As the spectroscopy shows, very many rotational levels are nearly isoenergetic ($\pm 0.2\ cm^{-1}$) thereby increasing the probability that a particular rotational state selected by the radiation field will be able to mix vibrational levels and conserve angular momentum. The effect of long-range collisions would then be related to an intramolecular coupling which slightly perturbs energy levels and also results in a broadened linewidth. Both of these effects would suppress absorption through either a smaller effective Rabi frequency (if the net perturbation of levels leads to $\Delta \gg \omega_R$) or a larger effective linewidth. Nevertheless, it is not at all clear theoretically whether or not separating level shifts and widths in this manner correctly describes what occurs in coupled oscillators in the context of the OBE formalism.

An additional feature of this model is that oscillator strength would be spread over a larger number of states. Some of these states may be detuned ($\Delta \gg \omega_R$) with respect to the laser frequency just as some states may be brought into resonance. If the net effect, however, is to decrease the effective oscillator strength, i.e., ω_R relative to Δ, the overall effect would be to suppress the probability of absorption. As was shown in the discussion of Fig. 12, reduction of the Rabi frequency by a weighting factor $\exp[-p\gamma\rho(E)]$ qualitatively reproduces the experimental results in calculations involving a single ladder. Moreover, the fact that the effect of different collision partners correlates with the long-range attractive part of the potential as has been found for radiationless transitions is consistent with, although does not prove, a hypothesis of collision-induced mixing of background states with the pumped mode, leading to a reduction in the Rabi frequency.

It is clear from this discussion that a simple explanation of the pressure dependence is not at present possible. The salient feature of these experiments, nevertheless, is the demonstration that in a system for which ω_R is small and a large number of rotational ladders exist, very weak long range interactions are sufficient to perturb the system. A complete treatment of the dynamics, including accurate spectroscopic parameters, collision-induced perturbations, and interaction with the radiation field, will be required to provide a full description of these pressure effects.

ACKNOWLEDGMENTS

The authors wish to thank Dr. H. W. Galbraith and Dr. J. Ackerhalt for help in computer modeling and

insightful discussions. We also thank Dr. E. Thiele, Dr. M. Goodman, Dr. J. Stone, and Dr. G. W. Flynn for their provocative comments. This work was carried out at Brookhaven National Laboratory and supported in part (DMB) under contract with the U.S. Department of Energy through its Office of Basic Energy Sciences and in part (MNS and JIS) by the Air Force Office of Research, Grant AFOSR-78-3725.

[1]H. W. Galbraith and J. Ackerhalt, in *Laser-Induced Chemical Processes*, edited by J. I. Steinfeld (Plenum, New York, 1981), pp. 1–44.
[2]C. D. Cantrell, S. M. Freund, and J. L. Lyman, in *Laser Handbook*, edited by M. L. Stitch (North–Holland, Amsterdam, 1979), Vol. 3, pp. 485–576.
[3]P. A. Schulz, Aa. S. Sudbo, D. J. Krajnovich, H. S. Kwok, Y. R. Shen, and Y. T. Lee, Annu. Rev. Phys. Chem. 30, 379 (1979).
[4](a) J. S. Francisco, W. R. Lawrance, J. I. Steinfeld, and R. G. Gilbert, J. Phys. Chem. 86, 724 (1982); (b) J. S. Francisco, Zhu Qingshi, J. I. Steinfeld, and R. G. Gilbert, Appl. Phys. B 28, 184 (1982).
[5]J. S. Francisco, J. I. Steinfeld, and R. G. Gilbert, Chem. Phys. Lett. 82, 311 (1981).
[6](a) W. D. Lawrance, A. E. W. Knight, R. G. Gilbert, and K. D. King, Chem. Phys. 56, 43 (1981); (b) J. E. Eberhardt, R. R. Knott, A. J. Pryor, and R. G. Gilbert, *ibid.* 69, 45 (1982).
[7]J. W. Hudgens and J. D. McDonald, J. Chem. Phys. 76, 173 (1982).
[8]J. L. Lyman, L. J. Radziemski, Jr., and A. C. Nilsson, IEEE J. Quantum Electron. QE-16, 1174 (1980).
[9](a) C. C. Jensen, T. G. Anderson, C. Reiser, and J. I. Steinfeld, J. Chem. Phys. 71, 3648 (1979); (b) C. Reiser, J. I. Steinfeld, and H. W. Galbraith, *ibid.* 74, 2189 (1981); (c) M. Dubs, D. Harradine, E. Schweitzer, J. I. Steinfeld, and C. Patterson, *ibid.* 77, 3824 (1982).
[10](a) P. F. Moulton, D. M. Larsen, J. N. Walpole, and A. Mooradian, Opt. Lett. 1, 51 (1977); (b) C. W. Patterson, R. S. McDowell, P. F. Moulton, and A. Mooradian, *ibid.* 6, 93 (1981).
[11]S. M. Adler-Golden, E. L. Schweitzer, and J. I. Steinfeld, J. Chem. Phys. 76, 2201 (1982).
[12](a) V. N. Bagratashvili, Yu. G. Vainer, V. S. Dolzhikov, S. F. Kol'yakov, A. A. Makarov, L. P. Malyavkin, E. A. Ryabov, E. G. Silkis, and V. D. Titov, Appl. Phys. 22, 101 (1980); (b) JETP Lett. 30, 471 (1979); (c) V. N. Bagratashvili, Yu. G. Vanier, V. S. Dolzhikov, V. S. Letokhov, A. A. Makarov, L. P. Malyavkin, E. A. Ryabov, and E. G. Silkis, Opt. Lett. 6, 148 (1981).
[13]P. Esherick, A. J. Grimley, and A. Owyoung, Proc. Vth International Conference on Laser Spectroscopy, Alberta, Canada, 1981.
[14](a) R. J. Orr and G. F. Nutt, Opt. Lett. 5, 12 (1980); (b) J. Mol. Spectrosc. 84, 272 (1980); (c) R. J. Orr, J. G. Haub, G. F. Nutt, J. L. Steward, and O. Vozzo, Chem. Phys. Lett. 78, 3 (1981).
[15]D. M. Brenner, K. Brezinsky, and P. M. Curtis, Chem. Phys. Lett. 72, 202 (1980).
[16](a) J. C. D. Brand, J. H. Callomon, D. C. Moule, J. Tyrrell, and T. H. Goodwin, Trans. Faraday Soc. 61, 2365 (1965); (b) O. A. Frenzel, K. E. Blick, C. R. Bennett, and K. Niedenzu, J. Chem. Phys. 53, 198 (1970); (c) J. R. Lombardi, *ibid.* 52, 6126 (1970); (d) J. C. D. Brand, J. L. Hardwick, and K. -E. Teo, J. Mol. Spectrosc. 57, 215 (1975); (e) D. A. Condirston, A. R. Knight, and R. P. Steer, Chem. Phys. Lett. 86, 254 (1982).
[17](a) M. F. Goodman, J. Stone, and D. A. Dows, J. Chem. Phys. 65, 5052 (1976); (b) J. Stone, M. F. Goodman, and D. A. Dows, *ibid.* 65, 5062 (1976).
[18]S. S. Alimpiev, N. V. Karlov, S. M. Kikiforov, A. M. Prokhorov, B. G. Sartakov, E. M. Khokhlov, and A. L. Shtarkov, Opt. Commun. 31, 309 (1979).
[19]C. W. Patterson, R. S. McDowell, P. F. Moulton, and A. Mooradian, Opt. Lett. 6, 93 (1981).
[20]I. P. Herman and J. B. Marling, Chem. Phys. Lett. 64, 75 (1979).
[21]J. C. Stephenson, D. S. King, M. F. Goodman, and J. Stone, J. Chem. Phys. 70, 4496 (1979).
[22]I. Hanazaki, K. Kasatani, and K. Kuwata, Chem. Phys. Lett. 75, 123 (1980).
[23]A. C. Baldwin, J. R. Barker, D. M. Golden, R. Duperrex, and H. van den Bergh, Chem. Phys. Lett. 62, 178 (1979).
[24]S. K. Sarkar, V. Parthasarathy, A. Pandey, K. V. S. Rama Rao, and J. P. Mittal, Chem. Phys. Lett. 78, 479 (1981).
[25]D. M. Brenner, J. Chem. Phys. 74, 2293 (1981).
[26]M. Spencer, J. I. Steinfeld, and D. M. Brenner, J. Chem. Phys. 75, 3153 (1981).
[27]D. M. Brenner, J. Phys. Chem. 84, 3341 (1980).
[28]D. M. Brenner and D. W. Peters, J. Chem. Phys. 76, 197 (1982).
[29]D. M. Brenner, J. Chem. Phys. 74, 494 (1981).
[30]D. M. Brenner (unpublished results).
[31]I. E. Coop and L. E. Sutton, Trans. Faraday Soc. 35, 505 (1939).
[32]F. W. Birss (private communication) and based on F. W. Birss, S. D. Colson, and D. A. Ramsay, Can. J. Phys. 51, 1031 (1973).
[33]J. H. Carpenter, D. F. Rimmer, J. Q. Smith, and D. H. Whiffen, J. Chem. Soc. Faraday Trans 2 71, 1752 (1975).
[34]H. -M. Lin, M. Seaver, K. Y. Tang, A. E. W. Knight, and C. S. Parmenter, J. Chem. Phys. 70, 5442 (1979).
[35](a) L. Allen and J. Eberley, *Optical Resonance and Two-Level Atoms* (Wiley, New York, 1975); (b) D. Larsen and N. Bloembergen, Opt. Commun. 17, 254 (1976).
[36]S. -C. Lin and J. H. Morris, J. Quant. Spectrosc. Radiat. Transfer 17, 577 (1977).
[37](a) M. F. Goodman and E. Thiele, Phys. Rev. A 5, 1355 (1972); (b) J. Stone, E. Thiele, and M. F. Goodman, J. Chem. Phys. 59, 2909 (1973).
[38]M. F. Goodman, J. Stone, and E. Thiele, J. Chem. Phys. 63, 2929 (1975).
[39]D. Hodgkinson (to be published).
[40]See A. H. Zewail, Acc. Chem. Res. 13, 360 (1980), and references therein.
[41]Zhu Qingshi, M. N. Spencer, J. I. Steinfeld, and D. M. Brenner (unpublished data).
[42]M. A. Hoffbauer, W. R. Gentry, and C. F. Giese, in *Laser-Induced Processes in Molecules*, edited by K. L. Kompa and S. D. Smith (Springer, Berlin, 1979), pp. 252–254.
[43](a) M. P. Casassa, D. S. Bomse, J. L. Beauchamp, and K. C. Janda, J. Chem. Phys. 72, 6805 (1980); (b) M. P. Casassa, D. S. Bomse, and K. C. Janda, *ibid.* 74, 5044 (1981).
[44]M. N. Spencer, Ph.D. dissertation, MIT, Cambridge, Massachusetts, 1982.
[45]D. L. Holtermann, E. K. C. Lee, and R. Nanes, J. Chem. Phys. 76, 3341 (1982).